The effects of carbon deposition on catalyst deactivation in high temperature Fischer-Tropsch catalysts

Veronica A. Patterson

A thesis submitted for the degree of PhD
at the
University of St Andrews

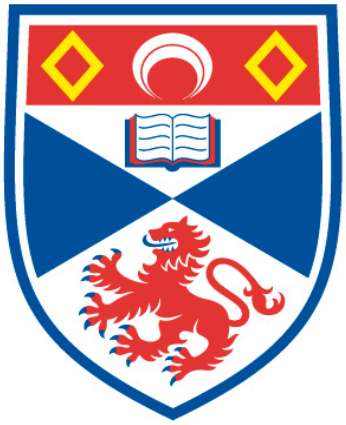

2012

Acknowledgements

Praise be to God who took my crazy childhood dream and made it a reality.

Thank you to Sasol for funding my studies and giving me the opportunity to become the best scientist I can be. I can only endeavour to show my gratefulness through hard work and loyalty to the company.

I would like to thank my industrial supervisor, Paul Webb, for the tremendous amount of time and effort to get this work going. Thanks for trusting me with this wonderful project, I've enjoyed working on it. I've really learned a great deal from him, not only about chemistry but also taking a result and turning it into something better. His guidance, endless patience and motivation are much appreciated.

I am most grateful to Catherine Botting, who introduced me to the world of and trained me on the MALDI-TOF MS. Thank you for coming to my aid whenever the instrument lost the will to live. I also appreciate the hours spent proof reading and giving quick feedback.

Thank you to everyone at STUK, you guys were wonderful to work with. Thanks for always being so eager to teach me new things and quick to help me out with emergency experiments. A special thanks to Phil Landon for training me on the Raman and all your help. You were always a trustworthy source of useful publications. I miss those insults in the lab. Many thanks to Johan Labuschagne for always being available to chat about the project. A special thanks to Carol Read, David Smith and Leigh-Anne de Jongh for making Spongebob corner so much fun. I miss you guys every day.

I'm also thankful for the time taken by Maropeng Ngobeni for facilitating the work at Sasol Technology R&D and for editing some of my manuscripts.

My dear St Andrews friends: Rebecca Atkinson, Vinet Coetzee, Jacorien and William Gabrielli, Elizabeth Tapscott thank you for helping me stay sane through the Scottish winters with regular beatings, feedings, walks on the beach and flick nights. Thank you for always caring and making me feel part of a special family. I'm sure each of you could write a chapter after all those hours of having to listen to my anti-social thesis banter.

Thanks to my family for reminding me where home is, and for keeping me in the circle of love. I know it wasn't easy having one lost soul away all the time. My dearest parents, thank you for reminding me of the dream when I lost my way. Thank you for all your support and encouragement. You never doubted me. This thesis is dedicated to you.

Declarations

I, Veronica Audrey Patterson, hereby certify that this thesis, which is approximately 50 000 words in length, has been written by me, that it is the record of work carried out by me and that it has not been submitted in any previous application for a higher degree.

I was admitted as a research student in June 2007 and as a candidate for the degree of Doctor of Philosophy in June 2007; the higher study for which this is a record was carried out in the University of St Andrews between 2007 and 2011.

Date ..... signature of candidate …….....

I hereby certify that the candidate has fulfilled the conditions of the Resolution and Regulations appropriate for the degree of Doctor of Philosophy in the University of St Andrews and that the candidate is qualified to submit this thesis in application for that degree.

Date ……..... signature of supervisor …….....

In submitting this thesis to the University of St Andrews I understand that I am giving permission for it to be made available for use in accordance with the regulations of the University Library for the time being in force, subject to any copyright vested in the work not being affected thereby. I also understand that the title and the abstract will be published, and that a copy of the work may be made and supplied to any bona fide library or research worker, that my thesis will be electronically accessible for personal or research use unless exempt by award of an embargo as requested below, and that the library has the right to migrate my thesis into new electronic forms as required to ensure continued access to the thesis. I have obtained any third-party copyright permissions that may be required in order to allow such access and migration, or have requested the appropriate embargo below.

The following is an agreed request by candidate and supervisor regarding the electronic publication of this thesis:

Embargo on both all of printed copy and electronic copy for the same fixed period of 2 years on the following grounds: publication would preclude future publication.

Date ……..... signature of candidate ……..... signature of supervisor …….....

Table of Contents

List of Figures

List of tables

Abstract

In this work, carbonaceous deposits on spent HTFT catalysts were investigated. This research was required in order to better understand the observed loss in productivity observed in the industrial reactors, with the aim of improving the economy of the HTFT process. A host of complementary techniques were employed to systematically determine the composition of a typical catalyst recovered from a reactor. Spent HTFT catalysts are comprised of magnetite and a mixture of iron carbides as well as adsorbed hydrocarbon products (soft carbon) and hard carbon. Reaction initiates at the particle surface and along the promoter-rich grain boundaries toward the core of the grains. A partially reacted particle would therefore have a core-shell structure, with magnetite representing the unreacted region of the catalyst. The reacted region consists of a porous carbonaceous matrix with soft carbon and carbide crystallites nestled in this matrix. The hard carbonaceous species is a mixture of polymeric carbon and polycyclic aromatic hydrocarbons. The particle structure is linked to the sample preparation method and an alternative method yielding catalyst particle with uniformly distributed promoter elements could be beneficial.

Investigating carbonaceous species is a complex process, and development of a fresh methodology would aid in the quest for insight into the nature of carbonaceous species in various systems. A new approach which entails a combination of the traditional techniques combined with MALDI-TOF MS enabled a deeper investigation. Additional aspects such as the molecular weight distributions along with known information about crystallinity and morphology of the catalyst provide a comprehensive study of carbonaceous material. Polymeric carbon and very large polycyclic aromatic hydrocarbons constitute hard carbon and can be observed with minimal sample preparation procedures.

The evolution of the HTFT catalysts was investigated as a function of time-on-stream. This enabled us to study the effects of increasing amounts of hard

carbon on the activity and the chemical and physical properties of the catalysts. The catalyst activity was found to decrease with increasing hard carbon content, although the effect of carbon deposition cannot be distinguished from phase transformation (oxidation) which occurs simultaneously. A method to quantify the amount of hard carbon, which progressively builds up on the catalyst, was demonstrated. This required a great deal of method development, which provides a platform for future investigations of these catalysts. Importantly, it allows predictions of the amounts of carbon that will be deposited after a certain reaction time. This allows more efficient regulation of catalyst replacement.

The production of fine carbon-rich particles in the industrial reactor poses a major problem in the process. Carbon deposition leads to an increase in particle diameter with time on-stream. Permissible levels of hard carbon were identified, beyond which the mechanical strength of the catalyst particles deteriorate. This leads to break-up of the particles and therefore fines formation. The surface area and pore volume generally increase with progressive deposition of hard carbon, while the bulk density of the catalyst material exhibits a linear decrease with carbon build-up.

A mechanism is proposed for hard carbon formation which apparently occurs through the dissociative adsorption of CO to form a carbon monolayer. This is followed by polymerisation of the carbon atoms. Meta-stable interstitial carbides are formed at the iron-carbon interface. Owing to a carbon concentration gradient between the top of the surface and the bottom of the metal or carbide particle, carbon diffusion across the crystal (carbide decomposition) and grows as a PAH molecule lifting the iron carbide away from the particle. As this corrosion process is intrinsic to iron-based catalysts, a catalyst that contains sulphur is proposed for future development.

1. INTRODUCTION

1.1 Fischer-Tropsch Synthesis

In the early 20th century Germany, many research efforts were directed towards finding a process that would utilise the abundant coal reserves. Franz Fischer and Hans Tropsch were working at the Kaiser Wilhelm Institute for Coal Research in Mülheim, Ruhr. Their aim was to produce hydrocarbon molecules from which fuels and chemicals could be made, using coal-derived gas (Fischer & Tropsch, 1923). The technology first found industrial application in the 1930's, where potential products and co-products were soon identified. Continued interest in the technology was due to strategic and political considerations, such as South Africa that had no crude oil but abundant coal reserves.

The world-wide prediction of rising crude oil prices was the driving force for Sasol's first Fischer-Tropsch Synthesis (FTS) plant (Moodley, 2008) based on synthesis gas, a mixture of hydrogen and carbon monoxide, derived from coal employing an iron-based catalyst. The first synthesis reaction was obtained in the Synthol plant based in Sasolburg, South Africa in 1955 (Dry, 1981). The discovery of huge oil fields in the Middle East, however, repressed the predicted rise in oil price. This led to diminished interest in FTS until the early 1970's saw a significant rise in oil price due to a series of events that were initiated by the outbreak of the Yom Kippur War in October 1973 (Steynberg, 2004). The increase in oil price proved favourable for the economics of FTS in South Africa, which resulted in the construction of two Sasol plants, each producing more than ten times the amount of fuel of the original plant in Sasolburg.

FTS converts synthesis gas to liquid fuels that are suitable for use in standard motor vehicles as well as other valuable chemicals. The economic viability of a commercial FT plant is highly dependent on the crude oil price, which has fluctuated considerably during the past few decades. The renewed interest in FTS lies in the demand for fuels that meet stringent specifications in order to

protect the environment. Synthetic fuels are much cleaner than those derived from crude oil.

FT technology usually involves three basic steps, namely synthesis gas preparation, FTS and product upgrading. Fischer-Tropsch synthesis uses alternative feedstocks to oil. These feedstocks are usually coal or natural gas and the technology associated with the conversion of syngas from these feedstocks being called coal-to-liquid (CTL) or gas-to-liquid (GTL), respectively. The use of biomass feedstock as an environmentally friendly alternative source of carbon is currently in the research stage, and the technology associated with FTS from this feedstock is called biomass-to-liquid (BTL).

Although all the Group VIII metals are active for Fischer-Tropsch synthesis (Vannice, 1975), it is only Ni, Co, Fe and Ru that exhibit sufficient CO hydrogenation activity for commercial applications (Davis, 2007). Ni catalysts are strongly hydrogenating, thereby producing excessive amounts of methane. Ru is expensive and is also too rare to consider the use of this catalyst in industrial operations. The current industrial catalysts are based on Co and Fe, where the product selectivity is strongly dependent on the choice of catalyst.

Products such as methane, synthetic gasoline and waxes, and alcohols are formed. Water is a major by-product of FTS and, owing to the prevalence of water-gas shift activity, carbon dioxide can also be formed (Patzlaff *et al*., 1999). Water-gas shift activity is mainly observed with iron-based catalysts, which facilitates the use of this catalyst with coal or biomass-derived syngas with a low H_2/CO ratio.

The Fischer-Tropsch process is performed under two different regimes, namely high temperature and low temperature (Dry, 2002). In high temperature Fischer-Tropsch synthesis (P~20 bar; T~300-350 °C), mainly hydrocarbons in the range of C_1-C_{20} are produced, *i.e*. products in the

gasoline boiling range, low molecular weight olefins and some oxygenates. The low temperature process (P~20 bar; T~220-240 °C) is mainly used for the production of high molecular weight linear waxes (Dry, 2002).

The iron-based catalyst currently used by Sasol for high-temperature FTS are prepared by fusion of iron oxide together with chemical promoter, K_2O, and structural promoters such as MgO and Al_2O_3 (Dry, 2004). These catalysts are preferentially reduced in H_2 at 350-450 °C. Exposure of the reduced catalysts to syngas leads to rapid transformation from metallic iron into interstitial iron carbides due to migration of the carbon atoms originating from the CO into the metal lattice (Dry, 2004). After completion of the carbiding process the deposition of carbon continues. Herein lays the main challenge in the design of the iron-based FTS catalyst. These catalysts have high deactivation rates during operation and the cost of constant catalyst replacement is very unfavourable from a commercial point of view.

1.1.1 Reaction pathways in the Fischer-Tropsch synthesis

The Fischer-Tropsch synthesis is a polymerisation reaction, in which the monomers are being produced *in-situ* from the gaseous reactants hydrogen and carbon monoxide. Thus, all reaction pathways proposed in the literature will have three main reaction steps, *i.e*.

1. generation of the chain starter (initiation)
2. chain growth (propagation)
3. desorption (termination)

Numerous reaction pathways have been proposed to explain the observed product distribution in FT synthesis. It can be assumed that not a single reaction pathway exists on the catalyst surface during the FT synthesis, but rather a number of parallel operating pathways. The four most popular mechanisms are the ‘alkyl’, ‘alkenyl’, ‘enol’ and ‘CO-insertion’ mechanisms (Claeys and van Steen, 2004).

The alkyl mechanism is presently the most widely accepted mechanism for chain growth in the FT synthesis (Claeys and van Steen, 2004). Chain initiation takes place *via* dissociative CO-chemisorption, by which surface carbon and surface oxygen is generated. Surface oxygen is removed from the surface by reaction with adsorbed hydrogen yielding water or with adsorbed carbon monoxide yielding carbon dioxide. Surface carbon can be subsequently hydrogenated yielding in consecutive reaction, CH, CH_2 and CH_3 surface species. The CH_3 surface species is regarded as the chain initiator, and the CH_2 surface species as the monomer in the reaction scheme. Chain growth is thought to take place by successive incorporation of the monomer, CH_2 surface species. Product formation takes place by either β-hydrogen abstraction or hydrogen addition yielding 1-olefins and *n*-paraffins as primary products, respectively (Fischer and Tropsch, 1926; Craxford and Rideal, 1939).

In the enol mechanism (Storch *et al*., 1951), chemisorbed CO is hydrogenated to an enol surface species. Chain growth occurs through a condensation reaction between enol species with elimination of water. The occurrence of branched hydrocarbons is thought to originate from the involvement of a CHROH surface species. Termination of the chain growth process occurs by desorption of oxygenates and 1-olefins.

In the CO-insertion mechanism (Pichler and Schulz, 1970) chemisorbed CO is the monomer. The chain initiator is thought to be a surface methyl species. Chain growth takes place by CO-insertion in a metal-alkyl bond leading to a surface acyl species. The elimination of oxygen from the surface species leads to the formation of the enlarged alkyl species. Product desorption can take place by hydrogen addition and β-hydrogen elimination of the alkyl or oxygen containing surface species, leading to the formation of *n*-paraffins, 1-olefins, aldehydes and alcohols.

In the alkenyl mechanism (Maitlis *et al*., 1996, 1999), the formation of the first C-C bond is thought to occur through the coupling of methylidyne (CH) and

methylene (CH_2) to form a vinyl surface species ($CH=CH_2$) favoured according to theoretical calculations (Trinquier & Hoffmann, 1984), which is considered as the chain initiator. Chain propagation involves the addition of a methylene species to a surface vinyl species, yielding a surface allyl species. This is followed by an allyl-vinyl isomerisation forming a surface alkenyl species. Product desorption involves the hydrogen addition to an alkenyl species yielding 1-olefins.

Carbon and hydrogen readily dissolve in the typical Fischer-Tropsch metal catalysts. Reasonable amounts of methyl in equilibrium with methylene must be present on a metal in order to be active as a Fischer-Tropsch catalyst (Nolan *et al*., 1998); this was confirmed by Alstrup and Tavares (1993) who argued that during the deposition of carbon from methane, the conversion of surface methyl to surface methylene is rate limiting. It is known that methyl, methylene, methyne and ethylidyne species adsorb preferentially in the three-fold hollow site formed by adjacent metal atoms (Yang *et al*., 1995).

Trinquier and Hoffman (1984) investigated the orbital symmetry requirements for the reaction of two metal-carbon σ bonds to react to form a C_2 species and reported that this would occur when the two carbons are bound to the same metal atom (reductive elimination). It is therefore likely that a surface methyl or methylene species, which was shown to interconvert easily (Zaera, 1992), can react with a dissolved carbon from the bulk to form the C_2 species. This surface C_2 species could possibly rearrange to vinyl as suggested by Maitlis *et al*. (1996, 1999) to be the chain initiation species for the Fischer-Tropsch reaction. In addition, a dissolved hydrogen atom sitting in the site directly below a methyl would preferentially react to form methane on a Ni catalyst as opposed to a surface hydrogen species (Johnson *et al*., 1992).

The formation of carbonaceous materials could be explained by furthering the surface reactions of hydrocarbon species on a metal surface. Adsorbed methyl nestled between three adjacent metal atoms can dissociate to form a surface CH species. These CH species can then recombine to form adsorbed

C_2H_2 (Yang *et al*., 1995). Near saturation coverage of the resulting C_2H_2 can trimerise to C_6H_6 on the surface. The dehydrogenation of C_6H_6 at elevated temperatures leads to the formation of polycyclic aromatic hydrocarbons.

1.1.2 Products of Fischer-Tropsch synthesis

A variety of products of different chain length with different functionality is formed in Fischer-Tropsch synthesis. The main products of the FT synthesis are n-olefins (mainly α-olefins) and *n*-paraffins, while oxygenates and branched compounds can also form (Claeys and van Steen, 2004). The actual product distribution of a Fischer-Tropsch process depends on reaction variables such as temperature and partial pressures of the reactants and product water, the reactor system used, as well as the properties of the catalyst.

The variety in composition of Fischer-Tropsch products comprising of hundreds of individual compounds shows a remarkable order with regard to the class and size of the product compounds (Schulz and Claeys, 1999). A number of kinetic models for the Fischer-Tropsch product distribution have been developed. The Anderson-Schulz-Flory distribution is the simplest of these kinetic models (Schulz and Claeys, 1999).

The basis of the Anderson-Schulz-Flory (ASF), as well as all the other polymerisation kinetics, is the generally accepted principle that Fischer-Tropsch reaction proceeds *via* the addition of a C_1 monomer (Schulz and Claeys, 1999). The carbon number dependency of the product distribution can be described by:

$$M_N = (1-\alpha).\alpha^{N-1} \qquad (3)$$

if the rate of addition of C_1 monomers relative to the rate of desorption is independent of the carbon number of the growing chain. M_N is the mole fraction of the products with carbon number N and α is the chain growth

probability. The so-called Anderson-Schulz-Flory plots are obtained by plotting M_N versus N on a semi-logarithmic plot, yielding a linear relationship, from which the chain growth probability is obtained. The chain growth probabilities of typical FT processes are illustrated in Figure 1.1 below.

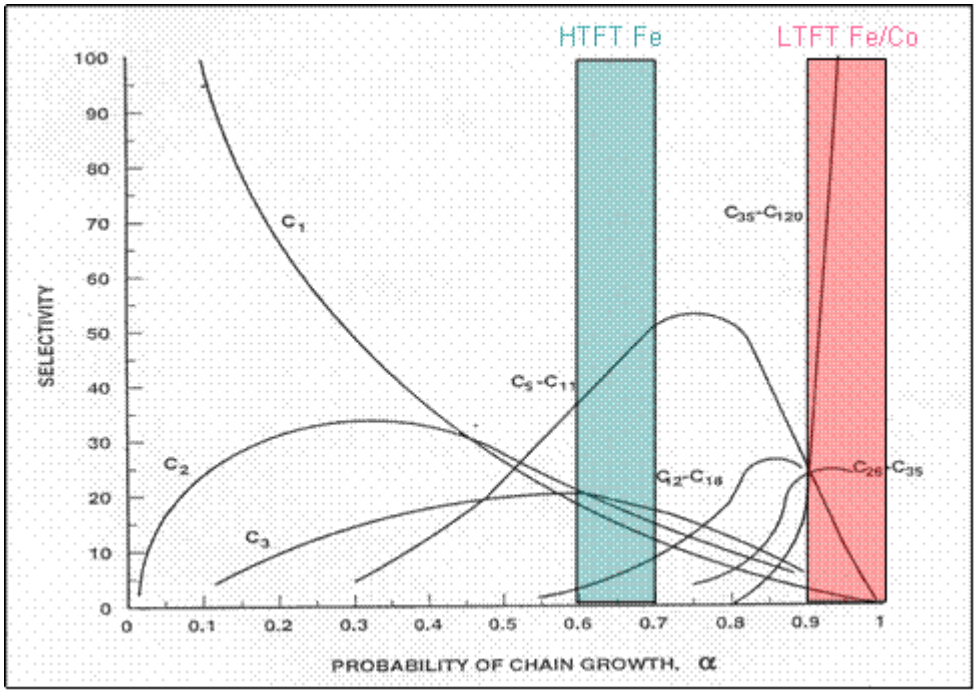

Figure 1-1: Chain growth probability of typical FT processes

While the product distribution in FT follows the ASF statistics, some deviations were also noted. The noted empirical deviations of the Fischer-Tropsch product distribution from the theoretically predicted ASF product distributions are:

- Higher than expected methane content *i.e.* low chain growth probability for C_1 surface species (Schulz *et al*., 2002)
- Relatively low ethene yield, which has been explained by strong re-adsorption of ethene leading to chain initiation and chain growth (Schulz and Claeys, 1999; Schulz *et al*., 2002)
- Increase in chain growth probability in the range C_7-C_8, indicative of increasing *n*-olefin readsorption for further chain growth (Schulz *et al*., 2002).

The high temperature Fischer-Tropsch (HTFT) synthesis is performed at conditions where condensation of higher carbon number products does not take place (Dry, 1996). This leads to decreased readsorption of higher carbon number olefins and therefore less secondary chain growth of these products.

1.2 Iron-based catalysts for Fischer-Tropsch synthesis

The iron-based FTS catalyst system has been a subject of research for over 80 years, but the exact structural composition of the active species remains controversial. Fe_3O_4 (Reymond *et al*., 1982; Kuivila *et al*., 1989; Butt, 1991), α-Fe (Niemantsverdriet *et al*., 1980; Ott et al., 1980; Loaiza-Gil et al., 1999; Dwyer & Somorjai, 1978) and iron carbides (Amelse *et al*., 1978; Raupp & Delgass, 1979a, b; Shroff *et al*., 1995; Dictor & Bell, 1986; Jung & Thomson, 1992) have all been reported as the active phase in FTS. Stabilisation of the active catalyst remains a challenge despite vast research efforts into the mechanisms of deactivation in these catalysts. An appreciation of the structure and the role of the different iron and carbon species present during operation would provide insight into the deactivation behaviour of the iron-based FTS catalyst.

Iron-based catalysts undergo several phase transformations such as haematite to magnetite during pre-treatment, followed by reduction to Fe metal and subsequent formation of carbides in the presence of CO or syngas (Schulz *et al*., 1999). These iron carbides are regarded as the active phases of the catalyst during Fischer-Tropsch synthesis (Niemantsverdriet *et al*., 1980; Dry, 1990; Cheng *et al*., 2010). Several iron carbides can in principle be formed, but it is commonly accepted that Hägg carbide is the catalytically active phase for Fischer-Tropsch synthesis (Herranz *et al*., 2006; Niemantsverdriet *et al*., 1981; Rao *et al*., 1994; Xu *et al*., 2003; Prasad *et al*., 2008; Zhang *et al*., 2004).

Malan *et al*. (1961) showed the phase composition of the iron catalyst as a function of time on stream in the Fischer-Tropsch synthesis (see Figure 1.2).

The reduced catalyst contained α-Fe, which transformed rapidly into Hägg carbide (Fe_5C_2), cementite (Fe_3C) and magnetite (Fe_3O_4). The oxide phase Fe_3O_4 became more dominant with increasing time on stream, whereas the relative abundance of carbide became less. Furthermore, Hägg carbide transforms into Eckstrom-Adcock carbide (Fe_7C_3). It is indicated that with time on stream, the carbide phases become enriched with carbon (*i.e.* cementite → Hägg carbide → Eckstrom-Adcock carbide).

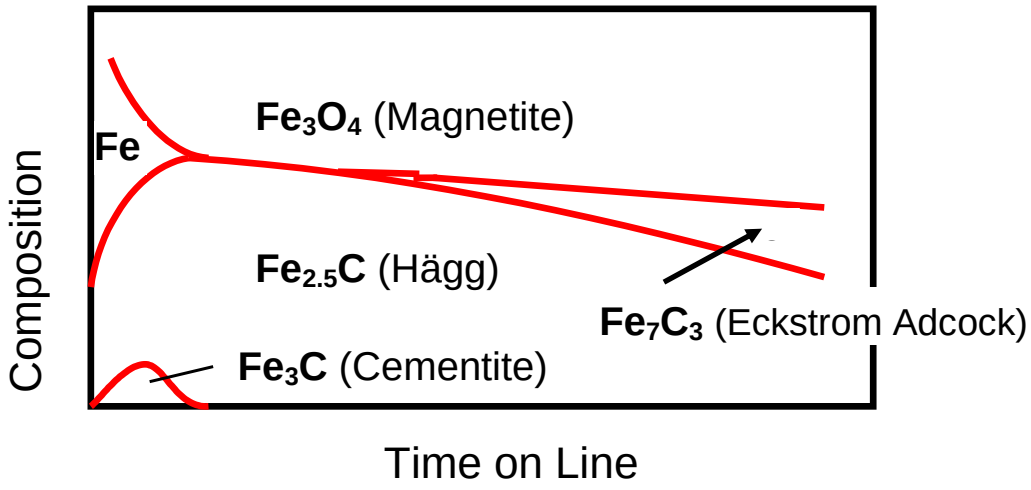

Figure 1-2: Phase change in iron-based catalyst as a function of time on-line (redrawn from Malan et al., 1961)

Inactive iron carbides for FTS have been identified, and in one such study Reymond and co-workers (1982) found $Fe_{20}C_9$ in a pre-reduced catalyst and Fe_2C in an unreduced catalyst. These authors also suggest that magnetite (Fe_3O_4) might be an active phase for the iron-based Fischer-Tropsch synthesis, based on the observation that the formation of this phase parallels the onset of FTS activity (Reymond *et al*., 1982). In a study of nanosized iron catalysts in slurry-phase FTS (Mahajan *et al*., 2003), the catalysts consisted of 88% magnetite and the balance was a mixture of carbides. The high activity and stability observed on these catalysts suggested that either magnetite was the active phase or the carbides were extremely active. Similarly, Loaiza-Gil and co-workers (1999) also ascribed FTS activity to Fe_3O_4 and metallic iron. The reasoning behind their hypothesis was that the catalyst consisted of 50% Fe_3O_4, 31.1% α-Fe and only 18.9% Fe_5C_2. An XPS study (Kuivila *et al*., 1989)

also showed that Fe_3O_4 was active for synthesis. The study also showed that activation of the catalyst particles was accompanied by a high rate of surface carbon deposition, and the near-surface region was converted to carbide. The surface carbon deposition continued throughout the reaction, and was reported to result in loss of activity. This contradicts the hypothesis of Dictor and Bell (1986), who reported that magnetite is inactive for FTS. These researchers performed Fischer-Tropsch synthesis over unpromoted and K-promoted iron oxide catalysts. They observed a delay at the start of the reaction, at which time the catalyst was being reduced to the active catalyst. Reduction is known to proceed *via* Fe_3O_4 to metallic Fe, which rapidly carburises to the active phases α-Fe and/or χ-$Fe_{2.2}C$. A Mössbauer study performed by Rao *et al*. (1994) also exposed a correlation between FT activity and the Fe_5C_2 content in the catalyst. Hayakawa and co-workers (2006) also linked the activity of their iron-based catalyst with the reduction of Fe_3O_4 and the subsequent appearance of Hägg carbide phase.

Fe_3C and $Fe_{2.5}C$ formed as nuclei on the catalyst surface were found to be the active phases for Fischer-Tropsch synthesis (Podgurski *et al*., 1950). Shroff and co-workers (1995) also believe that magnetite has negligible Fischer-Tropsch activity, whereas the carbide formation was accompanied by high activity. The conversion of near-surface layers of Fe_3O_4 to FeC_x is reported to be sufficient for the formation of active sites for FTS (Li *et al*., 2001). Therefore, an erroneous assignment of the active phase can be made in magnetite-rich catalysts.

In a study of the site requirements in iron-catalysed Fischer-Tropsch synthesis, Li and co-workers report that the rate of formation of Fe_3O_4 was similar to the rate of conversion to FeC_x (Li *et al*., 2002). It was postulated that since the appearance of both these phases coincided with the detection of hydrocarbon products, either one or both these phases can provide the catalytic site required for Fischer-Tropsch synthesis. The fact that Fe_3O_4 and FeC_x easily interconvert as a result of elementary reaction steps in the

reaction makes the assignment of catalytic activity to a specific phase irrelevant.

Both iron carbide and oxide phases occur simultaneously on the Fischer-Tropsch catalysts. The carbide phase is believed to be active towards dissociation of CO and formation of hydrocarbons, while the oxide phase seems to be the most active for the water gas shift reaction (van der Laan & Beenackers, 2000; Prasad *et al*., 2008).

1.2.1 Effect of particle size on carbide phase

Raupp and Delgass (1979a, b, c) in an investigation of FTS on precipitated iron-based catalysts at 250 °C reported that the carbide phase formed on supported Fischer-Tropsch catalysts depends on the particle size and support material. Small iron particles on silica favour the formation of the unstable ε-Fe_2C and ε'-$Fe_{2.2}C$, while large particles form χ-Fe_5C_2. It was further revealed by simultaneous spectroscopic and kinetic measurements in this study that incorporation of carbon in the iron particles controls the number of active sites on the surface.

The effect of particle size on the iron carbide phase was also observed by Jung *et al*., (1982b). It was reported that the support has a strong influence on the extent of dispersion of the metal, so that silica-supported iron catalysts which form smaller iron particles readily form $Fe_{2.2}C$ upon exposure to FT conditions (Amelse *et al*., 1978). The highly dispersed particles were also found to have a lesser tendency to deactivate by the deposition of carbonaceous species.

The effect of Mn on a Fe/Cu/Si catalyst was investigated by Campos and co-workers (2010). It was hypothesised that the Mn-substitution of octahedral Fe-sites in Fe_3O_4 occurs, which leads to the formation of smaller iron carbide crystallites. The workers therefore ascribed a decrease in carbon deposition to the formation of these smaller crystallites, since deleterious carbon

deposition is assumed to occur predominantly on large iron carbide particles (Jin & Datye, 2000; Shroff *et al*., 1995; Arakawa & Bell, 1983). The benefits of Mn promotion of an iron-based catalyst appear to be more evident when the catalyst is pre-treated in CO. In this case, the stabilisation of active carbonaceous intermediates is enhanced (Herranz *et al*., 2006).

1.2.2 Adsorption and reaction on Hägg carbide surfaces

It is important to consider the adsorption of synthesis gas on Hägg carbide surfaces, as well as the reactions that are favoured in order to understand the activity of this phase towards FTS. Bulk Hägg carbide structures have been well characterised by X-Ray Diffraction (XRD), but since these materials are not stable in air, there is no experimental characterisation of the surfaces (Du Plessis *et al*., 2007). This makes the choice of appropriate surface models for mechanistic studies by Density Functional Theory (DFT) challenging. It is therefore useful to conduct a theoretical analysis of the trends of surface stability for Hägg carbide. This work was performed by Steynberg and co-workers (2008), who identified the (010) as the most stable and the (101) as the least stable low Miller index surface. A large number of surfaces are shown to share similar surface energies and it is therefore concluded that it is not appropriate to assign a single representative active surface for Fischer-Tropsch synthesis.

A series of papers on the adsorption of H_2, CO and syngas on specific Fe_5C_2 surfaces were published by the group of Jiao. The first of these papers addressed the adsorption of CO on the (001), (100) and (110) surfaces of Fe_5C_2 (Cao *et al*., 2004). CO is reported to preferentially adsorb at a 3-fold hollow site at low CO coverage. The donation and back-donation of the surface iron orbitals and adsorbing CO molecule orbitals are essential in CO activation. The electrons in the HOMO of a CO molecule are donated to the LUMO of the surface iron atoms. In turn, the d electrons on the HOMO of the surface iron atoms are donated back to the π antibonding LUMO of the adsorbed CO molecule, resulting in weakening of the strong CO bond. The

adsorption of hydrogen on the Fe_5C_2 surfaces was subsequently studied (Cao *et al*., 2005a). Iron carbide can be transformed into metallic iron under H_2 atmospheres and it was previously reported that the carbon in iron carbide can be reduced to CH_x (x = 1-3) fragments as detected by infrared spectroscopy (Bian *et al*., 2001; Bian *et al*., 2002). Again, adsorption is favoured in the 3-fold hollow site. The most stable surface species are dissociated hydrogen and C_sH (where s denotes surface species) for the (001) and (110) surfaces which have carbon atoms within the surface. At high coverage on the (001) surface, C_sH_3 was also found to be favoured on a 3-fold site. This is in contrast to the tetravalence rule suggested by Zheng *et al*. (1988) for the binding of the simplest hydrocarbon fragment on the (111) surface of transition metals to complete their tetravalence, e.g., C_sH_3 at on-top, C_sH_2 at bridge and C_sH at 3-fold sites. Finally, DFT calculations of synthesis gas adsorption on Fe_5C_2(001), (110) and (100) were performed to identify stable intermediates during Fischer-Tropsch synthesis (Cao *et al*., 2005b). Dissociated hydrogen and adsorbed CO was found in 2-, 3- and 4-fold sites on the (001) and (110) surfaces, along with C_sH, C_sCO, C_sHCO, C_sH_2CO and $C_sC_2O_2$. On the (100) surface which has only iron atoms on the surface layer, dissociated hydrogen and CO is preferentially adsorbed in on-top and 2-fold configurations.

The hydrogenation of an adsorbed ketene molecule (formed by CO-insertion) was also studied on Fe_5C_2(001) (Cao *et al*., 2007). It was found that this would preferentially proceed *via* dissociation leading to the formation of hydrocarbons rather than stepwise hydrogenation with the formation of ethanol. The adsorption and reaction of surface carbon species on Fe_5C_2(001) was also investigated (Cao *et al*., 2008). In the absence of hydrogen, a carbon atom was found to adsorb at a 4-fold site when the CO coverage is low. These surface carbons can couple to form clusters, chains and eventually graphitic carbon. The presence of hydrogen is reported to inhibit the coupling of carbon atoms. The most stable adsorbed sites for CH_x (x = 1-3) fragments is 4-fold for CH and CH_2, while a 2-fold site is stable for CH_3. The CH and CH_3 are found to be the most stable species.

1.3 Catalyst Deactivation

In heterogeneous catalysis, one of the major problems associated with the operation is loss of activity and/or selectivity with time on stream, *i.e.* deactivation and degradation. This process occurs simultaneously with the main reaction and is both of chemical and physical nature (Bartholomew, 2001). Time scales for catalyst deactivation vary considerably, but it is inevitable that all catalysts will decay. Although catalyst deactivation is unavoidable, some immediate consequences can be postponed or even avoided. The extent and rate of deactivation therefore greatly impacts the design and operation of commercial processes. It is therefore important to understand the deactivation mechanisms. This understanding would provide a foundation for designing stable catalysts and optimising processes to slow catalyst deactivation.

Deactivation can occur by several routes (Forzatti and Lietti, 1999; Bartholomew, 2001) namely poisoning, fouling, thermal degradation or sintering, solid-solid transformations and mechanical deactivation or attrition. Poisoning is the loss of activity due to the strong chemisorption of impurities in the feed stream on the active sites. Fouling is the physical deposition of species from the fluid phase onto the catalyst surface and in catalyst pores. Sintering refers to the loss of active surface *via* structural modification of the catalyst. This is generally a thermally activated process and is physical in nature. Solid state transformation is the process of deactivation that can be viewed as an extreme form of sintering occurring at high temperatures and leading to the transformation of one crystalline phase into a different one. Mechanical deactivation of a catalyst can also occur, especially in fluidised-bed reactors in which case the fines can be carried away with the product flow (Moulijn *et al*., 2001).

Coking refers to the active surface being covered by carbonaceous residues (usually referred to as coke or carbon). This occurs as a side reaction for

catalytic reactions involving hydrocarbon or even carbon monoxide and carbon dioxide. Usually a distinction is made between coke and carbon, although the difference is rather arbitrary. Carbon is considered the product of CO disproportionation, where coke refers to the material originating from decomposition or condensation of hydrocarbons (Forzatti and Lietti, 1999). Carbonaceous deposits are not necessarily harmful (Menon, 1990). The deactivating influence of coke in coke insensitive reactions depends on the location of the coke in terms of blocking active sites and the nature, structure and morphology of coke that is formed. The amount of coke deposited only becomes important in coke-sensitive catalytic reactions. Coke can even be beneficial in some cases (Menon, 1990). A few examples include the ability of coke to avoid excessive hydrogenolysis which leads to a run-away exothermic reaction in catalytic reforming and the ability of coke to stabilise defects on a silver surface, where CO oxidation was found to depend on the number of defects of the silver particles (Meima *et al*., 1987).

1.3.1 Catalyst Deactivation in the Fischer-Tropsch Process

There are several factors involved in the decay of FT catalysts. These include the presence of high molecular weight waxes resulting in diffusion restrictions, poisoning by H_2S and other sulphur-containing compounds in the feed gas, transformation of the active phase, hydrothermal sintering and coke or carbon deposition (Dry, 2004). These factors contribute differently to deactivation depending on the temperature at which FTS is performed. The emphasis of the literature reviewed in this section will be on carbon deposition.

1.3.1.1 Carbon deposition

A principal cause of iron Fischer-Tropsch catalyst deactivation is believed to be the transformation of either active surface carbon species resulting from CO dissociation or active iron carbide phases to inactive carbon and/or carbide forms (Krebs *et al*., 1979; Dwyer and Hardenbergh., 1984; Pijolat *et al*., 1987; Galuszka *et al*., 1992; Jung and Thomson, 1992, Bukur *et al*., 1995b; Eliason and Bartholomew, 1999; Prasad *et al*., 2008; Loaiza-Gil *et al*.,

1999; de la Peña O'Shea *et al*., 2007). In the high temperature operation carbon is deposited at a fairly constant rate (Steynberg, 2004).

There are three main models that are used to describe iron catalysts during FTS and their time-dependent behaviour. These models, first distinguished by Niemantsverdriet and van der Kraan (1981) are referred to as the carbide model, the competition model and the slow activation model. These three models all ascribe deactivation to the deposition of carbon on the catalysts. In the carbide model, the active phase is considered to be bulk iron carbide with active surface sites. Bulk carbide plays an important role in controlling the number of active sites on the surface. Metallic iron is considered inactive for FTS. The competition model appoints surface iron atoms as the active species. This model assumes that surface carbide is a common precursor for bulk carburisation, FTS and formation of inactive surface carbon. Dissociation of CO is considered to be the rate-determining step. The slow activation model assumes that CO dissociation is very fast. Sufficient carbon is therefore available on the surface for both hydrocarbon synthesis and bulk carburisation. Hydrogenation is believed to occur at a surface complex consisting of a certain configuration of iron, carbon and hydrogen. The activity of FTS is initially slow since these complexes are formed at a low rate.

Carbon deposition is generally believed to occur by CO disproportionation *via* the Boudouard reaction:

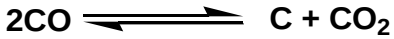

The following elementary steps can be used to describe carbon formation (Tavares *et al*., 1994)

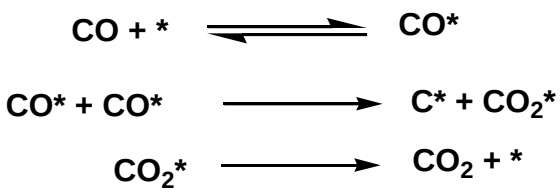

Nolan *et al*. (1998) proposed a reaction scheme for carbon incorporation involving two different types of active site

$$CO + * + \$ \rightleftharpoons C\$ + O*$$

$$CO + O* \rightleftharpoons CO_2 + *$$

$$C\$ \rightleftharpoons \underline{C} + \$$$

where * and $ designate the two types of sites and C represents carbon in solid solution with the catalyst metal.

This reaction can be altered to account for the presence of hydrogen as in the Fischer-Tropsch reaction:

$$CO + H_2 \rightleftharpoons C + H_2O$$

Different kinds of carbon-containing species have been reported to form during Fischer-Tropsch synthesis following pre-treatment by H_2, CO and syngas *i.e.* atomic carbon, polymeric surface carbons, two different iron carbides ($Fe_{2.2}C$ and $Fe_{2.5}C$), ordered and disordered graphitic carbon (Xu & Bartholomew, 2005). However, the operation conditions in the study by Herranz *et al*. (2006) more closely match those of industrial conditions, and subsequently yield different iron carbide phases. Herranz and co-workers therefore adapted the route (Figure 1.3) proposed by Xu and Bartholomew for the formation of these carbonaceous species following pre-treatment:

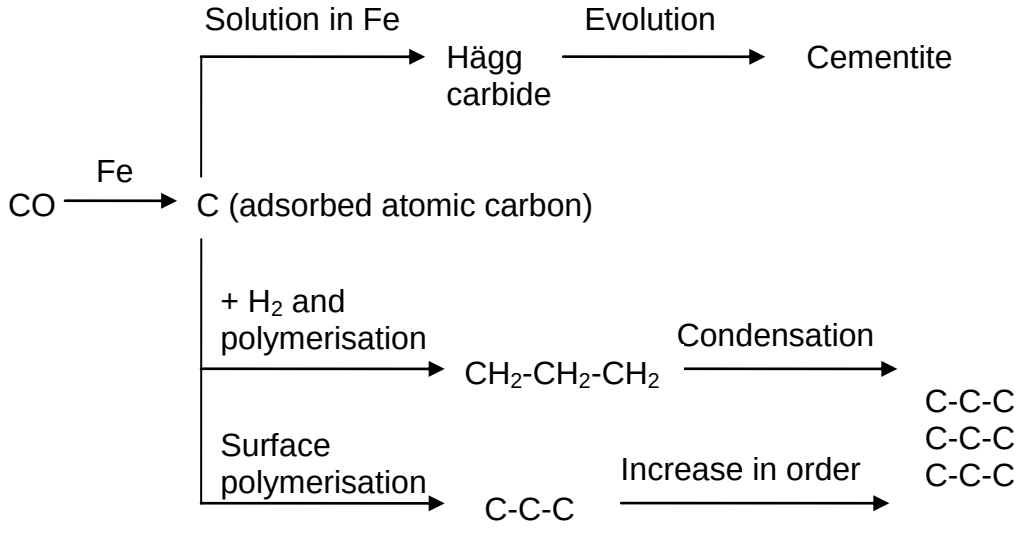

Figure 1-3: Routes of formation of carbonaceous species after pre-treatments in CO and syngas (redrawn from Herranz et al., 2006)

Niemantsverdriet *et al*. (1980) studied the behaviour of metallic iron catalysts during the Fischer-Tropsch synthesis. Using X-ray diffraction and Mössbauer spectroscopy they found four iron carbide phases (θ-Fe_3C, χ-Fe_5C_2, ε'-$Fe_{2.2}C$ and Fe_xC) but from the calculation on the basis of iron carbide structures, significantly more carbon than expected was found after 6.5 h reaction time. It was also observed that the catalyst started to deactivate in this time frame, which led to the conclusion that excessive amounts of inactive carbon was the main cause of catalyst deactivation.

Ott and co-workers (1980) investigated the rate of carbon deposition on catalyst composition over Fe-Ru alloys. It was reported that the pure Ru and Ru doped with 3% Fe showed no carbon build-up and therefore exhibit steady activity and selectivity with time on-stream. Increasing the Fe content, however, resulted in carbon being incorporated into the bulk Fe followed by a carbon overlayer being deposited which reduces the specific activity.

Carbon deposition as the cause for the deactivation of FT catalysts is not universally accepted. In an investigation of the Fischer-Tropsch activity on a promoted iron catalyst using H_2/CO and H_2/CO_2 gases, Riedel and co-workers (2003) monitored the amount of carbon on the catalyst as a function of time on-stream by atomic absorption spectroscopy. The activity did not decline even though the resulting carbon build-up decreased the surface area and pore volume of the catalyst. They also reported the consumption of α-Fe and the respective formation of Fe_5C_2 (measured by Mössbauer spectroscopy) coinciding with the onset of Fischer-Tropsch activity. This led to the conclusion that α-Fe is not active as a Fischer-Tropsch catalyst. The lack of deactivation was explained by the active species remaining on the surface of the catalyst. X-ray photoelectron spectroscopy showed that the atomic surface ratio of K to Fe increases when the activity increases, indicating a migration of K from the bulk of the catalyst to the surface. This migration of K was also reported by Prasad and co-workers (2008) on an iron-based catalyst

used for carbon dioxide hydrogenation. XPS measurements revealed that the active K promoter compound is not covered by the deposited carbon but rather sits on top of the carbon layer in a study of FTS on iron foils (Bonzel & Krebs, 1981). Sommen and co-workers (1985) also reported that although carbon filaments were formed in their investigation, the active iron crystallite stayed on the surface due to carbon deposition starting at the interface of the iron crystallites and the carbon support and thereby lifting the crystallite from the surface.

1.3.1.1.1 Factors that influence the rate of carbon deposition

Previous studies have shown that the rate and mechanism involved in carbon deposition depend on the reaction conditions namely temperature, reactant partial pressures and the catalyst itself (Steynberg, 2004). The reaction steps become considerably more complicated when hydrogen is included, since certain hydrocarbon intermediates also play a role (Nolan *et al*., 1998).

The influence of promoter on FTS and ultimately also the rate of formation of free carbon in Fischer-Tropsch synthesis was studied by Dry *et al*. (1970a). The authors consider the influence of Lewis basic (electron donating) promoters on the rate of the Boudouard reaction. It was found that the addition of basic promoters such as Na_2O and K_2O led to an increase in the rate of carbon formation. The more basic K had a higher promotional effect on FTS and carbon formation. This correlation between potassium promotion and the deactivation of catalysts by blocking of the active sites due to an increase in deposited carbon was established by various researchers (Kölbel *et al*., 1951; Anderson *et al*., 1952; Dry, 1981; Bonzel & Krebs, 1981; Arakawa & Bell, 1983; Bukur *et al*., 1990). It was found by Dry *et al.* that structural promoters (SiO_2, Al_2O_3 and CaO) had no significant effect on the intrinsic rate of carbon formation, although the most basic CaO showed a slightly higher rate. Combining the basic promoters with structural promoters it was found that the total electron donating potential of the basic promoters was reduced leading to reduced carbon deposition rates per unit iron area.

In the next paper in the series (Dry *et al*., 1970b) the authors investigated the effect of temperature and of gases and vapours present during Fischer-Tropsch synthesis on the formation of carbon. A ten-fold difference in the rate of carbon deposition was reported between 285 and 338 °C. There was a slight increase in the rate of free carbon formation with water vapour, hydrogen and oxygenates, but this increase was not related to the amount of each of the gases added.

The rationalisation for all these gases having a similar influence on the rate of carbon deposition was that water, aliphatic acids, alcohols and ketones decomposed to form molecular hydrogen. The role of this hydrogen was to enhance the CO adsorption by reduction of iron carbide to metallic iron. Alternatively, the hydrogen acts as an electron donor which would enhance the metal to carbon bond and weaken the carbon to oxygen bond in adsorbed CO.

The rate of carbon deposition was later found to be proportional to the value of $P_{CO}/(P_{H2})^2$ present in the feed (Dry, 1981). This relation is significant since an increase in the operating pressure which is accompanied by a higher hydrocarbon production rate would result in a decrease in the rate of carbon deposition.

Krebs *et al*. (1979) studied the hydrogenation of CO over iron foils. It was found that the hydrogenation activity of the iron foil decreased faster at higher temperature and higher $CO:H_2$ ratios. By Auger Electron Spectroscopy (AES) and X-ray Photo-electron Spectroscopy (XPS) it was found that there were two forms of carbon, namely carbidic and graphitic carbon that could be distinguished on the surface of the foils. The formation of the carbidic carbon layer is believed to result in an increase in the rate of CO hydrogenation, while the production of graphitic carbon coincided with a decrease in activity; therefore deactivation was attributed to the growth of carbonaceous over-layers.

The hydrogenation of CO and CO_2 over iron foils was investigated by Dwyer and Somorjai (1978). Since the iron surface is active after being covered by a near monolayer quantity of carbon, the iron carbide phase is initially postulated to be the active phase. This surface is assumed to compete for hydrogenation of the surface carbide and catalysed reduction of CO to produce multilayers of carbon which poison the active surface within 4 hours. Increased partial pressures of H_2O and CO_2 do not inhibit carbon deposition, which lead to the interpretation that a few iron sites are extremely active in this reaction. It was later noted by Dwyer and Hardenbergh (1984) that there is a difference between the deactivation rates on iron foils and precipitated Fischer-Tropsch catalysts. These researchers found that powders were less susceptible to the formation of graphitic carbon, although these materials were eventually poisoned by graphite at temperatures above 275 °C.

Bukur *et al*. (1995c) studied the effects of pre-treatment on a precipitated iron catalyst promoted with Cu and K, which was tested in a fixed-bed reactor. The catalysts pre-treated with H_2 were transformed to metallic iron (α-Fe) or mixtures of α-Fe and Fe_3O_4, while CO and syngas pre-treated catalysts were found to form mostly Hägg carbide. The H_2 pre-treated catalyst showed no deactivation even at very long times on stream and was explained by the higher surface concentration of hydrogen that somehow stabilised the activity of the catalyst with the disadvantage of producing lighter hydrocarbon products. The CO and syngas pre-treated catalysts were found to deactivate with time on stream, and in this study it was attributed to the conversion of Hägg carbide to less active oxide phases as well as the build-up of inactive carbonaceous species on the catalyst surface. The influence of the pre-treatment method on FTS and deactivation rates therefore seems to be important. It was found by Reymond and co-workers (1982), in a study of reduced and unreduced Fe_2O_3 during reaction with H_2 and CO that inactive carbon led to deactivation. Pre-reduced catalyst was found to be more susceptible to deactivation.

Shroff *et al*. (1995) investigated the effect of various activation and reaction treatments on the resulting phase transformation in a precipitated FT catalyst. It was observed that when the catalysts are exposed to FT conditions, transformation to the carbide phase occurs. The activation process only determines the rate of this transformation. Magnetite transforms into smaller crystallites of iron carbide. Furthermore, the deposition of carbon on the surface of the carbide causes separation of these crystallites from each other and is also responsible for deactivation by physical covering of the active sites on the catalysts.

1.3.1.2 Inter-conversion of carbides as a cause of deactivation

This section discusses the inter-conversion of iron carbide phases as the main mechanism of deactivation. The importance of inter-conversion in this regard is that free carbon is formed in the decomposition of carbides. Interestingly, both decomposition of the iron carbides (Eliason & Bartholomew, 1999; Jung and Thomson, 1992; Mansker *et al*., 1999) and carbon uptake (Pijolat *et al*., 1987) have been reported as responsible for deactivation. In an investigation on the carburisation of pure iron samples at 500 °C in CO-H_2-H_2O-H_2S gas mixtures, Schneider and co-workers (2000) reported the formation of Fe_3C and Fe_5C_2. Both carbides decomposed to iron and graphite in this study. This decomposition leads to disintegration of the carbide layer into particles, which are preserved in a coke matrix.

Pijolat *et al*. (1987) studied the deactivation of a Fe/Al_2O_3 catalyst. In addition to deactivation by coverage of the metallic surface with graphitic layers within the first few minutes of reaction, these authors propose the progressive uptake of C in $Fe_{2+x}C$ (decreasing x) as a contributing factor at longer times on-stream. They used results obtained by Mössbauer spectroscopy to show that the catalyst activity for FTS scaled linearly to the stoichiometry of the $Fe_{2+x}C$ phase present.

Active CO hydrogenation catalysts exhibit high reactivity for CO dissociation, the initial step in the synthesis of hydrocarbons from synthesis gas (Eliason & Bartholomew, 1999). This surface carbon can then either react, or remain on the surface and eventually form inactive deposits. Eliason and Bartholomew proposed that in addition to the formation of graphitic carbon, catalysts deactivate by the conversion of carbon-rich $Fe_{2.2}C$ to Fe_5C_2 and finally to Fe_3C. However, no evidence is presented to support this hypothesis. Interestingly, it is also reported that carbon deposition occurs more slowly on a potassium-promoted catalyst.

Jung and Thomson (1992) proposed the deactivation of iron catalysts for FTS to be a result of the transformation of $Fe_{2.2}C$ to Fe_5C_2. In addition, the workers state that the carbon resulting from this decomposition of $Fe_{2.2}C$ can act as nucleation sites which lead to build-up of inactive carbon which blocks the active sites.

1.4 Carbonaceous Species in HTFT

Fischer-Tropsch synthesis is thought to occur *via* CO dissociation which leads to the formation of surface carbon (Claeys & van Steen, 2004). This surface carbon can be hydrogenated in the formation of product molecules. Alternatively, the surface carbon can recombine to form carbon clusters yielding a stable graphene layer on metal surfaces (Kalibaeva *et al*., 2006). Finally, surface carbon can also diffuse into the metal lattice which leads to the formation of carbides or carbon enrichment of existing carbides.

Matsumoto and Bennett (1978), in an investigation of Fischer-Tropsch synthesis over a fused iron catalyst, reported that methanation and carburization occur *via* the same reaction intermediate, namely a C^* moiety. It was found that the bulk catalyst after reaction was Hägg carbide (Fe_2C). The total carbon as calculated from the CO consumption was reported to increase almost linearly with an increase in the duration of exposure to CO.

The following sections therefore discuss the formation of possible carbonaceous material.

1.4.1 Graphene

The occurrence of graphite-like carbonaceous deposits is commonly proposed in FTS systems. Graphene consists of a single layer of sp^2-hybridised carbon atoms densely packed into a benzene-ring structure. It is the basic building block of graphite, nanotubes and fullerenes. In graphite, each carbon atom is covalently bonded to three other surrounding carbon atoms (Allen, 2010). The formation of graphene has been investigated by DFT studies. A theoretical study of graphene formation on a fcc-Co(111) surface was performed by Swart and co-workers (2008), since this was proposed as a possible intermediate in the formation of carbonaceous deposits on cobalt-based Fischer-Tropsch catalysts. DFT calculations indicate that carbon clusters (specifically linear) tend to be more stable than atomic carbon species. Ring structures can also be formed, but pronounced stabilisation is only observed with an infinite aromatic ring structure. Larger aromatic structures are significantly more stable than linear clusters, with graphene the most stable of all the structures. In terms of surface coverage, island formation was found to be more favourable than an even distribution. In a later investigation (Swart *et al*., 2009) it was reported that the energy barrier for a graphene layer sliding is lower than lifting off the surface. In addition, it was found that these fcc-Co(111) surfaces reconstruct when carbon is adsorbed (Ciobîcă *et al*., 2008).

Carbon clustering on a Ni(111) surface was investigated by *ab initio* simulation (Kalibaeva *et al*., 2006). This surface was found to be stable when it was either clean or fully covered by carbon in a graphitic form. This graphitic carbon is reported to be in the 'on-top' configuration. Carbon clusters are more stable than dispersed carbon. In a later study by Wang *et al*. (2007), the thermodynamic stability of a graphite monolayer on Ni was also reported. The stability is in the order of: graphitic monolayer > C in bulk > carbon chain >

small cluster > atomic carbon. These authors, however, found that the carbon preferentially adsorbs on a 3-fold hollow site.

In a study of carbon deposition and hydrocarbon formation on various group VIII metal catalysts, the mobility of carbon from subsurface sites is found to be similar to carbon diffusion in the catalyst metal, since similar activation energies were obtained for carbon filament growth and carbon diffusion (Nolan *et al*., 1998). In terms of Fischer-Tropsch synthesis, carbon and hydrogen dissolve in the typical catalyst metals and this dissolved hydrogen is believed to control the branching of products in higher hydrocarbons. The deposition of carbon can only occur once it has dissolved in the catalyst metal. Surface vinyl species that are intermediates in the Fischer-Tropsch synthesis may polymerise to form graphene (Nolan *et al*., 1998).

Graphitic carbons formed in the absence of hydrogen, were observed on a Fe(100) surface (Panzner & Diekmann, 1985). Graphitic and chemisorbed carbon was observed simultaneously. The graphite is reported to form multilayer islands on the iron surface, with the chemisorbed carbon arranged in the space between these islands.

1.4.2 Carbon Filaments

Carbon filaments are often formed in hydrogen-rich environments under HTFT conditions. Sommen and co-workers (1985) investigated the conversion of syngas into C_2 and C_3 olefins on carbon-supported Fe catalyst. Thermogravimetric studies revealed the deposition of carbon exceeding that of carbide formation and surface monolayers. TEM showed that carbon filaments were formed with an iron crystallite on top, due to carbon deposition starting at the interface of the iron crystallites and the carbon support and thereby lifting the crystallite from the surface.

Ando and Kimura (1989) investigated the effect of hydrogen partial pressures on carbon deposition on iron. An 80%CO-20%H_2 gas mixture at 650 °C

produced the highest amount of carbon, and although both laminar and filamentous carbon was observed after completion of the deposition it was the relative amount of filamentous carbon that was greatly increased in the presence of hydrogen. The iron substrate formed Fe_3C due to the high temperatures at which the reaction was performed, and the authors reported local breakage of the iron surface. Laminar carbon is postulated to nucleate on the surface and grow by surface carbon atoms, while filaments grow by catalytic action of iron particles moving into the laminar carbon by repetitive formation and decomposition of Fe_3C.

Carbon whiskers have been reported on nickel-based reforming catalysts (Dias & Assaf, 2004; Gould *et al*., 2008; Trimm, 1999). Trimm (1999) proposes that the growth of carbon whiskers occurs by dissolution of adsorbed carbon in the nickel lattice, initially forming nickel carbide. This carbon diffuses through the metal particle to a grain boundary. The carbon therefore precipitates out and lifts the nickel particle at the tip of a growing whisker.

A three-step carbide cycle is also proposed as an alternative mechanism (Dias & Assaf, 2004). The first step is the formation of a carbon monolayer followed by the formation of a graphitic carbon by polymerisation of the carbon atoms. The third step occurs as a result of a carbon concentration gradient between the top of the surface and the bottom of the particle. This leads to carbon diffusion across the crystal and eventually the growth of a carbon whisker.

This type of mechanism is further explained by Grabke *et al*. (2001) as the growth of graphite into the carbide because the graphite nucleates on the metal carbide sites and then grows vertically into the carbide. This is due to the iron atom at the interface moving outward through the graphite flakes. This process occurs on metals which dissolve carbon and do not form stable carbides and therefore become oversaturated, forming graphite (Grabke *et al*., 2001).

Carbon deposition can occur in the form of either carbon filaments or graphite. In the catalytic disproportionation of CO it was found that a lamellar form of graphite forms on the surface of a catalyst particle, while when hydrogen is present the deposition of carbon occurs by the growth of filaments (Nolan *et al*., 1994). It is proposed that this growth of graphitic carbon occurs on the outside of the particle and the number of graphene layers that can form depends on the metal used in the reaction.

Hydrogen and sulphur apparently have similar effects during carbon deposition, namely that the ensembles required in the formation of a graphene layer by a network of carbon atoms on the surface of the catalyst, is hindered by the presence of other elements adsorbed on the surface. The effect of sulphur adsorption on a cobalt catalyst used to catalyse the decomposition of ethylene was studied by Kim and co-workers (1993). The sulphur pre-treatment of the metal was found to dramatically increase the weight percentage of carbon filaments produced during reaction. The carbon filaments produced also became less graphitic with the addition of sulphur to the system. Similarly, it was stated that the nucleation of graphitic carbon on an iron catalyst needs an ensemble of several sites and that the presence of even less than a monolayer of sulphur can disturb the occurrence of an ensemble (Grabke *et al*., 2001).

1.5 Aim and Objectives

The aim of this thesis is to investigate the carbonaceous deposits on a spent HTFT catalyst in order to understand the mechanism of this detrimental build-up. This work is focused on *ex-situ* studies of as-received samples from the SAS, Pilot Plant and Berty reactors.

The general objectives are:

- To investigate the composition of the spent catalyst and also the general structure of these particles. This can give insight into the deactivation process.
- Developing a method to determine the chemical nature and structure of the carbonaceous species. This information can be used to reduce deactivation in future optimisations of the HTFT process.
- Examining the evolution of the catalyst with time on-stream. This will enable us to monitor chemical and physical properties as a function of progressive carbon build-up.

1.6 Outline of the Thesis

The effects of carbon deposition on composition and chemical and physical properties of HTFT catalysts can be helpful in obtaining an understanding of the mechanisms responsible for the loss in productivity with time on-stream. This knowledge might aid in the future design of novel catalysts with extended lifetimes. This work is focused on determining the composition and structure of used HTFT catalysts and in this way obtain an appreciation of how this catalyst evolves over time. The complex chemical structure of the iron-based catalysts and the fact that the active sites are created *in-situ* complicates interpretation of the effect of carbon on the catalyst. The main reason for this complication is that the bulk of the catalyst does not necessarily reflect what the active surface species is comprised of. There have been many proposed mechanisms for catalyst deactivation but this is clearly a multifaceted process that probably involves all these mechanisms to some extent.

Chapter 3 shows the complications involved in studying the spent catalyst obtained from the SAS reactor. Temperature Programmed Oxidation (TPO) in conjunction with XRD and Raman Spectroscopy was employed in the determination of the composition of the catalyst as well as providing a way to simplify the characterisation by selectively fractionating the constituents of the catalyst. Studying the catalysts obtained from a Pilot Plant reactor proved to

be helpful in interpretation. The structure of the catalyst was also determined by Raman mapping and other imaging techniques.

Chapter 4 demonstrates the development of MALDI-TOF MS in the investigation of several carbonaceous deposits. The application of this technique to the species typically deposited on spent HTFT catalyst can provide an additional method to determine the mass distributions of the carbonaceous deposits. High Resolution Transmission Electron Microscopy (HRTEM) and Raman Spectroscopy are also employed to determine the chemical nature of the deposits.

Chapter 5 draws together the techniques developed in Chapters 3 and 4 for the investigation of spent HTFT catalysts obtained from a laboratory-scale Berty reactor. Although this reactor fails at mimicking the SAS reactor, studying these catalysts is invaluable in gaining insight into how the catalyst composition changes with time on-stream. The Berty experiments allow for determination of the mechanism and the rate of carbon formation. Evolution of the catalysts in terms of chemical and physical properties is also demonstrated in this work.

2.EXPERIMENTAL

In the field of catalysis, characterisation is one of the key disciplines. Through characterisation the composition, morphology and structure of a typical catalyst can be determined. In the case of spent catalyst, the importance of characterisation is more prominent, since the usual activity and selectivity measurements to determine catalyst performance is not available. The use of several imaging and spectroscopic techniques provided a great deal of structural and chemical information, respectively. Physical properties of the catalyst particles also constituted a crucial aspect of this investigation. The introduction of MALDI-TOF MS analysis to the deposits on spent catalyst required a great deal of development, and proved to be a valuable tool in understanding the nature of carbonaceous deposits.

This chapter details the materials used throughout the investigation. In the case of the spent catalyst, these were not prepared in-house but were received from various sources within Sasol. The methods of preparing these samples for analysis are also presented here. Finally, the various techniques employed are introduced briefly and exact descriptions of the instrumentation and methodologies are portrayed.

2.1 Solvents and Chemicals

The solvents were supplied by Fischer Scientific (UK) and were used without further purification. All chemicals used as matrices were from Fluka (UK). All the gases used in the experiments were supplied by BOC (UK).

2.2 Fresh catalyst

The fresh catalyst is a fused iron oxide catalyst which is similar to the ammonia synthesis catalyst. There is an inhomogeneous distribution of promoter elements within particles of different size, which originates from the sample preparation method. The molten iron and promoter-rich silicate phase is cast into ingots for cooling. This silicate phase does not form a solid

solution with the iron oxide phase, resulting in this material being forced towards the grain boundaries between the iron oxide crystallites when it solidifies. Since the rate of cooling is higher at the edges of the ingots, the particles formed in these cooler parts are smaller, whereas the particles formed in the slower-cooling region would typically be larger and consist of several grains. Subsequent crushing and grinding of the fused catalyst therefore leads to breakage occurring preferentially along these grain boundaries. The higher promoter levels of the smaller particles are associated with greater surface area. Several particle size fractions of the spent catalyst were sieved by Johan Labuschagne (Sasol R&D, Sasolburg, South Africa) using Madison Test Sieves placed on a Fritsch Analysette 3 PRO vibrating plate. The particle sizes were as follows: <45 μm, 45-75 μm, 75-150 μm and >150 μm. The iron content of these particles as a function of particle size is indicated in Table 2.1 below, while the potassium contents are reported in arbitrary units normalised to the >150 μm fraction. The other structural and chemical promoters have been omitted from this thesis due to Intellectual Property (IP) restrictions.

Table 2-1: Chemical composition of Fused Fe catalyst

	Total Fe (%)	K
>150 μm Fused	71.1	1.0
75-150 μm Fused	70.7	1.4
45-75 μm Fused	71.0	1.2
<45 μm Fused	70.8	2.0

2.3 Spent Cat-1

The catalyst samples used were equilibrium catalysts i.e. not all of the particles have experienced the same length of time on-stream, obtained from the Sasol Advanced Synthol (SAS) Fluidised-Bed Reactor located at Secunda, South Africa. These catalyst particles are a mixture of catalyst particles that have been exposed to Fischer-Tropsch conditions for different periods of time. The catalyst removal takes place under normal HTFT conditions and the catalysts are immediately exposed to air. The composition of these catalyst particles as a function of particle size is given in Table 2.2.

Total Fe and C are expressed as percentage values, while the potassium contents are given in arbitrary units normalised to the >150 µm fraction.

Table 2-2: Chemical composition of Spent Cat-1 fractions

	Total Fe (%)	Total C (%)	K
>150 µm	67.5	6.8	1.0
75-150 µm	65.8	9.5	1.0
45-75 µm	63.5	14.9	1.2
<45 µm	57.8	23.9	2.1

2.4 Spent Cat-2

One of the major problems associated with understanding carbon build-up on the SAS catalyst is that it is an equilibrium catalyst. Therefore the composition of the Synthol catalyst following Fischer-Tropsch Synthesis (FTS) on a Pilot Plant system was studied, where all catalyst particles have experienced the same exposure to synthesis gas. It is worth noting, however, that since the flow regime is different within the Pilot Plant reactor compared to the SAS reactor, a direct comparison between the two recovered catalysts is not possible. The fused catalyst was exposed to Fischer-Tropsch conditions within the Pilot Plant reactor. The duration of this exposure to syngas under reaction was 5 days. These catalytic materials were cooled in-situ under a flow of an inert gas. Once the catalyst had cooled down to room temperature, the particles were removed from the reactor.

2.5 Spent Cat-3

The fused catalyst was exposed to FTS conditions for different periods of time in a Berty micro-reactor. In a Berty micro-reactor there are no restrictions on the initial particle size distribution since the catalyst bed is fixed. Therefore, a narrow fraction of particle sizes was used in the tests. The fused catalyst was further sieved and only the 45-75 µm fraction was used for FTS in the laboratory scale Berty micro-reactor. Five reactor runs were carried out by Kim Easton (Sasol R&D, Sasolburg, South Africa) and the duration of the runs was 1, 3, 9, 15 and 25 days. These Spent Cat-3 samples can be distinguished by the number of days in parenthesis, e.g. Spent Cat-3(1) is the catalyst

recovered from the Berty reactor after 1 day on-line. Cooling of the samples was performed under an inert atmosphere and subsequently poured out into a container with dry ice. The compositions of the catalysts as a function of time on-stream are given in Table 2.3.

Table 2-3: Chemical composition of Spent Cat-3 catalysts

	Total Fe (%)	Total C (%)
Spent Cat-3(1)	69.6	6.8
Spent Cat3(3)	70.0	10.1
Spent Cat-3(9)	66.3	12.2
Spent Cat-3(15)	61.1	14.6
Spent Cat-3(25)	62.7	17.9

2.6 Oxidation experiments

Oxidation experiments were performed in a sample boat sitting in a long quartz tube, which was placed in a horizontal tube furnace (Lenton Thermal Designs). Temperature was controlled by a K-type thermocouple placed in the porcelain heating cylinder within the surrounding furnace. The holding time was found empirically to ensure that all of the species associated with a certain oxidation peak in the Temperature Programmed Oxidation (TPO) profile was removed. The heating rate was 10 °C/min. The first oxidation was performed by heating up to 340 °C, where it was kept for 4 hrs. The second oxidation was carried out at 450 °C for 1 hr. The final oxidation was at 800 °C and held at that temperature for 1 hr. The gas used was air, and the flow rate was maintained at about 50 mL/min. Cooling was performed by simply switching off the furnace.

2.7 Surface area and pore volume

Brunauer-Emmett-Teller (BET) is an analysis technique for the measurement of the specific surface area of a material. The concept of the theory extends on the Langmuir theory, which is a theory for monolayer molecular adsorption. In this case multilayer adsorption is described, with the following hypotheses: (a) gas molecules physically adsorb on a solid in layers infinitely; (b) there is

no interaction between each adsorption layer; and (c) the Langmuir theory can be applied to each layer.

Brunauer-Emmett-Teller (BET) surface area and pore volume analysis of the catalysts was performed on a Gemini VI Surface Area and Pore Volume Analyser (Micromeritics, Dunstable UK). Thermal desorption of wax was performed under N_2 flow in a quartz tube placed in a horizontal tube furnace fitted with a Eurotherm temperature controller. The ramp rate was 5 °C/min up to 440 °C where it was kept for 2 hrs. Thermal desorption under reduced pressure was performed in the same way but with reduced pressure applied at both ends of the tube.

2.8 Soxhlet extraction

Soxhlet extraction is a continuous solid/liquid extraction. Soxhlet extraction is only required where the desired compound has a limited solubility in a solvent, and the impurity is insoluble in that solvent. If the desired compound has a significant solubility in a solvent then a simple filtration can be used to separate the compound from the insoluble substance.

Solvent extraction of spent catalyst samples was performed by means of Soxhlet extraction. Xylene or dichloromethane were used as solvents, while a cellulose extraction thimble was used. After extraction for 24 hrs, the solvent was removed by means of a rotary evaporator, yielding the extracted compound. The non-soluble portion of the extracted solid was dried and also kept for analysis.

2.9 Resin fixing

Samples were fixed in Epoxy Resin. This was performed by mixing the Struers EpoFix Resin with the EpoFix Hardener in a 15:2.5 ratio and adding the sample to this. This mixture was poured into a mould to set overnight. This disc was then polished down successively using 600, 800, 1200 and 2500

grinding paper (Buehler Ltd.) followed by a polishing cloth used in conjunction with 6, 3 then 1 µm diamond paste (MetPrep Ltd.).

2.10 Matrix Assisted Laser Desorption/Ionisation-Time of Flight Mass Spectrometry

Matrix Assisted Laser Desorption/Ionisation-Time of Flight Mass Spectrometry (MALDI-TOF MS) is based on a highly laser light absorbing matrix material being mixed with the analyte and allowing the mixture to dry into a crystalline deposit. The analyte is desorbed and ionised as intact gas-phase ions through the excitation of the matrix material by a high intensity laser pulse (Dass, 2007). The ionisation step is illustrated in Figure 4.10 below.

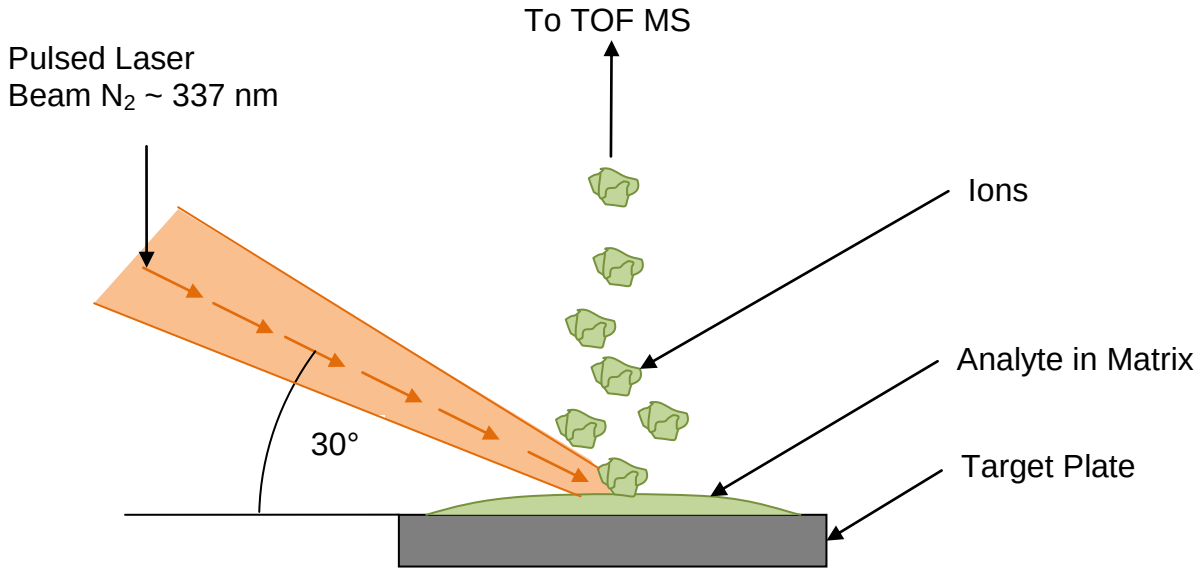

Figure 2-1: MALDI-TOF MS sample ionisation

The ions are then accelerated by a strong electric field and allowed to drift along a flight tube at a velocity related to their mass-to-charge ratios (m/z) before reaching the detector. The instrument discriminates the ions by their time-of-flight, which in turn is related to their m/z (Figure 4.11).

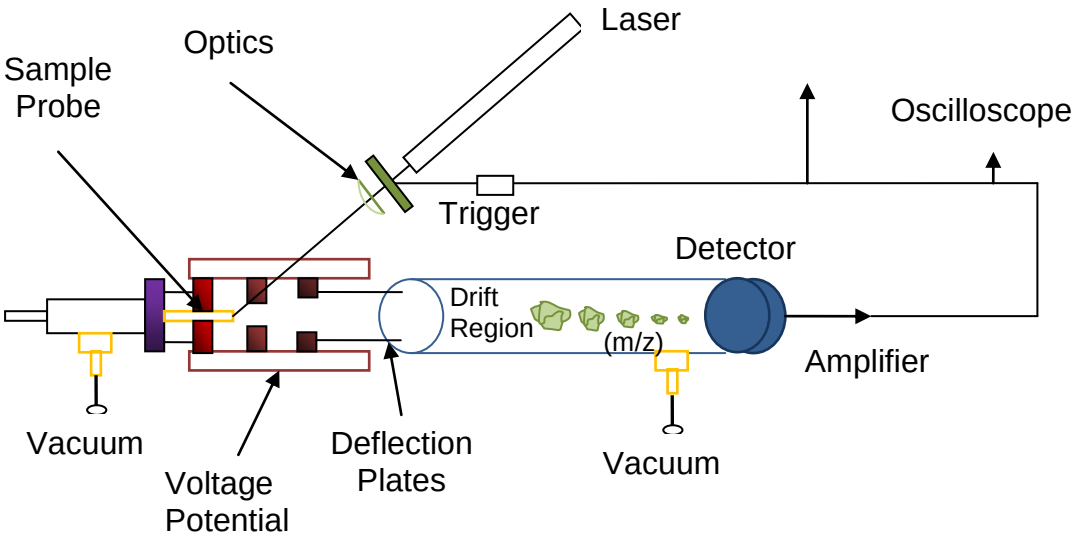

Figure 2-2: Schematic of a MALDI-TOF mass spectrometer

MALDI-TOF MS is considered a soft ionisation technique. Materials which possess limited functionality need a matrix that efficiently absorbs the frequency of laser light. This leads to ionisation and subsequent desorption of the matrix molecules which carry the analyte molecules along into the gas phase with very little or no fragmentation (Karas & Hillenkamp, 1988).

MALDI-TOF MS has been used for the characterisation of a wide range of carbonaceous materials. Materials such as carbonaceous pitches (Edwards *et al.*, 2003; Edwards & Thies, 2005; Domin *et al.*, 1997; Edwards & Thies, 2006; Cervo & Thies, 2007; Cervo *et al.*, 2008; Cristadoro *et al.*, 2009), synthesised insoluble giant polycyclic aromatic hydrocarbons (Przybilla *et al.*, 2000; Simpson *et al.*, 2002; Thomson *et al.*, 2007), carbonaceous deposits on spent zeolite catalysts (Feller et al., 2003a; Cerqueira et al., 2005), diesel particulate matter (Carré *et al.*, 2004), technical waxes (Kühn *et al.*, 1996), paraffins (Pruns *et al.*, 2002), diamond-like or graphitic carbon (Šedo *et al.*, 2006), carbon nano- and microparticles (Gherghel *et al.*, 2002), coal derived liquids (Herod *et al.* 2000; Johnson *et al.*, 1998; Miller *et al.*, 1998), crude oil (Dutta & Harayama, 2001) and soot materials and pyrolysis products (Mathieu *et al.*, 2007; Shukla *et al.*, 2008; Bauer *et al.*, 2007; Fletcher *et al.*, 1998; Dobbins *et al.*, 1995; Dobbins *et al.*, 1998; Apicella *et al.*, 2006; Dobbins *et al.*, 2006; Apicella *et al.*, 2007; Apicella *et al.*, 2004) have been characterised using

MALDI-TOF MS. The significance of these studies is that MALDI-TOF MS was demonstrated for the analysis of solid and slightly-soluble materials.

In the study of mixtures using MALDI-TOF MS it is important to consider different ionisation efficiencies of the various materials. This ionisation technique may also be biased towards smaller molecules within a particular class of species, since these ionise more easily. Factors that play a role in discrimination of high masses includes desorption/ionisation efficiency of the molecules (Domin et al., 1997; Johnson et al., 1998), transmission down the flight tube and the mode of detection (Nielen, 1999). The technique is not quantitative and is known to misrepresent species by the intensity of peaks. It is therefore important to study different standard materials individually in order to understand their behaviour with this ionisation technique.

One of the key issues in traditional MALDI-TOF MS sample preparation is making good mixtures of the analyte and the matrix. It was originally believed that the analyte had to be soluble in a suitable solvent to enable co-crystallisation of the analyte and matrix. Slow crystallisation at room temperature resulted in problems with segregation between sample, cationisation salt and matrix (Nielen, 1999). Improved results were reported (Vorm *et al.*, 1994) by the thin layer method, wherein a matrix layer is prepared first and allowed to crystallise followed by the sample and then dried. Electrospray deposition is reported to be one of the most promising techniques for sample preparation of synthetic polymers since small and evenly-sized co-crystals are formed (Axelsson *et al.*, 1997). Przybilla and co-workers (2000) developed a new method of sample preparation for the analysis of insoluble polycyclic aromatic hydrocarbons (PAHs). The analyte and matrix were mechanically mixed (mortar and pestle grinding) without any solubilisation procedures. This method produced very good mass spectra and is easy to apply to most samples (Skelton *et al*., 2000; Trimpin *et al*., 2001). This is therefore the preparative method of choice in the characterisation of all samples in this study.

The quality of a measured MALDI-TOF MS spectrum also depends strongly on the matrix used in the analysis. The typical matrices used in the characterisation of carbonaceous material include 7,7,8,8-tetracyanoquinodimethane (TCNQ), 1,8,9-anthracenetriol (dithranol), α-cyano-4-hydroxycinnamic acid (HCCA) and 2,5-dihydroxybenzoic acid (DHB). Since the carbonaceous deposits on a spent catalyst comprise a mixture of various types of species, it is important to consider the ionisation efficiency of each species by the different matrices. The determination of the nature of the deposits would be simplified if the different matrices could selectively ionise a particular class of species. In the case of nonpolar matrices and analytes, it has been reported that matrices only ionise the analyte molecule when the ionisation energy of the analyte is lower than the ionisation energy of the matrix (Macha *et al.*, 1999). TCNQ has the advantage that molecules with little or no chemical functionality can be analysed (Przybilla *et al.*, 2000), since the electron accepting properties of the matrix promotes the formation of radical cations. It is therefore a suitable matrix for the characterisation of large hydrogen-deficient molecules such as polycyclic aromatic hydrocarbons. The matrices listed above as well as Ag^+ (in the form of silver nitrate), which is typically used as a cationising agent, were therefore used in the MALDI-TOF MS characterisation of the catalyst recovered from the Pilot Plant and SAS reactors. In the case of Ag^+, ionisation is believed to take place through the formation of adducts (Ehlers *et al.*, 2001). MALDI-TOF MS imposes a major limitation on the analysis of the light hydrocarbons that contribute to molecular growth due to the vacuum experienced by the sample during mass spectrometry (Mathieu *et al.*, 2007). Volatile species can therefore not be detected by this technique.

Mass spectra were recorded using a Micromass Tof Spec 2E equipped with a nitrogen laser operating at 337 nm. An ion extraction voltage of 20kV was used. The flight tube was used in reflectron mode for all the analyses. Only positive ions were examined in this study.

The standard materials and spent catalyst samples were prepared for characterisation by grinding equal volumes of the analyte and matrix (7,7,8,8-tetracyanoquinodimethane (TCNQ), 2,5-dihydroxybenzoic acid (DHB), α-cyano-4-hydroxycinnamic acid (HCCA), 1,8,9-anthracenetriol (dithranol) or $AgNO_3$) together. A small volume of water was then added to the mixture to make slurry, which was then pipetted onto a spot on the target plate. This was then dried in air at room temperature. Once dry, the plate was placed in the instrument for laser ablation.

The laser scanned across the area of the sample and at least 50 spectra were acquired of each material, and in each case the spectrum reported is the average of these individual spectra. This minimises variations in concentration in different regions of the sample due to inhomogeneity. Suppression was not applied to the lower masses in any of the analyses.

2.11 Scanning Electron Microscopy

A scanning electron microscope (SEM) is a type of electron microscope that images a sample by scanning it with a high-energy beam of electrons in a raster scan pattern. The electrons interact with the atoms that make up the sample producing signals that contain information about the sample's surface topography. The most common imaging mode collects low-energy (<50 eV) secondary electrons that are ejected from the k-orbitals of the specimen atoms by inelastic scattering interactions with beam electrons. Due to their low energy, these secondary electrons come from the a depth of only 50 to 500 Å within the sample surface (Skoog *et al*., 1998). Alternatively, when a primary beam of energy hits the sample, electrons can collide with the atoms in the sample and be scattered back. If the sample contains regions with atoms or phases that are heavier than the surroundings, it can be distinguished due to a higher yield of backscattered electrons (Niemantsverdriet, 1993). These backscattered electrons originate deeper in the sample.

Scanning electron microscopy (SEM) images were collected using a JEOL JSM-5600 Scanning Electron Microscope. For imaging the voltage was set to 5 kV with a working distance of 6 mm. An Oxford INCA Energy 200 Electron Dispersion Spectroscopy (EDS) was also used to determine the elemental composition of the various types of particles. In this case the voltage was set to 20 kV with a working distance of 25 mm.

The samples fixed in Epoxy Resin were characterised using a Hitachi S4800 SEM operated between 5 and 20 kV. This instrument was equipped with a backscatter detector which is particularly suited to identifying different phases by the relative intensities observed.

2.12 High Resolution Transmission Electron Microscopy

Transmission Electron Microscopy is an imaging technique whereby a beam of electrons is focused onto a specimen causing an enlarged version to appear on a fluorescent screen or layer of photographic film. Transmission of the electron beam without losing energy occurs in samples depending on thickness and density (Niemantsverdriet, 1993). This technique is used to determine the morphology of the catalyst particles, as well as an estimate of the crystallite size. The d-spacings measured in the high resolution mode can be used to determine the nature (phase) of the species.

Characterisation by High Resolution Transmission Electron Microscopy (HRTEM) was performed on a JEOL JEM-2011 operated at 200 kV by Ross Blackley (School of Chemistry, University of St Andrews). The samples were dispersed using ethanol and allowing this slurry to dry on a carbon coated copper grid.

2.13 Temperature Programmed Oxidation

In temperature programmed reaction methods, a chemical reaction is monitored continuously with a linear increase in the temperature. This technique is easily applied to most catalysts and qualitative interpretation is

rather straightforward (Niemantsverdriet, 1993). The catalyst is typically placed within the reactor and heated while the thermal conductivity detector (TCD) measures the gas content before and after the reaction. It is known that various species will undergo oxidation at different temperatures. The onset of this oxidation can also be affected by the ramp rate, and this should be borne in mind when drawing comparisons between studies. TPO has been extensively used to investigate coke or carbonaceous species in different catalytic systems (Spivey & Roberts, 2004). It provides information on the oxidation rate of coke and also the location (Catalysed vs. Non-catalysed) and composition (carbon/hydrogen ratio). In the case of monitoring the oxidation process *via* CO_2, it is essential that complete oxidation occurs. Carbonaceous material can be present in several forms and these could ideally be distinguished using TPO. Galuszka *et al*. (1992) investigated the TPO of carbonaceous species and on iron catalysts. The authors observed at least five different forms of carbonaceous material (aliphatic, aromatic, oxygenated, carbidic and amorphous carbons) deposited on oxide-supported iron FT catalysts. The results generated in this study should provide a useful comparison.

The TPO experiments were carried out in a U-type quartz reactor on a Micromeritics AutoChem2920 (Micromeritics Instrument Corp., USA). The behaviour of the spent catalyst materials were investigated by temperature-programmed experiments including oxidation, reduction and desorption. The samples were heated within a regulated furnace and the temperature was measured by a thermocouple placed 2 mm above the sample. The bottom of the tube was plugged with quartz wool to prevent the sample from going through. The tube was placed into the furnace and gas was allowed to flow through the sample at a flow rate of 50 mL/min. The heating ramp rate was set at 10 °C/min from ambient temperature up to 800 °C. Profiles were generated by measurements which were taken once every 5 seconds using a thermal conductivity detector.

The oxidation experiments were performed using 10% O_2/He, while the reductions were performed with 10% H_2/Ar. The 10% O_2/He was passed through a moisture and hydrocarbons scrubber (manufactured in-house) before entering the system. He gas was used in most desorption and pre-treatment experiments. In all cases the gas flow rates were maintained around 1000 mL(NTP)/(g_{cat}. min). A Thermostar Pfeiffer Vacuum Quadrupole Mass Spectrometer was used to measure changes in the partial pressure of C, CH_3, O_2, H_2O, CO and CO_2 as the samples were heated.

2.14 Raman Spectroscopy

Raman spectroscopy is based on inelastic scattering of photons which lose their energy by exciting vibrations in the sample (Smith & Dent, 2004). Monochromatic light in the visible, near infrared or near ultraviolet range is typically used. The majority of photons undergoes scattering without energy exchange *i.e.* Rayleigh scattering which is very intense compared to Raman scattering. The Raman effect occurs when a molecule is excited to a virtual energy state and then decays to a new vibrational level. The difference in energy between the original state and this new (virtual) state leads to a shift in the emitted photon's frequency away from the excitation wavelength. The scattering occurring in this way results in the Stokes band. Conversely, an anti-Stokes shift takes place when a photon brings a vibrationally excited molecule to the virtual energy state and then decays to the ground state. The anti-Stokes band normally has much lower intensity than the Stokes band (Niemantsverdriet, 1993). These scattering processes are depicted in Figure 2.3 below.

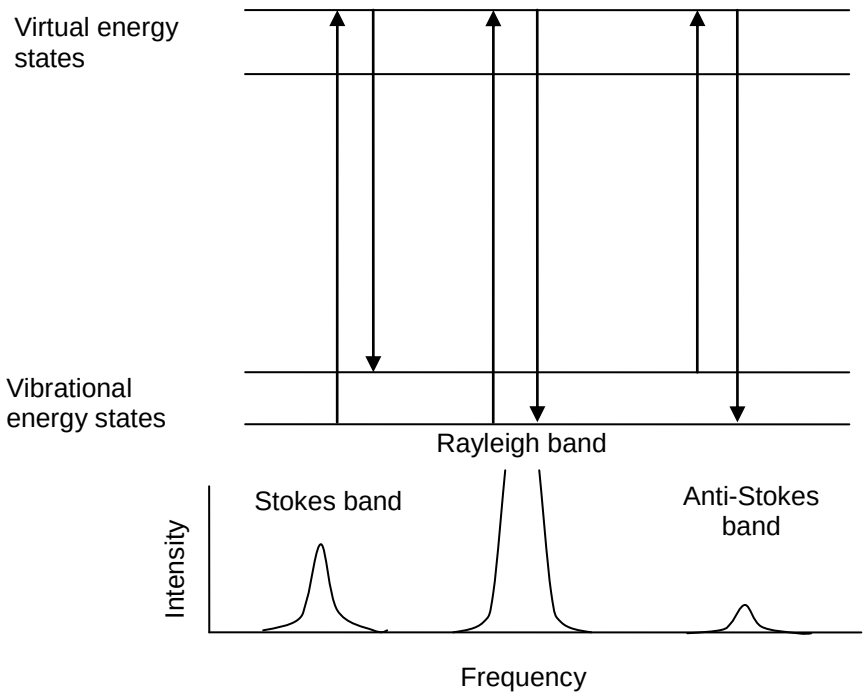

Figure 2-3: The Raman effect: incident light is scattered by the sample without losing energy (Rayleigh band) or inelastically producing an excited vibrational mode (Stokes band) or de-excited mode (anti-Stokes band). Redrawn from Niemantsverdriet (1993)

The Raman effect differs from fluorescence, where in the latter incident light is completely absorbed and the system is transferred to an excited state. It can then go to a lower state only after a certain resonance lifetime. This fluorescence can obscure weak signals (Freeman, 1974). It is also possible with this technique for the sample to be heated up and subsequently damaged/decomposed by the incident light (Niemantsverdriet, 1993). Care should be taken to minimise this effect since it could lead to incorrect interpretation of the sample composition or phase.

Raman spectra were recorded using a Horiba Jobin Yvon Labram HR 800 UV spectrometer. The experiments were performed at an excitation wavelength of 514 nm. Small quantities of powdered samples were placed on a glass slide for analysis. In recording spectra of these powdered samples, care was taken to use a representative sample. Raman mapping was performed by Paul Webb (Sasol Technology UK, St Andrews).

Selected experiments were performed by Philip Landon (Sasol Technology UK, St Andrews) using a spectroscopic cell. The desired gases pass downwards through the sample bed and then exit the cell. Approximately 25-50 mg of sample was used for these experiments. Once the sample was loaded into the cell it was placed under the microscope of the Raman spectrometer.

2.15 X-Ray Diffraction

X-ray diffraction (XRD) is a versatile, non-destructive technique that can be used to identify crystalline phases in a catalyst, as well as providing an indication of the crystallite size. XRD is the elastic scattering of X-ray photons by atoms in a periodic lattice. X-rays have sufficiently high energies to penetrate solids and thereby probe their internal structure (Niemantsverdriet, 1993). In phase scattered monochromatic X-rays results in constructive interference. The angles (2Θ) that lead to constructive interference can be used to determine the corresponding lattice spacings through the Bragg relation (Equation 2.1). These lattice spacings are characteristic of a certain compound.

$$n\lambda = 2d\sin\Theta \qquad \text{Equation2.1}$$

where n is the integer called order of the reflection, λ is the wavelength of X-rays, d is the distance between two lattice planes and Θ is the angle between the incident ray and the scattering planes. This is shown in Figure 2.4.

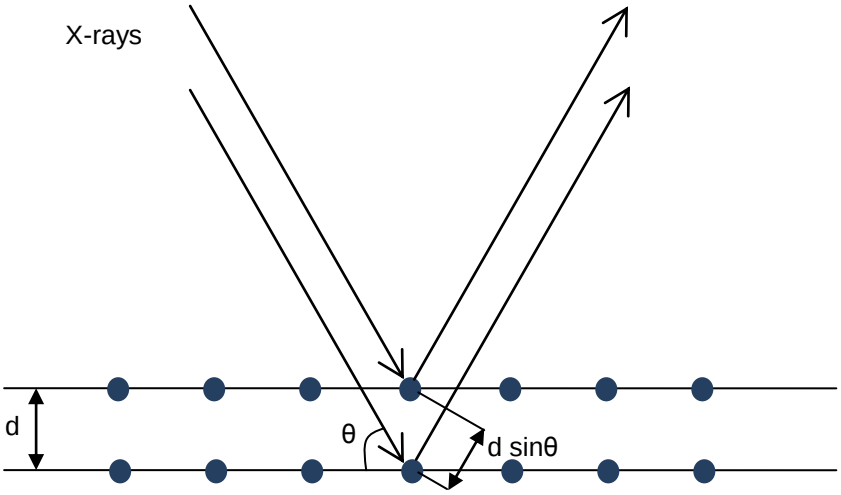

Figure 2-4: Bragg diffraction: two beams with identical wavelength approach a crystalline solid and are scattered off two different atoms within it. The lower beam traverses an extra length of 2dsinθ

Powder XRD data were collected on a Stoe STADI/P diffractometer operating in transmission mode with $FeKa_1$ radiation (l = 1.936 Å) to eliminate iron fluorescence. The X-ray diffractometer tube was operated at the following settings:

- Voltage 33 kV
- Current 30 mA
- 2θ range 10° - 90°
- Step width 0.01°
- Step duration 1.8 seconds

The observed diffraction peaks were assigned by referring to the International Centre for Diffraction Data (ICDD) supplied PDF-2. Quantitative phase analysis using the Rietveld technique was used to determine the relative amounts of different crystalline phases in the catalyst samples using GSAS software.

X-ray Diffraction (XRD) coupled with quantitative phase analysis using the Rietveld technique can be used to determine the relative amounts of different crystalline phases in the catalyst samples (Young, 1995). Surface phases may only comprise a small fraction of the bulk solid and may therefore not be detectable by X-ray diffraction analysis. A number of repeating unit cells yield

a diffraction pattern with identifiable peaks. The shape and width of diffraction peaks is determined by the order and size of the crystallites. The Rietveld technique uses the proportionality between the measured diffraction intensities and the amount of a particular crystalline phase in a sample. This proportionality is non-linear due to matrix absorption effects (Rietveld, 1969). Rietveld quantification on good diffraction data has to account for sample texture and amorphous components within the sample.

The peak profiles are a convolution of the sample dependent effects with the instrumental contributions. Instrumental contributions to peak profiles include the energy distribution of the incident radiation and aberrations due to the experimental geometry and optical components. The main refinement technique used by GSAS (Larson & Von Dreele, 1987) is the method of least squares and is performed by the program GENLES. In general the expressions for the calculated values corresponding to the set of crystallographic observations are transcendental and thus the least squares minimization function is nonlinear and the process is iterative. The minimization function in GENLES can be made up of several components.

2.16 X-ray Photoelectron Spectroscopy

X-ray photoelectron spectroscopy (XPS) is a quantitative spectroscopic technique very often used in the field of catalysis, yielding information about the elemental composition and the oxidation state of elements at the surface. XPS is based on the photoelectric effect, whereby an atom absorbs a photon of energy and ejects a core or valence electron:

$$E_k = h\nu - E_b - \varphi \qquad \text{Equation 2.2}$$

where E_k is the kinetic energy of the photoelectron, hv is the energy of the incident X-rays being used, E_b is the binding energy of the photoelectron and φ is the work function of the spectrometer. X-ray sources that are typically used include monochromatic Mg Kα and Al Kα. The measured parameter is the intensity of photoelectrons as a function of their kinetic energy, or more often their binding energies.

An XPS spectrum also contains Auger peaks, which arise from the transition of an electron in an atom filling an inner-shell vacancy and subsequently causes the emission of another electron. Since the XPS peaks are plotted against binding energies, Auger peaks are also plotted in this way although the Auger electrons have fixed kinetic energies. Auger peaks can be distinguished by recording the spectrum at two different X-ray energies; XPS peaks occur at the same binding energies while the Auger peaks will shift.

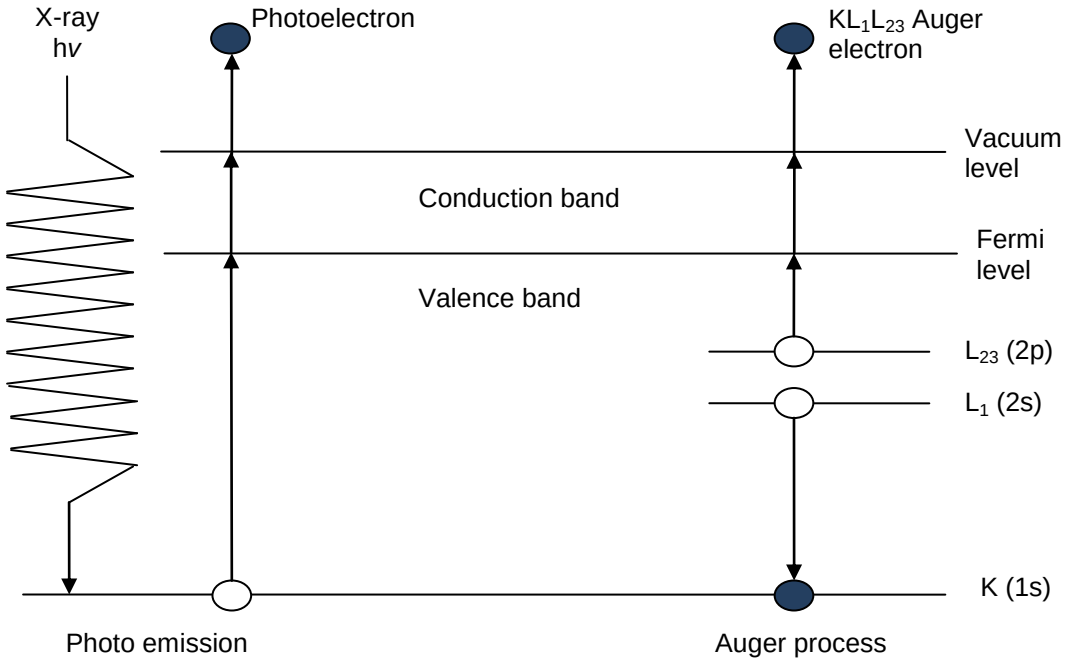

Figure 2-5: Photoemission of a photoelectron occurs by absorption of an incident X-ray photon (Left). The atom stays behind as an unstable ion. The Auger process is the relaxation of this ion by filling the core hole with an electron from a higher shell. The energy released is taken up by the Auger electron (Right)

Sample composition can be determined because elements are characterised by a set of binding energies. Photoelectrons used in XPS typically have kinetic energies ranging from 0.2 to 1.5 keV, while the probing depth varies between 1.5 and 6 nm (Niemantsverdriet, 1993). In order to calculate concentrations a structure model needs to be assumed. The general expression for the intensity of an XPS peak is:

$$I = F_x S(E_k)\sigma(E_k)\int_0^{\infty} n(z)e^{-z/\lambda(E_k)\cos\theta}dz$$

Where I is the intensity of the peak, F_x is the X-ray flux on the sample, $S(E_k)$ is the transmission function, $\sigma(E_k)$ is the cross-section for photoemission, n(z) is the concentration, z is the depth below the surface, $\lambda(E_k,z)$ is the mean free path of the photoelectron at kinetic energy E_k through the material present at depth z and θ is the take-off angle.

In addition to different elements yielding different binding energies, the chemical state of the atom also results in slight differences in the binding energy. These chemical shifts typically range from 0 – 3 eV. The binding energy increases with an increase in the oxidation state. It is important to consider the occurrence of charging during the measurement of electrically insulating samples due to photoelectrons leaving the sample. A positive charge on the sample with lead to a shift of all XPS peaks to higher binding energies. This can be overcome by calibrating using the binding energy of a known compound.

XPS was performed by David Morgan (Cardiff University) using a Kratos Axis Ultra DLD spectrometer equipped with a monochromatic Al K_α X-ray source (75 W). The analyser pass energy was either 160 eV (survey scans) or 40 eV (detailed elemental scans). Samples were mounted using double-sided adhesive tape. The data were analysed using the Casa XPS software. Sputtering experiments were performed using 5 kV Ar^+ ions for a duration of 30 minutes, with spectra recorded throughout this treatment.

2.17 Size Exclusion Chromatography

Size Exclusion Chromatography (SEC) is a chromatographic method in which molecules in solution are separated by their size, not by molecular weight. It is a well established technique in the determination of molecular masses of high molecular weight organic compounds (Wu, 1995). Packings for SEC consist of small silica or polymer particles containing a network of uniform pores into which solute and solvent molecules can diffuse. Smaller molecules are effectively trapped and removed from the flow of mobile phase while in the

pores (Skoog *et al*., 1998). Molecules larger than the average pore size of the packing are excluded and therefore not retained; thereby being the first to elute. SEC differs from other chromatographic techniques since no chemical of physical interaction between the molecules and stationary phase occurs.

The sample was dissolved in the mobile phase to a final concentration of 5 mg/mL. Within the instrument, the mobile phase, which was pumped by a HPLC pump (LC1120, Polymer Laboratories) and fitted with an on-line degasser (PL-DG 802, Polymer Laboratories), was allowed to stabilise within the column. The 30 cm long, 7.5 mm outer diameter column was packed with 5 µm polystyrene-divinylbenzene polymer particles. The column was operated at 35 °C, at a mobile phase flow rate of 1 mL/min. The peaks were detected using refractive index (Waters 2410), dynamic light scattering (Precision Detectors Inc. PD200DLS Plus) and UV/VIS absorption (Polymer Laboratories LC1200, operated at variable wavelengths) detectors. At the start of each analysis, a blank was run to observe the peaks formed as a result of the gases absorbed in the solvent. If there were any impurities present in the column, it would be evident at this stage. The sample (100 µL) was then injected into the column. Recording was started immediately, so that a constant elution time could be recorded for a particular species. In order to calculate the molecular weight of the species, there has to be a difference between the refractive index of the solvent and that of the sample. Furthermore, the solvent should not be too volatile, since it might evaporate within the column, therefore leaving it dry. The solvents that have been used were decane, xylene, 1,2-dichlorobenzene, dichloromethane.

2.18 Mössbauer Absorption Spectroscopy

Mössbauer Absorption Spectroscopy (MAS) is based on the Mössbauer effect i.e. the recoil free resonant absorption of gamma rays in solids. This technique is relatively seldom used and is limited to elements that exhibit the Mössbauer effect. It is extremely useful in selectively probing the local environments of nuclei based on the shift and splitting of degenerate nuclear

energy levels caused by the interactions between electrons and nuclei, the so-called hyperfine interactions: electric monopole, electric quadrupole and magnetic dipole interactions (Maddock, 1997). MAS provides information about the oxidation states, magnetic fields, lattice symmetry and vibrations by accurately analysing the energy levels of the nucleus (Niemantsverdriet, 1993). The nuclei in the source of gamma rays need to be in the excited state and must be of the same isotope as the sample absorbing them. Gamma rays are produced by nuclear transitions from an unstable high-energy state, to a stable low-energy state. In solids, atoms are fixed in a lattice and can therefore not recoil as if they are free. This allows resonance to occur.

Many factors make Mössbauer parameters ambiguous and thus hinder the identification of species based on these parameters. These include: the superparamagnetic behaviour often found in very small crystallites, inter-particle interactions, mixture of phases, the presence of impurities, structural disorders, surface effects, sub-lattice occupancy imbalances, shape anisotropy and incoherent magnetisation reversal mechanisms (Murad & Cashion, 2004; Kuzman *et al*., 2003). These difficulties may be resolved if the measurements are performed at low temperatures. But, it often happens that data collected at low temperatures are similar and thus cannot be used for unambiguous identification (Kuzman *et al*., 2003). Only measurements performed in an external magnetic field can enable differentiation of materials on the basis of their distinct responses to the applied magnetic field and thus enable the identification of their magnetic states.

MAS measurements were performed by Lonzeche Lodya (Sasol R&D, South Africa) at room temperature and 4.2 K with and without a 10 T external magnetic field using an Oxford Instruments SpectroMag4000-10 cryomagnet constant acceleration spectrometer operating in transmission mode. The spectra were analyzed by means of a least squares program “Normos” that models their combination based on a Lorentzian line-shape profile. Metallic iron (α-Fe) was used to calibrate the velocity scale (i.e. all isomeric shift

values are reported relative to it). The iron content of each phase was determined from their relative areas of the absorption peaks.

2.19 Particle Size Analysis

Particle Size Analysis is an analytical technique by which the distribution of sizes in a sample of particulate material is measured. Modern light scattering instruments are becoming the particle analysis method of choice in most industries due to their analysis speed, wide size range, ease of use, flexibility, and reproducibility. In Laser Particle Size Analysis, the size of particles is measured using the diffraction and diffusion of a laser beam. During the laser diffraction measurement, particles are passed through a focused laser beam. These particles scatter light at an angle that is inversely proportional to their size. The angular intensity of the scattered light is then measured by a series of photosensitive detectors.

Particle size analysis was performed on a Micromeritics Saturn Digisizer 5200. The samples were dispersed into slurry using a 10 % Triton X-100 solution and water was used as the analysis medium. In all the analysis, the obscuration was between 15 and 20 %. The pump speed was 12 L/min.

The ultrasonic attrition studies were performed on a Malvern Mastersizer 2000 with the Hydro S dispersion cell. Dispersion of the samples was achieved using a 10 % Triton X-100 solution, but in this case a paste was made which ensured that sampling was done effectively. The dispersant used was water and the stirrer/pump speed was set to 3200 rpm. To get a base line, five measurements were performed. Ultrasound was applied at 50 % for the next six measurements (roughly 60 seconds). The sample was then left to allow the sonic energy to dissipate while a further three measurements were taken. Ultrasound was reapplied at 100 % for a further six measurements. Finally three post sonic measurements were taken. The scattering pattern was deconvoluted using the Mie theory which requires knowledge of the refractive index of the dispersant and the sample.

2.20 Sieving

Catalysts were sieved using an Analysette 3 PRO vibratory sieve-shaker (Fritsch, Kingston UK) using Test Sieves (Impact Test Equipment Ltd., Stevenston UK). The vibration amplitude was set to 0.3 mm and the sieve time was 2 hours with an interval after every 10 seconds.

2.21 Thermogravimetric Analysis

Thermogravimetric Analysis (TGA) determines changes in weight in relation to change in temperature. The mass of a sample is recorded continuously as a function of temperature or time as the temperature is increased, usually linearly (Skoog *et al*., 1998). Such analysis relies on a high degree of precision in three measurements: weight, temperature, and temperature change. As many weight loss curves look similar, the weight loss curve may require transformation before results may be interpreted. A derivative weight loss curve can identify the point where weight loss is most apparent. Similarly to TPO, the heating rate has a large impact on the onset temperature for thermal events. Resolution of overlapping events can be achieved by stepwise heating programmes. Simultaneous TGA-DTA/DSC measures both heat flow and weight changes in a material as a function of temperature or time in a controlled atmosphere. Simultaneous measurement of these two material properties not only improves productivity but also simplifies interpretation of the results. The complementary information obtained allows differentiation between endothermic and exothermic events with no associated weight loss (e.g. melting and crystallization) and those that involve a weight loss (e.g. degradation).

TGA was performed by Mark Kelly (Sasol Technology UK, St Andrews) using a Netzsch STA 449 F1 Jupiter® instrument by placing 20-30 mg of the catalyst samples in a pan into the instrument. Desorption experiments were performed in a He flow rate of 50 mL/min and the heating rate was set to 5 °C/min up to 600 °C. Oxidations were performed in 10 % O_2/He at a flow rate

of 50 mL/min and the heating rate was 10 °C/min to 800 °C. Data was analysed using the Netzsch Proteus Thermal Analysis software.

2.22 Nuclear Magnetic Resonance Spectroscopy

NMR spectroscopy is a technique that exploits the magnetic properties of certain atomic nuclei to determine physical and chemical properties of atoms or the molecules in which they are contained. It relies on the phenomenon of nuclear magnetic resonance and can provide detailed information about the structure, dynamics, reaction state, and chemical environment of molecules. It is one of the most powerful techniques for elucidating the structure of chemical species (Skoog *et al*., 1998).

^{57}Fe is a low sensitivity spin ½ nucleus. It has been shown that the presence of iron oxides, or more specifically Fe(III), results in an increase in the rate of surface relaxation (Keating & Knight, 2007). This is further exacerbated in the presence of magnetite which contains both Fe(II) and Fe(III) due to internal magnetic field gradients. This leads to paramagnetic broadening of the signals observed, and is the reason why NMR was very little used in this investigation.

Soluble fractions of samples were analysed by ^{1}H Nuclear Magnetic Resonance (^{1}H-NMR) using a Bruker Avance 300 spectrometer fitted with a BBFO probe-head. Data was analysed using TopSpin 2 software.

2.23 Gas Chromatography-Mass Spectrometry

Gas-Chromatography coupled with Mass Spectrometry (GC-MS) is a method that combines the features of gas-liquid chromatography and mass spectrometry to identify different substances within a test sample.

GC-MS was performed using an Agilent 6890 GC with a 5973 mass selective detector (MSD). The oven was initially at 40 °C and ramped up at 10 °C/min to 300 °C where it was kept for 20 minutes. An Agilent 122-0162 capillary

column with a length of 60 m, a diameter of 0.25 mm and a film thickness of 0.25 µm was used with an initial flow of 1mL/min. The MSD transfer line was heated to 280 °C. Data was acquired in scan mode between the masses of 25 and 550.

2.24 Microanalysis

The technique is traditionally applied to the analysis of organic compounds (Belcher, 1976), therefore the analysis of more demanding samples that combust slowly by automated elemental analysers has proven to be difficult. The characterisation of the HTFT catalyst is problematic due to the presence of the iron-based substrate, adsorbed wax that readily desorbs at elevated temperatures and oxidation-resistant carbonaceous species that need time to fully combust. To analyse a sample, a weighed quantity is introduced into a high temperature furnace and the sample is combusted in oxygen. Typically the sample is weighed into a tin container, which gives the advantage of strong exothermic combustion ensuring complete sample oxidation at approximately 1800°C. The resulting combustion products pass through specialised oxidation reagents to produce carbon dioxide (CO_2), water (H_2O), nitrogen (N_2) and N oxides from elemental carbon, hydrogen, and nitrogen, respectively. These gases are then passed over copper to remove excess oxygen and reduce the oxides of nitrogen to elemental nitrogen. Helium is used as the carrier gas. Other elements present are removed by the use of specialised combustion reagents.

Microanalysis is complicated by the presence of materials that are difficult to combust in the analysis (Etherington *et al.*, 2001) and thereby underestimating the amount of carbon and hydrogen within these samples. The detection and measurement of combustion products in microanalysis differ according to analyser type. These can be classed as either static or dynamic systems. In a dynamic system the sample is dropped into the combustion tube at a predetermined time to meet with an oxygen enriched atmosphere in a vertically arranged furnace. The samples are combusted on

top of previously combusted samples. In contrast, in a static system that has a horizontal combustion furnace, the sample is introduced *via* a ladle into the combustion tube comprising a pure oxygen environment. After combustion has occurred the sample residue is removed from the combustion tube. Detection in a static system is therefore highly accurate and precise (Etherington *et al.*, 2001).

Samples were submitted to London Metropolitan University for microanalysis. The instruments used were Carlo Erba CE 1108 and 1110 using combustion temperatures up to 1800 °C. Selected samples were sent to Exeter Analytical (UK) Ltd for analysis on a CE 440 elemental analyser.

3. THE STRUCTURE OF SPENT HIGH TEMPERATURE FISCHER-TROPSCH CATALYSTS

3.1 Introduction

The High-Temperature Fischer-Tropsch (HTFT) process is operated commercially by Sasol in Secunda to produce long chain hydrocarbons from synthesis gas, a mixture of carbon monoxide and hydrogen obtained from the gasification of coal. The reaction takes place in a Sasol Advanced Synthol (SAS) fluidised-bed reactor and employs an alkali-promoted iron-based catalyst (Dry, 1981). During operation the productivity of the system drops; this is ascribed to the build-up of carbon. The carbon results in changes in fluidisation dynamics and the loss of catalyst through cyclones, which diminishes the amount of material in the optimum temperature zone. This necessitates the constant on-line replenishment of fresh catalyst and removal of the equilibrium catalyst, a mixture of catalyst particles that have been exposed to Fischer-Tropsch Synthesis (FTS) conditions for different periods of time. The focus of this work is to investigate changes in composition due to the deposition and continuous build-up of carbonaceous species, and then to understand how these compositional changes affect chemical and physical properties. The aim is to develop an understanding of the mechanism by which carbonaceous deposits are formed on the catalyst and how this carbon build-up leads to loss of mechanical strength and eventually break-up of the catalyst particles. Understanding the mechanisms involved in the evolution of the catalyst with time on-stream during FTS could facilitate the design of catalyst and operating conditions that would minimise deactivation.

To gain insight into the mechanism, we are investigating catalyst structure and composition of the catalyst recovered from a SAS reactor. One of the major problems associated with understanding carbon build-up on Spent Cat-1 is that it is an equilibrium catalyst i.e. the recovered material contains an ensemble of particles that have been exposed to HTFT conditions for different durations. The catalyst also exhibits a large particle size distribution, which is

necessary in order to facilitate adequate fluidisation within the reactor and this further complicates determination of the origin of catalyst particle structure. However, a simplified picture can be obtained by investigating catalysts that have all been exposed to FTS conditions for the same length of time. This can be achieved by studying catalysts removed from the Pilot Plant reactor. Although operating conditions are very similar and the particle size distribution required for the SAS reactor is also used in the Pilot Plant reactor, there are differences between the operations of these two reactors. This is mainly due to the different flow regimes in the reactors. While the SAS reactor is a fluidised bed reactor, the Pilot Plant is operated as plug flow with significant back-mixing. However, despite these differences, the benefit of studying a simpler catalyst is still enormous.

The characterisation of carbonaceous deposits formed on a used catalyst is a complicated process. The surface species is comprised of a mixture of species not all contributing to deactivation. This includes adsorbed hydrocarbonaceous products from FTS. Also, the presence of the iron-based catalyst substrate makes analysis by traditional techniques commonly applied to organic species difficult. Several techniques are usually employed in the characterisation of spent catalysts. These include quantitative techniques such as Temperature-Programmed Oxidation (TPO) and Thermogravimetric Analysis (TGA) (Galuszka et al., 1992; Shroff et al., 1995), and spectroscopic methods namely Raman spectroscopy (Herranz et al. 2006; Loaiza-Gil et al., 1999; Ning et al., 2006; Pijolat et al. 1987) and X-Ray Photoelectron Spectroscopy (XPS) (Krebs et al., 1979; Ott et al., 1980; Bonzel & Krebs, 1980, 1981; Reymond et al., 1982; Dwyer and Hardenbergh, 1984; Loaiza-Gil et al., 1999; Shroff et al., 1995; Bukur et al., 1995a; de la Peña O'Shea et al. 2006; Butt, 1990; Riedel et al., 2003; Jin et al., 2002). X-Ray Diffraction (XRD) (Galuszka et al., 1992; Herranz et al., 2006 Jung and Thomson, 1992; Loaiza-Gil et al., 1999; Ning et al., 2007; Reymond et al., 1982; Shroff et al., 1995; Bukur et al., 1995a; Jin and Datye, 2000; Bukur et al., 1995c; Zhang et al., 2004) and Electron Microscopy (Shroff et al., 1995; Jin and Datye, 2000;

Mathieu et al., 2007; Janbroers et al., 2009; Jin et al., 2002) are often also used in the characterisation of spent catalysts.

HTFT catalysts recovered from the reactors are comprised of a mixture of species; therefore a method to simplify or fractionate the carbonaceous species is required. The simplest way to achieve this fractionation is perhaps by TPO. TPO of the catalyst can be used to gain insight into the species present on the catalyst and applying this knowledge to simplify the catalyst by sequential oxidation of various species. Identifying the number of species and the temperature at which oxidation events occur can give information about the nature of the species present. This information can subsequently be used in the selective removal of certain species. The results obtained in the characterisation of the spent HTFT catalysts are presented in the following section.

3.2 Results and Discussion

3.2.1 The Composition of a Spent HTFT Catalyst

3.2.1.1 As-received HTFT catalyst

A typical TPO profile of Spent Cat-1 shows several oxidation events occurring. An oxidation event can represent the combustion or partial oxidation of carbonaceous material, phase transformation of the iron-containing material or both of these events occurring simultaneously. The thermal conductivity detector (TCD) trace of this material is shown in Figure 3.1. The drawback of using the TCD trace is that it represents changes in thermal conductivity of the effluent gas caused by both oxygen consumption and the generation of all the combustion products. However, if this trace is used to qualitatively identify oxidation events, it can serve as a guide to the number and the reactivity of species. In Figure 3.1 there appears to be at least five oxidation events (labelled Peak I – Peak V) taking place. Assuming that each event represents oxidation of a different species the aim is to determine the nature of material associated with these oxidation events by

step-wise oxidation of the various species. Bulk and surface characterisation techniques can be used to analyse the material before and after each oxidation event. Then, starting with the simplest material which is obtained after complete oxidation (800 °C), the next step is to work back to reconstruct a picture of the species present in the original spent catalyst before any oxidation treatment was performed. The assumption in this approach is that all the species would combust completely and therefore contribute to the observed TPO profile and produce CO_2 and/or H_2O that can be detected by MS.

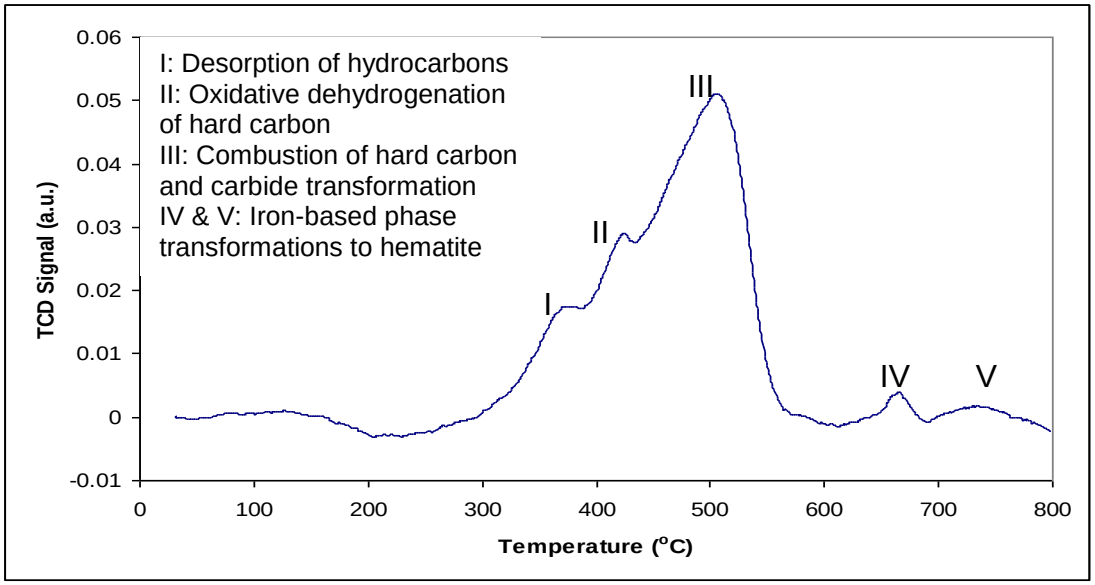

Figure 3-1: Temperature-programmed oxidation experiment of Spent Cat-1. This is a spent iron Fischer-Tropsch catalyst recovered from the Sasol Advanced Synthol (SAS) reactor. Standard TPO conditions: heating rate 10 °C/min in 10 % O2/He

XRD is an invaluable technique for determination of the bulk structure of the catalyst and is employed in this study to monitor any phase transformations of iron-based catalyst substrates. The XRD pattern of the spent catalyst refined by the Rietveld method (Rietveld, 1969) is indicated in Figure 3.2. It shows that the phase of the catalyst substrate is mostly magnetite (Fe_3O_4) with carbides consisting of Hägg carbide (Fe_5C_2) and Eckström-Adcock carbide (Fe_7C_3). The peaks associated with magnetite are indicated, while the carbide phases are grouped together for simplicity. The difference between the

experimental (red) and theoretical (green) XRD pattern is indicated by the pink curve plotted below the pattern.

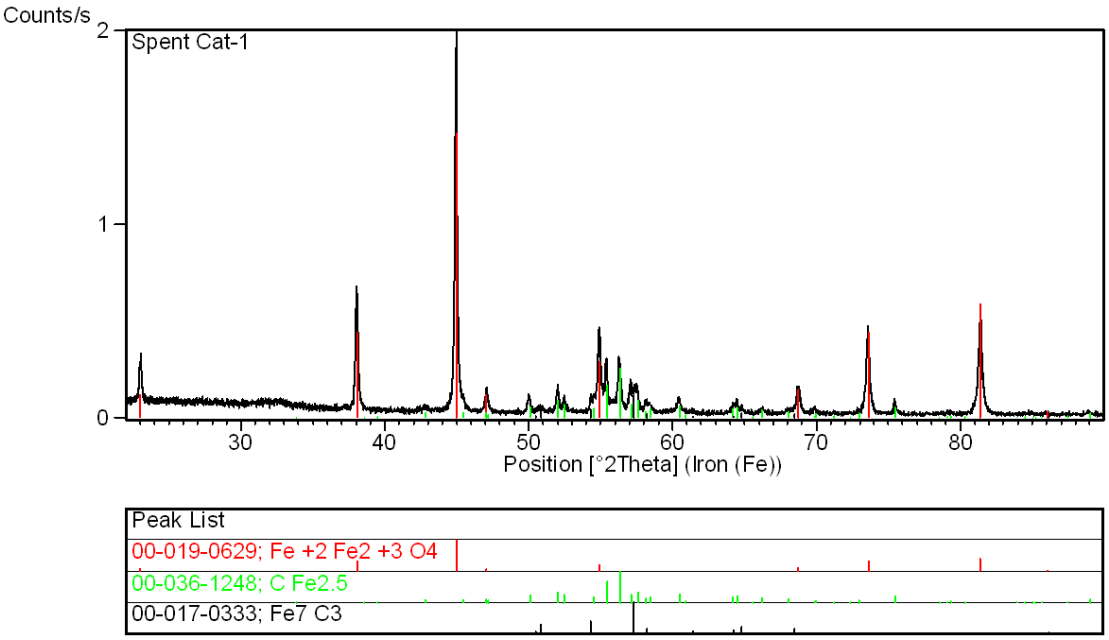

Figure 3-2: X-ray diffraction pattern of Spent Cat-1: a spent iron Fischer-Tropsch catalyst recovered from the Sasol Advanced Synthol (SAS) reactor. The experiment was carried out as follows: 33 kV, 30 mA, step width: 0.01°, step duration 1.8 seconds

Matching the XRD patterns to a specific phase is difficult (Janbroers *et al.*, 2009; Niemantsverdriet *et al.*, 1980; Jin & Datye, 1998a; Bukur *et al.*, 1995a) since these carbides exhibit similar XRD patterns and therefore Rietveld refinement was employed in the quantification of the phases. Table 3.1 shows the relative abundances of the various phases expressed as a mass percentage. Also indicated within the table are the PDF numbers of the various phases used in the refinement. The χ^2 value provides an indication of the goodness of fit in Rietveld refinement, which would be unity for perfect agreement between the calculated curve and the observed XRD pattern. The final χ^2 value obtained for the refinement was 1.179.

Table 3-1: Relative abundances (m/m %) of constituent phases of Spent Cat-1 determined by Rietveld refinement

Phases	PDF number	XRD
Magnetite	019-0629	74.1
Hägg carbide	036-1248	23.8
Eckström-Adcock carbide	071-0333	2.1

Raman spectroscopy is an easy and non-destructive technique for the characterisation of carbonaceous species. It was used to determine the surface composition of the spent catalyst since the typical analysis depth expected of this technique is typically believed to be around 1 μm, but this depth varies for different materials. Importantly, this technique is quite surface specific for the HTFT catalyst used in this work, where the average particle diameter is 60 μm. Raman spectroscopy is very useful in determining the nature of carbonaceous species; most carbonaceous materials exhibit a certain line-shape, intensity and position of D and G modes as well as some additional signature peaks. However, this information becomes lost in the characterisation of mixtures of species. Section 4.2.1.2 gives a full discussion of the application and interpretation of Raman spectra to the study of carbonaceous deposits found on typical HTFT catalysts.

The Raman spectrum (Figure 3.3, Section 3.2.1.2) shows that the surface of the spent catalyst is not comprised of any iron oxide phases (expected between 100 and 700 cm^{-1}) suggesting that the catalyst is completely covered by carbonaceous deposits. The two major vibrational modes around 1350 and 1600 cm^{-1}, commonly termed D and G modes, respectively, represent C-C bonds. The crystallinity of the carbonaceous material is reflected in the intensity of the D mode relative to that of the G mode. The modes associated with C-H bonds are typically observed as a shoulder at 1330 cm^{-1} and also at 2500 and 3250 cm^{-1}.

Performing the various techniques on the equilibrium catalyst, the next step was to study the catalyst subjected to oxidation and to compare the results with those described above. It was determined that performing oxidation of Spent Cat-1 at 340 °C removed aliphatic material associated with oxidation events I and II, while oxidation at 450 °C also removed event III from the TPO profile. Oxidation was complete after 800 °C. These samples were therefore prepared by performing oxidation in a bulk experiment. The following sections

discuss the characterisation of the material that remains after these sequential oxidation treatments have been performed.

3.2.1.2 HTFT Catalyst after bulk oxidation at 340 °C

Isothermal treatment at 340 °C followed by TPO of this material reveals that oxidation events I and II are no longer present. Considering the mild temperature at which these oxidation events occur, it was initially postulated that they are associated with the combustion of hydrogen-rich hydrocarbons (or soft carbon) adsorbed on the spent catalyst surface. This hypothesis is corroborated by the work of Galuszka *et al.* (1992), who assigned low-temperature oxidation events to aliphatic species present on supported iron catalysts. It should be noted that partial oxidation instead of complete combustion can occur. In addition, thermal desorption occurs simultaneously to oxidation. This renders TPO non-quantitative with respect to oxidation events I and II and will be discussed in detail in Section 3.2.1.5. Raman spectroscopy provides evidence for this assignment since the C-H modes present in the Raman spectrum shown in Figure 3.3 were essentially removed following the oxidation treatment. Figure 3.3 depicts the comparison between the spectra before and after oxidation at 340 °C.

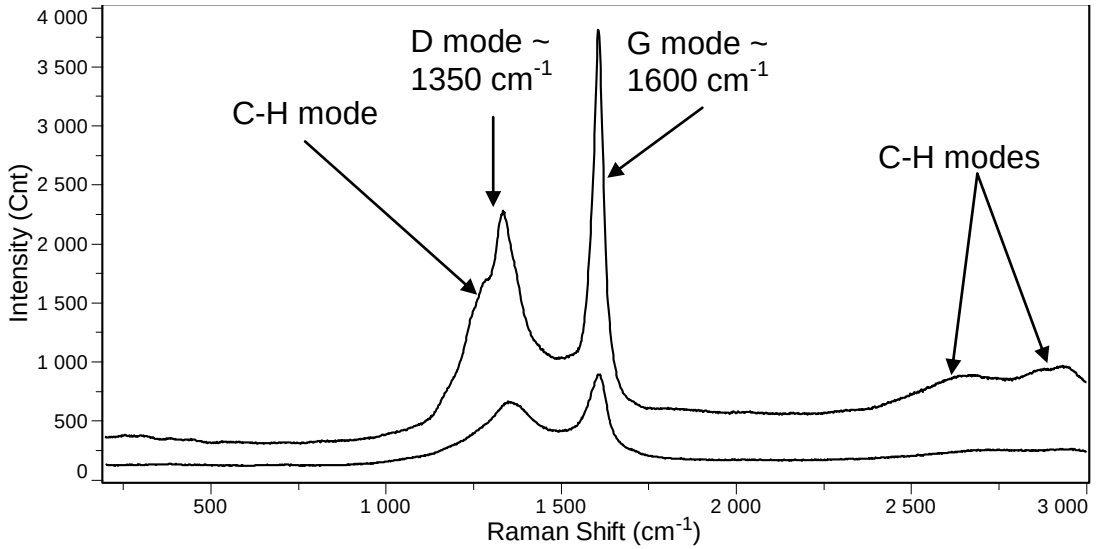

Figure 3-3: Raman spectrum of Spent Cat-1: a spent iron Fischer-Tropsch catalyst recovered from the Sasol Advanced Synthol (SAS) reactor before (upper) and after (lower) bulk oxidation at 340 °C. Excitation wavelength: 514 nm

Phase composition determined by XRD (Figure 3.4) is given in Table 3.2. The data reveals that the combustion of hydrocarbons was accompanied by phase transformation of some of the magnetite to maghemite and hematite. This data was refined to a final χ^2 value of 1.820. The carbide phases underwent minimal transformation during heat treatment.

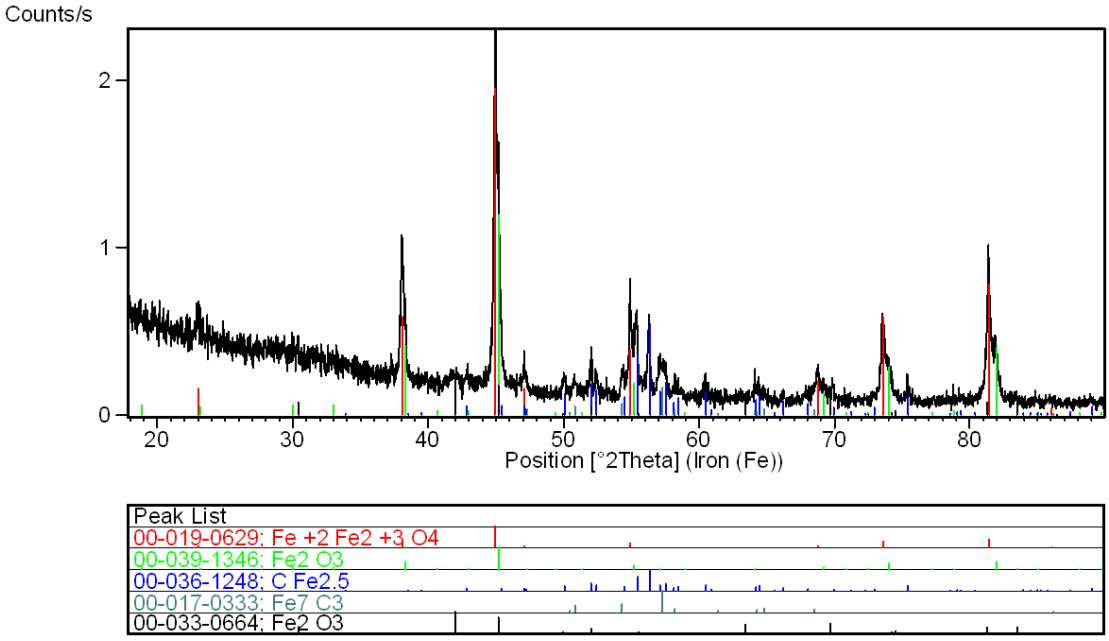

Figure 3-4: X-ray diffraction pattern of spent iron Fischer-Tropsch catalyst recovered from the SAS reactor following desorption at 340 °C. The experiment was carried out as follows: 33 kV, 30 mA, step width: 0.01°, step duration 1.8 seconds

Table 3-2: Relative abundances (m/m %) of constituent phases of Spent Cat-1 following desorption at 340 °C determined by Rietveld refinement

Phases	PDF number	XRD
Magnetite	019-0629	42.9
Maghemite	039-1346	27.9
Hägg carbide	036-1248	25.1
Eckström-Adcock carbide	017-0333	3.0
Hematite	001-1053	1.1

CHN microanalysis data is presented in Table 3.3. Briefly, this quantification provides an indication that in addition to this hydrogen-rich material that is oxidised and/or desorbed at 340 °C and the carbides that are present, there is additional carbon species that still remains intact after this oxidation

treatment. This material does not contain detectable amounts of hydrogen and will therefore be referred to as hydrogen-deficient carbonaceous species or hard carbon. This hard carbon must be present in oxidation event III, since there is no carbon left after oxidation treatment at 450 °C. Obtaining accurate CHN microanalysis data is not so straightforward and this will also be described further in Section 5.2.1.

Table 3-3: Carbon (total and carbide) and hydrogen content (m/m %) of Spent Cat-1 and catalyst material after oxidation at 340 °C and 450 °C

Samples	Total C	Carbidic C	H
Spent Cat-1	17.8	2.0	0.7
Ox 340 °C	10.2	1.6	<0.1
Ox 450 °C	<0.1	0	<0.1

3.2.1.3 HTFT Catalyst after bulk oxidation at 450 °C

Isothermal treatment at 450 °C followed by TPO of this material reveals that oxidation event III is no longer present. This oxidation treatment at 450 °C removes the hard carbonaceous material associated with Peak III. XRD (Figure 3.5) of the resultant material shows that carbides are no longer present following this oxidation treatment. This data is tabulated in Table 3.4. This material was refined to a final χ^2 value of 1.285. The corresponding Raman spectrum indicates that the main phase present on the surface of the catalyst is maghemite, as depicted in Figure 3.6. It should be borne in mind that if a small amount of magnetite surface species were also present, the modes associated with this iron oxide phase would be concealed by the presence of maghemite. The main feature characterising magnetite occurs around 650 cm^{-1}, while maghemite has a broad mode at about 700 cm^{-1} as well as the mode at 1400 cm^{-1}. It is important to note that the D and G modes associated with carbon are no longer present. Microanalysis of this material reveals that all the carbon is removed by this treatment (Table 3.3). The transformation of carbidic iron is known to occur at 550 °C (Galuszka *et al.*, 1992), which corresponds to Peak III. Based on these considerations, it was therefore believed that the oxidation event associated with Peak III

represented both the transformation of iron carbides to oxides as well as the combustion of the hydrogen-deficient carbonaceous species or hard carbon.

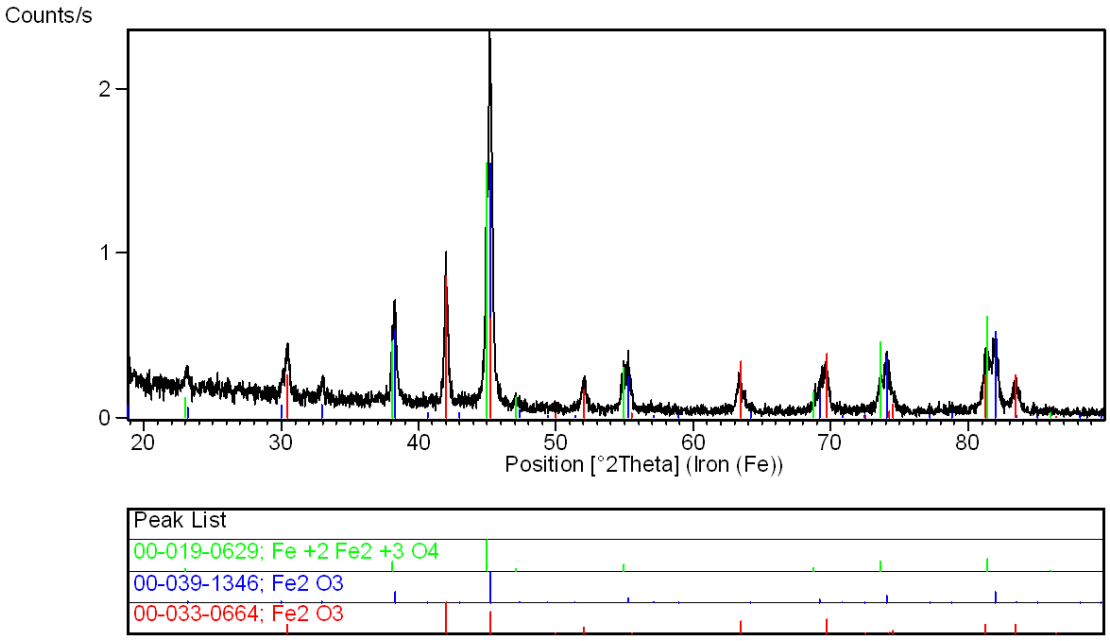

Figure 3-5: X-ray diffraction pattern of spent iron Fischer-Tropsch catalyst recovered from the SAS reactor following bulk oxidation at 450 °C. The experiment was carried out as follows: 33 kV, 30 mA, step width: 0.01°, step duration 1.8 seconds

Table 3-4: Relative abundances (m/m %) of constituent phases of Spent Cat-1 following desorption at 450 °C determined by Rietveld refinement

Phases	XRD	PDF number
Hematite	28.1	001-1053
Magnetite	29.1	019-0629
Maghemite	42.9	039-1346

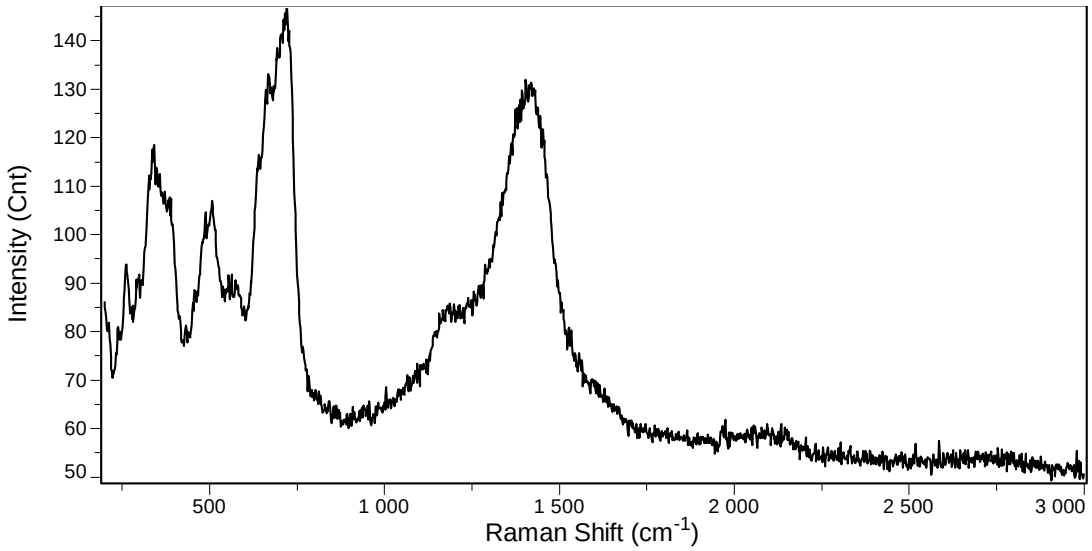

Figure 3-6: Raman spectrum of spent iron Fischer-Tropsch catalyst recovered from the SAS reactor following bulk oxidation at 450 °C. Excitation wavelength: 514 nm

The combustion temperature of hard carbonaceous species such as commercial graphite usually requires higher temperatures than 450 °C. However, by mixing this graphite with Spent Cat-1, it was demonstrated that oxidation of commercial graphite is catalysed by iron oxides and as such oxidation events for hard carbon on 'spent' catalysts may occur at significantly lower temperatures than expected, thereby giving credence to the assignment of Peak III to the combustion of hard carbon. The catalysing effect of iron oxide on the oxidation of carbon is widely applied in the manufacturing of steel.

3.2.1.4 HTFT Catalyst after bulk oxidation at 800 °C

The final isothermal oxidation at 800 °C followed by TPO showed that Peaks IV and V are no longer present. Both the XRD pattern (Figure 3.7) and Raman spectrum (Figure 3.8) reveal that the major phase present after this treatment is hematite, while refinement shows that there are still small amounts of magnetite present (Table 3.5). A final χ^2 of 1.178 was obtained. Hematite belongs to the D^6_{3d} crystal space group. Two A_{1g} (225 and 498 cm^{-1}) and five E_g modes (247, 293, 299, 412 and 613 cm^{-1}) are therefore expected in a Raman spectrum (de Faria et al., 1997). The additional mode at 650 cm^{-1} can be ascribed to magnetite. Since hematite is an antiferromagnetic material, the

collective spin movement can be excited in a magnon (de Faria et al., 1997). The feature at 1320 cm^{-1} is assigned to a two-magnon scattering from the interaction of magnons created on antiparallel close spin sites (de Faria et al., 1997).

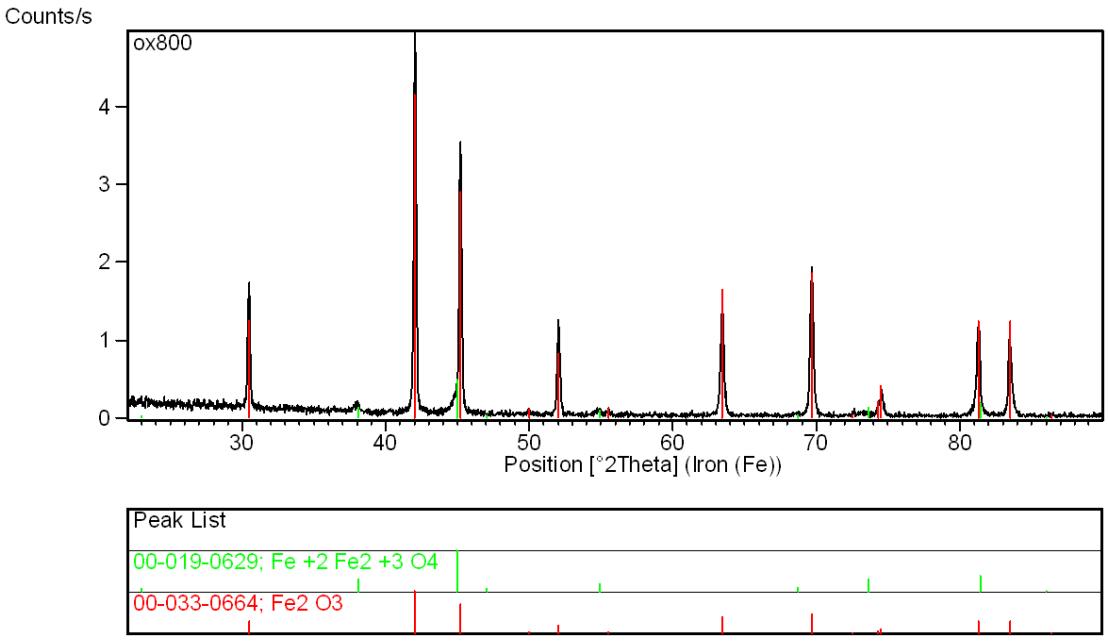

Figure 3-7: X-ray diffraction pattern of spent iron Fischer-Tropsch catalyst recovered from the SAS reactor following oxidation at 800 °C. The experiment was carried out as follows: 33 kV, 30 mA, step width: 0.01°, step duration 1.8 seconds

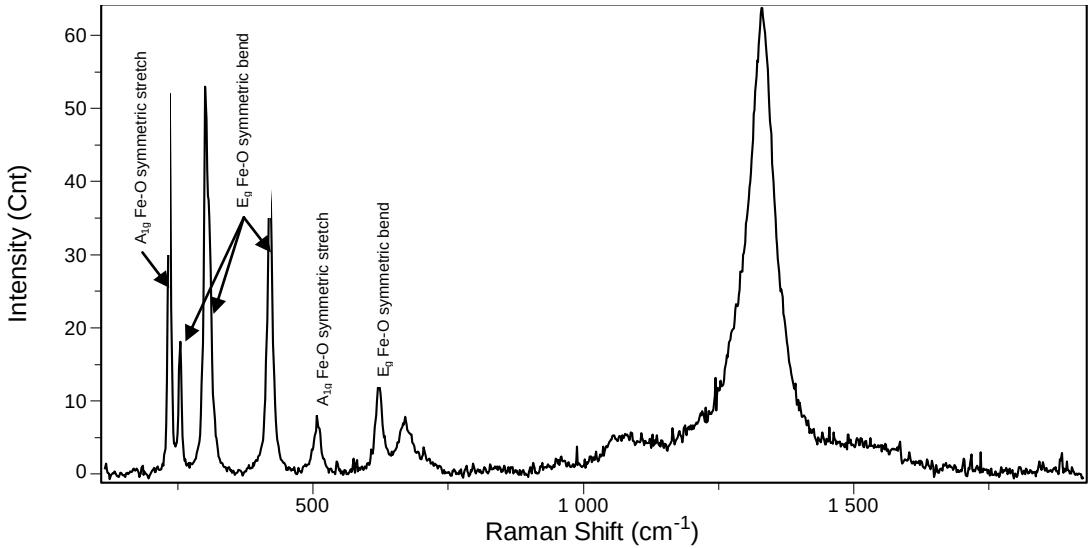

Figure 3-8: Raman spectrum of spent iron Fischer-Tropsch catalyst recovered from the SAS reactor following oxidation at 800 °C. Excitation wavelength: 514 nm

Table 3-5: Relative abundances (m/m %) of constituent phases of Spent Cat-1 following desorption at 800 °C determined by Rietveld refinement

Phases	XRD	PDF number
Hematite	92.9	001-1053
Magnetite	7.1	019-0629

3.2.1.5 Identification of events I and II

Soxhlet extraction (using xylene) of the catalyst recovered from the SAS reactor was also performed with the aim of simplifying TPO and spectroscopic data. The idea was that this treatment would selectively remove soluble species. In the extraction experiment, very little material was found in the solvent following *in vacuo* concentration. Consequently, it is believed that the extraction process seems to be rather inefficient at removing adsorbed hydrocarbons. However, there appears to be a change in the sample after Soxhlet extraction, as illustrated in Figure 3.9. Subsequent TPO reveals that only Peak II observed in the oxidation profile of Spent Cat-1 is removed, despite the fact that both Peaks I and II were initially assigned to hydrocarbon combustion. Therefore, if both these peaks represent hydrocarbons, the extraction process only removes the more oxidation-resistant hydrocarbons.

The extracted material should comprise the change in the TPO profile. Therefore, if Peak II represents the oxidation or desorption of hydrocarbons, then TPO of the extract after concentration might be expected to exhibit an oxidation event in this temperature range (~ 400 °C). However, instead of Peak II, the TPO profile (Figure 3.9) reveals events at Peaks III and IV only, which is associated with iron related phase transformations. This initially suggests that some fine iron-containing catalyst particles are removed/oxidised during extraction. TPO of the extract would therefore exhibit the events assigned to the transformation of iron carbides and oxides to hematite, namely events III and IV. However, GC-MS indicates that a homologous series of various olefins and paraffins as well as some aromatic and oxygenated species are present in the extract.

A complication in Soxhlet extraction stems from the porosity of the cellulose thimbles used during extraction, which is known to play a part in the quality of the extraction process. The reason for this is that some of the iron particulate fines present in the catalyst material can pass through the pores and into the soluble fraction. Evidence that this indeed occurs is provided by paramagnetic broadening of the solution as observed by ^{1}H solution-state NMR. In addition, material also appears to become trapped within the thimble, so that the dried extract only amounts to 0.6 wt% of the catalyst.

A shift in the temperature of the oxidation of catalyst from which carbonaceous species had been extracted on the TPO spectra has been reported previously (Xu & Bartholomew; 2005). This was ascribed to oxidation of the iron carbide nodules on the extracted catalyst. However, these researchers did not perform TPO of the extract. A further problem is that the Soxhlet extraction is performed in air at elevated temperatures and this can cause transformations and oxidation to occur. Similarly, in a study conducted by Mansker and co-workers (1999) it was reported that Soxhlet extraction results in subtle changes in catalyst composition and morphology due to the prolonged high temperatures at which this process is carried out. XRD of Spent Cat-1 following extraction revealed that the bulk phase of the catalyst remained largely unchanged after extraction.

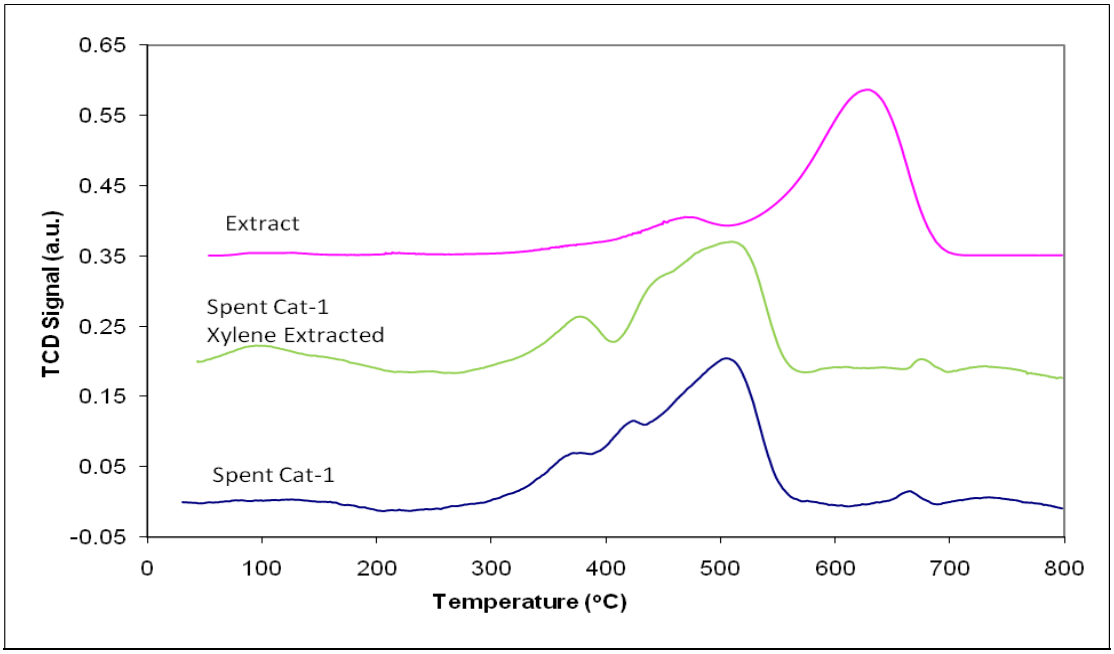

Figure 3-9: Temperature-programmed oxidation experiment of Spent Cat-1: a spent iron Fischer-Tropsch catalyst recovered from the SAS reactor before and after Soxhlet extraction and the extract. Standard TPO: heating rate 10 °C/min in 10% O_2/He

Interestingly, the TPO profile of the catalyst recovered from the Pilot Plant reactor (Figure 3.10) is similar to the Soxhlet-extracted Spent Cat-1 i.e. Peak II is not observed. This places further uncertainty on the initial assignment of Peak II to the combustion of soft carbon, since it is known from microanalysis that the hydrocarbon content of Spent Cat-2 is considerably higher compared to Spent Cat-1 (Table 3.6). Spent Cat-2 contains more carbonaceous material at the end of the five-day reactor run. The spent catalyst recovered from the Pilot Plant differs from the equilibrium catalyst obtained from the SAS reactor in several other ways. There is also the added complication that the reactor types are not the same in these two cases. This leads to different fluidisation dynamics experienced by the catalyst particles. We therefore postulated that the absence of Peak II in the SAS extracted catalyst (Figure 3.9) is due to oxidation of fine iron-containing particles that occurs during extraction. In line with this, it was hypothesised that there is less attrition occurring in the Pilot Plant, so that there are fewer fines produced in the process.

One of the original ideas concerning combustion of particles of different size is that smaller particles would combust more easily (at lower temperatures) due

to diffusion of oxygen occurring in the absence of transport limitations. The implication of combustion temperature being particle size dependent is that, since there are two distinct peaks that could represent hard carbon and carbides (Peaks II and III), a bimodal particle size distribution would be expected for Spent Cat-1. Particle size analysis (PSA) was performed to investigate the validity of this hypothesis. PSA was performed using a laser diffraction particle size analyser. Although most instruments from the various suppliers work on the same principle, there are minor differences in the design that render certain instruments unsuitable for the analysis of spent HTFT catalysts. The main obstacle that was encountered involved obtaining fluidisation of all the particles in the dispersant (water). Carbon-rich fines floated on the surface of the water and could therefore not be detected. This problem was remedied by pre-treating the particles using a 1% detergent solution. The large particles were also not detected due to settling within the sample chamber even at maximum flow rates. This difficulty was overcome by performing PSA in a Micromeritics' Saturn DigiSizer instrument, which is equipped with a rotor pump capable of high revolutions per minute. Figure 3.11 shows the particle size distribution of the fresh fused, Pilot Plant and SAS reactor catalysts. The particle diameters have been omitted for IP purposes. It is apparent that the catalyst recovered from the SAS reactor contains more fines. This bimodal distribution is in fact not observed and calls into question the postulate concerning particle size effects and the origin of oxidation event II.

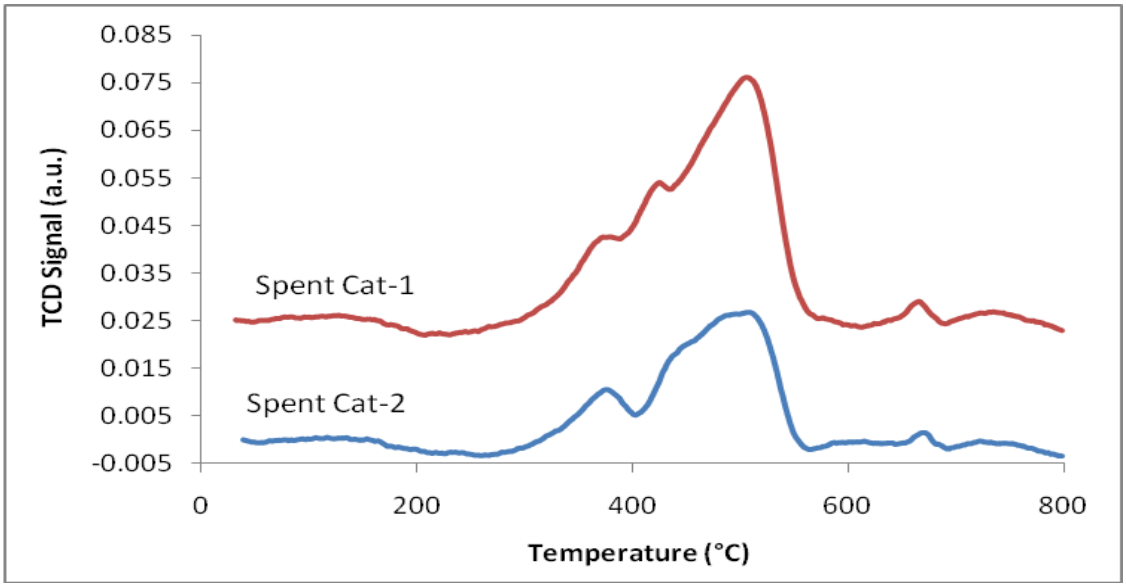

Figure 3-10: Temperature-programmed oxidation of Spent Cat-1 (spent iron Fischer-Tropsch catalyst recovered from the SAS reactor) and Spent Cat-2 (recovered from the Pilot Plant reactor). Standard TPO: heating rate 10 °C/min in 10% O_2/He

Table 3-6: Relative abundances (m/m %) of carbon and hydrogen in Spent Cat-1 and Spent Cat-2

Sample	C	H
SAS	17.8	0.7
Pilot Plant	68.0	4.5

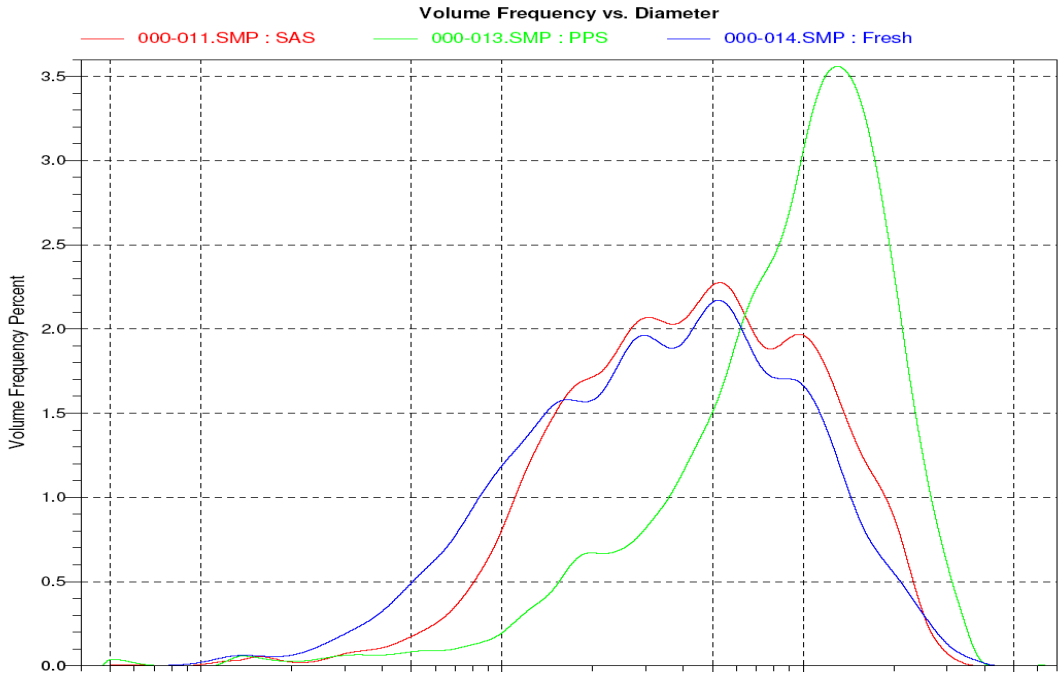

Figure 3-11: Relative particle size distributions of fresh fused (blue), Spent Cat-1 recovered from the SAS reactor (red) and Spent Cat-2 recovered from the Pilot Plant reactor (green). Micromeritics Saturn Digisizer 5200, obscuration: 15-20 %, pump speed: 12 L/min

Another possibility is a shift in oxidation temperature in particles with different amounts of iron oxides in contact with carbonaceous species. This idea originates from the ability of iron oxide to catalyse the combustion of carbonaceous species in contact with this phase. Spent Cat-1 contains a mixture of particles that have been exposed to FTS conditions for different durations. It is therefore possible that particles which have only been in the reactor for a short time contain iron oxide but has no deposited carbon associated with this phase. Also, broken-off particle fragments could be entirely made up of carbides and carbonaceous deposits. These possibilities render the study of catalysed oxidation in Spent Cat-1 difficult. The argument can be extended to Spent Cat-2, where the absence of Peak II suggests that only non-catalysed oxidation is occurring for this sample. Section 3.2.2 describes how SEM analysis of the Pilot Plant sample shows no particles with visible iron oxide in contact with the carbonaceous species, while phase analysis indicates that a considerable amount of iron oxide is present. We cannot neglect the contribution of this proposal in identifying the event responsible for Peak II. A more fundamental approach to identifying Peaks I and II is described below.

During bulk isothermal oxidation, wax is desorbed from the spent catalyst, which deposits on the cooler parts of the tube as well as transfer lines. However, Soxhlet extraction fails to remove the material associated with Peak I which was initially ascribed to hydrocarbonaceous material, largely on the basis of CHN analysis (Table 3.3). It was therefore shown that the extraction process is inefficient and that the subsequent change in the TPO profile of the catalyst after extraction is associated with oxidation that occurs during extraction. This raises the question of the nature of hydrocarbons associated with Peak I. The following studies were therefore performed.

CHN microanalysis of the different samples before and after the oxidation and desorption treatments is key in determining the amount of carbon and hydrogen present at each stage. The total carbon and hydrogen content

measured on the Pilot Plant sample was found to be 68.01 % and 4.49 %, respectively. After performing a thermal desorption treatment at 550 °C to remove the adsorbed wax on the catalyst, the carbon content increases to 73.66 % and the hydrogen decreases to 1.70 %. This suggests that the method of analysis underestimates the carbon content when wax is present on the catalysts. This can be attributed to the wax blocking the pores of the catalyst, thereby interfering with the combustion of carbonaceous material by means of mass transport limitations. However, due to the excessively high temperature at which the thermal treatment was performed, thermal cracking of the soft carbon or wax to form hard carbon (instead of desorption) cannot be excluded. The desorbed wax was also characterised by microanalysis, yielding a carbon content of 85.03 % and hydrogen content of 14.48 %. This may represent an aliphatic hydrocarbon with a relatively low degree of unsaturation.

The location of the wax was investigated by Brunauer-Emmett-Teller (BET) surface area analysis. It has been reported that the surface area of the fresh catalyst after activation (reduction) is 5-15 m^2/g (Steynberg, 2004). BET was applied to the characterisation of the equilibrium catalyst obtained from the Pilot Plant reactor. It was shown that the surface area of these materials is very low (4 m^2/g). Once the catalysts were subjected to thermal desorption, it was found that the measured surface areas increased to about 20 m^2/g. This confirms that the wax had probably become trapped within the pores of the carbonaceous matrix because these molecules condense in the pores under normal Fischer-Tropsch conditions.

GC-MS of the desorbed material indicates the presence of a homologous series of paraffinic material in the C_{10} – C_{20} range in addition to a mixture of oxygenates. It should be noted that higher masses may be present but the technique only allows temperatures of up to 350 °C in order to minimise column bleed. TPO was also used to investigate Spent Cat-2 after wax desorption in order to verify that this wax-like material is associated with Peak I. TPO analysis of the material following desorption at 450 °C (Figure 3.12)

shows that Peak I is significantly diminished confirming the original assignment of Peak I being associated with hydrocarbons.

Identification of this wax during TPO suggests that there are two competing processes i.e. thermal desorption and temperature programmed oxidation occur simultaneously. While oxidation should be quite easy to detect, desorption products will not necessarily be sufficiently volatile to be detected. We have observed that the instrument becomes blocked with these materials over time.

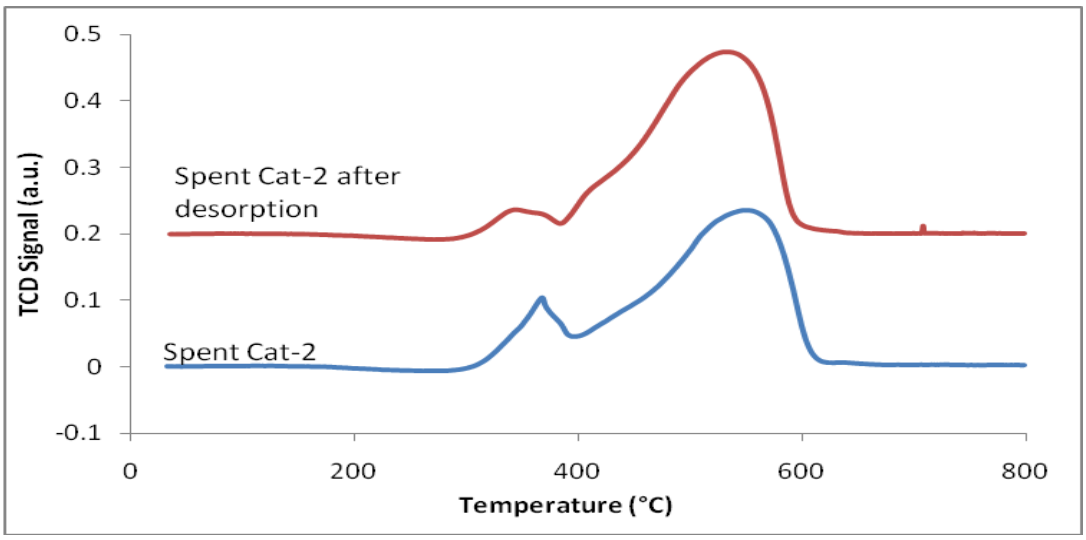

Figure 3-12: Temperature-programmed oxidation of Spent Cat-2: a spent iron Fischer-Tropsch catalyst recovered from the Pilot Plant reactor before and after thermal desorption at 340 °C. Standard TPO: heating rate 10 °C/min in 10% O_2/He

The TCD profile of Spent Cat-1 can be better understood by studying the C, CH_3, H_2O, CO and CO_2 traces represented by 12, 15, 18, 28 and 44 Da cations from the mass spectrometer, respectively. This data is presented in Figure 3.13. Peak I is mainly associated with CH_3, which suggests fragments produced from hydrocarbons desorbing from the surface of the catalyst. Monitoring for larger hydrocarbon fragment ions was complicated due to ambiguity in the assignment. Furthermore, observation of some deposition of the heavier hydrocarbons in the instrument indicates that these materials are not likely to reach the detectors. This confirms the observations made by CHN

and GC-MS of the desorbed material responsible for Peak I as mainly saturated hydrocarbons.

Peak II corresponds to mainly H_2O and also some CO_2 production, indicating a high H:C ratio in the hydrocarbon species being combusted. This suggests that these hydrocarbons are not readily desorbed from the catalyst at Peak I and are therefore still present on the spent catalyst for oxidation at this temperature. Alternatively, it could be argued that this species is readily oxidised due to higher reactivity as in unsaturated light hydrocarbons. Finally, these species might be trapped within the catalyst pores. It is also possible that Peak II represents the evaporation of product water, since more H_2O is detected and the H_2O and CO_2 traces do not have the same shape. Regarding the postulate of Peak II being associated with a dehydration process, it is expected that the equilibrium catalyst removed from the SAS reactor still contains products. Upon cooling, the heavier hydrocarbons and water condense within the pores of the catalyst. The thermal energy supplied during TPO is likely responsible for the release of these FT products. Spent Cat-2 is different in the sense that flow is switched to N_2 at reaction temperature and is then gradually cooled. This allows the water to escape. It was previously observed that during oxidation of carbonaceous deposits, the oxidative dehydrogenation occurs at a lower temperature than the removal of carbon through CO and CO_2 (Li & Brown, 1999). This is the most likely explanation for Peak II in the TPO profile of Spent Cat-1.

Peak III is associated with CH_3, H_2O and CO_2 production, as well as CO and C which follow a similar trace to the CO_2. This indicates that these are probably fragments produced by the harsh electron ionisation method used in the MS and the CO is therefore less likely to result from partial oxidation. The fact that CH_3 is detected at two distinct temperatures suggests that the location is different for the hydrocarbons desorbing at higher temperatures. It was demonstrated earlier in this section, that wax becomes trapped within the pores.

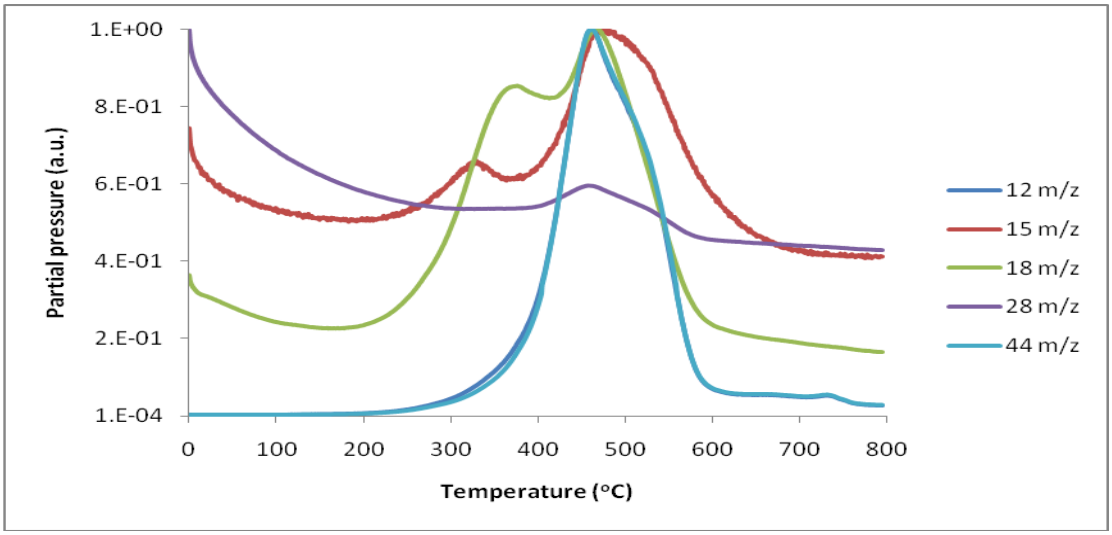

Figure 3-13: Temperature-programmed oxidation-mass spectrometry traces of selected ions generated during a standard TPO of Spent Cat-1: a spent iron Fischer-Tropsch catalyst recovered from the SAS reactor. Standard TPO: heating rate 10 °C/min in 10% O_2/He

The CH_3 trace (Figure 3.14) can be used to explain the major differences between Spent Cat-1 and Spent Cat-2. The other traces from the MS data of Spent Cat-2 are quite similar to those of Spent Cat-1 and are therefore not shown. While Spent Cat-1 has hydrocarbons desorbing at two temperatures, Spent Cat-2 only has a very intense CH_3 desorption at the temperature range of Peak I. Since Spent Cat-2 has experienced a shorter time under HTFT conditions, it is possible that the hydrocarbons that are slightly more resistant to desorption have not yet formed after 5 days on-stream. This idea could be used to explain the absence of a CH_3 peak in the temperature range of Peak III.

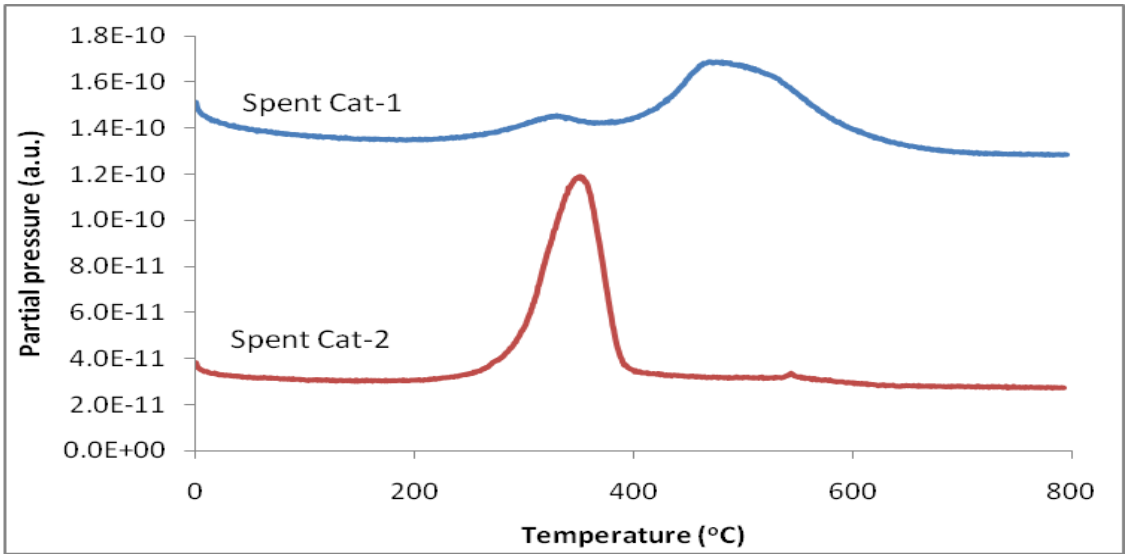

Figure 3-14: Temperature-programmed oxidation-mass spectrometry trace of 15 m/z representing CH_3^+ ion of Spent Cat-1 (recovered from the SAS reactor) and Spent Cat-2 (recovered from the Pilot Plant reactor)

TPO often forms the basis of quantitative interpretations reported in the literature (Fung & Querini, 1992). However, simultaneous thermal desorption and partial oxidation processes complicate attempts to perform quantitative analysis. Quantitative X-ray photoelectron spectroscopy (XPS) of the samples after oxidation indicates that the atomic percentage of oxygen is increased on the surface of the catalysts oxidised at 340 and 450 °C (Table 3.7). This suggests that partially oxidised carbonaceous species are present on the surface of the catalyst.

Table 3-7: Atomic percentages of Spent Cat-1 before and after oxidation at 340 °C and 450 °C determined by quantitative XPS

Sample	Fe (%)	C (%)	O (%)
SAS	1.2	89.3	8.2
Ox 340 °C	5.7	70.4	22
Ox 450 °C	21.1	19.8	52.4

In summary, the catalyst is characterised by five events including one desorption and four oxidation steps. These are assigned as follows: I represents desorption of hydrocarbons; II is associated with oxidative dehydrogenation of hard carbon; III represents the combustion of hard carbon and carbide phases and IV and V are iron phase transformations to hematite.

3.2.2 Structure of Spent High Temperature Fischer-Tropsch Catalysts

Particles of the equilibrium catalyst recovered from the SAS reactor are illustrated in a SEM image in Figure 3.15. Energy-dispersive X-ray spectroscopy (EDX) reveals that the small particles have higher carbon content than the large particles. This is presented in Figure 3.16. The results should only be interpreted semi-quantitatively for these inhomogeneous powdered samples, since the signal strength (in eV) for a particular element depends on the angle at which the X-ray beam impacts the particle. The particles of different size are apparent in the SEM image and some of the particles seem to have a soft overlayer as seen in the close-up image of the surface of a large particle (Figure 3.15(b)).

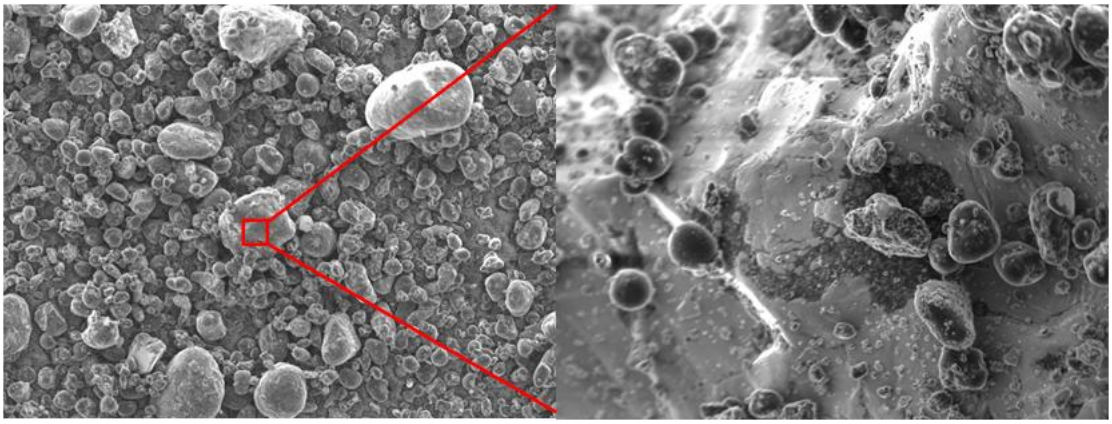

Figure 3-15: Scanning electron microscopy image of Spent Cat-1 (spent iron Fischer-Tropsch catalyst recovered from the SAS reactor) particles of various sizes (left) and close-up of the surface of a large particle (right). JEOL JSM-5600, voltage: 5 kV, working distance: 6 mm

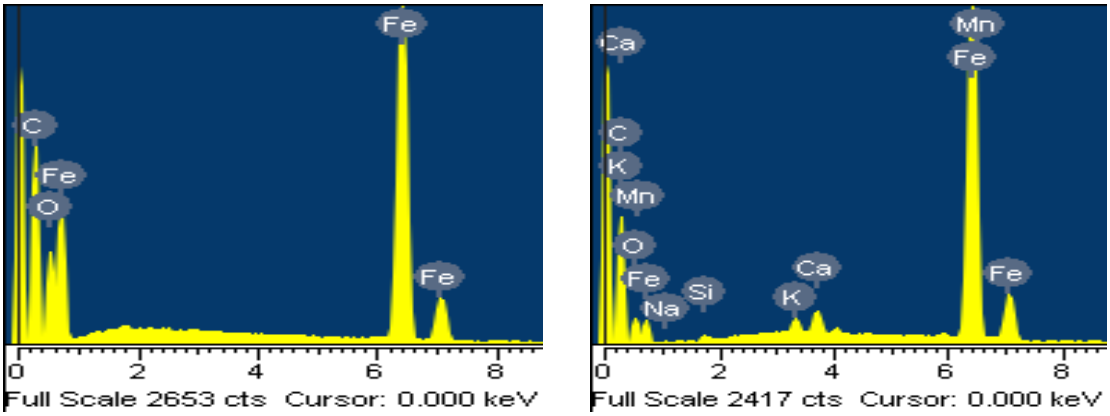

Figure 3-16: Energy dispersive X-ray spectra of large (left) and small (right) particles of Spent Cat-1 (recovered from the SAS reactor). Oxford INCA Energy 200, 20 kV, 25 mm

Figure 3.17 indicates that the particles of Spent Cat-2 have a distribution of particles of different size. The surface of this catalyst does not appear identical to Spent Cat-1 and the fines on the surface are fewer.

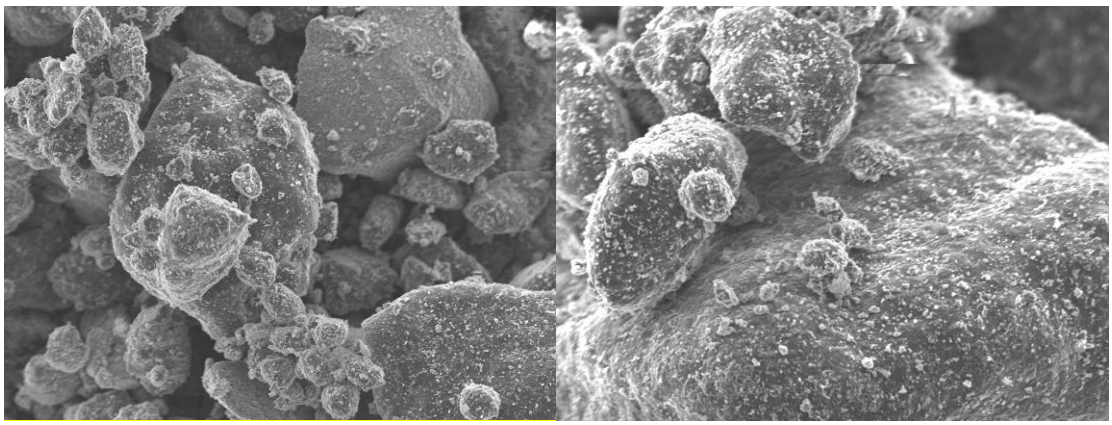

Figure 3-17: Scanning electron microscopy images of Spent Cat-2 (spent iron Fischer-Tropsch catalyst recovered from the Pilot Plant reactor) particles

In order to assess the validity of the assignment of the structure, a Spent Cat-1 sample was fixed in resin and polished. The advantage of this technique is that the internal structure can be scrutinised. SEM imaging of such a particle is shown in Figure 3.18. This clearly shows a core-shell structure, but with the added complexity of the presence of several cores within the larger particles separated by veins.

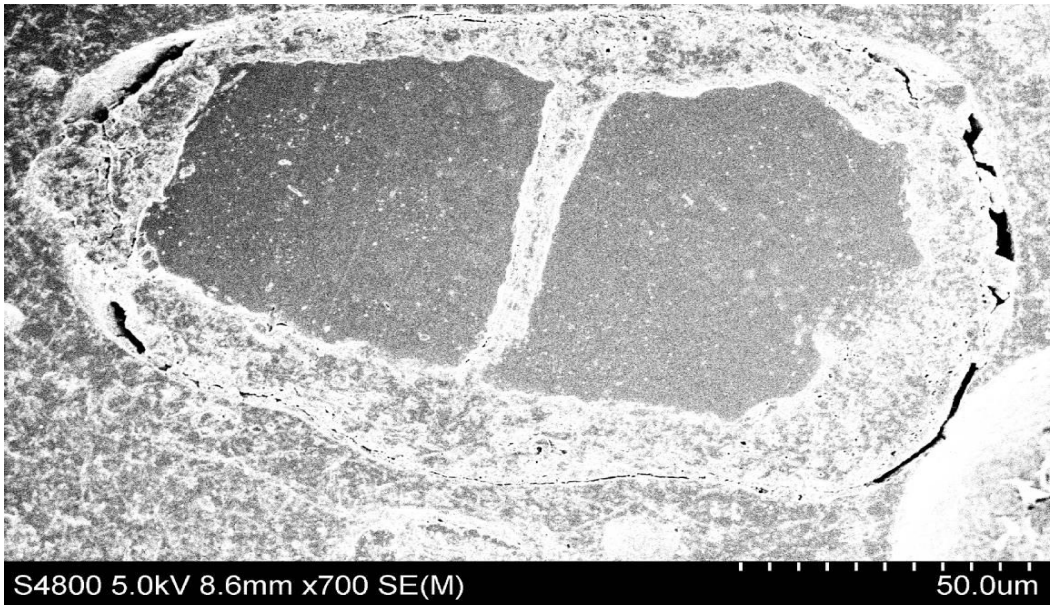

Figure 3-18: Scanning electron microscopy image of polished segment of Spent Cat-1 (spent iron Fischer-Tropsch catalyst recovered from the SAS reactor) particle. Hitachi S4800 SEM, 5 kV, 8.6 mm

It is postulated that during preparation of the catalyst, crushing of the particles leads to single grains or large particles comprised of several grains, where these grains are separated by promoter-rich silicate boundaries. Optical microscopy combined with Raman mapping of polished Spent Cat-1 particles fixed in resin clearly shows small particles made up of a single grain and larger particles comprised of several grains separated by carbon-rich grain boundaries (Figure 3.19). The individual grains appear to have a magnetite core (green) and carbonaceous material (red) as the shell. From the Raman map of the used catalyst, FTS appears to initiate at the outer surface of the particle and from the grain boundaries containing a high concentration of promoter elements.

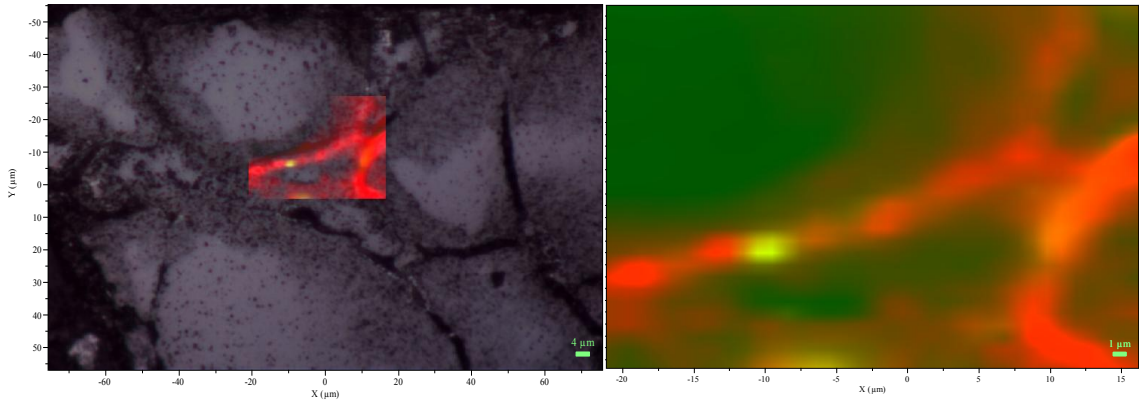

Figure 3-19: Raman map of polished segment of Spent Cat-1: a spent iron Fischer-Tropsch catalyst recovered from the SAS reactor. Carbonaceous material is shown in red and the magnetite in green

The polished catalyst samples were investigated using Backscattered Scanning Electron Microscopy (BSEM) in order to observe the contrast between the various phases present. The visibility of iron carbide should then depend on the size and location of the crystallites, the energy of the incident electrons and the size of the electron probe (Liu, 2000). Since it is known from Raman mapping experiments that the core of the grain consists of magnetite while the shell is mostly carbonaceous, the latter seemed to be the most likely location for carbide crystallites. It should be borne in mind that iron carbides are not Raman active; if this phase was present within the magnetite phase, the magnetite map would be expected to appear at a lower intensity in the regions where these carbides occur. Figure 3.20 shows an image of a partially reacted catalyst particle from the SAS reactor. There appears to be a sharp contrast between the mass of free carbon and some crystallites, which are believed to be carbides, nestled in the carbonaceous matrix. This corresponds to the findings of Caceres (2006) where Fe_5C_2 platelets were formed with a reported width of 100-300 nm and thickness of 30-50 nm by reacting syngas over α-Fe porous aggregate catalyst. These platelets were also to be found in a matrix of carbon. This demonstrates the stability of these iron carbide phases in air in the absence of passivation. Dry (1990) has also reported a magnetite core surrounded by a carbonaceous layer consisting of carbide crystallites embedded in this carbon matrix. Table 3.8 shows the phase composition of Spent Cat-1 determined by XRD and Mössbauer Absorption Spectroscopy (MAS), verifying the observation of the oxide core. The higher

carbide content measured by MAS reveals that there are small carbide crystallites present that cannot be detected by XRD.

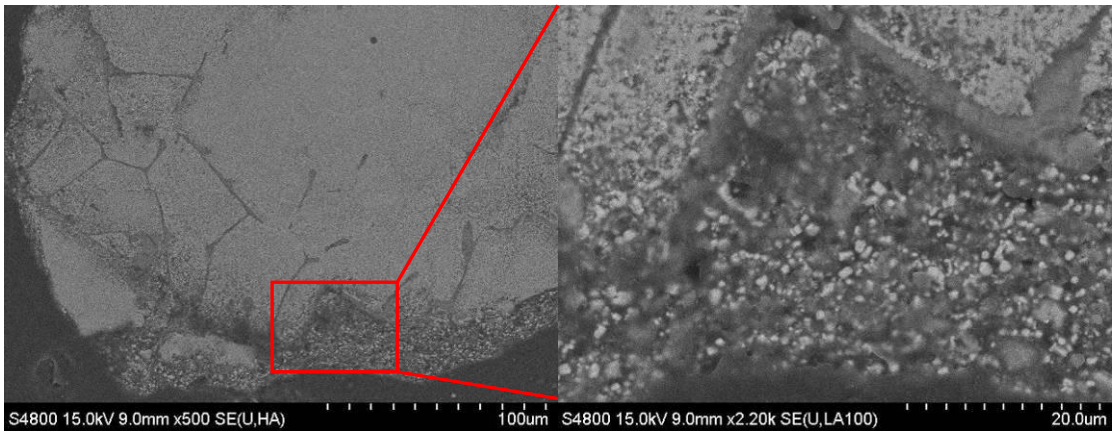

Figure 3-20: Backscatter scanning electron microscopy image of polished segment of Spent Cat-1 (spent iron Fischer-Tropsch catalyst recovered from the SAS reactor) particle (right) and close-up of carbonaceous region (left)

Table 3-8: Relative abundances (m/m %) of constituent phases of Spent Cat-1 determined by XRD and MAS

	Conditions (T, B_{app})	**Magnetite**	**Hägg carbide**	**Fe carbide**
XRD	-	74.1	23.8	2.1
MAS	298K, 0 T	61 ± 2	37 ± 2	2 ± 1
MAS	4.2 K, 0 T	54 ± 2	46 ± 2	-
MAS	4.2 K, 10T	56 ± 2	44 ± 2	-

BSEM images of the polished catalyst particles in resin (Figure 3.21) illustrate that Spent Cat-2 particles have no visible iron oxide core after 5 days on stream. This contradicts phase analysis data (Table 3.9) which indicates that there is still a considerable amount of magnetite present. The magnetite is probably present within the carbonaceous matrix. The size of the carbide crystallites measured in this image indicates that they are between 300 and 800 nm in diameter.

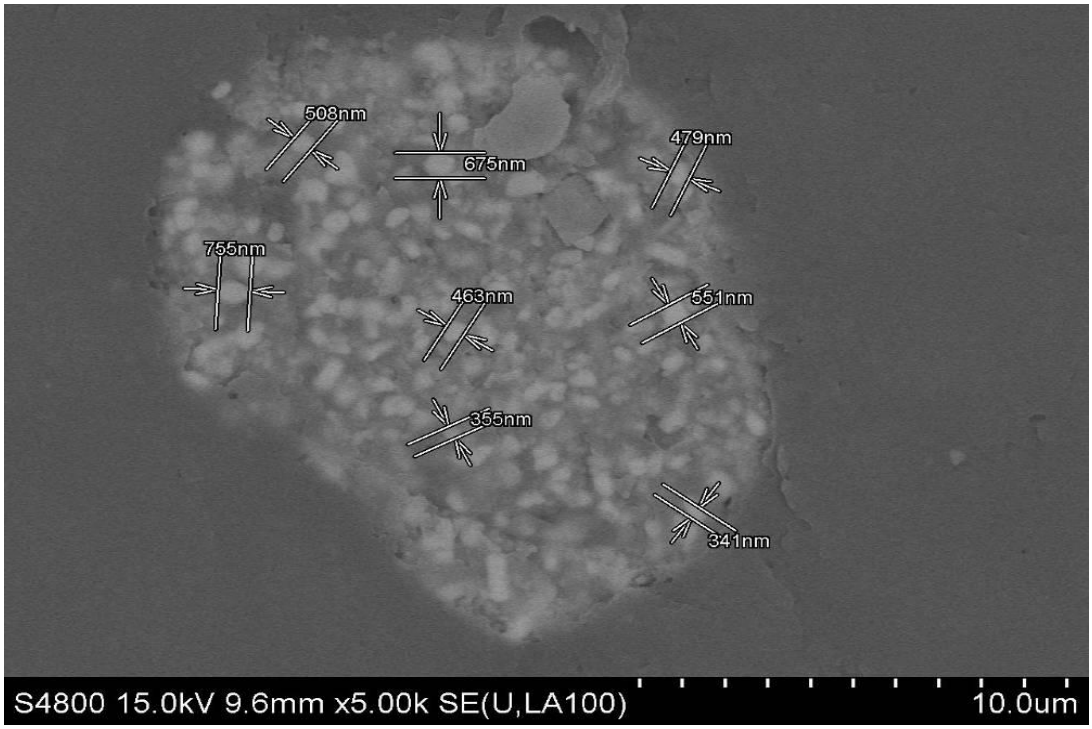

Figure 3-21: Backscatter scanning electron microscopy image of polished segment of Spent Cat-2: a spent iron Fischer-Tropsch catalyst recovered from the Pilot Plant reactor

Table 3-9: Relative abundances (m/m %) of constituent phases of Spent Cat-2 determined by XRD and MAS

	Conditions (T, B_{app})	Magnetite	Hägg carbide	Fe carbide	Hematite
XRD	-	49.1	46.2	4.7	-
MAS	298K, 0 T	48 ± 2	49 ± 2	-	3 ± 1
MAS	4.2 K, 0 T	51 ± 2	46 ± 2	-	3 ± 2
MAS	4.2 K, 10T	54 ± 2	43 ± 1	-	3 ± 1

3.2.3 Origin of Carbon-rich Fines

The composition of the equilibrium catalyst recovered from the SAS reactor indicates that the smaller particles are richer in carbon and carbide phases (Table 3.10 and 3.11). Quantitative XRD shows that the relative abundance of iron carbides decreases with an increase in particle size. CHN microanalysis also indicates that as the particle size increases, the amount of carbon relative to iron becomes less.

Table 3-10: Relative abundances (m/m %) of constituent phases of sieved Spent Cat-1 following desorption

Fraction	Magnetite	Hägg carbide	Eckström-Adcock carbide	X^2
<20 µm	59.9	37.5	2.6	2.141
20-32 µm	72.7	25.7	1.6	1.764
32-38 µm	75.4	22.9	1.7	1.312
38-45 µm	78.6	20.0	1.4	1.144
45-53 µm	80.8	17.9	1.3	1.338
53-63 µm	82.6	15.9	1.5	0.998
63-75 µm	90.2	8.5	1.3	1.017
>75 µm	88.3	9.7	2.0	0.857
PDF number	019-0629	036-1248	071-0333	-

Table 3-11: Relative abundances (m/m %) of carbon and hydrogen in the various Spent Cat-1 fractions

Fraction (µm)	C	H
<20	25	0.7
20-32	20.21	0.52
32-38	16.72	0.39
38-45	15.75	0.4
45-53	13.46	0.31
53-63	11.63	0.26
63-75	9.95	0.24
>75	8.41	0.17

3.3 Discussions

The aim of this chapter was to determine the composition of a typical spent Fischer-Tropsch catalyst. The catalysts studied herein were an equilibrium catalyst (recovered from the Sasol Advanced Synthol (SAS) reactor) and a sample where all the particles had experienced the same length of time on-stream (recovered from the Pilot Plant reactor). The approach was to use a combination of sequential Temperature-programmed oxidation (TPO) along with X-ray diffraction (XRD) and Raman spectroscopy. It was found that the spent catalyst consists of hydrocarbons, hard carbon, iron carbides and iron oxide.

A further aim was to determine the structure of a spent Fischer-Tropsch catalyst. The structural evolution of the catalyst reveals the mechanism of

catalyst break-up, and is therefore an important part of the study. This was investigated by a combination of imaging techniques. A core-shell structure was observed, where the core consists of magnetite while the shell is comprised of a hard carbon matrix with embedded iron carbide crystallites and wax. Carbon-rich fines were identified and their origin was related back to the catalyst preparation method.

The phase composition of the as-received high temperature Fischer-Tropsch (HTFT) catalyst from the SAS reactor was determined by XRD. The results indicate that magnetite and Hägg carbide are the main phases present, while some Eckström-Adcock carbide was also observed. Magnetite and Hägg carbide are associated with most iron-based catalysts during and after Fischer-Tropsch synthesis (FTS) (Ning *et al.*, 2006; Reymond *et al.*, 1982; Shroff *et al.*, 1995; Bukur *et al.*, 1995a; Zhang *et al.*, 2004; Jin & Datye, 1998a), irrespective of whether the studies were conducted on catalysts used for the low- or high-temperature FTS regimes. Additional iron carbide phases frequently observed by XRD are $Fe_{2.2}C$ and Fe_3C, depending on the reaction conditions and nature of the iron catalyst (Niementsverdriet *et al.*, 1980) as well as the size of the iron particles (Raupp & Delgass, 1979b; Jung *et al.*, 1982). Fe_7C_3 is not commonly found in spent FT catalysts, but has previously been observed by Mansker *et al.* (1999) and Hayakawa *et al.* (2006) in their catalysts. Mansker and co-workers performed their experiments in a slurry reactor using precipitated catalysts and found Fe_7C_3 to be the major phase. The catalysts were activated in H_2 or CO at 280 °C, 0.78 MPa for 8 h, and subsequently reacted in syngas with a H_2/CO ratio of 2/3 at 260 °C, 1.48 MPa. Transformation of this phase to Fe_5C_2 was ascribed to a loss in catalyst activity. Hayakawa and co-workers only found Fe_7C_3 in a copper-free catalyst after reaction. The catalyst was reduced in a slurry phase for 3 h at 300 °C, 0.1 MPa in syngas with a H_2/CO ratio of 1. FTS was performed at 260 °C, 2 MPa and the H_2/CO ratio was also 1 in this case. These authors, however, postulated that Fe_7C_3 was less active than Fe_5C_2. It appears from these reports that Fe_7C_3 is only formed in significant amounts when the H_2/CO ratios are relatively low. This is related to the rate at which carbon dissociates and

the subsequent rate of conversion to hydrocarbon products. In a hydrogen-lean environment the rate of hydrocarbon synthesis is limited by the availability of hydrogen on the surface, thereby favouring the incorporation of carbon into the bulk of the catalyst and deposition of carbon on the catalyst surface. This is also in line with the competition model proposed by Niemantsverdriet and van der Kraan (1981). The catalyst becomes increasingly oxidised after each oxidation treatment, but the additional iron oxide phases do not reflect the phase composition of a typical spent catalyst.

It should be noted that careful passivation of an iron-based Fischer-Tropsch catalyst is normally necessary for ex-situ analytical studies (Shroff and Datye, 1996; Janbroers *et al.*, 2009). It is reported that carbon is freed and deposited as a separate amorphous phase on oxide surfaces upon re-oxidation (Janbroers *et al.*, 2009). Since neither the Fischer-Tropsch catalysts recovered from the SAS nor the Pilot Plant reactors were passivated after reaction, it is possible that the observed amounts of magnetite were increased due to oxidation on exposure to air. However, if these iron-containing species are covered by a carbonaceous shell, we believe that re-oxidation of surface carbides will be minimised. Oxidation of the surface carbide crystallites would only result in an incremental phase transformation, since the bulk catalyst remains unchanged.

The typical TPO profile of the HTFT catalyst recovered from the SAS reactor has five peaks. The first and second events in the TPO were initially ascribed to combustion of hydrocarbons. However, failure to remove Peak I in Spent Cat-1 after Soxhlet extraction led to further investigation. It was found that oxidation of fine iron-containing particulates occurred during extraction. The TPO profile of the spent catalyst from the Pilot Plant reactor also does not have Peak II. The question of the particle size dependence of combustion temperature was raised and subsequently dismissed since a bimodal particle size distribution was not observed. It was postulated that the temperature of oxidation of hard carbon and transformation of iron carbides to iron oxides depends on the amount of carbonaceous material in contact with iron oxide,

since the presence of an oxide core catalyses the combustion of the carbonaceous species. Two distinct peaks suggest the presence of particles containing no iron oxide. The investigation was not straightforward in the catalyst from the SAS reactor, since this is an equilibrium catalyst. The catalyst from the Pilot Plant reactor suggests that this possibility cannot be discarded. BET, CHN and GC-MS investigations proved that the first event observed during TPO is due to desorption of mainly saturated hydrocarbons. TPO-MS as well as GC-MS was used to show that the second event represents the oxidative dehydrogenation of hard carbon. The other three events represent the combustion of hard carbon and phase transformations.

The approach in Section 3.2.1 relies on the ability of TPO to accurately represent all species present. While useful information could still be obtained from the temperatures at which certain events occur as well as simultaneous XRD and Raman studies, it was shown that TPO cannot be interpreted quantitatively. This limitation in the interpretation of TPO data exists in complex samples comprised of mixtures of species including volatile or oxidation-resistant materials such as saturated hydrocarbons or polyaromatic hydrocarbons. This is because quantitative interpretation of the amounts of CO_2 and H_2O produced during combustion would be erroneous i.e. not all of the carbonaceous material present combusts to form these products; some of it is desorbed. This can be partly overcome by introducing a thermal desorption step in the catalyst characterisation which would remove the saturated hydrocarbons and facilitate the oxidation of unsaturated species i.e. the use of TGA/TPO. TPO is a simple technique but it should be borne in mind that interpretation can be rather complex when other processes are competing with oxidation.

Raman spectroscopy presents an idea of the structure of the spent catalyst particles from the SAS reactor. The iron oxide core is completely enveloped by the carbonaceous overlayer and only an oxidation treatment to 340 °C reveals the iron oxide core (Section 3.2.1.2). It was therefore postulated that the catalyst has a core-shell type structure. It is known from XRD that the

catalyst is composed of iron oxide and iron carbide, while TPO has indicated the presence of hard and soft carbon. A core-shell structure has been proposed previously for iron-based FT catalysts (Li *et al.*, 2001; Davis, 2009; Dry, 1990). The structure of a single grain of spent HTFT catalyst can therefore be depicted as shown in Figure 3.22 below. The magnetite core is surrounded by a carbonaceous overlayer. Iron carbide crystallites can be found within this overlayer. The carbonaceous matrix is also porous and wax becomes trapped within these pores.

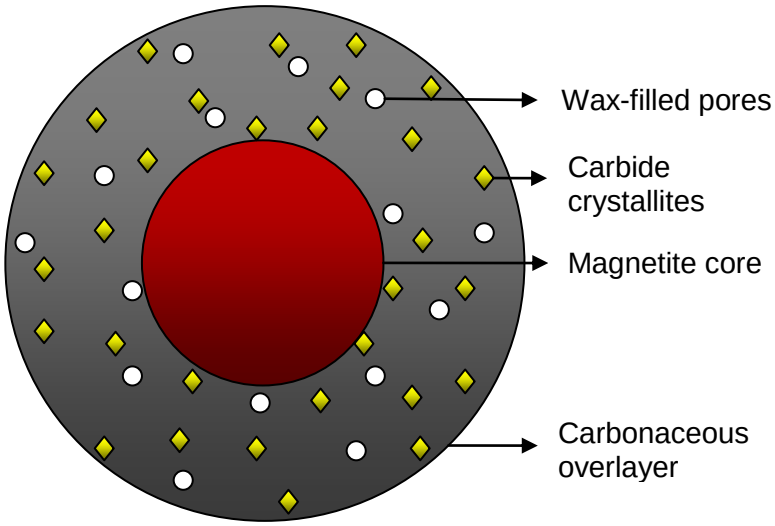

Figure 3-22: Schematic of a typical spent HTFT catalyst grain. Several grains are often grouped together in larger particles and are separated by grain boundaries

The origin of this structure can possibly be linked back to the evolution of the catalyst when it is exposed to HTFT conditions. After catalyst activation the outer layers are reduced to metallic iron, while the core remains oxidic. Upon exposure to syngas the iron is transformed to highly dispersed iron carbides due to the reducing atmosphere (Li *et al.*, 2002). During FTS, reactants are transported to active sites within the catalyst where they react to form hydrocarbons and water as products (Davis, 2009; Dry, 1990). These researchers offer re-oxidation as the most likely explanation for a magnetite core. The shell contains various iron carbide phases and hard carbon with adsorbed hydrocarbons.

Section 3.2.3 presents data showing that smaller particles are richer in carbon and iron carbide phases. This raises the question of the origin of these carbon-rich fines. The milled fresh catalyst already contains fine particles since a particular particle size distribution is required for fluidisation purposes within the reactor. In this fine fraction there are also separate alkali-silicate particles that break away from the particles during milling (Steynberg, 2004). Since the small particles have a higher surface area per unit mass and are therefore richer in promoter elements, it is to be expected that Fischer-Tropsch activity and subsequently also the rate of carbon deposition would be enhanced on these particles. It is well accepted that potassium leads to an increased rate of carbon deposition (Kölbel *et al.*, 1951; Anderson *et al.*, 1952; Dry, 1981; Bonzel & Krebs, 1981; Arakawa & Bell, 1983; Bukur *et al.*, 1990). This is one possible mechanism for the formation of carbon-rich fines within the reactor. The alternative mechanism in the formation of these carbon-rich fines is through chemical and physical attrition processes, which would result in the formation of carbide crystallites and also particles breaking along the brittle carbonaceous grain boundaries.

Essentially these two mechanisms both have their origin in the manner in which the catalyst is prepared. The particle size distribution and inhomogeneous incorporation of promoter elements originates from the sample preparation method where the molten iron and silicate-rich promoter oxide mixture is rapidly cooled in ingots. The cations of added structural promoters (Al_2O_3, MgO, etc.) enter into solid solution in the magnetite phase (Dry, 1981). An Al^{3+} ion can replace Fe^{3+} and Mg^{2+} can replace Fe^{2+} in the magnetite lattice, for instance, and are therefore atomically dispersed in the magnetite. The promoter-rich silicate phase does not form a solid solution with the iron oxide phase, resulting in this material being forced towards the grain boundaries between the iron oxide crystallites when it solidifies. Similarly, potassium ions are too large to fit into the magnetite lattice structure. Subsequent crushing and grinding of the fused catalyst then leads to higher promoter levels per mass of iron on the smaller particles as verified by this investigation.

The formation of iron particles with promoter-rich inclusions during catalyst preparation creates weaknesses in the structure since these silicate-rich inclusions are brittle compared to the iron phase. During grinding the particles would therefore preferentially break along these inclusions. Small particles with individual grains (promoters on the surface) and large particles consisting of an agglomerate of grains (promoters on surface and along the inclusions) can be formed. In the case of the large particles, the catalytic reaction will be initiated at the promoter-rich sites, thereby creating weak points and this again occurs along the grain boundaries. The carbon-rich grains will therefore be easily broken off, creating carbon-rich fines. Designing a catalyst with a uniform distribution of promoter elements throughout the particle would be a fair attempt at circumventing the production of fines during the HTFT process. However, the fluidisation dynamics need to remain the same in the reactor.

The formation of carbon-rich fines is strongly associated with the drop in productivity in the SAS reactor (Dry, 1990). We have proposed a simplified model for the evolution of particle structure in the SAS reactor (Figure 3.23). The activated catalyst particles in the reactor are initially mostly metallic iron. In the FTS environment, these metallic iron atoms are rapidly transformed into highly dispersed carbide phases (Dry, 1981, Li *et al.*, 2002). The carbides form as nanometer sized crystallites and stick to the core because of the carbonaceous matrix. These carbide particles form the site of Fischer-Tropsch synthesis, therefore adsorbing reactants and catalytically transforming them into hydrocarbon products and water (as a by-product). These are then desorbed from the catalytic sites. As the hydrocarbon species on the surface grow to long-chain hydrocarbons, they are less easily desorbed from the catalytic sites. The water also becomes trapped by dense carbide layers (Li *et al.*, 2001), amorphous carbon (Sarkar *et al*.; 2007) or heavy wax products (Gormley *et al.*, 1997) within these catalyst particles. This leads to gradual oxidation of the particles. The iron carbides on the surface serve as sites for carbon enrichment, either within the metal lattice to form carbon-rich iron carbides or as hard carbon deposits. These carbon-rich sites lead to stress

within the catalyst particle resulting in breakage of these grains from the rest of the particle. This leads to large particles that are rich in magnetite and small particles rich in carbides and carbonaceous deposits.

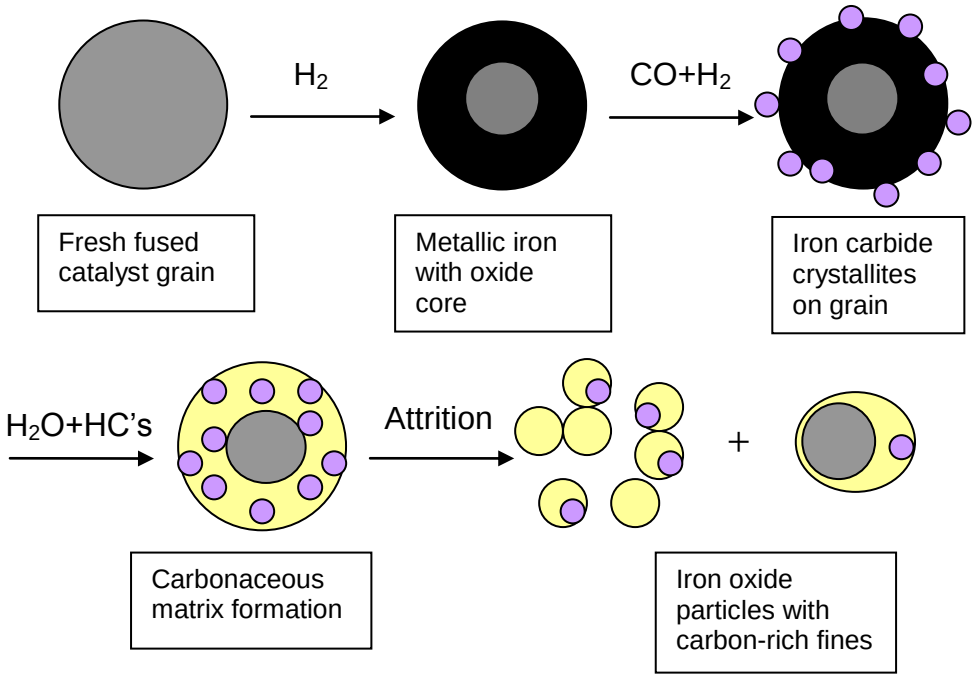

Figure 3-23: Simplified model of evolution of catalyst in HTFT synthesis. Phase transformations and the build-up of carbon is inherent to the process, which ultimately leads to attrition

Similar models have been proposed in the literature for the evolution of iron-based catalysts (Shroff *et al.*, 1995; Davis, 2009; Dry, 1990; Li *et al.*, 2002). The rate of carbide formation and size of these crystallites is affected by the presence of a potassium promoter (Li *et al.*, 2002). The formation of carbon-rich fines is mostly ascribed to attrition and is also observed in a precipitated catalyst. This suggests that the preparation method for a fused catalyst perhaps contributes to physical attrition, while the formation of iron carbide

crystallites and carbonaceous deposits plays a role in the corrosion or chemical attrition of most iron-based catalysts. While it is easy to understand physical attrition as the preferential breakage of particles along grain boundaries during fluidisation, chemical attrition perhaps requires further clarification. In the carbidisation process, it is known that carbon is rapidly

deposited and taken up in the metallic phase, which leads to supersaturation of the metal at the metal-carbon interface (Grabke *et al*., 2001). Small interstitial carbide crystallites are formed at the sites where the carbon comes into contact with an iron atom. The carbide crystallites are enveloped by deposited carbon. This carbon-rich environment then leads to decomposition of the carbides, resulting in iron crystallites embedded in the carbonaceous matrix. These metallic sites promote further carbon uptake, leading to continued carbon deposition. This carbidisation therefore results in corrosion, which is the break-up of bulk metal into metal powder. This occurrence is hence commonly termed metal dusting, the inhibition of which will be discussed in Section 5.3. This process decreases the structural integrity of the particle and facilitates physical attrition. During fluidisation, attrition can therefore not only occur along grain boundaries, but also shatter the carbonaceous matrix resulting in the formation of carbon- and carbide-rich fine particles.

3.4 Concluding remarks

The composition of a spent iron-based Fischer-Tropsch catalyst recovered from Sasol reactors has been determined by systematically using Temperature-programmed oxidation (TPO) with several complementary bulk and surface characterisation techniques. This approach of determining catalyst composition had several challenges. The typical catalyst recovered from the Sasol Advanced Synthol reactor exhibits five peaks in a TPO profile each representing a desorption/oxidation event. The TPO profiles cannot be interpreted quantitatively, since partial oxidation and thermal desorption occur simultaneously. The catalyst is comprised of adsorbed hydrocarbons, hydrogen-deficient carbonaceous species, iron carbides and iron oxides.

The structure of the catalyst has been determined by several imaging techniques along with Raman mapping. It was initially proposed that the spent catalyst has a core-shell type structure, but this was found to be a simplified model of the true structure. From the way in which the fused catalyst is

prepared, the catalyst particles can be made up of several grains separated by promoter-rich veins. The reaction initiates at the surface of the catalyst and along the grain boundaries that are high in promoters and so transform to a mixture of hard carbonaceous material and iron carbides surrounding a magnetite core. The carbides crystallites embedded in the carbonaceous shell were observed by Backscatter Scanning Electron Microscopy. A model for the evolution of a catalyst structure of the high temperature Fischer-Tropsch catalyst is proposed, explaining the evolution of the catalyst throughout the lifetime of the catalyst. The origin of carbon-rich fines is attributed to physical and chemical attrition processes, inherent to the catalyst preparation method and iron-catalysts, respectively. This is directly linked to the observed drop in productivity on the Sasol Advanced Synthol reactors.

4. THE NATURE OF CARBONACEOUS SPECIES

4.1 Introduction

Catalysts employed in the production or transformation of hydrocarbons are often prone to deactivation by coke. The formation of coke also occurs in high temperature Fischer-Tropsch (HTFT) catalysts (Dry, 2004). However, it is worth specifying that a loss of activity with the formation of coke is not observed in HTFT synthesis on the basis of micro-reactor studies. Instead, we believe that the catalysts experience a drop in productivity due to changes in fluidisation dynamics, which leads to a decrease in the mass of catalyst found in the optimal temperature zone for FTS. Regardless, the process of hard carbon formation leads to changes in the physical characteristics of the catalysts, which ultimately requires catalyst replenishment. The cost involved in the purchase of fresh catalysts could be significantly reduced if the build-up of coke could be prevented. In order to understand the mechanism of this carbon formation, the chemical nature of the carbonaceous species must first be determined.

Carbonaceous deposits which form on Fischer-Tropsch catalysts within the HTFT process are structurally complex and can be comprised of adsorbed products, hydrogen-deficient amorphous and graphite-like carbon. A wide range of techniques have been applied to the study of carbonaceous material. Several techniques including Raman spectroscopy, X-Ray Photoelectron Spectroscopy (XPS) and High Resolution Transmission Electron Microscopy (HRTEM) are often employed to determine the chemical structure of carbonaceous species, while Thermogravimetry and Temperature Programmed Reduction (TPR) or Oxidation (TPO) are employed to determine the quantity and reactivity of these materials. Several complementary techniques are in fact required to obtain an accurate depiction of the nature of carbonaceous deposits.

Carbonaceous material deposited in catalytic systems similar to the HTFT process has been studied by XPS and Auger Electron Spectroscopy (AES)

(Krebs *et al.*, 1979; Ott *et al.*, 1980; Bonzel & Krebs, 1980; Bonzel & Krebs, 1981; Reymond *et al.*, 1982; Dwyer and Hardenbergh, 1984; Loaiza-Gil *et al.*, 1999; Shroff *et al.*, 1995; Bukur *et al.*, 1995a; Butt, 1990; Riedel *et al.*, 2003; Jin *et al.*, 2002), High Resolution Transmission Electron Microscopy (HRTEM) (Helveg *et al.*, 2004; Jin and Datye, 2000; de la Peña O'Shea *et al.* 2006; Janbroers *et al.*, 2009; Mathieu *et al.*, 2007; Sarkar *et al.*, 2007; Park & Baker, 1999; Gherghel *et al.*, 2002; Jin *et al.*, 2002) and Raman Spectroscopy (Galuszka *et al.*, 1992; Herranz *et al.* 2006; Loaiza-Gil *et al.*, 1999; Ning *et al.*, 2006; Pijolat *et al.* 1987; de la Peña O'Shea *et al.* 2006). In all these studies, the presence of graphitic material was reported to be deposited on the surface of the spent catalysts.

It is worth noting that the spectroscopic tools described herein are typically not developed for the study of structurally complex carbonaceous material, which proves to be a challenge in its own right. Thus, a significant amount of technique development has formed a necessary part of the work described in this chapter. This development, together with the often overlooked shortfalls of several characterisation methods will be described in detail.

4.2 Results and Discussion

4.2.1 The Nature of Carbonaceous Deposits on HTFT Catalysts

The investigation of the nature of carbonaceous deposits on HTFT catalysts is complex and therefore requires the use of several techniques. Chapter 3 describes the presence of several carbonaceous species in a typical spent HTFT catalyst. The aliphatic hydrocarbons which are collectively referred to as soft carbon are adsorbed on the catalyst surface and trapped within the porous carbide/carbon structure (Section 5.2.4.2). The hard carbon is traditionally believed to be graphitic in nature (Dry, 2004), but understanding the exact nature of this material is important since this hard carbon is responsible for the observed losses in productivity in the SAS reactor.

4.2.1.1 High-Resolution Transmission Electron Microscopy

HRTEM images obtained in this study revealed lattice fringes with 3.36 Å d-spacing which corresponds to the (002) plane of graphite on Spent Cat-1 (Figure 4.1). These graphitic materials were also observed on model supported catalysts after exposure to CO (Jin & Datye, 2000). Amorphous carbon is usually located on the surface of carbide crystallites (Jin & Datye, 2000; Jin *et al.*, 2002; Janbroers *et al.*, 2009). The identification of amorphous carbon which forms on the Hägg carbide crystallites ($d_{(310)}$ = 2.93 nm) confirms the presence of this additional carbon form.

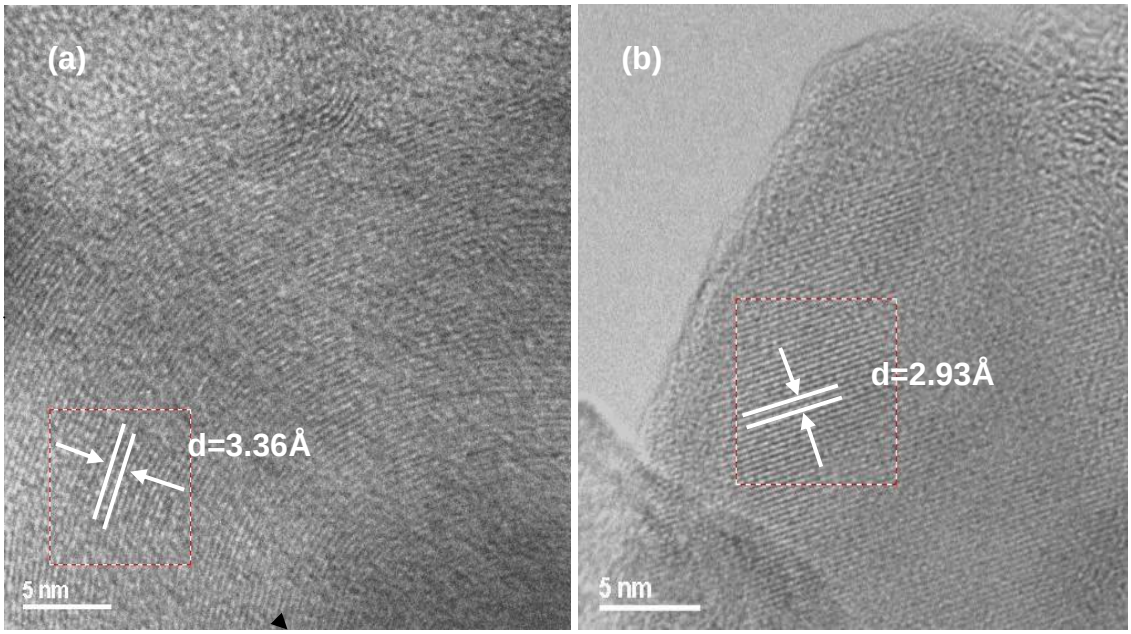

Figure 4-1: High resolution transmission electron microscopy images of Spent Cat-1 showing (a) graphitic carbon and (b) Hägg carbide and amorphous carbon. This is a spent iron Fischer-Tropsch catalyst recovered from the Sasol Advanced Synthol (SAS) reactor. JEOL JEM-2011, 200 kV

4.2.1.2 Raman Spectroscopy

Figure 4.2 shows a typical Raman spectrum of the equilibrium catalyst from the SAS reactor. The two major vibrational modes around ~1350 and ~1600 cm^{-1}, commonly termed D and G modes respectively, represent C-C bonds in deposits typically present in iron-based catalysts after exposure to CO or syngas (Herranz *et al.*, 2006). The D mode at 1350 cm^{-1} represents the level of disorder or amorphous content in carbonaceous materials (Ning *et al.*,

2006). The ordered G peak at ~1600 cm^{-1} (Lazzeri *et al.*, 2006; Piscanec *et al.*, 2007) and disordered D peak at ~1350 cm^{-1} (Ferrari & Robertson, 2000) are usually assigned to the phonons of E_{2g} and A_{1g} modes respectively. The G peak is due to bond stretching of all pairs of sp^2 atoms in both rings and chains, while the D peak is due to the breathing modes of rings (Ferrari & Robertson, 2000). Most carbonaceous materials exhibit a certain line-shape, intensity and position of D and G modes and sometimes signature peaks in addition to the D and G modes but this information becomes lost in the characterisation of mixtures of species. Raman bands of iron carbides would be expected between 200 and 600 cm^{-1} (Bi *et al.*, 1993) from Fe-C bonds. Nevertheless, the lattice vibrational modes of an iron carbide crystal are all Raman inactive (Park *et al.*, 2001).

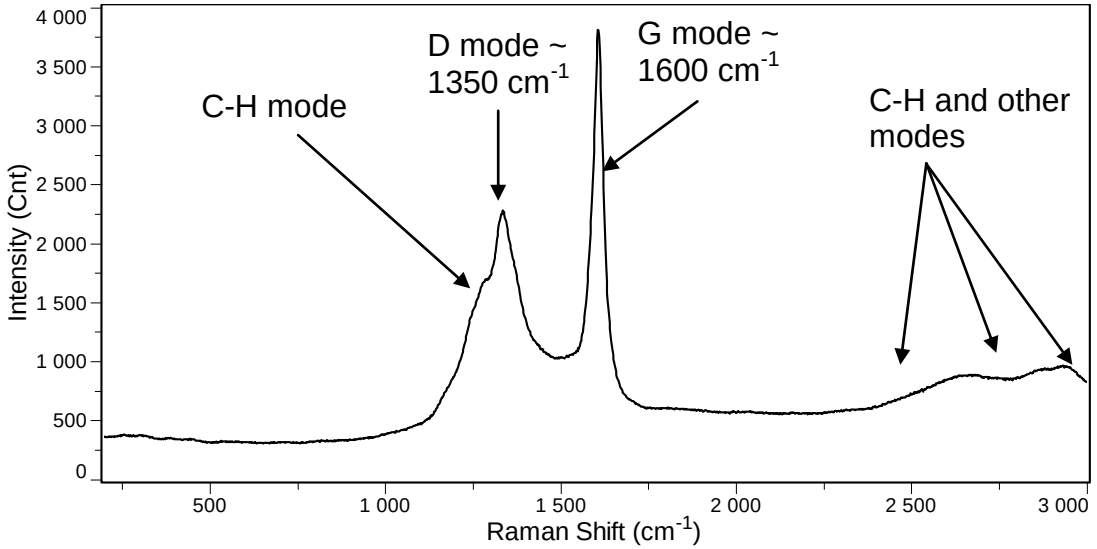

Figure 4-2: Raman spectrum of Spent Cat-1: a spent iron Fischer-Tropsch catalyst recovered from the SAS reactor. Excitation wavelength: 514 nm

Graphene is known to exhibit very characteristic Raman spectra. A typical Raman spectrum of a commercial graphite sample is presented in Figure 4.3. Verification that carbonaceous material is graphitic is obtained by the second disorder peak at ~2700 cm^{-1} (Ferrari *et al.*, 2006), which is historically named G' since it is usually the second most prominent peak after G. In an investigation by Park *et al.* (2001) where iron ores were reduced to cementite and accompanied by hard carbon formation in Ar-H_2-CH_4 gas mixtures, the G'

mode was observed but in this case no hydrocarbons were formed and the modes at 2950 and 3200 cm^{-1} were assigned to overtones and a combination of the D and G bands. However, for the study of HTFT catalysts, the presence of adsorbed hydrocarbons could possibly obstruct certain features of these materials if they were indeed present on the spent catalyst. In-situ annealing experiments of commercial graphite as well as Spent Cat-1 was therefore carried out in an inert atmosphere, and a Raman spectrum collected at several points on the heating ramp. Commercial graphite underwent this treatment and it was found that at room temperature there is a small D mode which disappears upon heating (Figure 4.4). This shows that the defects are removed by this treatment, since the G and G' modes remain. This observation supports the increase of crystallinity with annealing procedures at high temperatures (Gruber *et al*., 1994).

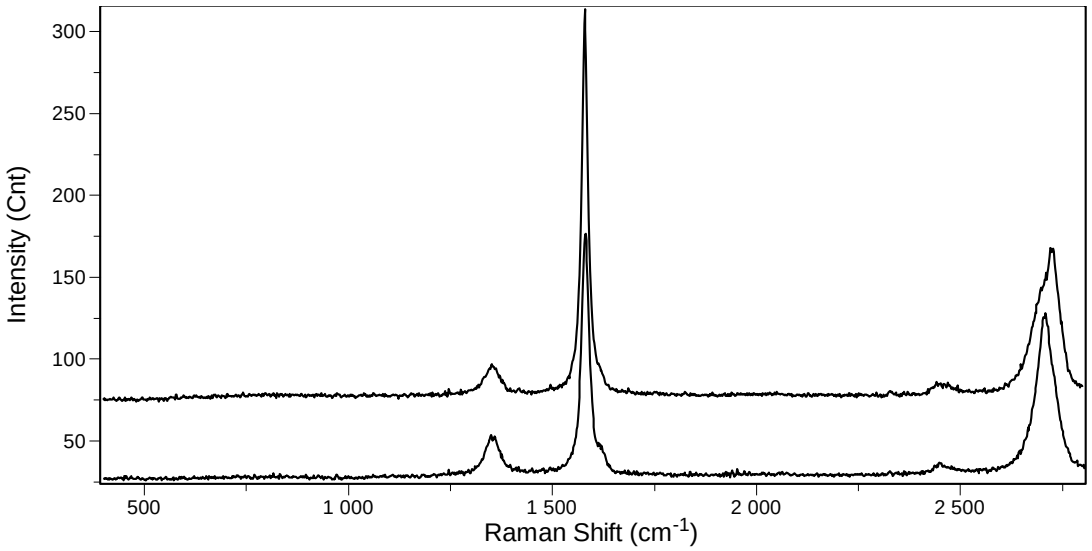

Figure 4-3: Raman spectrum of commercial graphite recorded in Ar at room temperature before (upper) and after (lower) annealing. Excitation wavelength: 514 nm

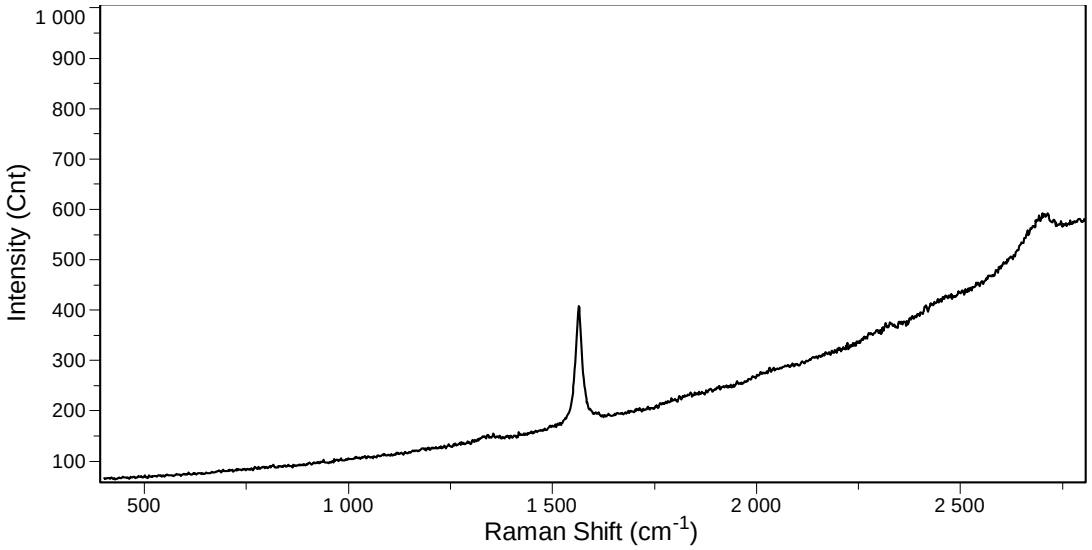

Figure 4-4: Raman spectrum of commercial graphite recorded in Ar at 800 °C. Excitation wavelength: 514 nm

In an attempt to extract additional information from the Raman spectra of Spent Cat-1, these samples were also subjected to annealing treatments. In the case of the equilibrium catalyst sample from the SAS reactor, annealing appears to remove all the bands associated with hydrocarbons (Figure 4.5). At 800 °C there are two small peaks that appear between 2400 and 2500 cm^{-1}, which disappear after cooling. The Raman spectrum of the annealed SAS after cooling down to room temperature exhibits the D, G and the G' mode. This provides evidence that the carbonaceous material on Spent Cat-1 exhibits at least some characteristics of graphitic carbon. However, since it is known that annealing increases the crystallinity of graphitic material, we cannot rule out the possibility that this spectrum is not a true reflection of the hard carbonaceous deposits on Spent Cat-1.

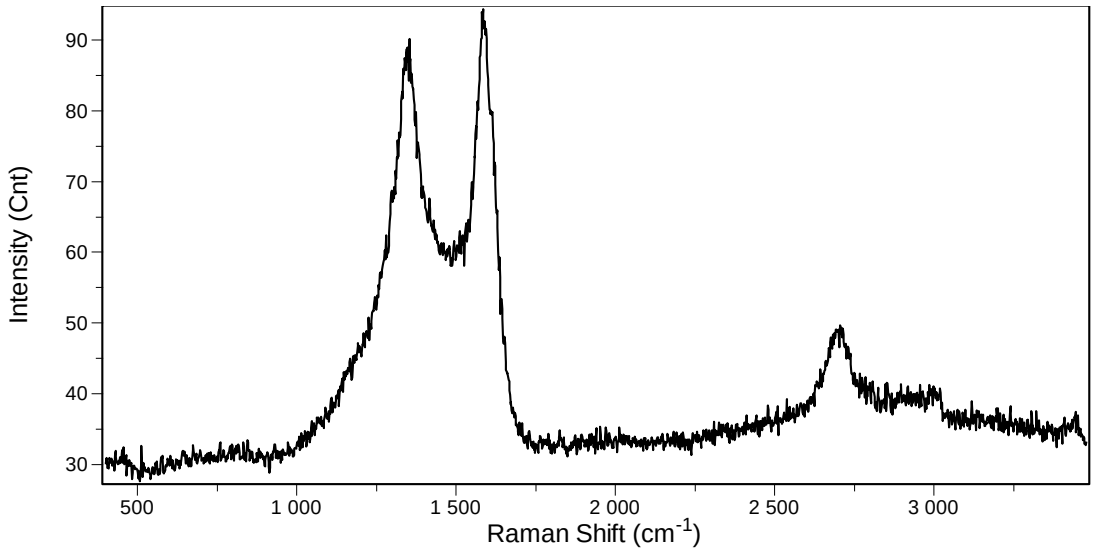

Figure 4-5: Raman spectrum recorded in Ar after cooling from 800 °C of Spent Cat-1 (spent iron Fischer-Tropsch catalyst recovered from the SAS reactor). Excitation wavelength: 514 nm

4.2.1.3 X-Ray Photoelectron Spectroscopy

XPS has the advantage of being able to detect iron carbide phases that are characterised by a peak at 283.3 eV (Bonzel & Krebs, 1980; Dwyer and Hardenbergh, 1984; Butt, 1990; Kuivila *et al.*, 1988; Loaiza-Gil *et al.*, 1999; Reymond *et al.*, 1982). This technique can be used to distinguish between CH layers (285.5 – 285.9 eV) (Dwyer and Hardenbergh, 1984; Paál *et al.*, 2005) and graphitic material (284.4 – 284.7 eV) (Bonzel & Krebs, 1980; Casanova *et al.*, 1983; Dwyer and Hardenbergh, 1984; Kuivila *et al.*, 1988; Loaiza-Gil *et al.*, 1999; Reymond *et al.*, 1982; Shang *et al.*, 2008). Oxygenated species occur at higher binding energies (286 – 290 eV) (Rodriguez *et al.*, 2001; Shang *et al.*, 2008). XPS is highly surface-specific (up to approximately 7 nm) due to the short range of the photoelectrons that are emitted from the solid.

XPS of the catalyst recovered from the SAS reactor reveals a spectrum (Figure 4.6) that indicates the presence of largely carbonaceous material on the surface of the catalyst. Surface charging during the measurements has resulted in a 3-4 eV shift to lower binding energies. This was observed by the Si 2p peak which normally occurs at a binding energy of 103.4 eV. The spectrum could therefore be charge-corrected. The surface of Spent Cat-1

does not appear to contain any iron carbides (expected at 704 eV), while only small quantities of iron oxide phases are present. There is 8% oxygen detected on the surface. Although the spent catalysts recovered from the SAS reactor are not protected against oxidation once they have been removed from the reactor, this does not seem to result in extensive oxidation of the catalyst surface. The Fe 2p peak at 711 eV confirms the presence of surface magnetite (Kuivila *et al.*, 1988).

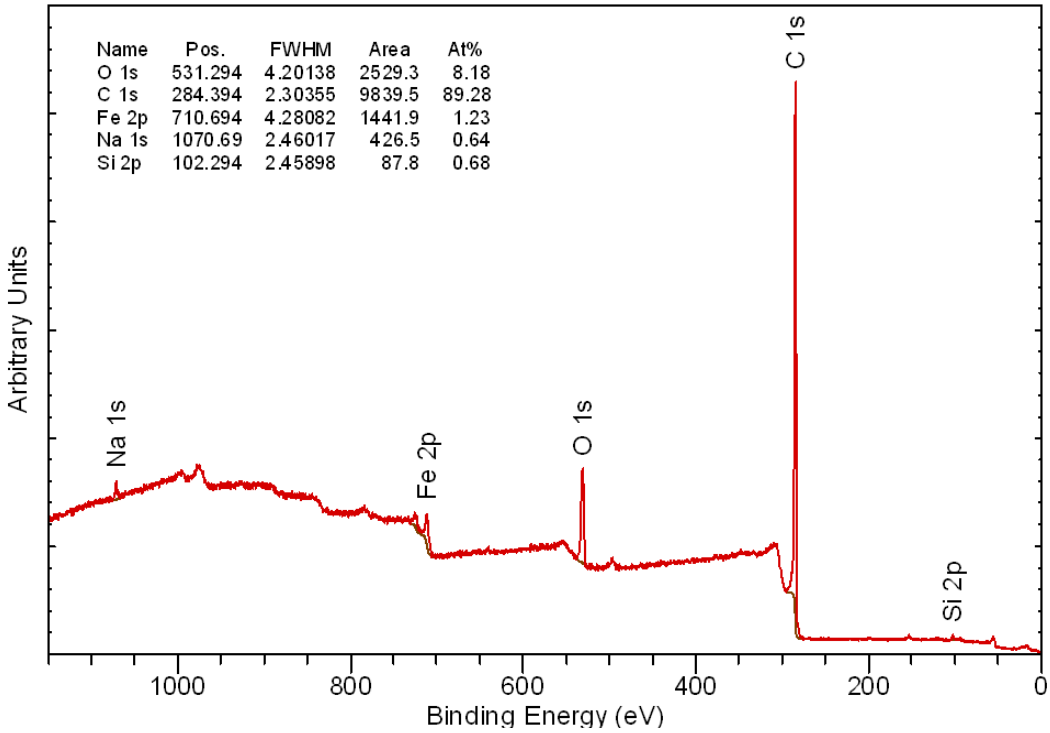

Figure 4-6: X-ray photoelectron spectrum of Spent Cat-1: a spent iron Fischer-Tropsch catalyst recovered from the SAS reactor. Kratos Axis Ultra DLD, monochromatic Al Kα X-ray source (75 W), 160 eV

The deconvoluted C1s region (Figure 4.7) should be considered with caution since charge correction of the spectrum was performed. Taking into account the crystallinity of the carbonaceous material as determined by Raman spectroscopy, the main peak at 284.5 eV is likely representing graphitic carbon while the peak at 285.0 represents hydrogenated carbon. The deconvolution is subject to certain assumptions that are made as to the number of peaks or types of carbon that are present on the surface of Spent Cat-1. Paál *et al.* (2005) assigned the lower binding energy peaks to the

presence of deactivating disordered carbon. We currently assign peaks at these binding energies wholly to graphite. The higher binding energy peaks are associated with oxygenated species such as ketones or alcohols (Riedel *et al.*, 2003; Loaiza-Gil *et al.*, 1999, Shang *et al.*, 2008).

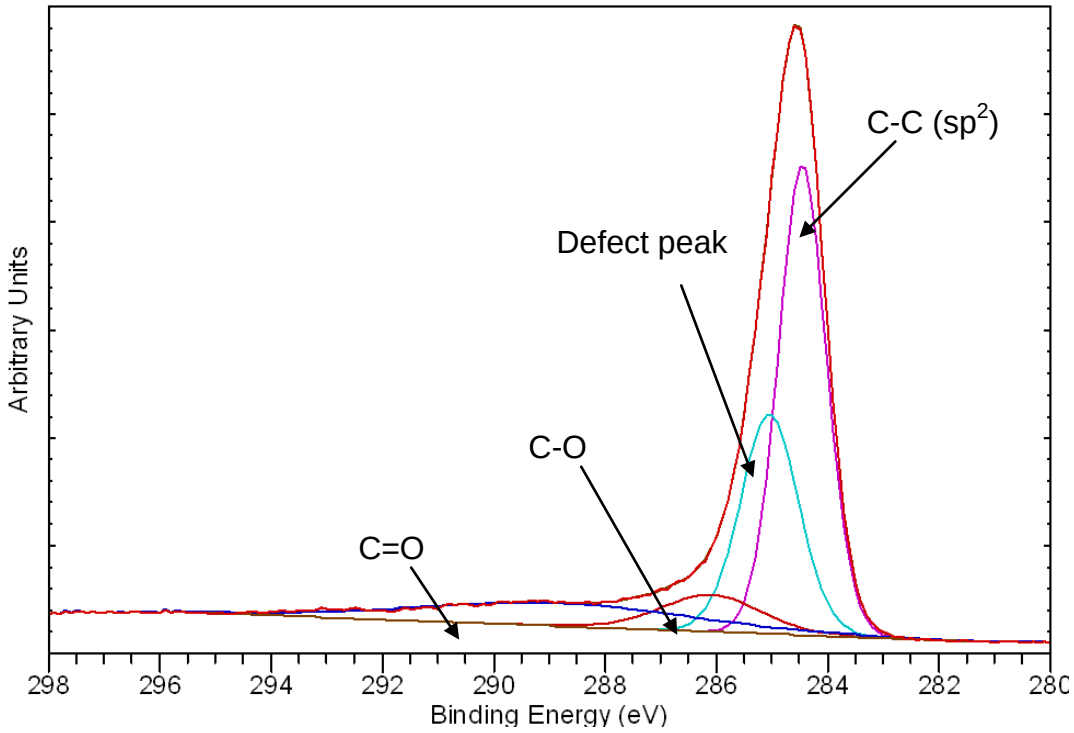

Figure 4-7: X-ray photoelectron spectrum showing C1s region of Spent Cat-1: a spent iron Fischer-Tropsch catalyst recovered from the SAS reactor deconvoluted into component peaks. Analyser pass energy: 40 eV

It is surprising that carbide peaks are not observed since XRD and Mössbauer spectroscopy detect considerable amounts of these phases. In an investigation on the activation of precipitated iron Fischer-Tropsch catalysts by Shroff *et al*. (2005), a similar result was obtained and was ascribed to the carbide crystallites being covered by amorphous carbon films which attenuate the Fe2p carbide signal. Argon sputtering was therefore applied to the surface of Spent Cat-1 and the results are shown in Figures 4.8 and 4.9, with the sputtering time increasing from the bottom spectrum to the top. From the changes in the C1s region (Figure 4.8) it is apparent that the carbon includes more amorphous phases such as the disordered carbon peak around 283.9 eV (Paál *et al*., 2005), since the observed peak is increasing in broadness.

This peak broadening indicates that different carbon phases occur deeper in the catalyst. The carbide peak still does not appear which is probably due to the crystallites being undetectable in the large mass of carbonaceous matrix. Alternatively, the signal from this phase could be much weaker than the carbon signal. The Fe2p region (Figure 4.9) shows the transition from magnetite to metallic iron (Kuivila *et al.*, 1988) with an increase in sampling depth. This could indicate the loss of the passivation layer on the surface of the catalyst. Ion bombardment could also induce phase transformations, so the Fe2p region should be considered with caution. The observation that magnetite (~ 711 eV) is reduced to metallic iron (707 eV) is corroborated by the decrease in the intensity of the carbon peak, which probably acts as a reductant in this case.

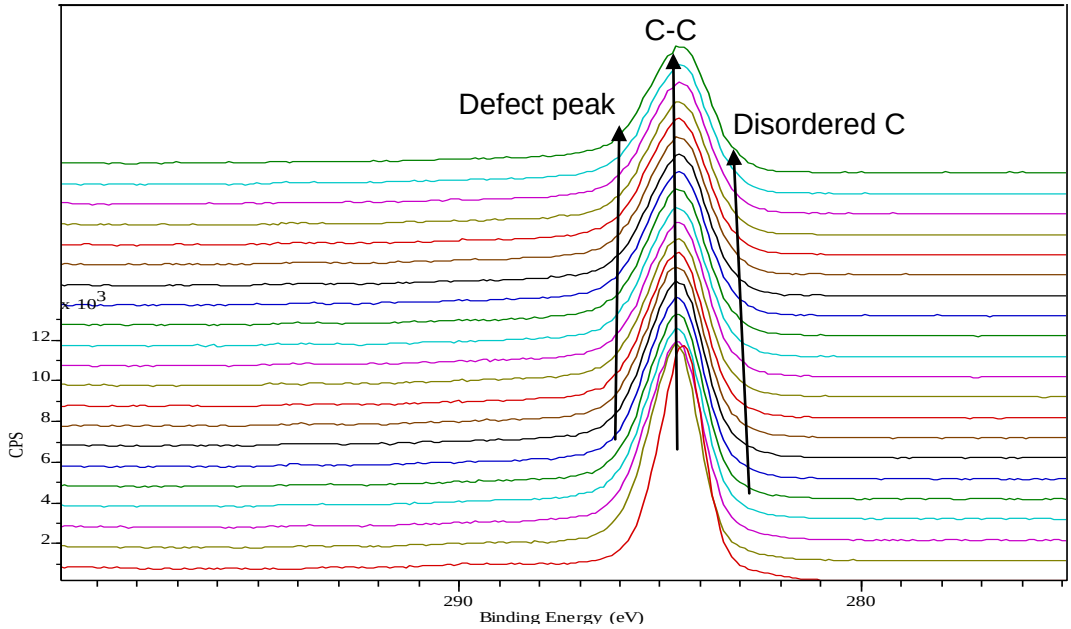

Figure 4-8: X-ray photoelectron spectrum showing C1s region of Spent Cat-1: a spent iron Fischer-Tropsch catalyst recovered from the SAS reactor. Sputtering time increases from bottom to top. 5 kV Ar ions, 30 minutes

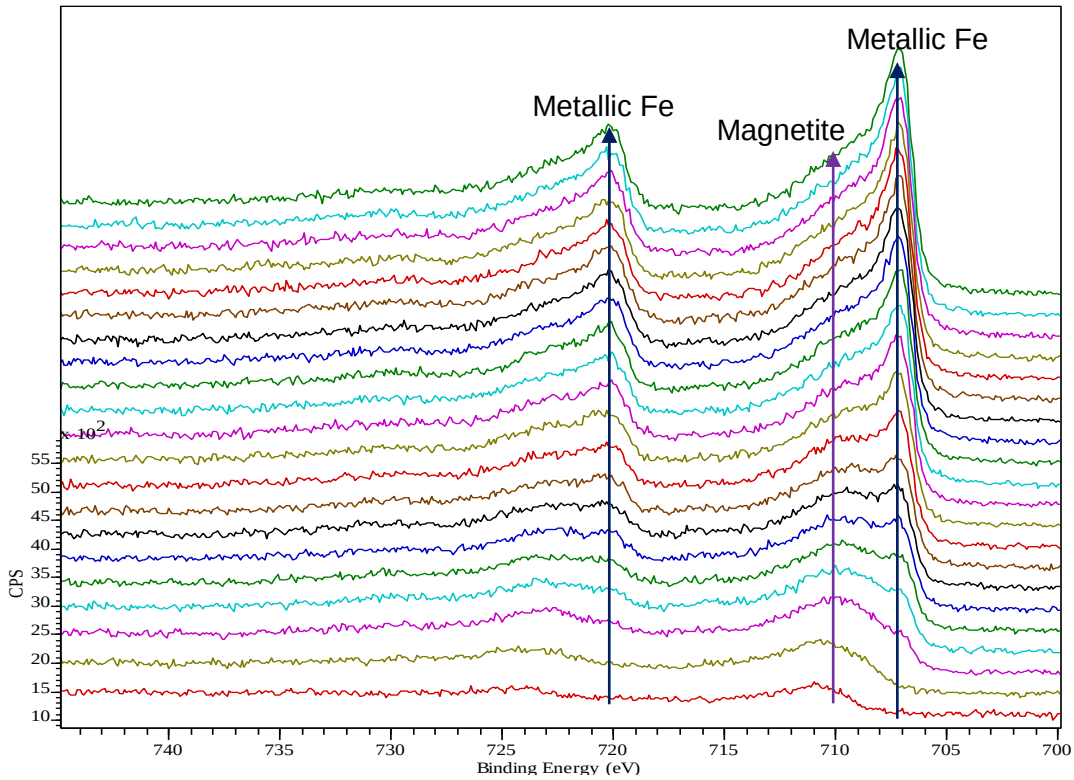

Figure 4-9: X-ray photoelectron spectrum showing Fe2p region of Spent Cat-1: a spent iron Fischer-Tropsch catalyst recovered from the SAS reactor. Sputtering time increases from bottom to top. 5 kV Ar ions, 30 minutes

From the typical techniques used to study carbonaceous deposits it appears as if the species on the spent catalyst recovered from the SAS reactor is largely amorphous but with some graphitic content, and the crystallinity of these deposits can be increased by annealing experiments.

4.2.1.4 Matrix-Assisted Laser Desorption/Ionisation Time-Of-Flight Mass Spectrometry

An aspect of the nature of the carbonaceous deposits, namely the mass distributions, has not yet been considered. Mass distributions can also provide information on the nature of carbonaceous species. The application of MALDI-TOF MS to the investigation of carbonaceous deposits on spent catalysts is a promising new area of research.

Spent Cat-2 will be described first. The main issue with the spent catalyst recovered from the Pilot Plant reactor is the large amount of adsorbed wax on these catalysts, and how this would affect the observed mass distribution. The mass distribution when 7,7,8,8-tetracyanoquinodimethane (TCNQ), dithranol (Figure 4.10) or $AgNO_3$ (Figure 4.11) was used as a matrix shows a very complex mass distribution. The spectrum exhibits a sinusoidal mass distribution where the peaks are 1 Da apart. Within the distribution, alternate peaks seem to have higher intensity (2 Da apart). The sinusoidal curve has peaks at 12 Da increments.

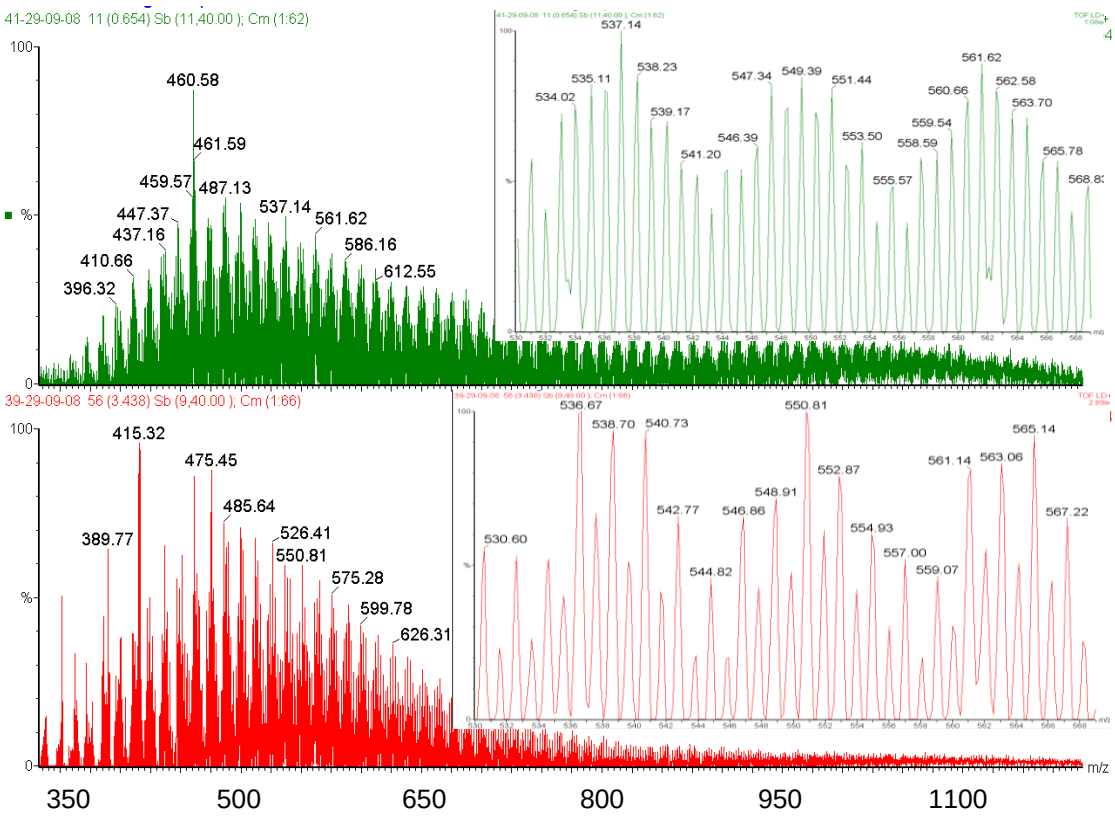

Figure 4-10: MALDI-TOF mass spectrum of Spent Cat-2: a spent iron Fischer-Tropsch catalyst recovered from the Pilot Plant reactor with TCNQ (bottom) and Dithranol (top) as matrices. Micromass Tof Spec 2E, laser: 337 nm, ion extraction voltage: 20kV, reflectron mode

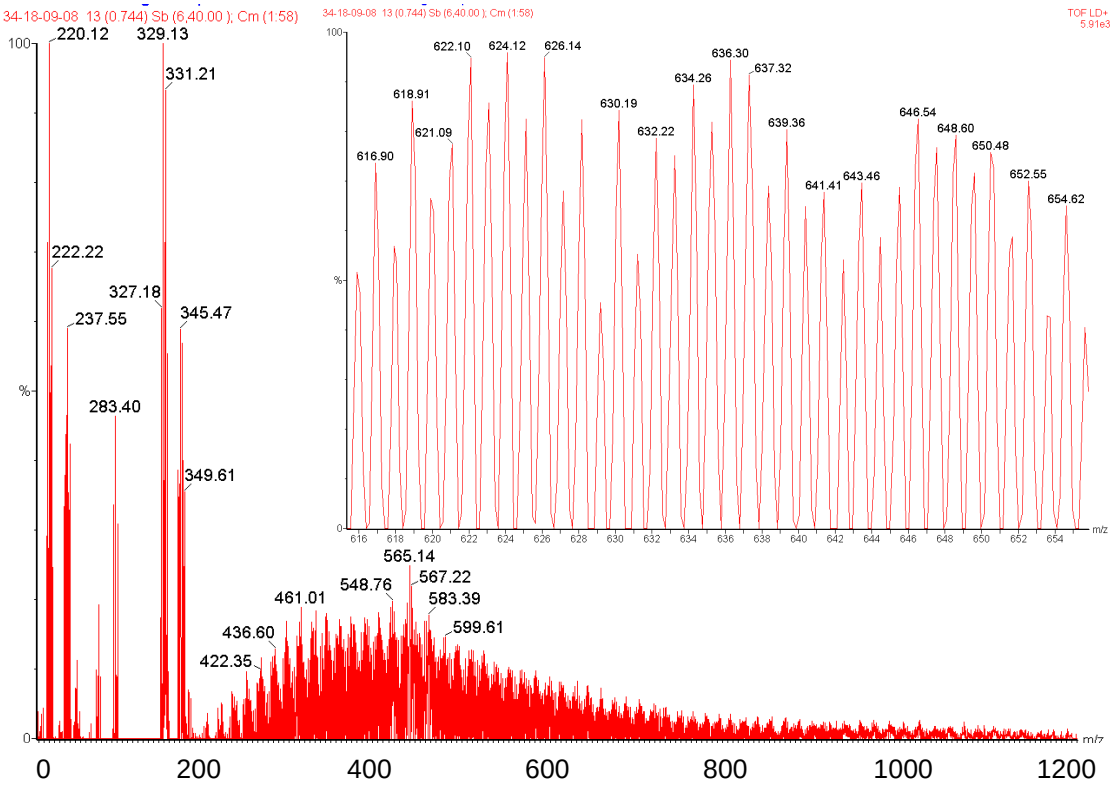

Figure 4-11: MALDI-TOF mass spectrum of Spent Cat-2: a spent iron Fischer-Tropsch catalyst recovered from Pilot Plant reactor with AgNO3 as matrix

Performing thermal treatment of Spent Cat-2 results in desorption of substantial amounts of wax, which was also characterised by MALDI-TOF MS. The mass spectrum of the desorbed wax depicted in Figure 4.12 has a simplified mass distribution compared to Spent Cat-2, indicating that this desorption selectively removes this wax. The 1 Da mass separations now appear in clusters with 14 Da separations between corresponding peaks. The MALDI-TOF MS, when $AgNO_3$ is used, shows that the wax desorbed from this spent catalyst sample has a mass distribution with maximum intensity observed at 465 Da which extends up to about 900 Da. However, this represents the mass of adduct formed when a silver ion replaces a proton of the wax molecule (Section 4.2.2.2). The adduct of $C_{25}H_{52}$ is the peak with maximum intensity, although it should be noted that saturated hydrocarbons are not necessarily the only constituent of this desorbed material. The peaks at ~775 Da and ~1000 Da represent clusters of silver ions. The TCNQ spectrum shows quite clearly that this mass distribution is shifted down by roughly 110 Da, which represents the mass of Ag^+. The fact that the presence

of this adsorbed wax was not immediately obvious in Spent Cat-2 (Figure 4.11) indicates a very important aspect of how, in a mixture of materials with different ionisation efficiencies, it is easy to misinterpret the type of species present. It would appear that the presence of wax complicates characterisation by MALDI-TOF MS because the relative intensity of the 12 Da peaks (in Figure 4.10) is so much greater than the peaks representing the wax.

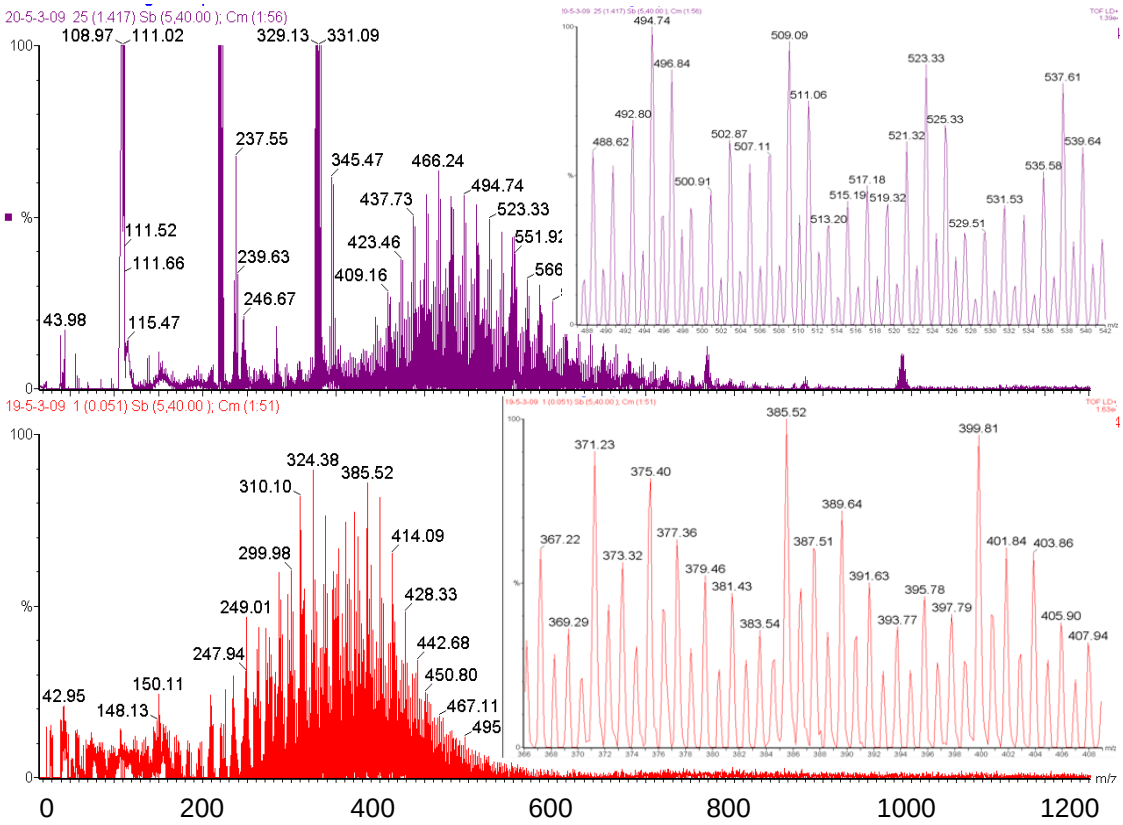

Figure 4-12: MALDI-TOF mass spectrum of wax desorbed from Spent Cat-2: a spent iron Fischer-Tropsch catalyst recovered from the Pilot Plant reactor with AgNO3 (top) and TCNQ (bottom) as matrices

MALDI-TOF MS of Spent Cat-1 will now be discussed. Figure 4.13 shows the MALDI-TOF mass spectrum of Spent Cat-1 using TCNQ as matrix. The masses below 400 Da can be attributed to the matrix, and therefore only the broad feature consisting of a series of peaks 12 Da mass separations with a maximum intensity around 500 Da is associated with the deposits on the

catalyst surface. Masses of up to 1500 Da can be detected on Spent Cat-1 using this matrix. Similar observations were made when dithranol was used as a matrix. However, the peaks for this matrix extend to around 450 Da. The maximum intensity of the distribution is also around 500 Da. The 12 Da mass separations again suggest polymeric carbon.

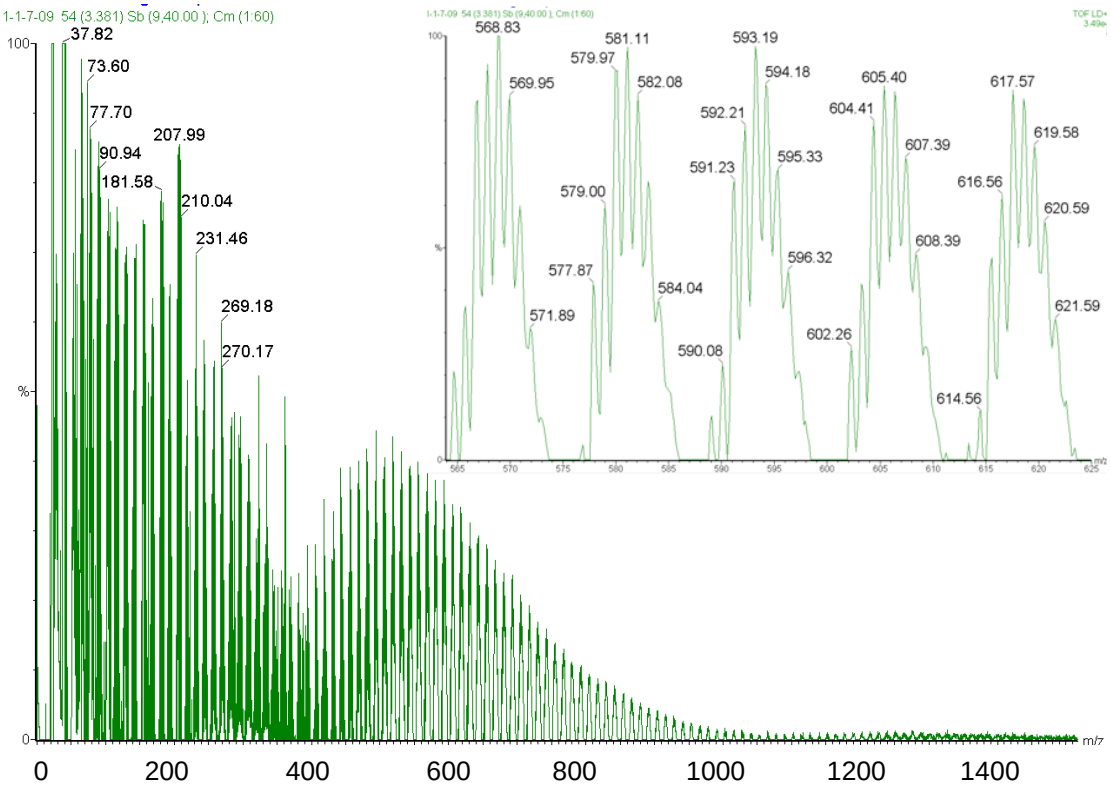

Figure 4-13: MALDI-TOF mass spectrum of Spent Cat-1: a spent iron Fischer-Tropsch catalyst recovered from the SAS reactor with TCNQ as matrix

Spent Cat-1 which was oxidised in air at 340 °C was also investigated by MALDI-TOF MS, and the mass spectrum is given in Figure 4.14. Compared to the mass distribution of the as-received catalyst, this distribution shows very little material on the surface, indicating that the most reactive surface species have been selectively removed by this treatment. The separation between the peaks is 24 Da throughout the indicated range. This distribution also does not exhibit a continuum of peaks and appears to be simplified by the oxidation treatment. This observation alludes to the possibility that the appearance of 12 Da peak separations in Figure 4.13 is associated with two overlaid sub-distributions with 24 Da increments. The one sub-distribution would then be

off-set from the other by 12 Da. This rationalisation was proposed by Apicella *et al*. (2004) who observed polycyclic aromatic hydrocarbons in the analysis of soot. Alternatively, the polymeric carbon species (12 Da separations) could be more easily oxidised at 340 °C compared to PAHs. Therefore, due to the enhanced ability of the carbon cations to "fly" due to the size of these species, we see 12 Da separations before oxidation. Only once these species are removed can the low-intensity peaks associated with PAHs be observed. Due to the different ionisation efficiencies of the various molecules typically found on a spent catalyst, MALDI-TOF MS might not be the easiest technique for this analysis.

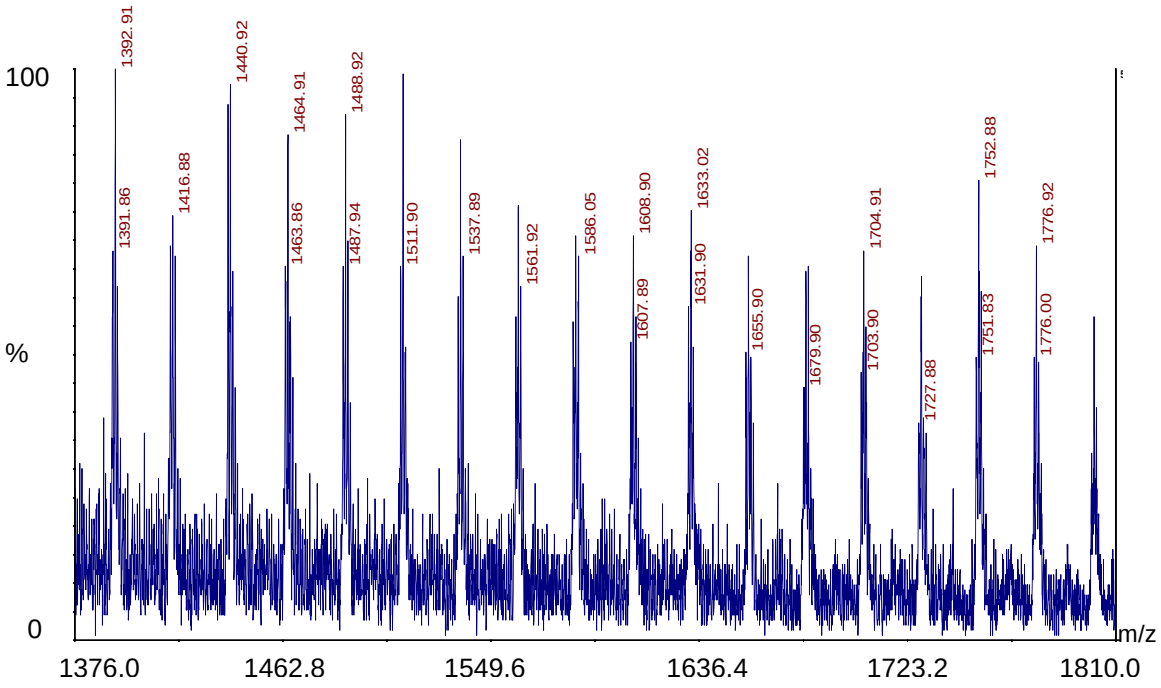

Figure 4-14: MALDI-TOF mass spectrum of spent iron Fischer-Tropsch catalyst recovered from the SAS reactor oxidised at 340 °C with TCNQ as matrix. ABSciex 4800, reflectron mode

The MALDI-TOF mass spectrum of Spent Cat-1 with silver nitrate is shown in Figure 4.15. The same broad mass distribution can be seen, but the masses detected are much higher than with the previous matrices, extending to at least 5000 Da. Considering that silver ions are conventionally believed to ionise saturated hydrocarbons, it was initially assumed that the observed mass distribution is due to wax molecules with chain lengths up to about C_{280}. However, closer inspection of the peaks revealed a continuum of masses,

while at high masses (beyond 1200 Da) the separation changes from 12 Da to 24 Da. This indicates that the mass distribution does not represent saturated hydrocarbons, since this would produce 14 Da separations. In the lower mass region there is a continuum of peaks. It appears as if several sub-distributions are present although fragmentation is a more likely explanation due to the higher laser powers employed in the analysis. The 24 Da increments indicate that the deposits on Spent Cat-1 might be polycyclic aromatic in nature.

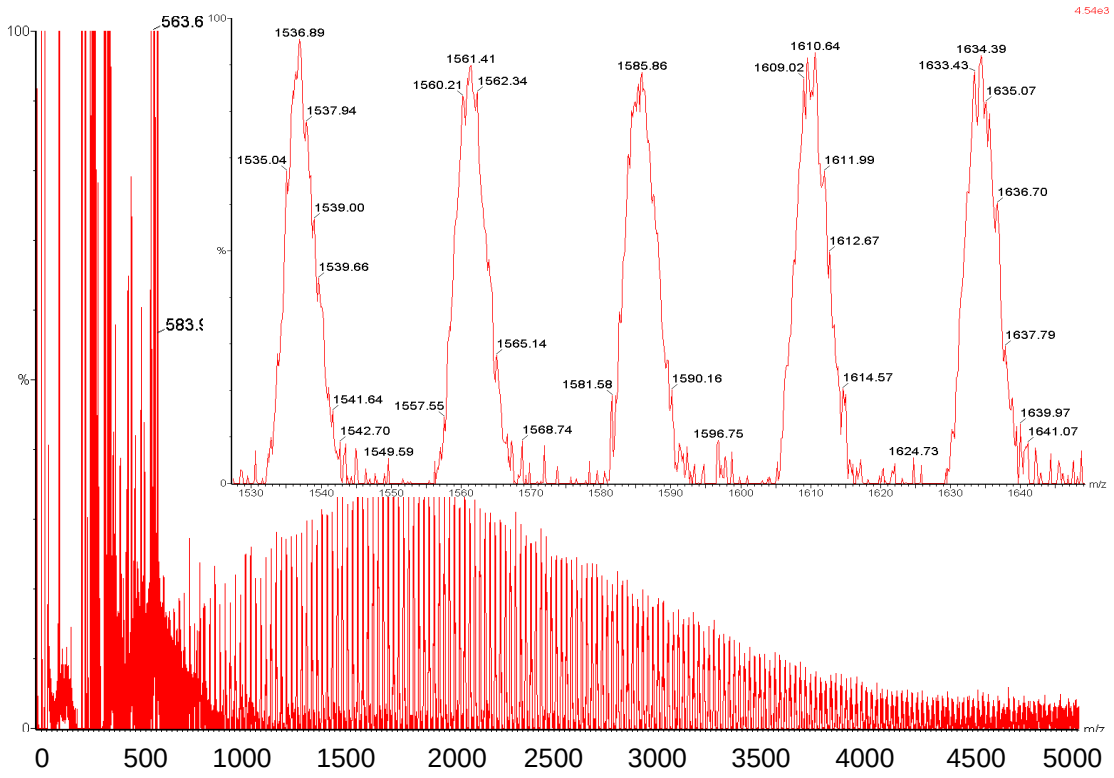

Figure 4-15: MALDI-TOF mass spectrum of Spent Cat-1: a spent iron Fischer-Tropsch catalyst recovered from SAS reactor with $AgNO_3$ as matrix

4.2.2 Development of MALDI-TOF MS for Other Applications

4.2.2.1 Spent Cobalt Catalyst

The deactivation of the low temperature Fischer-Tropsch (LTFT) cobalt-based catalyst is believed to be due to the formation of aliphatic hydrocarbons which become trapped within the pores and this subsequently leads to mass transfer limitations of the reactants to the active catalytic surface (Steynberg, 2004). The spent cobalt catalyst is regenerated to remove coke build-up and

reactivated for further use. Regeneration causes changes to the cobalt catalyst which lowers the activity, probably due to the severe conditions experienced by the catalysts during regeneration (Saib *et al*., 2010). Regeneration follows a solvent wash/oxidation/reduction sequence. It would be assumed that all coke is removed during oxidation; however, when subsequent reduction with H_2 is performed, methane is released indicating hydrocracking of some residual carbon forms. Due to the low quantities of deleterious carbon on the catalyst, this characterisation is not straightforward. Furthermore, not all carbon present is responsible for deactivation since adsorbed products are also present on the catalyst. The investigation therefore requires a systematic approach, which involves studying the catalysts at various stages along the regeneration cycle.

The spent cobalt-based catalyst used in the LTFT process was characterised by MALDI-TOF MS and showed mass distributions with a maximum around 500 Da and 14 Da separations (Figure 4.16). These 14 Da increments are believed to represent a homologous series of hydrocarbons. These clusters occur up to a molecular mass of about 1500 Da, beyond which it is difficult to distinguish the peaks from the background noise. This was observed with both $AgNO_3$ and TCNQ (not shown) as matrices, which indicates that these two matrices ionise the same types of species on the spent cobalt catalyst surface, but with different efficiencies. The fact that 14 Da mass gaps are obtained by TCNQ suggests that the mass distribution could not represent purely aliphatic hydrocarbons since it is known that a cationising agent is normally required to produce signals in the analysis of large saturated hydrocarbons (Kühn *et al.*, 1996; Pruns *et al.*, 2002). Small enough molecules could, however, be ionised as intact ions even without a matrix (LDI-TOF MS). Similar observations i.e. 14 Da separations were made by Feller *et al.* (2003a) in the study of carbonaceous deposits on a spent zeolite catalyst. Particularly, they report naphthalene with an increasing number or length of side chain (Feller *et al.*, 2003a). This mass distribution in Figure 4.19 could therefore arise from molecules comprising an aromatic or polycyclic aromatic head with an aliphatic tail(s). In an attempt to verify the ionisation efficiency of these

types of species by various matrices, we prepared eicosyl benzene (aromatic head with a C_{20} tail). However, due to the comparatively low molecular weight of this species (358.66 Da), it could easily be ionised by the laser. Ideally, the size of the aromatic head or the length or number of side-chains could be increased to contain at least 40 carbon atoms. This investigation was abandoned since preparing a molecule well in excess of 600 Da (therefore requiring a matrix to assist in the ionisation process) would be difficult. Ideally, this analysis would be performed using commercially available pure standard materials.

The spent cobalt catalysts were extracted and subsequently treated by hydrogenation. There are differences between the observed mass spectra before and after a wax extraction process and also after the hydrogenation step. This hydrogenation is known to catalytically hydrocrack the adsorbed aliphatic hydrocarbons to produce methane. The spectra shown in Figure 4.16 indicate that the wax extraction is not efficient at removing all the wax. However, the fact that the remaining wax is made up of low molecular weight material, which should be easiest to extract, suggests that this material might be more difficult to remove due to it being trapped within the pores of the catalyst. In a study of the coke produced during commercial Resid fluid catalytic cracking (designed to convert 100% residue from the atmospheric distillation tower), a similar observation was made of surface and trapped molecules, but in this case the distinction was easier since the types of species in the two locations were different (Cerqueira *et al.*, 2005). The advantage of having a technique which is suitable for characterisation of the adsorbed wax present on the spent catalyst is that the extraction process can be monitored, thereby facilitating the design of a more suitable extraction process for the regeneration of the catalyst. The final hydrogenation reveals that only masses associated with Ag^+ are observed, indicating complete hydrocracking of the adsorbed hydrocarbon species.

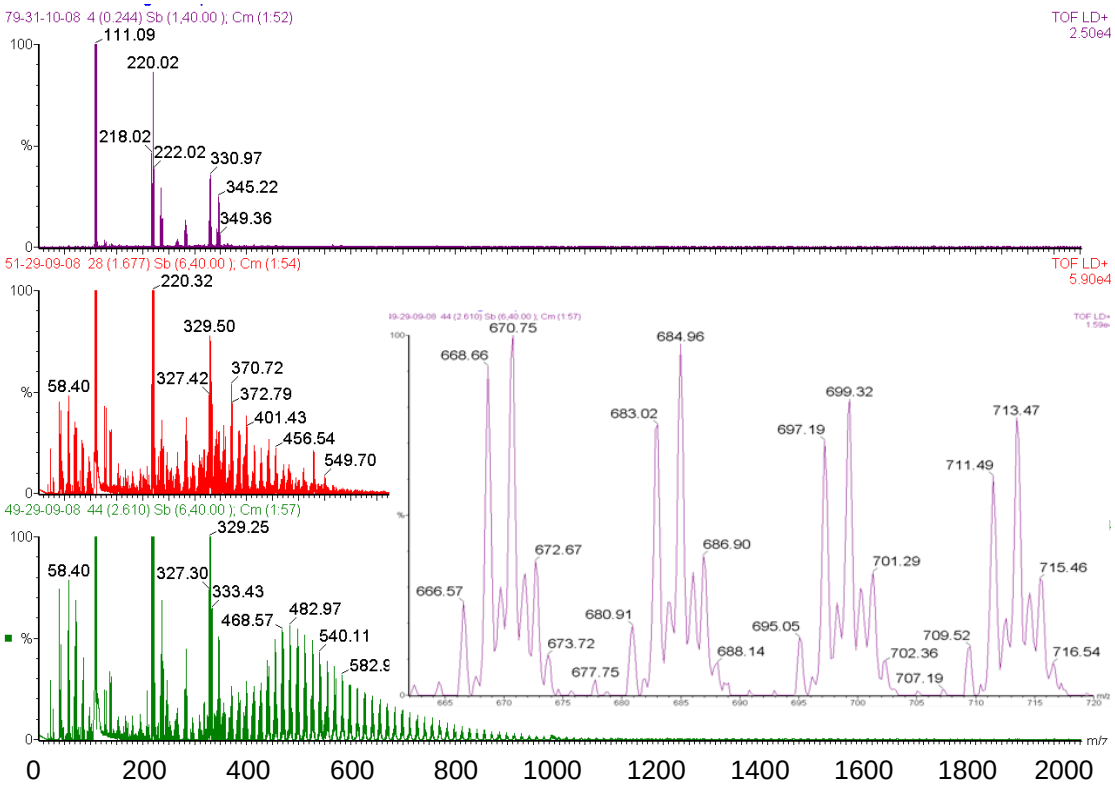

Figure 4-16: MALDI-TOF mass spectrum of cobalt catalyst after 150 days on-stream with $AgNO_3$ as matrix in wax (bottom), wax extracted (middle) and hydrogenated (top)

The spectrum of the wax-extracted end-of-run cobalt catalyst (Figure 4.17) clearly illustrates the inefficiency of the wax extraction process. In this spectrum there are peaks visible up to 3000 Da due to the longer time the catalyst remained in the reactor. This indicates that the molecules that make up carbonaceous deposits progressively increase in molecular weight during FTS. The mass distribution shows that a broad mass distribution stays behind after this extraction. The insert shows 14 Da mass separations indicating a homologous series of hydrocarbons.

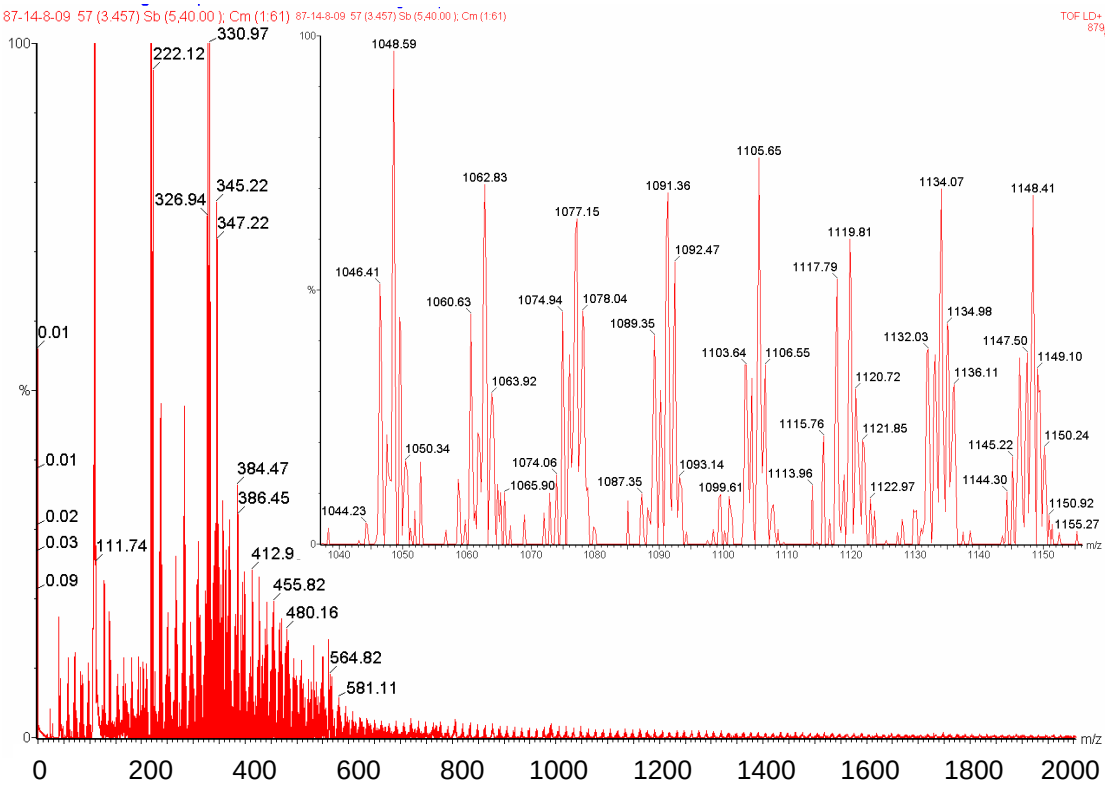

Figure 4-17: MALDI-TOF mass spectrum of wax-extracted cobalt catalyst after 200 days on-stream with AgNO3 as matrix

An important observation in this study was that, after oxidation treatment of the wax extracted catalyst, the mass separations changed to 12 Da. In addition, only carbonaceous species with a molecular weight below 800 Da remains. From the previous section, peaks separated by 12 Da are normally assigned as carbon clusters or polymeric carbon. Removal of the wax, which is probably easier to ionise, facilitates detection of this species and demonstrates the importance of different ionisation efficiencies of species. Alternatively, we have to consider the possibility that this material is formed or chemically transformed during oxidation. It has been reported that after oxidation, higher temperatures are required to hydrogenate this species (Saib *et al*., 2010). This provides support for the transformation of these species during oxidation.

The nature of the deposits on the spent cobalt-based catalysts was determined by combining the difference in ionisation ability of the matrices

with the observed mass distributions obtained by MALDI-TOF MS. The 14 Da mass separations do not necessarily indicate the presence of a homologous series of hydrocarbons, but could also contain an aromatic component. As adsorbed products are condensed in the pores of the recovered catalyst, it becomes more difficult to transport them out under reaction conditions and they become trapped within the pores. The exact structure and relative aromaticity of the carbonaceous material could be determined by performing ^{13}C NMR of the soluble fraction which can be extracted.

4.2.2.2 Wax Analysis

The major product synthesised in the LTFT reactors at Sasol is wax. Most of these waxes are available commercially, although some low-value wax fractions are usually hydrocracked to yield predominantly diesel boiling range hydrocarbon product (Steynberg, 2004). The LTFT wax is normally analysed by High-Temperature Gas Chromatography (HTGC). However, by using this technique only about 60% of the product wax could be accounted for. This is observed in the Anderson-Schulz-Flory distribution of the products as determined by HTGC, where it is seen that the distribution tails off around $C_{110}H_{222}$. This is due to an upper limit in molecular weight of 1545 Da for the wax samples that could be analysed by HTGC, due to restrictions imposed by maximum usable temperature of the column. MALDI-TOF MS was therefore investigated to see if it was a superior method in the analysis of these industrial wax materials. Saturated hydrocarbons are notoriously difficult to analyse by mass spectrometry (Pruns *et al*., 2002).

The characterisation of wax standards was performed to establish the suitability of MALDI-TOF MS to the type of species typically found in the LTFT reaction. In MALDI-TOF MS saturated hydrocarbons are generally characterised by mixing this species with a cationising agent. Silver cations are conventionally used for this purpose and ionisation is believed to take place through the formation of adducts (Ehlers *et al.*, 2001).

The waxes used were C_{40}, C_{46}, C_{50} and C_{60}. The MALDI-TOF mass spectrum of the C_{40} wax is given in Figure 4.18. The spectrum indicates that the m/z given by this technique includes the molar mass of a silver cation and this is within 1% of the expected value (670.08 Da for the ^{107}Ag isotope). This discrepancy is due to differences in calibration, but it is not a significant problem since the mass distributions are more concerned with the separation between peaks and the range of molecular weights rather than exact masses of molecules. Importantly, there is very little fragmentation of the wax molecules taking place, indicating that the silver nitrate is an appropriate matrix material for the characterisation of waxes since it promotes ionisation of the molecules and absorbs the laser light. TCNQ does not produce a mass spectrum for the wax standards.

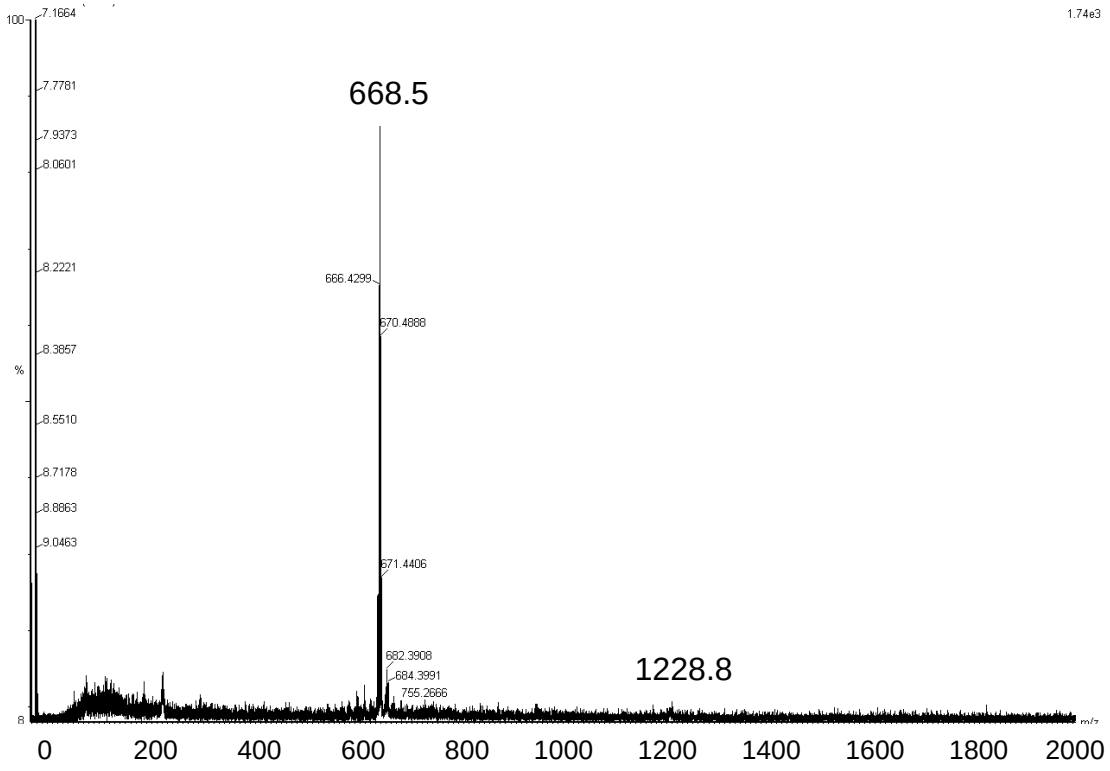

Figure 4-18: MALDI-TOF mass spectrum of C40 standard wax with $AgNO_3$ as matrix

Figure 4.19 shows the mass spectrum of the C_{50} wax and it is apparent that there are some m/z values greater than the sum of the wax and the silver cation. This suggests that there are not only adducts formed between a single wax molecule and a cation, but that additional analyte molecules or fragments

can adhere to these adducts, or alternatively that clusters containing multiple cations can form adducts with a single wax molecule. Alternatively, these additional peaks might be due to impurities in the wax standards.

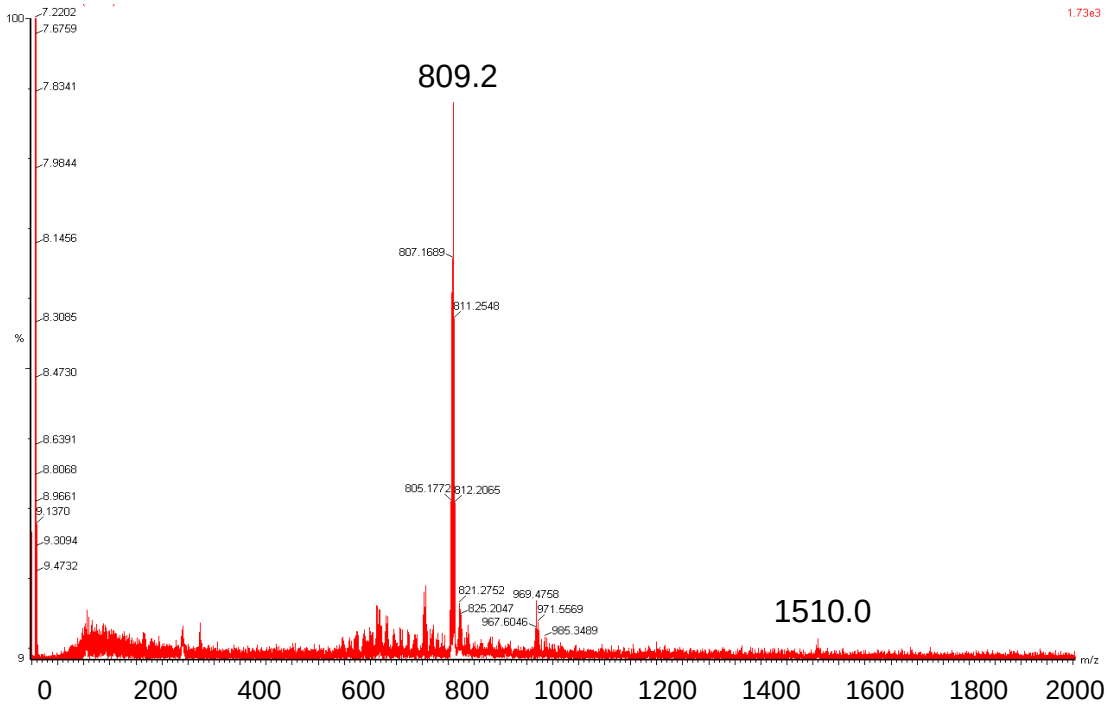

Figure 4-19: MALDI-TOF mass spectrum of the C50 standard wax with $AgNO_3$ as matrix

The MALDI-TOF mass spectrum of wax obtained from a slurry phase reactor (Figure 4.20) represents a broad product distribution of molecules of various chain lengths. This is consistent with the progressive chain growth mechanism by which the Fischer-Tropsch synthesis occurs (Schulz and Claeys, 1999). Closer observation of the individual peaks reveals that the m/z values in each case differ by 14 Da which can be explained by the addition of a CH_2 to the wax molecules. It would appear as if there is a maximum chain length of about C_{120}. In the mass distribution, the two prominent peaks at 769.4 and 989.2 Da are due to silver clusters. The mass distribution is well resolved up to a mass of about 2000 Da.

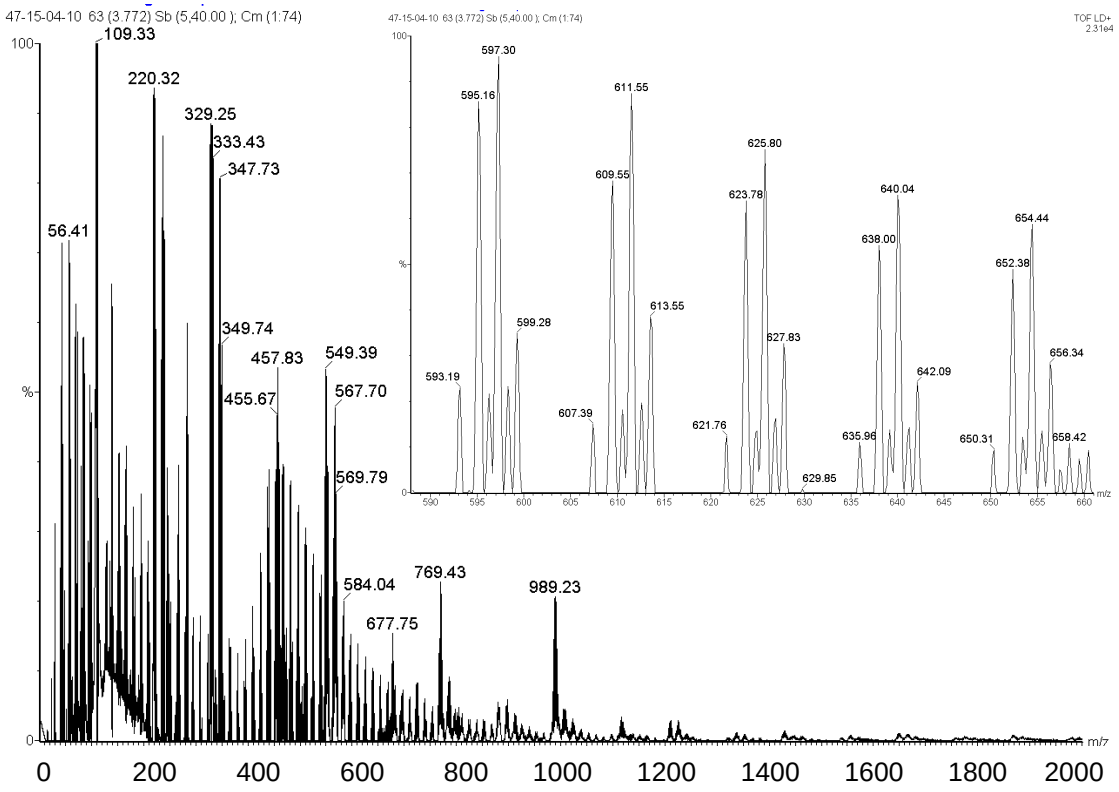

Figure 4-20: MALDI-TOF mass spectrum of a slurry phase reactor wax with $AgNO_3$ as matrix

4.3 Discussion

The aim of this chapter was to investigate the nature of the carbonaceous deposits found on spent high temperature Fischer-Tropsch catalysts. While several techniques are routinely being used to study carbonaceous species, there are still significant challenges with the interpretation of results. Therefore complementary techniques provided a good overview of different aspects, and substantiated certain results. Method development also constituted a large part of this chapter, in order to make mass spectrometry (with soft ionisation) accessible to these solid samples with high molecular weight species.

Carbonaceous deposits on spent HTFT catalysts are comprised of hydrogen-rich soft carbon and hydrogen-deficient hard carbon. Soft carbon consists of a complex mixture of paraffinic and olefinic hydrocarbons as well as oxygenated species. Hard carbon contains both polymeric carbon and polycyclic aromatic

hydrocarbons (PAHs) with a molecular weight range of 800 to 5000 Da. This hard carbon is predominantly amorphous, although the species grow to large sheets that bear a resemblance to graphene. The hard carbon forms a porous matrix in which soft carbon becomes trapped and carbide crystallites are embedded.

High Resolution Transmission Electron Microscopy (HRTEM), Raman spectroscopy and X-ray Photoelectron Spectroscopy (XPS) were employed in the characterisation of carbonaceous deposits. Characterisation of spent catalysts using only HRTEM provides limited information since PAHs and graphitic carbon exhibit the same fringes. The fact that the HRTEM images show characteristic graphite fringes along with the iron carbides might be misleading since it is known that crystalline graphite does not account for all hard carbon measured by microanalysis. Additionally, the relative amount of crystalline graphite is too small (compared to the iron-containing phases) to even be detected by X-ray Diffraction (XRD) and Mössbauer spectroscopy. The lattice fringes observed by HRTEM that are most readily associated with graphite are also characteristic of PAHs. This was observed by Mathieu and coworkers (2007) in their study of soot materials where the PAHs formed had a molecular weight of no larger than 600 Da, implying that PAHs adopt the characteristics of graphene/graphite irrespective of the size or crystallinity of the molecules. In HRTEM the electron beam focuses on only a very small part (up to 50 nm) of the surface of the spent catalyst which can be up to 200 µm in diameter and can therefore not provide a representative image of the surface deposits. Additional techniques are therefore required that can characterise a larger portion of the catalysts.

In Raman Spectroscopy the D and G modes representing C-C bonds are well understood. In addition to these modes, there are also other modes associated with carbonaceous material. One such mode is the G' mode occurring at 2700 cm^{-1}. The increasing intensity of G' was observed by Park *et al.* (2001) with an increase in duration under carburisation conditions, but the origin of this mode only became clear in the study of graphene layers

performed by Ferrari *et al.* (2006). The relative intensity of the G' to the G peak is correlated with the number of graphene layers (Park *et al.*, 2010). The C-H stretching modes associated with adsorbed hydrocarbon species are observed from 2500 to 3250 cm^{-1}, although overtones and a combination of D and G bands also occur in this region (2700, 2950 and 3200 cm^{-1}). In addition to these modes, there is also a C-H bending mode at 1330 cm^{-1} (Ferrari & Robertson, 2001). In a pure hydrocarbon species, the relative intensity of this mode to the D and G modes indicates the hydrogen content of the material. This, however, cannot be applied where a mixture of carbonaceous species is present on the surface. The absence of iron oxides in the Raman spectrum Figure 4.2 (expected around 500 cm^{-1}) suggests that the catalyst is completely covered by these carbonaceous deposits, since Raman spectroscopy samples within 1 µm from the surface, depending on the constituent phases. The relative intensity of the D to the G mode in the Raman spectrum suggests that the hard carbon is not crystalline, confirming XRD data where graphite is not observed. Annealing experiments show that upon removal of aliphatic hydrocarbons graphene-type carbon is exposed, or that this graphene-type carbon can be formed during this treatment.

Further attempts at obtaining more information from the Raman spectrum included deconvolution. Deconvolution of the simplified (wax removed) Raman spectrum of the catalyst recovered from the SAS reactor could provide quantitative information on the remaining carbonaceous material (Beyssac *et al*., 2003). Removing the wax produces a spectrum where the shoulder at 1330 cm^{-1} is absent (see Section 3.2.1.2, Figure 3.4). Sadezky *et al*. (2005) demonstrates a suitable approach in the deconvolution of soot and related carbonaceous species, where the observed modes are fitted to four Lorentzian-shaped bands (G, D1, D2, D4) at about 1580, 1350, 1620 and 1200 cm^{-1} and a Gaussian-shaped band (D3) at ~1500 cm^{-1}. In particular, the authors state that structural information can be obtained from the width of the D1 band at ~1350 cm^{-1}. With the C-H modes absent from the spectrum of the Spent Cat-1 (Figure 3.4), fitting the broad D4 band ascribed to sp^2-sp^3 bonds can therefore be performed without interference. This characterisation is,

however, limited by the experimental reproducibility of the spectra as well as statistical uncertainties of the curve fitting. In addition to the inherent subjectivity of deconvolution, the carbonaceous material that remains on Spent Cat-1 after wax removal is a mixture of material of different molecular weights (shown in Section 4.2.1.4.). Although the difficulties in quantitatively characterising disordered and heterogeneous carbonaceous materials could possibly be overcome by area mode microspectroscopy (Beyssac *et al*., 2003), deconvolution of the Raman spectrum of Spent Cat-1 was not performed.

XPS has the advantage of being able to detect iron carbide phases. C 1s signals of carbides and hydrocarbons are often strongly overlapping (Dwyer and Hardenbergh, 1984; Loaiza-Gil *et al.*, 1999). Ning and co-workers (2006) therefore reported that XPS is not necessarily a suitable technique for characterising the graphite-like carbonaceous species on the Fischer-Tropsch catalyst unless careful deconvolution is performed. Despite these efforts, carbide signals were not observed, even after Ar^+ ion sputtering. Chapter 3 details how XRD and Mössbauer spectroscopy detected a considerable amount of iron carbide present in the spent catalyst. Carbide crystallites were shown to agglomerate to units that are typically 500 nm in diameter by Backscatter Scanning Electron Microscopy (Section 3.2.2). Although Shroff and co-workers (1995) found that carbide phases were revealed after Ar^+ bombardment, these catalysts contained less carbonaceous deposits than is present in Spent Cat-1, since their catalysts were characterised after only 2 h of activation treatment in CO or syngas.

A fresh approach to the characterisation of carbonaceous species was through Matrix-Assisted Laser Desorption/Ionisation-Time of Flight Mass Spectrometry (MALDI-TOF MS). The spectra of the carbonaceous material typically include a sinusoidal distribution of peaks that are 1 Da apart. The spacing between maxima can provide an indication of the nature of the most easily ionisable species present without studying specific masses. The main concern at this stage is to distinguish between aliphatics, polymeric or

polycyclic aromatic hydrocarbons. Observing 14 Da separations, indicative of the addition of a methylene unit, can be further examined by performing GC-MS of the solvent-soluble portion of the sample. In this way, paraffins, olefins and some oxygenates were identified. Previous observations which involved 12 Da mass separations were ascribed to carbon cluster series formed on soot particles (Fletcher et al., 1998). There is little information available on the formation and structure of this carbon. Deposition of free or polymeric carbon has been proposed as the deactivation mechanism in iron-based Fischer-Tropsch catalysts (Xu & Bartholomew, 2005; Herranz *et al*., 2006), and we believe that this type of species would give 12 Da separations.

The interpretation of complex MS data of coal and coal-derived samples is simplified by the presence of heteroatoms (Herod *et al.* 2000; Johnson *et al.*, 1998). More information can then be obtained by higher resolution, which would allow distinction between various isomers. However, due to the complexity of the distributions from the deposits on the HTFT catalysts we did not attempt to assign individual peaks.

In terms of the question of whether different matrices can be used to selectively characterise different classes of species, it appears as if very similar molecules are ionised in each case by $AgNO_3$, dithranol and TCNQ. In most cases the mass distributions are very similar. It is clear from the range of the distribution that $AgNO_3$ is able to ionise larger molecules than TCNQ and is therefore a better matrix in the characterisation of spent HTFT catalysts. There is also good agreement between the mass distributions obtained when using the different matrices. Observing the 2 Da gaps with both $AgNO_3$ and TCNQ implies that the isotopes of Ag do not contribute significantly to the observed mass distributions. The mass distribution possibly represents most of the able-to-fly material present on this HTFT spent catalyst, although not quantitatively. The 2 Da gaps that are observed could be explained as molecules with a varying degree of unsaturation. These homologous series are each characterised by 14 Da separations between peaks, but is sometimes overshadowed by the 12 Da gaps (representing more easily

ionisable species). Furthermore, 1 Da separations might suggest isotopic abundance for the carbon atoms present in the molecules. However, the relative abundance of ^{13}C is considerably lower than the peaks observed in these spectra. This 1 Da separation in the low mass regions therefore points to the cumulative effect of isotope peaks for a mixture of species.

In the mass spectra of Spent Cat-1, 24 Da separations that were observed require further discussion. It is known that aromatic hydrocarbons can be formed within the HTFT process. These products are thermodynamically favoured at these conditions as aromatisation is an endothermic reaction (Steynberg, 2004). Since MALDI-TOF MS is a soft ionisation technique, very little fragmentation is expected to occur at higher mass regions during analysis and the observed distribution is therefore likely to be the result of a growing series of molecules as opposed to fragmentation. The progressive growth of these PAHs as demonstrated by Yang and co-workers (2008) can eventually lead to the formation of graphene under the correct conditions, which is the most stable species (Swart *et al.*, 2008). A well-accepted mechanism for the growth of PAHs is the Hydrogen Abstraction C_2H_2 Addition (HACA) mechanism (Frenklach *et al.*, 1984; Frenklach, 2002; Bauschlicher *et al.*, 2002; Mathieu *et al.*, 2009; Unterreiner *et al.*, 2004). According to this mechanism, a PAH grows by the addition of an acetylene molecule and the abstraction of a hydrogen molecule. This implies that several PAH molecules in the growth stage will exhibit a mass spectrum containing peaks separated by 24 Da, as observed in this work. It is important to note that we are not suggesting that the HACA mechanism is responsible for growth of PAHs on HTFT catalysts, but merely aim to indicate that the growth of PAHs can lead to 24 Da separations.

The observation of PAHs has mostly been associated with soot in a premixed hydrocarbon-oxygen flame (Bockhorn *et al.*, 1983; Apicella *et al.*, 2006; Apicella *et al.*, 2007; Fletcher *et al.*, 1998; Dobbins *et al.*, 1995; Dobbins *et al.*, 1998; Apicella *et al.*, 2004; Violi, 2004), pyrolysis experiments (Mathieu *et al.*, 2007; Shukla *et al.*, 2007, Shukla *et al.*, 2008), or in the emissions from diesel

engine combustion (Dobbins *et al.*, 2006) and carbonaceous pitches (Cervo & Thies, 2007). It was also observed by Cerqueira and co-workers (2005) that such PAHs (mainly 50 Da gaps) were trapped in the mesopores of a zeolite catalyst used in fluid catalytic cracking. In addition to 24 Da increments, Bauer and co-workers (2007) also observed peaks spaced 37 and 50 Da apart that were ascribed to C_2, C_3H and C_4H_2 units according to the growth of PAHs by the HACA and Phenyl Addition/Cyclisation (PAC) mechanisms. A schematic representation of these mechanisms is shown in Figure 4.21, and underlined in the same colours are some examples of 24 Da differences between molecules.

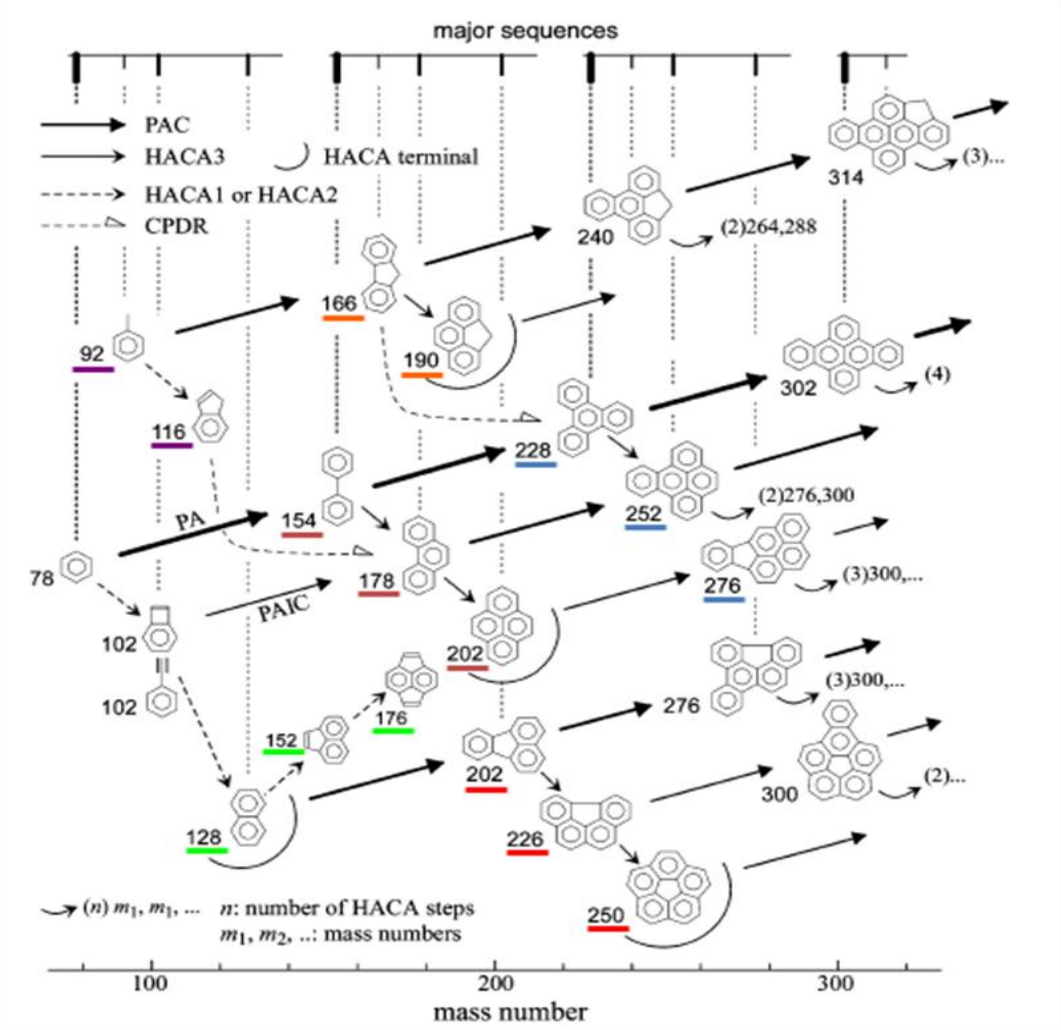

Figure 4-21: Schematic showing various mechanisms for the growth of PAHs (redrawn from Shukla et al., 2008)

An important consideration in the characterisation of materials using MALDI-TOF MS is the laser power used. Ideally, a range of laser powers is required

to obtain an accurate depiction of a sample with a broad mass distribution. This was demonstrated by Lázaro and co-workers (1997) who studied coal-derived liquids by MALDI-TOF MS. It is important to obtain spectra at the minimum laser power required to achieve ionisation. High laser power is required in order to detect high molecular mass species, but can lead to fragmentation and therefore incorrect characterisation of the sample due to distortion of the lower mass regions. Too low laser energy will not produce signals with sufficient intensity, and in this study the laser power was increased to the point where all of the analyte peaks were visible without saturating the detector. In some cases this led to deterioration of the low molecular weight region of the mass distribution. The benefit of using high and low laser powers to study a sample with a broad mass distribution is therefore clear. In the case of the $AgNO_3$ matrix a higher laser power is generally required to produce a mass distribution of the material adsorbed on the spent catalyst surface. In this case artificial peaks are observed that appear more pronounced than the rest of the mass distribution at high mass range. These peaks are separated by 108 Da and can be identified by their masses. This is clearly an artefact created by photo-dissociation of the matrix molecules as opposed to the presence of species present within the sample. However, increasing the laser power in this way renders peaks of up to much higher masses, making it very useful in characterisation. The distinction can easily be made between the peaks of Ag^+ clusters (108 Da separations) and the peaks of hydrocarbon species (12, 14 or 24 Da increments) known to be present.

Size-exclusion chromatography (SEC) could be used to study the efficacy of MALDI-TOF MS. SEC or gel permeation chromatography (GPC) is a well established technique in the determination of molecular masses of soluble organic compounds. The application of SEC to the waxes studied by MALDI-TOF MS was considered since it is well-known that MALDI-TOF MS is not a quantitative technique. This is because in MALDI-TOF MS, the peak intensity depends on the ionisation efficiency of that molecule. This effect is more prominent between different classes of compounds, where molecules which

exhibit limited functionality such as saturated hydrocarbons are difficult to ionise. In addition, within the same species, smaller molecules can desorb/ionise and fly more easily than larger ones. In the study of solvent-soluble carbonaceous material, the technique has been used independently (Räder *et al.*, 1996; Pindoria *et al.*, 1996; Johnson *et al.*, 1998), or for verification of results obtained from mass spectrometry (Kahr and Wilkins, 1993; Herod *et al.*, 2000; Kühn *et al.*, 1996; Domin *et al.*, 1997; Miller *et al.*, 1998). In these cases, the material being studied was soluble in the standard solvents at room temperature, but it was crucial to find a suitable solvent. In order to calculate the absolute molecular weight of the analyte species, there has to be a sufficiently large variation between the refractive index of the solvent and that of the analyte. Furthermore, the solvent should not be too volatile, since it might evaporate within the column. SEC of commercial waxes containing a broad mass distribution and with different melting ranges was undertaken in this work. The solvents used in the experiments included decane, xylene, o-dichlorobenzene and dichloromethane. Our work did not produce satisfactory results with the available experimental set-up. Future attempts at SEC of waxes should ideally include heating of the sample (minimum temperature of 100 °C) prior to injection and the use of columns better suited to this type of work. Although SEC could not be used to obtain results to compare to MALDI-TOF MS, this work was a good demonstration of how easy MALDI-TOF MS works for high molecular weight hydrocarbons.

4.3 Concluding remarks

Some commonly used techniques such as High Resolution Transmission Electron Microscopy, Raman spectroscopy and X-ray Photoelectron Spectroscopy were employed in the investigation into the nature of carbonaceous species typically found on spent iron-based catalysts recovered from high temperature Fischer-Tropsch reactors. These techniques fall short when working with inhomogeneous samples, although some useful information can be obtained. Large volumes of carbonaceous species in

complex spent catalyst structures also pose a challenge for the identification of the nature of deposited material.

In this chapter, a new technique for the determination of the nature of carbonaceous deposits, namely Matrix-Assisted Laser Desorption/Ionisation-Time of Flight Mass Spectrometry has been developed. As well as the range of the mass distribution, the separation between peaks can also provide information about the species present. The difficulties that might be encountered in the interpretation of the results have been highlighted. Despite these drawbacks, there is ample useful information that can be obtained on the chemical nature of carbonaceous deposits from these spectra. The technique is also easy to apply, qualitatively representative of the ionisable species and provides a quick indication of the nature of carbonaceous species.

The nature of the carbonaceous deposits was therefore identified as polymeric carbon and polycyclic aromatic hydrocarbons with a large molecular weight range. This hard carbon is predominantly amorphous, although the species grow to large sheets that bear a resemblance to graphene.

5.EVOLUTION OF CHEMICAL AND PHYSICAL PROPERTIES OF HTFT CATALYSTS WITH TIME ON-STREAM

5.1 Introduction

The objective in this section is to understand the factors that govern the rate of hard carbon formation and the mechanism by which it is formed. We also aim to understand structural changes associated with the build-up of carbonaceous deposits and the effects it has on the chemical and physical properties of the HTFT catalyst. In the commercial Sasol Advanced Synthol (SAS) reactors, online catalyst replacement is performed, which involves removing a portion of the spent catalyst and adding fresh catalyst at given intervals. As a result, investigating the chemical and physical properties of HTFT catalysts obtained from the SAS reactor is complicated since the particles have experienced different exposure times to HTFT conditions. The complications associated with studies of the catalyst recovered from the SAS reactor can be partly addressed by studying the catalyst from a Pilot Plant reactor where all the catalyst has experienced the same time on-stream (see Section 3.2.1.4). However, an understanding of the time-dependent structural evolution of the catalyst and the influence on chemical and physical properties as a function of duration under Fischer-Tropsch conditions is still lacking. In order to monitor the evolution of chemical and physical properties as a function of time on-stream, the Synthol catalyst was therefore exposed to Fischer-Tropsch synthesis conditions for different durations in a Berty micro-reactor to investigate the effect of exposure time on the composition and properties of the recovered catalyst. The spent catalysts obtained from these experiments will be referred to as Spent Cat-3(#), where # is the number of days the catalyst was exposed to HTFT conditions. The Berty reactor, shown schematically in Figure 5.1, is a gradientless reactor that circulates gas past a stationary catalyst bed. These reactors are operated at very similar conditions as the SAS reactor. The gas feed composition in the Berty micro-reactor is tuned to mimic a ‘slice’ at the inlet of the SAS reactor by co-feeding CO_2 as this would be present in the recycle stream to the SAS reactor. A key

advantage of a Berty micro-reactor is that the restrictions pertaining to the initial particle size distribution are different to that in the SAS and Pilot Plant reactor since there is no fluidisation in this reactor. Thus, a narrow fraction (45 – 75 µm) of particle sizes was used in the tests. There are several benefits to using a narrow size fraction; the most obvious being that the inhomogeneous distribution of promoter elements with particle size will be minimised, since the variation in promoter levels is strongly dependent on the particle size of the catalyst (see Section 2.2).

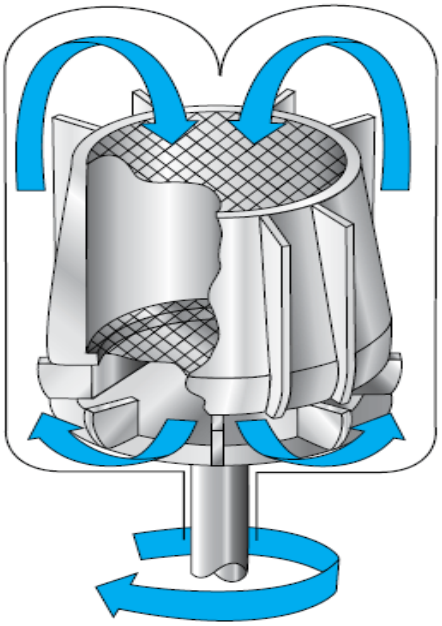

Figure 5-1: Schematic representation of a Berty reactor (image obtained from www.autoclaveengineers.com/products/catalytic)

Investigating the activity and selectivity is an important way to establish the effect of the catalyst composition on the performance during FTS. Insight into the chemical evolution of the HTFT catalyst can be obtained by investigating the composition and relating this to the catalytic performance, the amount and nature of the carbonaceous deposits. The physical evolution, which can be described as a change in the Geldart powder classification of the catalyst particles, has been postulated as the cause of detrimental transition in the fluidisation regimes within the SAS reactor (Steynberg *et al.*, 2004).

5.2 Results and Discussion

5.2.1 Quantification of Carbon

The easiest way to determine the total carbon content of the spent catalysts is by CHN microanalysis. The total carbon content of the catalysts recovered from the Berty reactor provides an indication of the evolution of the catalyst by deposition of carbonaceous species, as depicted in Figure 5.2. The samples were analysed as-received and the carbon content shows a general increase with time on-stream (TOS), but there is significant scatter. A transition in the amount of total carbon deposited over time appears to occur around 1 day on-stream from the data presented here, although this could be confirmed by further Berty experiments.

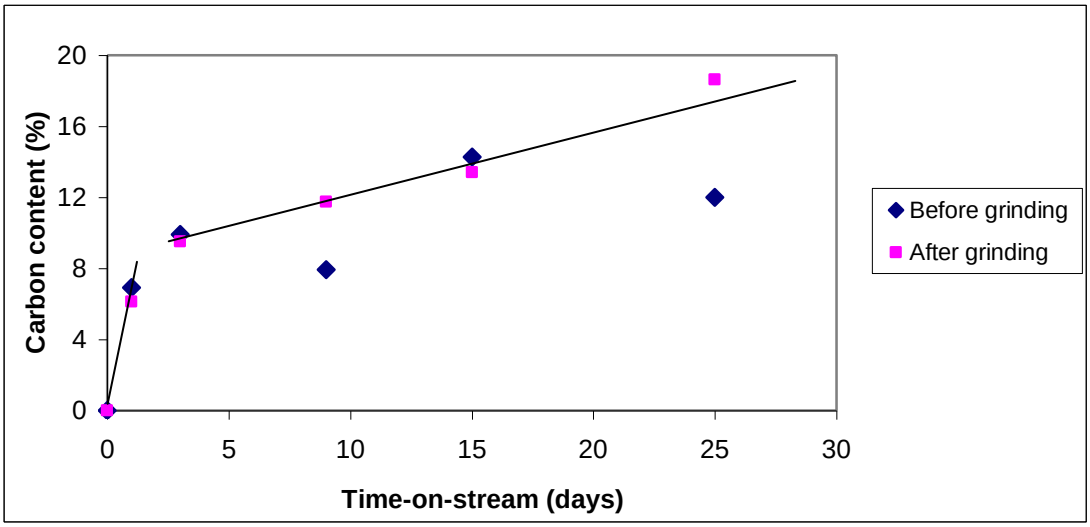

Figure 5-2: Total carbon content of spent iron Fischer-Tropsch catalysts from Berty reactor before and after grinding, shown as a function of exposure time to reaction conditions. Microanalysis performed on Carlo Erba CE 1108 or 1110

Microanalysis of the spent catalysts constitutes an important part of the characterisation process since the progressive deposition of carbon overlayers is the main factor influencing catalyst composition and possibly physical and chemical properties. However, obtaining reproducible results using CHN microanalysis was challenging for the Spent Cat-3 samples.

From the recognised difficulties in analysing the HTFT catalysts, simple mortar and pestle grinding was performed prior to subsequent analyses in

order to expose a greater surface area of catalyst material to the oxygen during combustion. These CHN results obtained are also depicted in Figure 5.2. The spent catalysts ground to a fine powder show a linear increase in the carbon content with TOS with the exception of the Spent Cat-3(1) catalyst (the catalysts are named according to the number of days spent in the Berty micro-reactor). The carbon content after 1 day on-stream probably represents mainly the formation of iron carbides, whereas all subsequent carbon deposits represent the build-up of hard and soft carbon. The hydrogen content, which gives an indication of the hydrocarbon (and moisture) content in the deposits, measured for all the catalysts was below the detection limit. This suggests that there was no soft carbon adsorbed on the Spent Cat-3 samples. However, monitoring the formation of water during the temperature-programmed oxidation (TPO-MS) of the Spent Cat-3 samples revealed that there is in fact some hydrogen associated with this catalyst *i.e.* H_2O is generated. It was also demonstrated in Section 3.2.1 that wax is desorbed from the catalyst without undergoing oxidation and would therefore not contribute to the amount of water monitored by mass spectrometry of the effluent. This inconsistency between these two techniques requires further investigation.

Thermogravimetric analysis coupled with differential scanning calorimetry (TGA-DSC) using an inert gas (He) was therefore applied to determine the temperature at which the endothermic event associated with desorption of wax occurs. Figure 5.3 indicates that this event which is accompanied by a mass loss of 1.9 % occurs around 440 °C. This temperature was therefore employed for thermal desorption of the Spent Cat-3 samples. It should be noted that the temperature at which the mass loss occurs is subject to the ramp rate, and could actually commence at a lower temperature. In addition, it was demonstrated in Section 3.2.1.5 that wax is detected at higher temperatures as well, which implies that the 1.9% reported here represents the minimum amount of wax present. The 20% mass loss commencing at 540 °C possibly represents the thermal degradation of hard carbon or phase transformation.

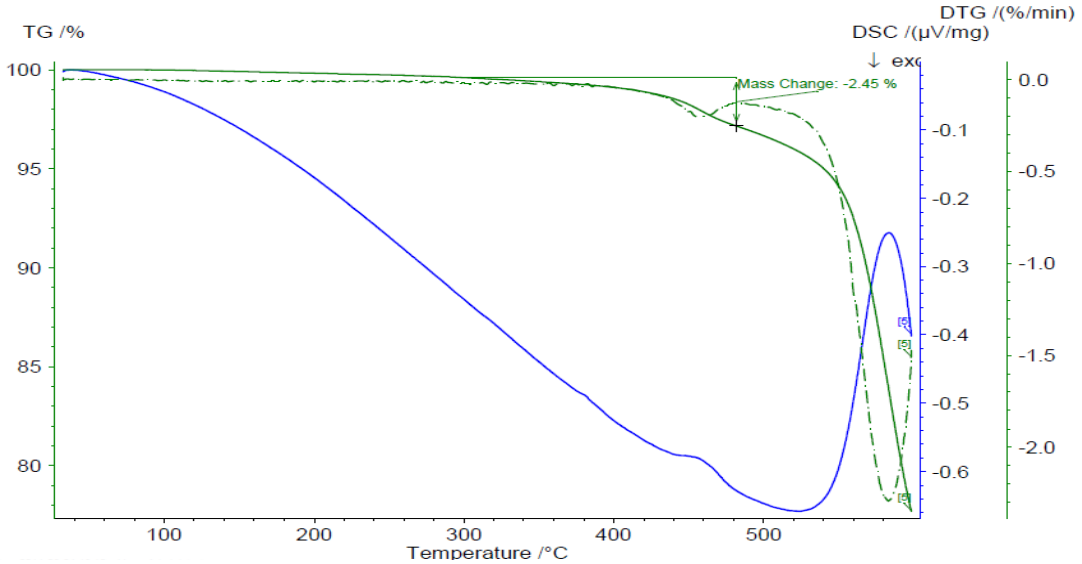

Figure 5-3: TGA-DSC of Spent Cat-3(25): a spent Fischer-Tropsch catalyst recovered from the Berty reactor after 25 days on-stream. Netzsch STA 449 F1 Jupiter®, He flow rate: 50 mL/min, 5 °C/min to 600 °C

The presence of adsorbed soft carbon demonstrates the limitations of the microanalysis technique used to collect the data presented in Figure 5.2 in detecting hydrogen on the catalyst.

A variation of the method of microanalysis, using a horizontal furnace, was therefore used to determine the carbon and hydrogen content of the Spent Cat-3 samples before and after desorption (Figure 5.4). Thermal desorption at 440 °C reduces the carbon content in these samples by 2-3 wt%. With an increase in TOS, the mass percentage of carbon present in the catalysts increases. This increase represents mainly hard carbon since the wax is mostly removed by thermal desorption, although changes in the relative amount of iron carbide also contribute to the observed trends.

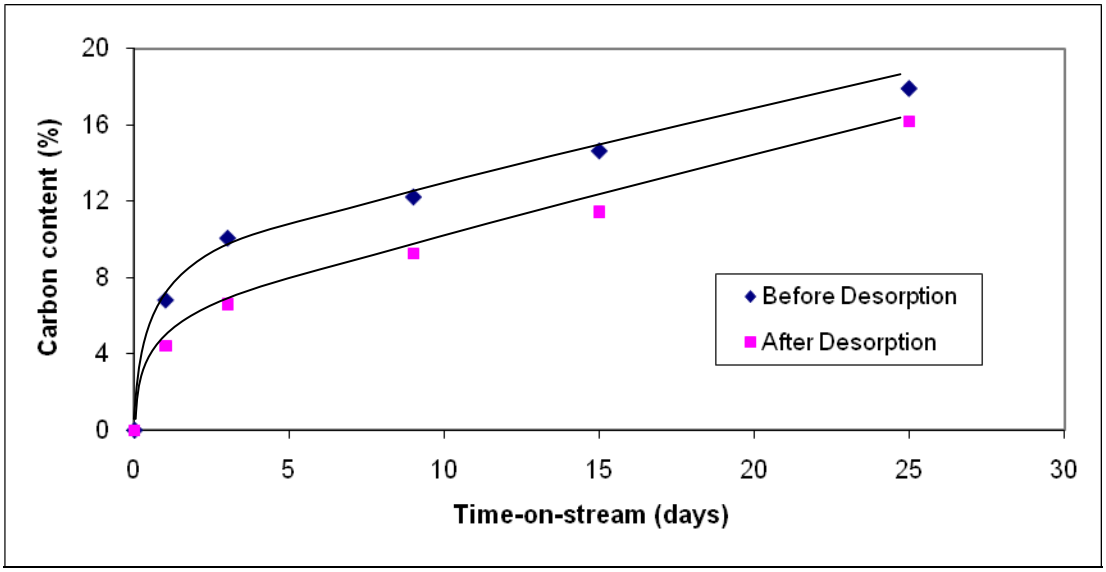

Figure 5-4: Total carbon content of spent iron Fischer-Tropsch catalyst samples recovered from the Berty reactor before and after wax removal by desorption at 440 °C, as a function of exposure time to reaction conditions. CE 440 elemental analyser

The presence of hydrocarbons is indicated by the occurrence of adsorbed hydrogen on the surface of the catalyst. The measured amount of hydrogen (Table 5.1) is very low and is merely an indication of the existence of hydrogen-containing species on the catalyst. The measurement also cannot discriminate between moisture and hydrocarbons. There appears to be a marked drop in the hydrogen content after thermal desorption. The hydrogen remaining after desorption is either associated with polycyclic aromatic hydrocarbons (PAHs) known to be adsorbed on HTFT catalysts (see Section 4.2.1.4) and/or wax that has not been effectively removed by the desorption treatment.

Table 5-1: Carbon and hydrogen content (m/m %) of Spent Cat-3 samples

	Before desorption		After desorption at 440 °C	
	C	H	C	H
Spent Cat-3(1)	6.81	<0.2	4.43	0.04
Spent Cat-3(3)	10.05	0.25	6.61	0.06
Spent Cat-3(9)	12.21	0.38	9.27	0.18
Spent Cat-3(15)	14.62	0.45	11.45	0.18
Spent Cat-3(25)	17.88	0.57	16.16	0.37

Phase analysis by XRD coupled with Rietveld refinement conducted on Spent Cat-3(25) catalyst after thermal desorption at 440 °C revealed that there is

significant phase transformation (Table 5.2) associated with this thermal treatment. This is associated with the excessively high temperature used during the desorption process. In addition, the presence of small amounts of oxygen in the N_2 gas that is used for desorption could also contribute to the phase transformation. The drop in mass percentage of carbon remaining is therefore not only due to desorption of hydrocarbons but also associated with these phase transformations, thereby complicating the carbon analysis. Since it has been shown that iron carbides and hard carbon oxidise at similar temperatures (Section 3.2.1), the main concern is that the amount of hard carbon determined for the catalysts after desorption at 440 °C will be inaccurate.

Table 5-2: Relative abundances (m/m %) of constituent phases of Spent Cat-3(25) catalyst before and after thermal desorption at 440 °C

	PDF number	Before desorption	After desorption
Hägg carbide	36-1248	35.9	16.8
Magnetite	19-0629	63.4	83.2
Cementite	3-0989	0.7	-
X^2	-	1.662	1.560

Thermal desorption was therefore performed at reduced pressure at 350 °C to minimise phase transformation. This temperature was specifically chosen since the catalysts typically experience these conditions during HTFT reaction. Table 5.3 shows the relative abundance of the constituent phases of the catalysts after vacuum desorption treatment at 350 °C. Figure 5.5 indicates that the relative abundance of carbide is similar before and after this treatment, which implies that performing the vacuum desorption at 350 °C is a suitable wax removal method. The catalysts at longer TOS show less of a change in the relative amount of carbide phases. This is probably due to the high concentration of hard carbon present in these samples, which protects the carbides from transformation. Carbon and hydrogen content of the catalysts before and after vacuum desorption at 350 °C is given in Table 5.4.

Table 5-3: Relative abundances (m/m %) of constituent phases of Spent Cat-3 samples after thermal desorption at 350 °C

	PDF number	Spent Cat-3(1)	Spent Cat-3(3)	Spent Cat-3(9)	Spent Cat-3(15)	Spent Cat-3(25)
Hägg C	19-0629	43.85	42.6	35.6	45.0	35.8
Magnetite	36-1248	56.15	57.4	64.4	55.0	64.2
X^2	-	0.980	0.931	0.900	1.037	0.983

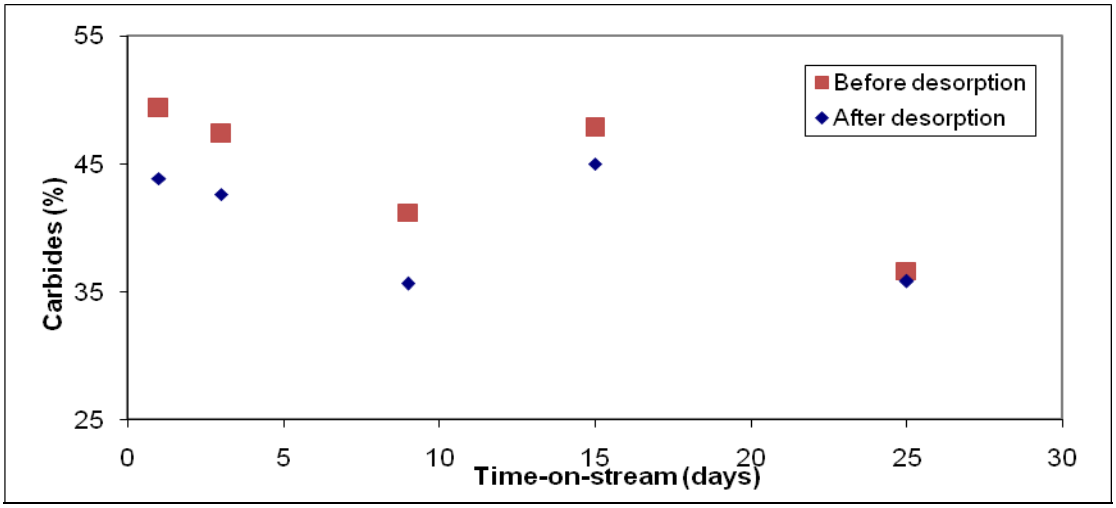

Figure 5-5: Total carbide content as determined by XRD of spent iron Fischer-Tropsch catalysts recovered from a Berty reactor, before and after wax removal by vacuum desorption at 350 °C. Spent Cat-3(15) removed after 15 days on-stream represents an anomalous data point.

Table 5-4: Carbon and hydrogen content (m/m %) of Spent Cat-3 samples before and after desorption at 350 °C

	Before desorption		After desorption at 350 °C	
	C	H	C	H
Spent Cat-3(1)	6.81	<0.2	6.41	0.1
Spent Cat-3(3)	10.05	0.25	9.35	0.16
Spent Cat-3(9)	12.21	0.38	11.63	0.28
Spent Cat-3(15)	14.62	0.45	12.73	0.32
Spent Cat-3(25)	17.88	0.57	16.79	0.47

One of the most important aspects to be considered is the rate at which hard carbon is deposited on the catalyst as this determines the frequency of on-line catalyst replacement in the SAS reactor. The total carbon, expressed in terms of the amount of iron present on the catalyst, can be classed into the different types namely soft, hard and carbidic carbon. Classifying the different carbon types in order to study the build-up of individual carbonaceous species would be beneficial in understanding the rates of formation of these individual

species. Specifically, the rate of hard carbon deposition can provide insight into the time-scale of productivity loss and changes in associated physical properties. Figure 5.6 shows this for the Spent Cat-3 samples before and after wax desorption. The rate of carbon deposition is indicated by the slope of the graph.

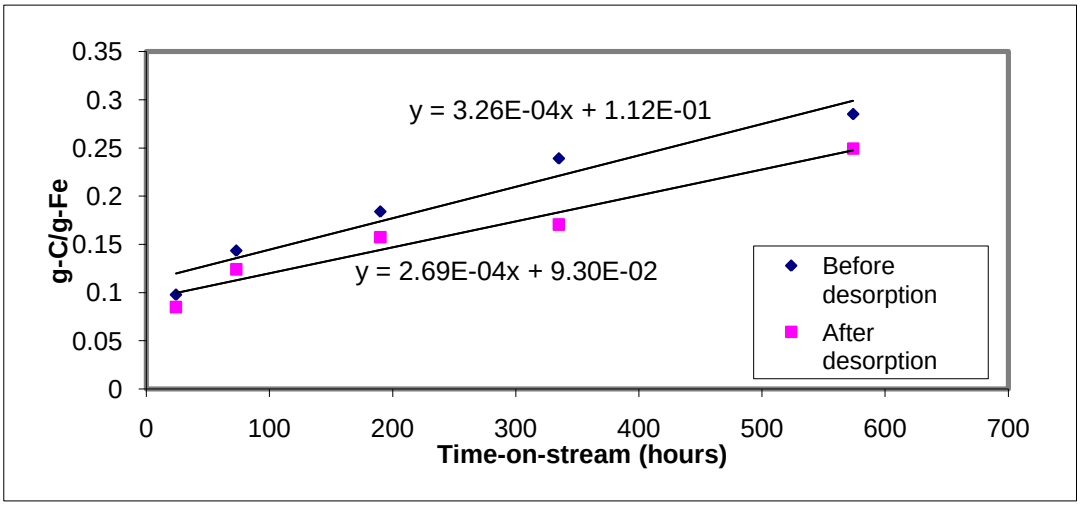

Figure 5-6: Rates of carbon formation in a Berty micro-reactor before and after wax removal by vacuum desorption at 350 °C. The slope of each graph represents the rate of carbon formation

The observation that hydrocarbons are desorbed from the catalysts recovered from the Berty micro-reactor elicited the need for thermal desorption of the samples prior to analysis. This is necessary in order to simplify the catalysts for subsequent quantification. The vacuum desorbed catalysts provide a platform for determining the rate of hard carbon formation since this treatment removes soft carbon without significantly affecting the hard carbon (carbides and hard carbon oxidise at similar temperatures and phase analysis shows very little oxidation of the carbides). The difference between the total mass of carbon and the mass of carbon in crystalline material (iron carbides) represents the amount of amorphous hard carbon and amorphous carbides. This is shown in Equation 5.1 below:

$$(C_{HardCarbon} + C_{Carbide})_{Amorphous} = C_{Total} - C_{CrystallineCarbide} \quad (5.1)$$

Determining the Fe content of the catalyst samples is a pivotal step in the quantification of carbon and was performed using elemental analysis. The mass percentage of Fe in the catalysts after vacuum desorption can be used to determine the amount of crystalline material that is present on the catalyst. This would allow scaling the mass of iron to the total mass of crystalline material through the relative abundance of oxide and carbide phases, using Equation 5.2:

$$M_{CrystallinePhases}\,\% = M_{Fe}\,\% \times \left(\left(\frac{M_{W,Fe_3O_4}}{3 \times M_{W,Fe}} \times f_{Fe_3O_4} \right) + \left(\frac{M_{W,Fe_5C_2}}{5 \times M_{W,Fe}} \times f_{Fe_5C_2} \right) + \left(\frac{M_{W,Fe_3C}}{3 \times M_{W,Fe}} \times f_{Fe_3C} \right) \right) \tag{5.2}$$

where $M_{CrystallinePhases}$ is the total mass percentage of the crystalline portion of the catalyst, M_{Fe} is the mass percentage of iron measured by elemental analysis, M_W is the molecular mass of the named phase and f is the mass fraction of the phase (determined by phase analysis). In order to determine the mass of the catalyst that is contributed by these crystalline phases, it was assumed that all Fe in the catalyst is present in the crystalline phase. In order to determine the phase compositions, quantitative XRD or Mössbauer Absorption Spectroscopy (MAS) data can be used. It will be demonstrated in Section 5.2.3.1 that the iron carbide content in this crystalline material is underestimated by XRD. This is because MAS is capable of detecting smaller crystallites and even amorphous materials, while it is known that XRD fails at detecting iron-containing species smaller than about 5 nm (Shroff *et al.*, 1995). It is therefore more reliable to determine phase compositions by MAS (Bukur *et al.*, 1995a; Galuszka *et al.*, 1992; Herranz *et al.*, 2006; Jin & Datye, 1998b; Loaiza-Gil *et al.*, 1999; Niemantsverdriet *et al.*, 1980; Pijolat *et al.*, 1987 Jung *et al.*, 1982a; Amelse *et al.*, 1978; Zhang *et al.*, 2004) where this is available. Although Figure 5.5 shows a slight phase transformation with thermal desorption, it was decided that MAS data before desorption would provide a better reflection of the phase composition. MAS data was not available for the Spent Cat-3 samples after thermal desorption.

Table 5.5 provides the composition of the Spent Cat-3 samples together with the mass balance. The degree of inaccuracy introduced by measuring the phase content by MAS before desorption is reflected in the total mass balance of the catalyst. The mass balances shown here therefore indicate that this method of determining the relative amounts of constituent species of the catalysts is within reasonable experimental error.

Table 5-5: Calculated carbon analysis of Spent Cat-3 samples after thermal desorption at 350 °C

Catalyst	Fe (%)	Total C (%)	Fe-containing phases (%)	Carbidic C (%)	Hard C (%)	Mass Balance
Spent Cat-3(1)	75.4	6.4	91.2	4.2	2.2	93.5
Spent Cat-3(3)	75.3	9.4	91.5	4.1	5.3	96.8
Spent Cat-3(9)	73.8	11.6	90.1	3.9	7.7	97.8
Spent Cat-3(15)	74.6	12.7	88.9	4.5	8.2	97.2
Spent Cat-3(25)	67.3	16.8	82.9	3.4	13.4	96.3

The rate at which hard carbon accumulates on the catalyst surface is the difference between the rates at which carbon adsorbs and then either hydrogenates or diffuses into the metal lattice to form bulk iron carbide. The rate of hard carbon formation can be determined by plotting the mass of hard carbon formed per unit mass of iron as a function of TOS (Figure 5.7). The slope of the graph at a particular point represents the rate of hard carbon formation. The rate of carbon formation R_{CF} is determined to be a function of TOS. For example, at 100 hours, $R_{CF,100} = 3.6\times10^{-4}\, gHC.gFe^{-1}.h^{-1}$, while at 400 hours the rate decreases to $R_{CF,400} = 2.0\times10^{-4}\, gHC.gFe^{-1}.h^{-1}$. This trend line passes through the origin, as expected. It is worth noting that the Spent Cat-3(15) catalyst exhibits different behaviour to the other samples; after desorption the amount of carbon per mass of iron is lower than expected.

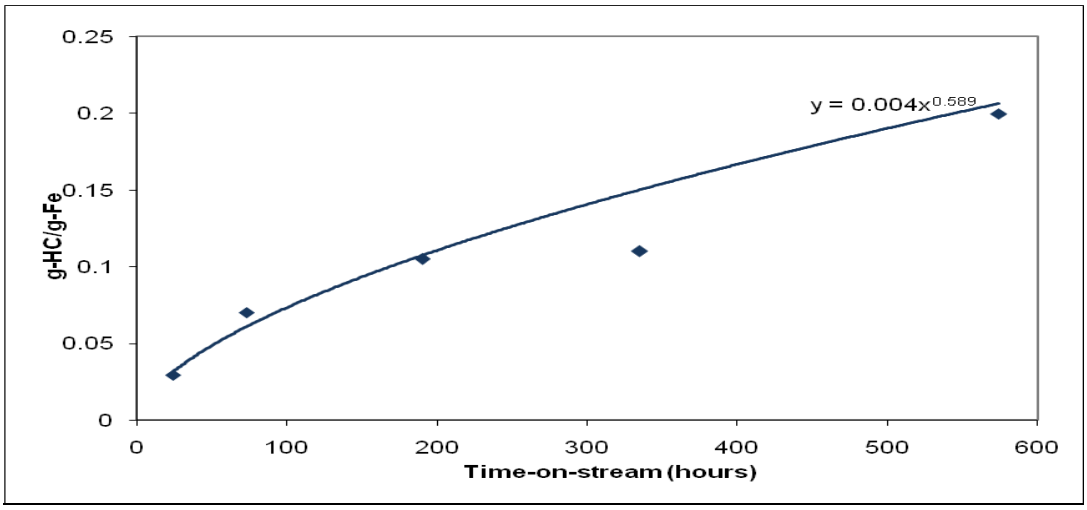

Figure 5-7: Rates of hard carbon formation of spent iron Fischer-Tropsch catalyst samples recovered from the Berty reactor, following wax removal by vacuum desorption at 350 °C, as a function of exposure time to reaction conditions

5.2.2 Evolution of HTFT Catalyst Structure

It is possible to understand the genesis of catalyst structure by studying the material that has experienced different durations of exposure to FTS conditions. Raman spectroscopy is an ideal tool for this application since this technique can be used to probe the surface of the spent catalyst powders. The Raman spectrum of Spent Cat-3(1) (Figure 5.8) exhibits strong magnetite modes between 200 and 800 cm^{-1} and broad C-C modes around 1350 and 1600 cm^{-1}. This can be ascribed to the small amount of hard carbon present after 1 day on-stream. The Raman spectra show a remarkable decrease in the intensity of the Fe-O modes relative to the C-C modes as a function of TOS, which indicates that the extent of carbon deposition is gradually increasing and thereby enveloping the catalyst. The relative intensities between the most intense modes characterising the magnetite and carbonaceous species, normalised to that of Spent Cat-3(25), is tabulated in Table 5.6. These results suggest the existence of a core-shell structure, as previously discussed in Section 3.2.2. Observing oxides using Raman implies that this phase is present near the surface. The fact that these samples are passivated after reaction suggests the possibility of these oxides forming by oxidation of surface carbides.

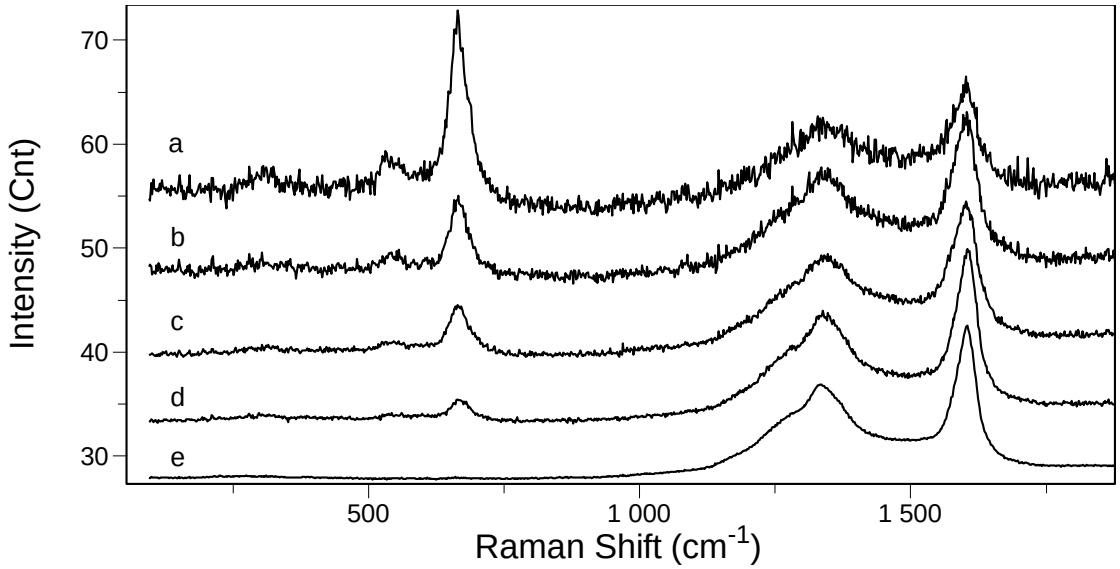

Figure 5-8: Raman spectrum of spent iron Fischer-Tropsch catalysts recovered from the Berty reactor after (a) 1, (b) 3, (c) 9, (d) 15 and (e) 25 days on-stream. Excitation wavelength: 514 nm

Table 5-6: Relative intensities of magnetite (650 cm^{-1}) to carbonaceous species (1600 cm^{-1}) in Spent Cat-3 samples normalised to Spent Cat-3(25)

	Berty1	**Berty3**	**Berty9**	**Berty15**	**Berty25**
$I_{Fe\text{-}O}/I_{C\text{-}C}$	27.9	16.4	8.5	6.6	1

The existence of a core-shell structure was therefore further investigated by imaging of the polished segments of the various catalysts. Although from the Raman spectra one can speculate the existence of a core-shell structure, the images (not shown) do not demonstrate this.

SEM images of the various Spent Cat-3 powders are shown in Figures 5.9-5.13. Enlarged images reveal differences with TOS, since the particles appear to become 'fluffy' after 9 days on-stream. The particles seem more broken and within the broken segments there are small particles that appear to be adhered to the larger ones.

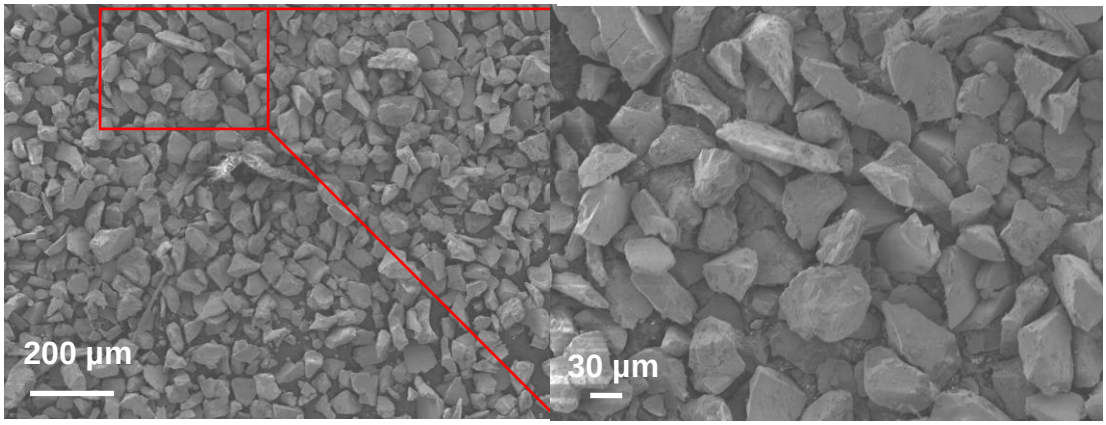

Figure 5-9: Scanning electron microscopy image of spent iron Fischer-Tropsch catalyst recovered from the Berty reactor after 1 day on-stream

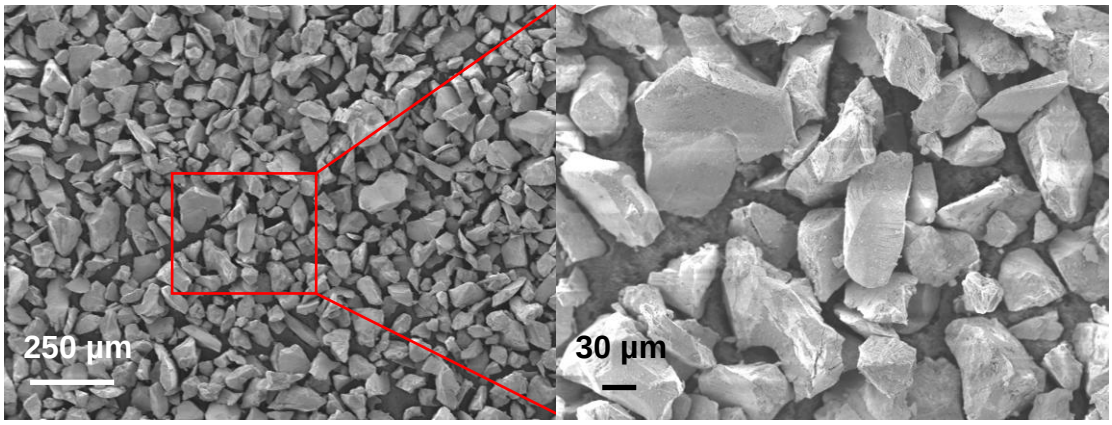

Figure 5-10: Scanning electron microscopy image of spent iron Fischer-Tropsch catalyst recovered from the Berty reactor after 3 days on-stream

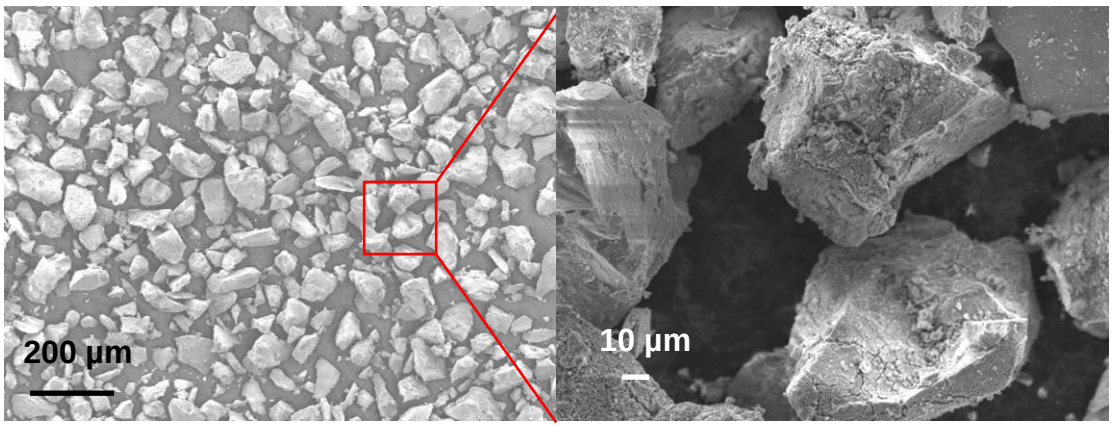

Figure 5-11: Scanning electron microscopy image of spent iron Fischer-Tropsch catalyst recovered from the Berty reactor after 9 days on-stream

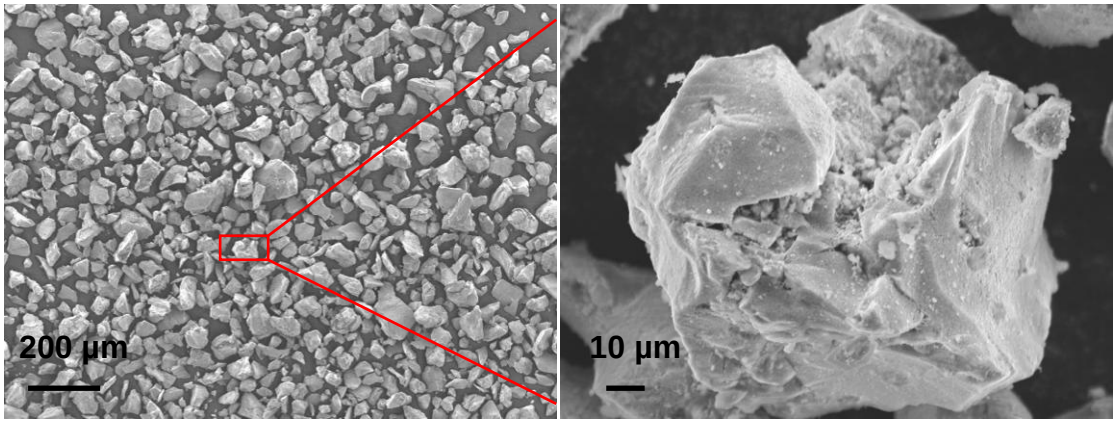

Figure 5-12: Scanning electron microscopy image of spent iron Fischer-Tropsch catalyst recovered from the Berty reactor after 15 days on-stream

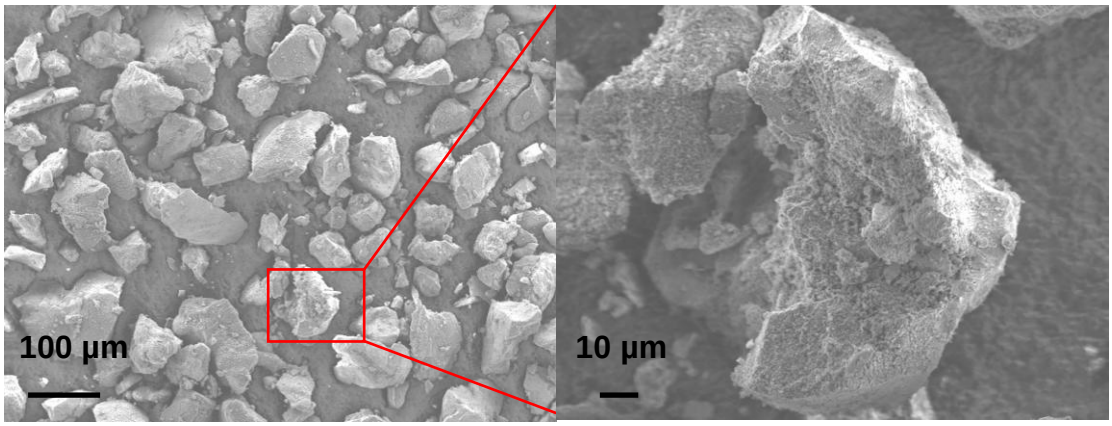

Figure 5-13: Scanning electron microscopy image of spent iron Fischer-Tropsch catalyst recovered from the Berty reactor after 25 days on-stream

5.2.3 Effects of Carbon on Chemical Properties

5.2.3.1 Phase-Activity Relationships

The iron-based FTS catalyst system has been a subject of research for over 80 years, but the exact structural composition of the active species remains controversial. Fe_3O_4 (Reymond *et al*., 1982; Kuivila *et al*., 1989; Butt, 1991), α-Fe (Niemantsverdriet *et al*., 1980; Ott et al., 1980; Loaiza-Gil et al., 1999; Dwyer & Somorjai, 1978) and iron carbides (Amelse *et al*., 1978; Raupp & Delgass, 1979a, b; Shroff *et al*., 1995; Dictor & Bell, 1986; Jung & Thomson, 1992) have all been reported as the active phase in FTS. It is well-known that the phase of a catalyst plays a crucial role in the catalyst performance. The approach in this section is therefore to present the activity data in terms of both the ($CO+CO_2$) and ($CO+H_2$) conversion, followed by the phase

compositions and then to identify any relationships between the activity and phase in order to obtain an idea of the apparent active phase.

($CO+CO_2$) conversion was calculated from the molar flow rates obtained from the GC-TCD analyses. CO_2 is co-fed to the Berty micro-reactors in order to mimic the conditions in the SAS reactor. The ($CO+CO_2$) conversion is defined as the amount of CO converted to hydrocarbon products only, as calculated from the $CO+CO_2$ mass balance:

$$(CO+CO_2)conversion = \frac{\left(\dot{n}_{CO,in} + \dot{n}_{CO_2,in}\right) - \left(\dot{n}_{CO,out} + \dot{n}_{CO_2,out}\right)}{\left(\dot{n}_{CO,in} + \dot{n}_{CO_2,in}\right)}.100\% \qquad (5.3)$$

Figure 5.14 depicts the ($CO+CO_2$) conversion for the Berty experiments and does not change significantly as a function of TOS. The significance of ($CO+CO_2$) conversion is that the amount of CO converted to CO_2 *via* the Water Gas Shift (WGS) reaction is excluded. At normal HTFT operating conditions the WGS reaction is known to be at equilibrium and therefore the ($CO+CO_2$) conversion includes the CO produced *via* the reverse reaction. The ($CO+H_2$) or syngas conversion with TOS is shown in Figure 5.15. There is a slight decrease in syngas conversion with TOS that is more pronounced in the case of the Spent Cat-3(15) reactor run. This reflects an increased rate of the WGS reaction with TOS. Commercially, the phase of the reduced (activated) iron catalyst is known to transform very rapidly (approximately 2 hours) to iron carbides and magnetite and remains fairly stable for extended periods within the commercial reactor (Dry, 1981). The activity results presented here do not necessarily demonstrate this catalyst stability as a function of TOS and could be attributed to several operational differences between the two methods, such as reactor type, temperature or partial pressures of the reactant and product gases.

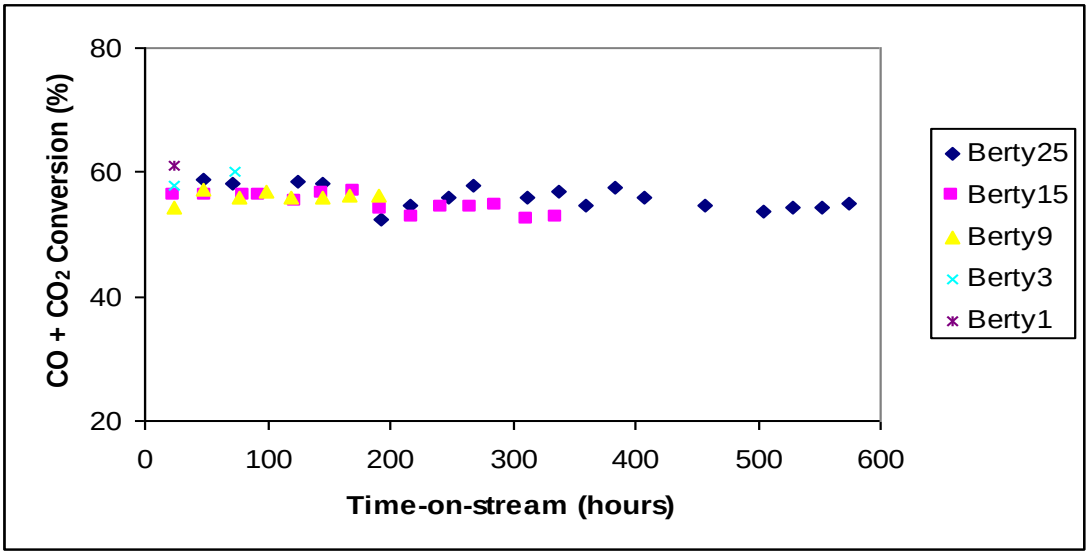

Figure 5-14: Variation in CO+CO2 conversions (%) for Berty reactor runs with time on-stream under Fischer-Tropsch reaction conditions

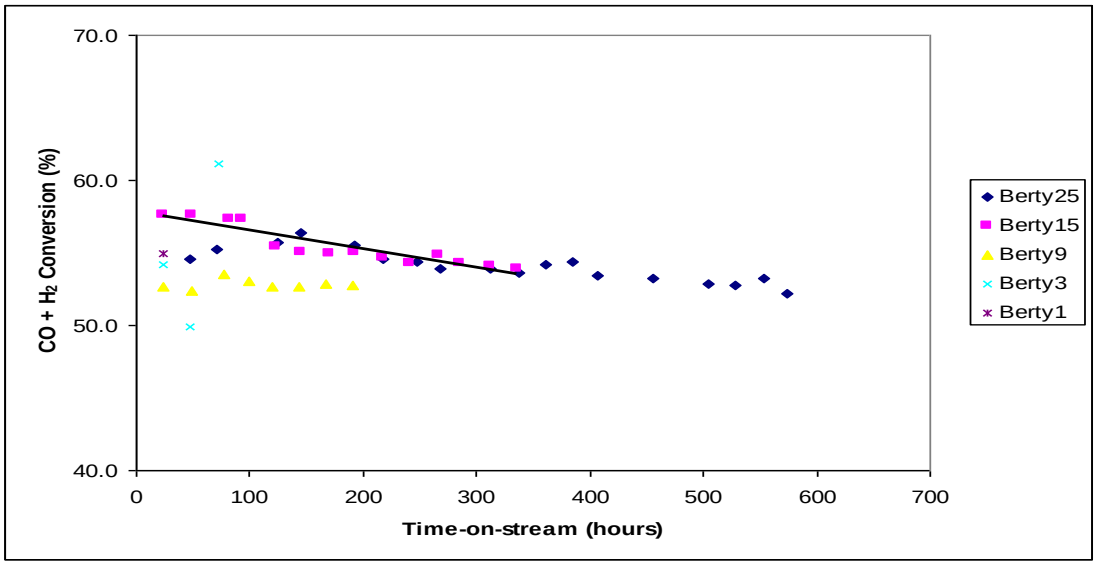

Figure 5-15: Variation in CO+H2 conversions (%) for Berty reactor runs with time on-stream under Fischer-Tropsch reaction conditions

XRD was employed to determine phase composition of the catalysts recovered from the Berty reactor following exposure to Fischer-Tropsch conditions for different durations. It is important to note that oxidation associated with exposure to air is believed to be minimised to a few nanometres (Shroff & Datye, 1996), since the catalysts were passivated using CO_2 upon removal from the Berty reactor. It is expected that oxidation will be greater on catalysts with more surface carbide crystallites. The powder

diffractograms obtained were refined by the Rietveld method. The relative abundance of the constituent phases is presented in Table 5.7. The samples were found to exhibit a slight decrease in relative amount of the carbide phases as a function of exposure time to Fischer-Tropsch synthesis conditions, as previously observed by Malan et al. (1961). This might be linked to oxidation of more surface carbides that are present at longer TOS. Spent Cat-3(15) does not follow this trend, and the anomalous behaviour of this sample corresponds to a larger decrease in syngas conversion. As described earlier, Spent Cat-3(15) has a higher WGS activity, producing more CO_2 than the other catalysts. A corresponding increase in the magnetite content would be expected for this catalyst since this phase is known to be active for WGS reaction (van der Laan & Beenackers, 2000; Prasad *et al.*, 2008). This is in fact not observed. In Section 5.2.1, it was demonstrated that the amount of hard carbon per mass of Fe is lower than expected. This suggests that there might be a difference in the amount of promoter elements present on this catalyst. Less potassium would lead to a decrease in FTS activity as well as carbon deposition, while the reducing environment owing to the production of more H_2 *via* the WGS reaction could still bring about carbide formation of the catalyst.

Table 5-7: Relative abundances (m/m %) of constituent phases of Spent Cat-3 samples (determined by XRD)

	PDF number	Spent Cat-3(1)	Spent Cat-3(3)	Spent Cat-3(9)	Spent Cat-3(15)	Spent Cat-3(25)
Hägg carbide	36-1248	47.8	46.1	37.1	47.5	35.9
Magnetite	19-0629	50.7	52.6	58.7	52.2	63.4
Cementite	3-0989	1.5	1.2	4.1	0.3	0.7
X^2	-	1.858	1.446	1.564	1.644	1.662

Mössbauer Absorption Spectroscopy (MAS) of the catalysts recovered from the Berty micro-reactor can provide additional information about the phases. Table 5.8 shows the phase composition for the various samples.

Table 5-8: Relative abundances (m/m %) of constituent phases of Spent Cat-3 samples (determined by MAS)

	Spent Cat-3(1)	Spent Cat-3(3)	Spent Cat-3(9)	Spent Cat-3(15)	Spent Cat-3(25)
Hägg carbide	58.1	56.2	54.5	64.1	51.0
Magnetite	41.9	43.8	45.5	35.9	49.0

Figure 5.16 shows the percentage of Hägg carbide (and cementite, if present) as determined by the two techniques. Although different relative abundance of the constituent phases was measured by XRD and MAS, Figure 5.17 shows that the carbide content follows similar trends. There is however higher carbide content measured by MAS, which suggests that there are small iron carbide crystallites present which are not detected by XRD. Figure 5.18 depicts the correlation between the end of run ($CO+H_2$) conversions and the total carbide and hard carbon contents. Therefore in Figure 5.17, we see the effects of phase transformation (oxidation) as well as hard carbon formation on the activity of the catalyst. Both factors affect FT activity. Using *in-situ* techniques to monitor the phase-activity relationships is therefore better.

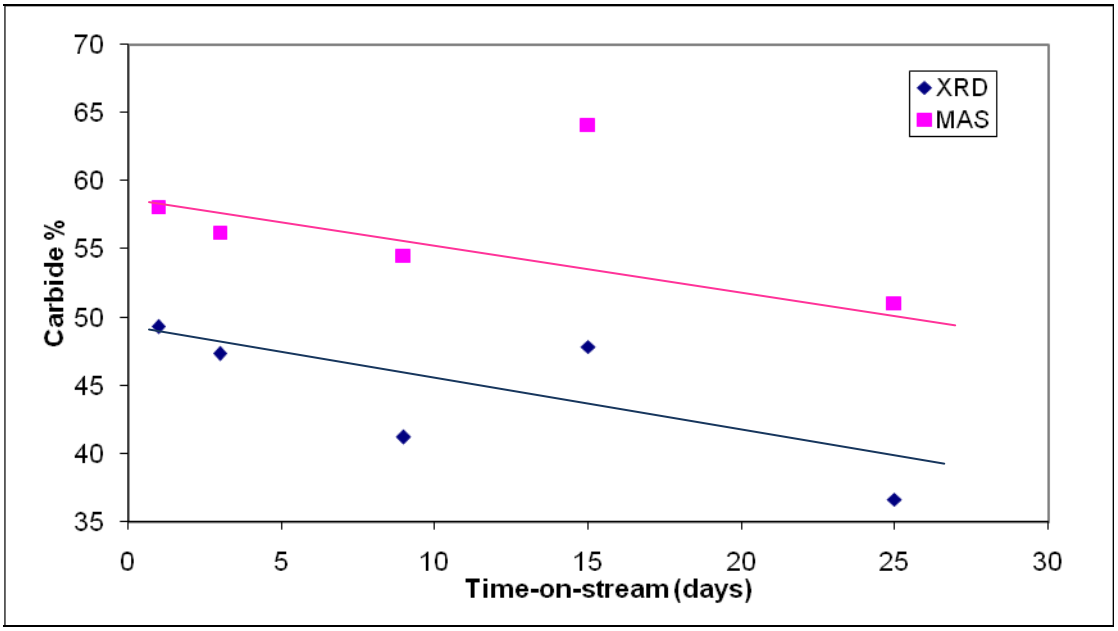

Figure 5-16: Relative abundance of total carbide phases present in spent iron Fischer-Tropsch catalysts recovered from the Berty reactor determined by XRD and MAS as a function of exposure time to reaction conditions

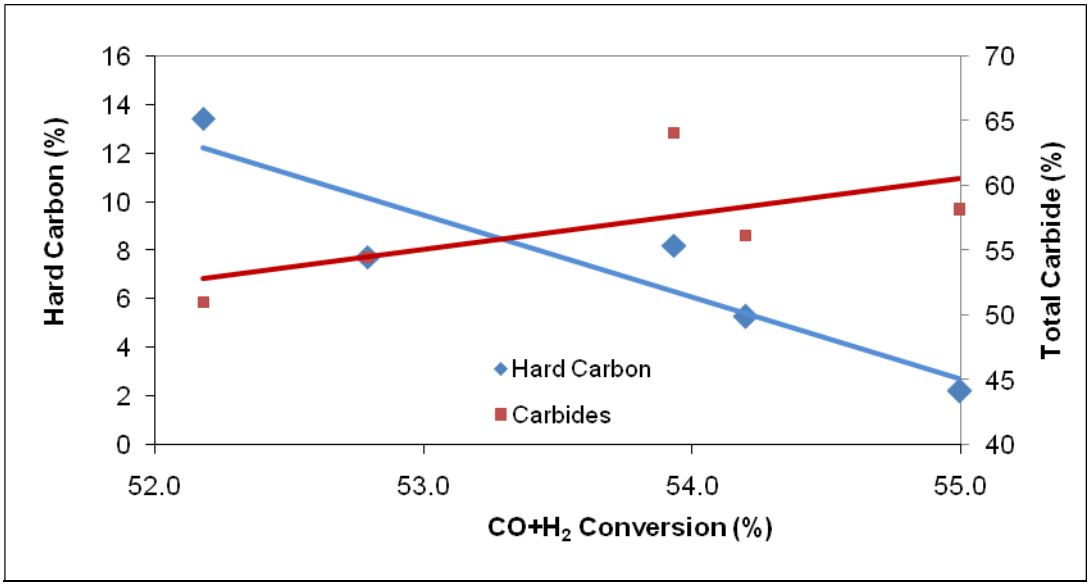

Figure 5-17: End-of-run CO+H2 conversions for spent iron Fischer-Tropsch catalysts recovered from the Berty reactor as a function of hard carbon and total carbide content determined by MAS

5.2.3.2 Mass distributions of carbonaceous deposits

The previous sections dealt with the amount of carbon that is deposited with TOS and the associated iron-related phases. In this section, MALDI-TOF MS data, which provides insight into the nature of hard carbon species, is discussed (see Section 4.2). The two matrices that were used in this investigation are $AgNO_3$ and 7,7,8,8-tetracyanoquinodimethane (TCNQ). Figure 5.18 shows the overlaid mass distributions of the various catalysts obtained from the Berty micro-reactor studies. It is demonstrated that the relative intensity of the carbonaceous deposits to matrix peaks (up to 400 Da) increases with TOS. This corresponds to the increase in carbon content measured for these catalyst materials. Spent Cat-3(1) has a very small mass distribution. This can be explained by the fact that the carbon present on the catalyst is predominantly associated with the iron carbide and that the deposition of free carbon (soft or hard) is still in its infancy. With an increase in TOS, catalysts have progressively more prominent mass distributions. Figure 5.19 indicates that the mass distribution is a continuum of peaks separated by 1 Da but with an underlying repetition of 12 Da. The mass distribution shown is very complex and a secondary distribution of 14 Da associated with a CH_2 repeating unit would be concealed by the main distribution. There are 2 Da

separations corresponding to varying degrees of saturation within each homologous series. Furthermore, in between these peaks are isotope peaks for ^{13}C, which explains why every second peak is slightly lower in intensity. Bearing in mind the isotopic abundance of ^{13}C is only 1.1%, it might seem unlikely that this is the only reason for this mass distribution. The cumulative effect of isotopic abundance was discussed in Section 4.2.1.4.

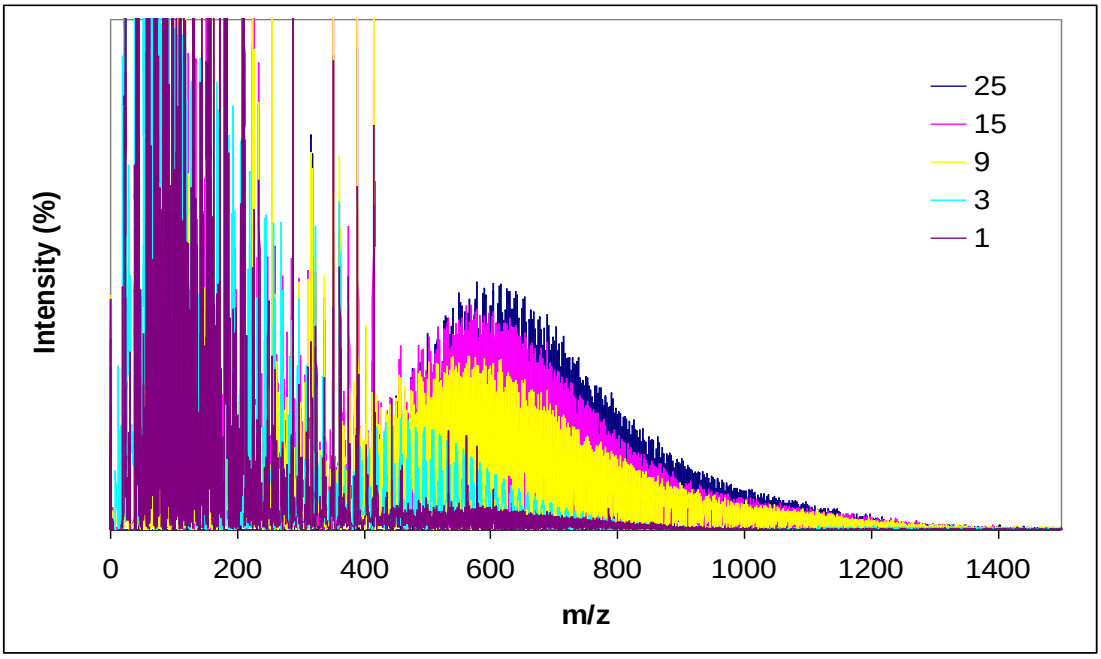

Figure 5-18: Overlaid mass distributions using TCNQ as matrix of spent iron Fischer-Tropsch catalysts recovered from the Berty reactor

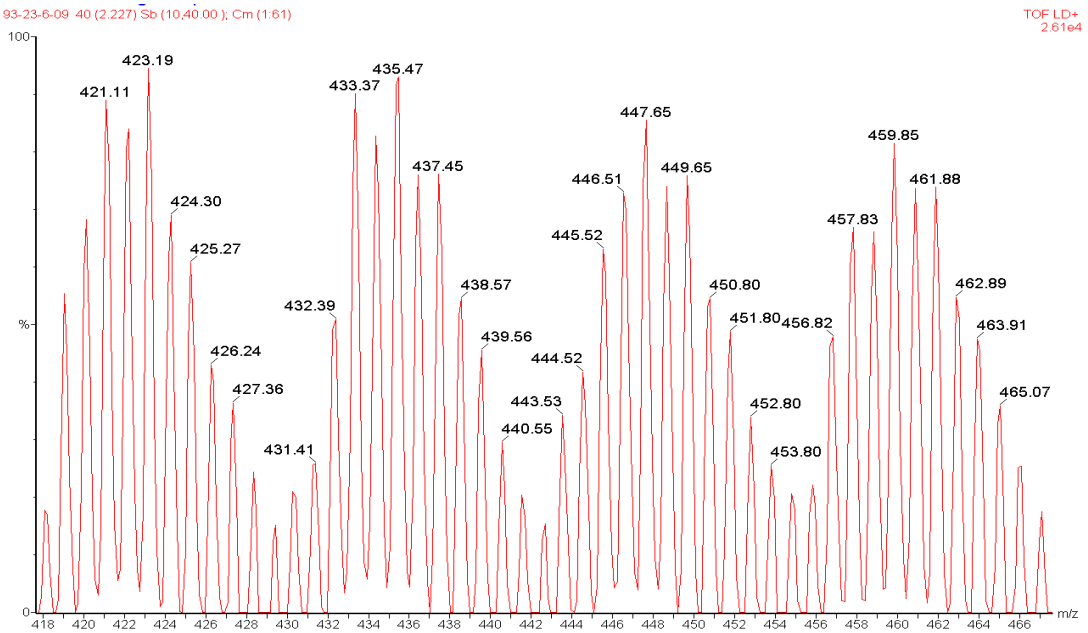

Figure 5-19: Mass distributions using TCNQ as matrix of spent iron Fischer-Tropsch catalyst recovered from the Berty reactor after 3 days on-stream

Figure 5.20 shows the various mass distributions of the Spent Cat-3 samples using $AgNO_3$ as matrix. The ranges of the mass distributions seem to increase as a function of TOS. The mass distribution is a continuum of peaks with separations of about 12 Da between the most intense peaks in the low mass range in each case. This indicates that the same polymeric carbon materials that are deposited on the catalyst recovered from the SAS and Pilot Plant reactors (see Chapter 4.2.1) are also found on these catalysts. There are peaks beyond 2000 Da for the catalysts that were removed from the reactor after 9, 15 and 25 days on-stream and it is noticeable at high masses that the mass distribution simplifies to 24 Da separations (indicative of PAHs). The mass distributions clearly show that there is a growth in the size and amount of PAHs that are present on the catalysts as a function of TOS. For TCNQ the mass distribution at low masses is a continuum of peaks (Figure 5.19), while the distributions do not extend further than 1200 Da (Spent Cat-3(25)). The information obtained from using $AgNO_3$ as a matrix is complementary to that obtained from TCNQ data in this case, since a combination of the two techniques can give a picture of the entire mass range of the distribution. The matrices therefore assist in the ionisation/desorption of molecules of different size. It should be borne in mind that the difference in laser power used for analysis using the two matrices plays an important role in the quality of the low mass region of the spectra. It is known that the lower molecular weight region of the mass distribution can be better analysed by using a lower laser power (Lázaro *et al*., 1997). Higher masses can be observed by increasing the laser power, but this is normally accompanied by a deterioration of the low mass region. This was explained in Section 4.2.2.2.

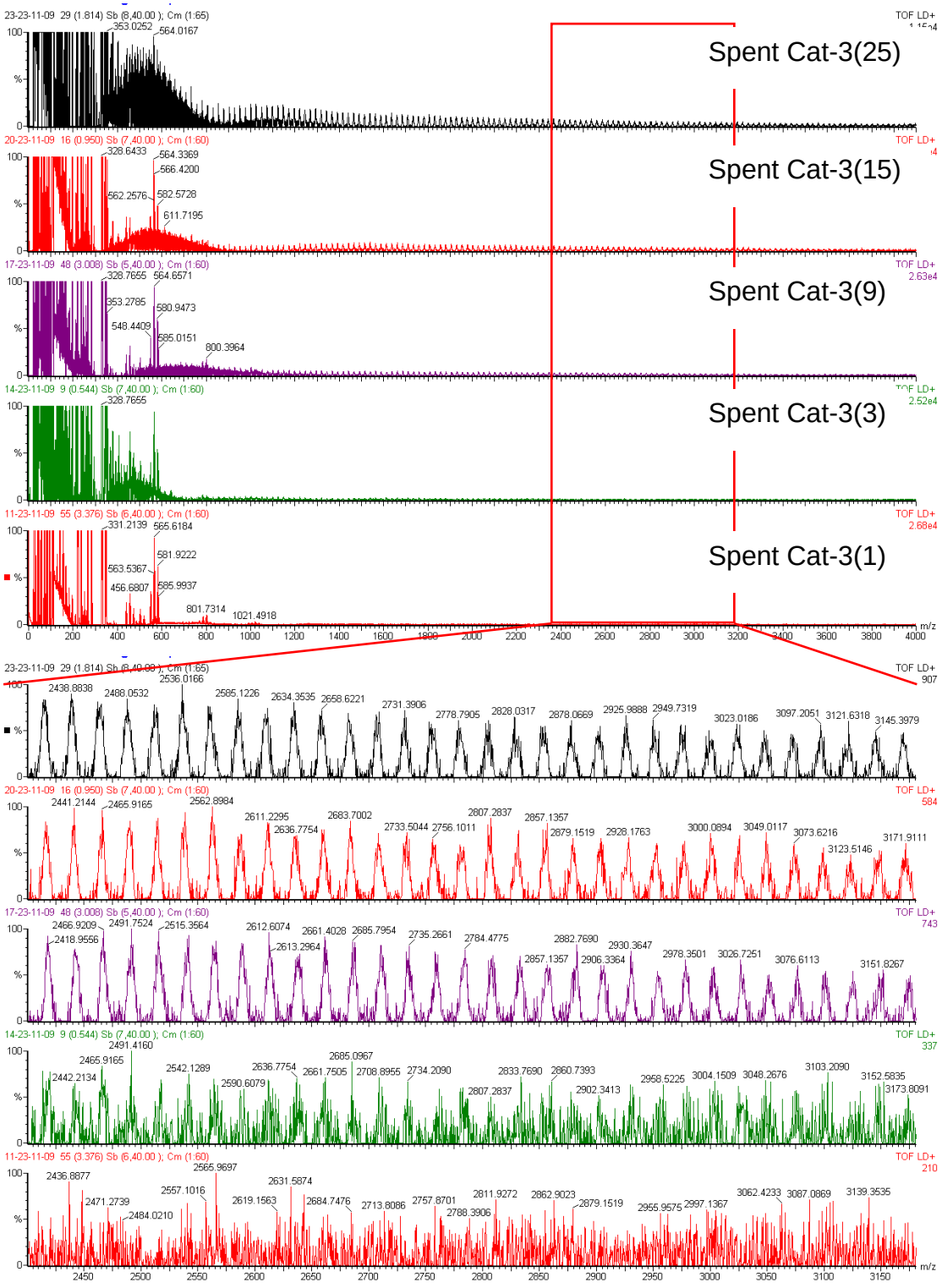

Figure 5-20: Mass distributions using AgNO3 as matrix of spent iron Fischer-Tropsch catalyst recovered from the Berty reactor after various exposure times to reaction conditions

5.2.3.3 Nature of deposits

Using HRTEM to study the morphology of the deposits on the spent Fischer-Tropsch catalysts obtained from the Berty micro-reactor revealed interesting features. Figures 5.21 – 5.23 show the HRTEM images of the catalysts obtained from the Berty reactor. There appears to be fringes associated with magnetite (Figure 5.21, left) and Hägg carbide as well as some amorphous carbon (Figure 5.21, right) located in the region of the iron carbides (Janbroers *et al.*, 2009; Jin & Datye, 2000) for the catalysts that experienced 1 and 3 days on-stream. In addition to lattice fringes ascribed to magnetite and Hägg carbide, there also appears to be filaments or whiskers present as illustrated in Figures 5.22 and 5.23 (left), for Spent Cat-3(9) and Spent Cat-3(15), which is not present in the other catalysts. The d-spacing in the filaments were measured and found to be 3.4 Å. This value corresponds to that of graphene nanoribbons synthesised from PAHs (Yang *et al.*, 2008). The carbonaceous deposits on Spent Cat-3(25) (Figure 5.23, right) have the large onion-ring type lattice fringes associated with polycyclic aromatic sheets (Mathieu *et al.*, 2007), which is formed in hydrogen-deficient environments (Nolan *et al.*, 1994). The nature of the carbonaceous deposits therefore appears to evolve as a function of TOS and is likely to be dependent on the localised availability of hydrogen at the active site.

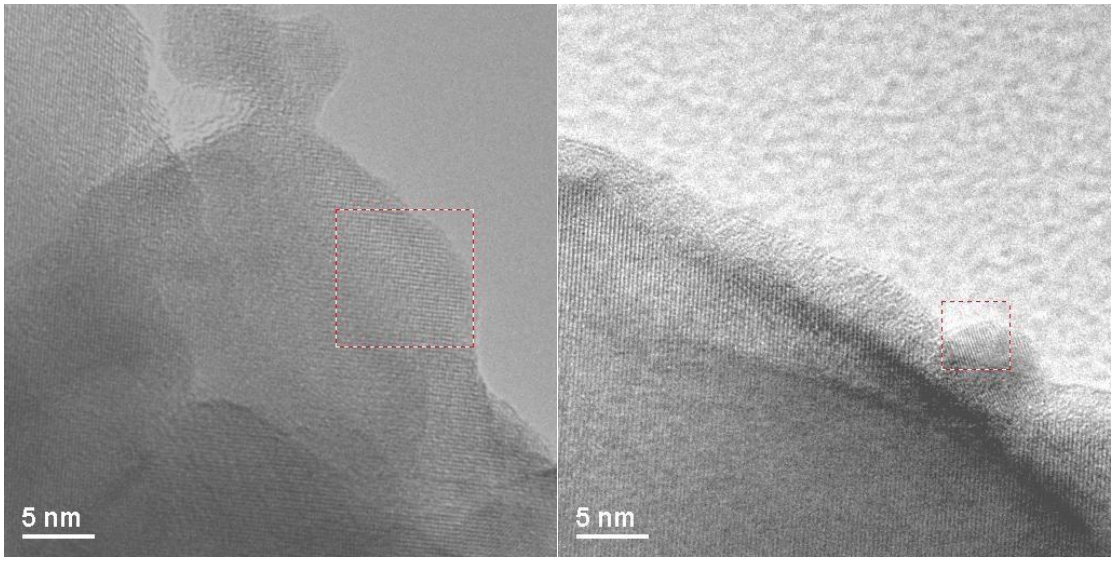

Figure 5-21: High resolution transmission electron microscopy images of spent iron Fischer-Tropsch catalyst recovered from the Berty reactor after 1 day on-stream (left) and 3 days on-stream (right)

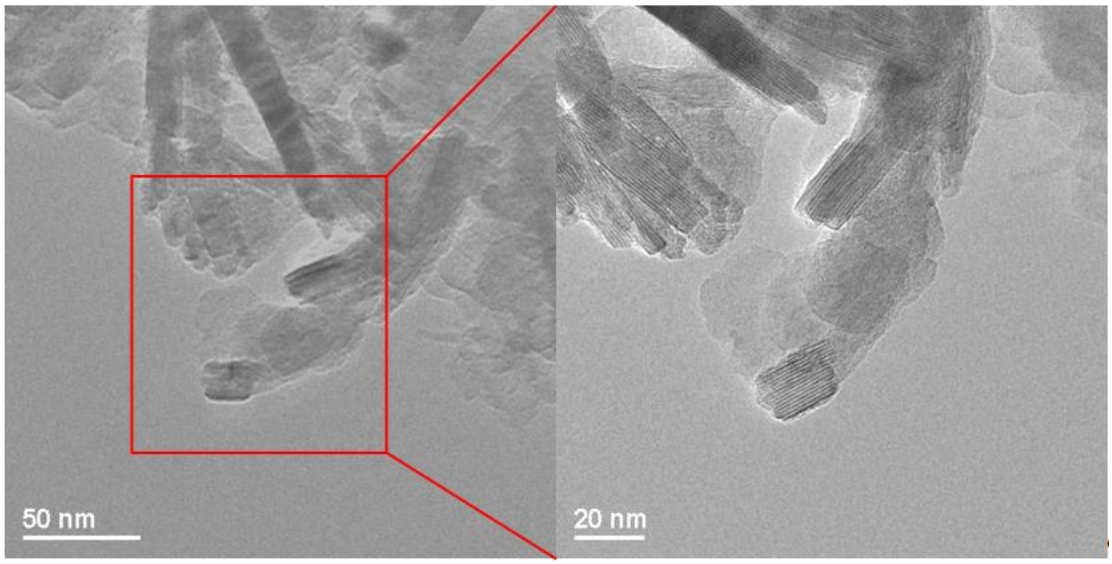

Figure 5-22: High resolution transmission electron microscopy image of spent iron Fischer-Tropsch catalyst recovered from the Berty reactor after 9 days on-stream

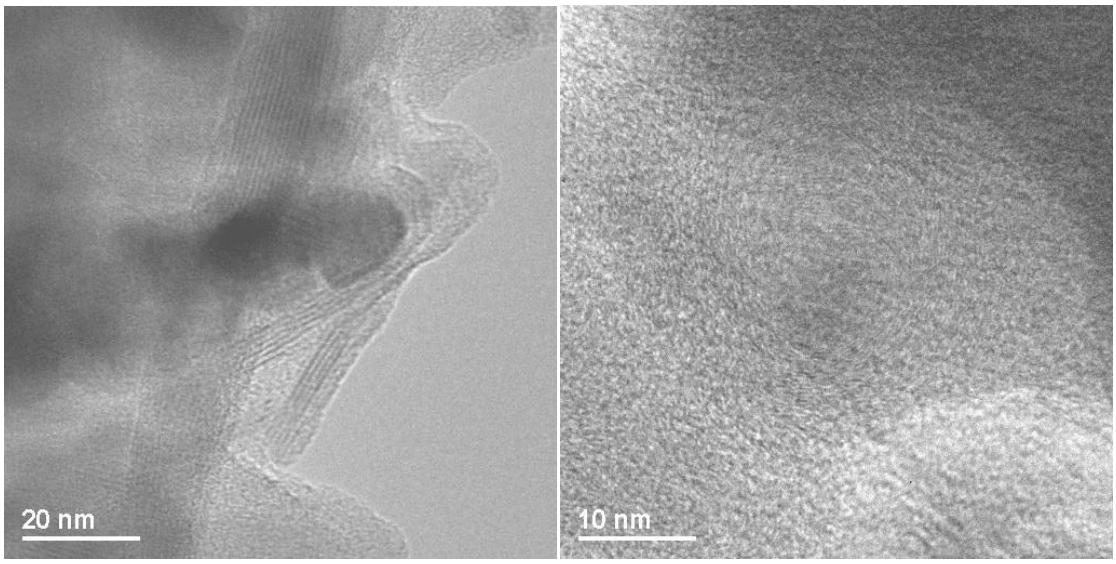

Figure 5-23: High resolution transmission electron microscopy images of spent iron Fischer-Tropsch catalyst recovered from the Berty reactor after 15 days on-stream (left) and 25 days on-stream (right)

5.2.4 Effects of Carbon on Physical Properties

5.2.4.1 Attrition studies

A serious problem in the use of iron catalysts in fluidised processes, in which the reactor bed contains gaseous or liquid products and the iron catalysts, is their tendency to undergo attrition during use. This can cause fouling of downstream equipment as well as making the separation of catalyst from products virtually impossible (Shroff *et al.*, 1995). Since the HTFT reaction is no exception, the aim in this section is to relate progressive changes in catalyst composition, through carbon build-up during FTS, to structural integrity in order to investigate the link between carbon deposition and loss of mechanical strength. This is necessary in order to ascertain the origin of carbon-rich fines that are produced in the fluidised SAS and Pilot Plant reactors (see Section 3.2.3). Progressive changes with TOS are studied through Berty experiments, which simplify the problem of studying structural integrity of an equilibrium catalyst. However, in a Berty micro-reactor the catalyst does not experience the harsh conditions that lead to attrition in a fluidised bed reactor. Therefore, mechanical strength needs to be determined *via ex situ* attrition studies. Our initial proposal was to use the American Society for Testing and Materials (ASTM) jet-impingement experimental set-

up, but this was impractical owing to the large amount of sample needed. Comparative attrition studies were performed by Zhao and co-workers using the jet-cup test and ultrasound, which were shown to produce similar results to the ASTM Standard Fluidised Bed. The advantage of these techniques is that they require less material (Zhao, 1999; Zhao, 2000). The decision was therefore taken to investigate attrition of the various Berty-recovered catalysts during particle size analysis (PSA) measurements and to cause break-up using ultrasound. It should be noted that it is not the intention to exactly replicate the fluidisation environment of the SAS reactors but rather to bring about break-up in a way that allows structural integrity of different materials to be compared easily.

Six particle size distributions (PSD) measurements were made during constant ultrasonic treatment. Figure 5.25 shows how the PSD, given as volume percentage versus particle diameter, changes with an increase in the number of ultrasound cycles. The PSD of Spent Cat-3(1) (Figure 5.24 (a)) is fairly constant, while Spent Cat-3(25) (Figure 5.24 (e)) shows a noteworthy change with increased duration under ultrasonic treatment. Spent Cat-3(3), Spent Cat-3(9) and Spent Cat-3(15) catalysts exhibit intermediate changes in PSD between these two extremes. Although all the samples exhibit a slight bimodal particle size distribution, there seems to be an increase in the volume percentage that is below 10 μm in diameter with TOS, which is probably brought about by progressive corrosion or chemical attrition of the catalyst during FTS. The benefit of using a narrow size fraction (45 – 75 μm) in the Berty experiments is clearly demonstrated in these results. The presence of fresh catalyst particles smaller than 20 μm in the normal particle size distribution might obscure the observation of carbon-rich particle formation caused by attrition.

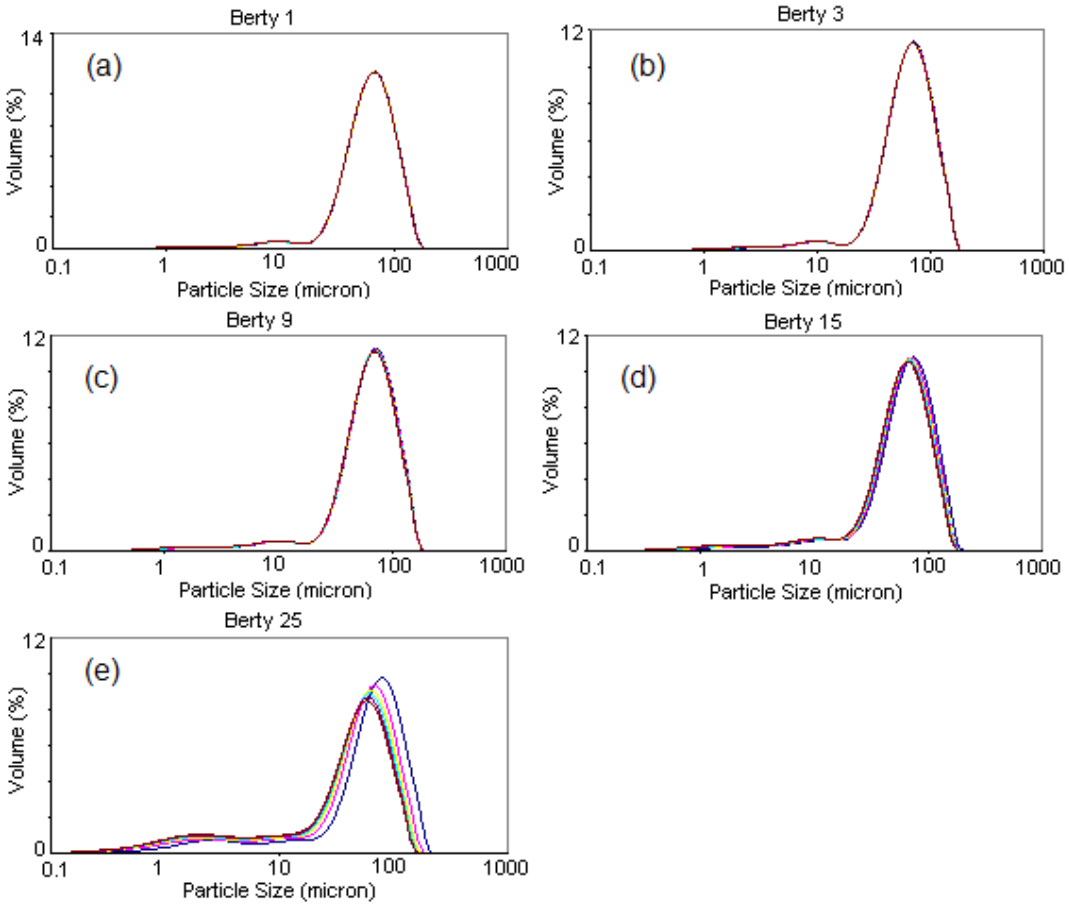

Figure 5-24: Changes in particle size distribution with number of cycles under ultrasound treatment for spent iron Fischer-Tropsch catalyst recovered from the Berty reactor after (a) 1, (b) 3, (c) 9, (d) 15 and (e) 25 days on-stream. Malvern Mastersizer 2000 with Hydro S dispersion cell, stirrer/pump speed: 3200 rpm

Changes in PSD can be expressed more clearly by studying the d(0.1), d(0.5) or d(0.9) of the distribution. D(0.9) is a diameter representing the upper diameter limit of 90 % (by volume) of the measured particles. Figure 5.25 shows the d(0.9) values of the five spent HTFT catalysts recovered from the Berty micro-reactor over six PSA measurement cycles during which ultrasound is applied. Firstly, in the initial PSA cycle before ultrasonic treatment, growth of the particles as a function of TOS under FT conditions can be observed. This is to be expected since the formation of a carbonaceous overlayer occurs and grows continuously with TOS. Similar results were reported by Sarkar *et al.* (2007) and Kalakkad *et al.* (1995) using iron-based catalysts in a slurry reactor. This growth of particles with TOS is the reason for the catalyst bed expansion that occurs in the SAS HTFT reactors (Dry, 2004). Secondly, Spent Cat-3(1) and Spent Cat-3(3) show very

little decrease in d(0.9) with an increasing number of cycles under ultrasonic treatment. However, Spent Cat-3(9) and Spent Cat-3(15) begin to show some loss of structural integrity as indicated by an eventual drop in d(0.9) values with successive cycles in ultrasound treatment. On Spent Cat-3(25) the amount of break-up, which is related to the build-up of carbon, is prominent. This attrition serves as an indication of the loss of structural integrity with time in the FT environment. The data below, where sonication is used to mimic the stresses caused by fluidisation, gives an indication of the origin of carbon-rich fines in the SAS reactor. This can be ascribed to chemical attrition associated with the formation of carbide crystallites and carbon deposition.

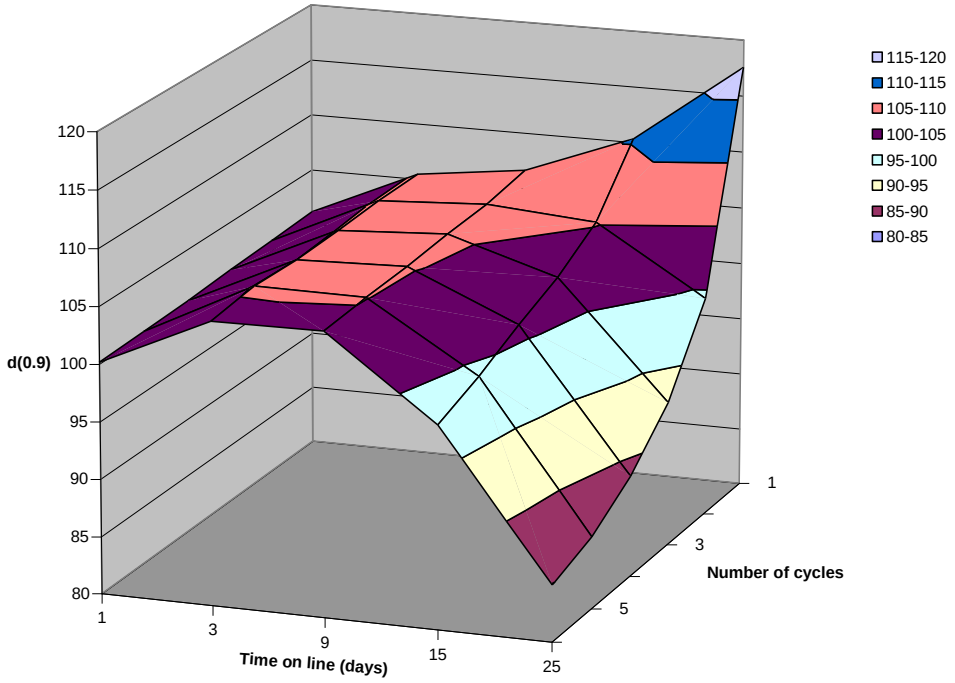

Figure 5-25: Variation in d(0.9) with number of cycles under ultrasound treatment for spent iron Fischer-Tropsch catalyst recovered from the Berty reactor at varying exposure times to reaction conditions

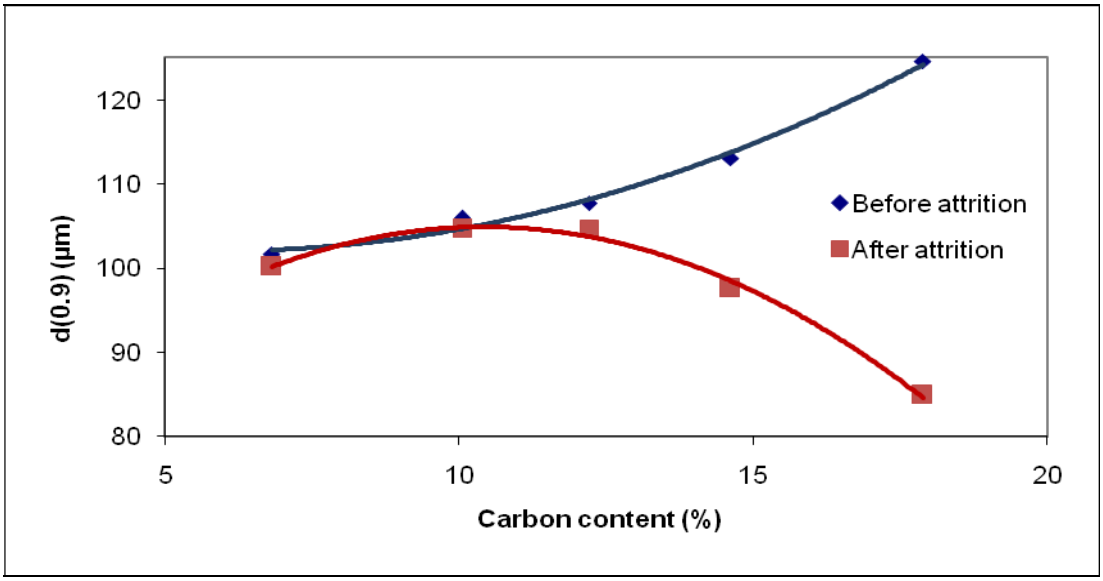

Figure 5-26: Variation in d(0.9) with total carbon content before and after attrition of spent iron Fischer-Tropsch catalysts recovered from the Berty reactor after various exposure times to reaction conditions

Figure 5.26 depicts the d(0.9) values as a function of carbon content. It can be clearly seen that, before attrition, d(0.9) increases with TOS associated with the deposition of carbon. After attrition, however, the drop in d(0.9) can be clearly seen beyond about 10 % carbon. This appears to be the critical point beyond which an excessive loss in mechanical strength and related operational problems is expected to occur. However, we concede that fluidisation dynamics within a reactor may change this critical point.

The volume percentage of fines (1-10 µm) present in spent HTFT catalyst can be related to the degree of phase transformation to carbides and in turn, chemical attrition. It was shown in Section 5.2.3.1 that the catalyst actually becomes oxidised with TOS. The observed phase composition is likely to be affected by oxidation of the carbide crystallites during reaction or upon exposure to air.

5.2.4.2 Surface Area, Porosity and Density Measurements

It is believed that the fluidisation problems within the commercial SAS reactor are strongly associated with a drop in density associated with the build-up of carbonaceous species (Dry, 2004). However, since the catalyst recovered

from the SAS reactor is an equilibrium catalyst it is difficult to monitor the progress of this postulated drop in density. The bulk density of catalyst samples recovered from the Berty reactors is determined in order to quantify the change as a function of TOS. The bulk density of these catalysts was determined by performing a simple measurement similar to the ASTM method for determination of tap density. In a typical measurement, a sample is poured into a vial of known volume. This is then tapped in order to cause settling and thereby pack the particles tightly. The mass of catalyst in the vial was then determined and used to calculate the bulk density.

The BET surface area and pore volume of the spent catalysts recovered from the Berty reactor studies were investigated to determine how these physical properties correlate with carbon build-up. Initially, the surface areas of the Spent Cat-3 samples were found to be extremely small. However, once the catalysts were heated in a flowing inert gas the surface areas increased. This suggests that the porous carbonaceous structure is blocked by the wax-type hydrocarbons that can be removed by this thermal desorption. These wax materials are formed and condense in the pores under normal Fischer-Tropsch conditions.

Figure 5.27 depicts the surface area after thermal desorption at 440 °C as a function of TOS. We observe an initial sharp increase in surface area, after which there is a slight decrease in the measured surface area. This initial increase can be attributed to the formation of highly dispersed iron carbide crystallites and deposition of the carbonaceous deposits upon exposure to FTS conditions, both of which are believed to be responsible for an increase in surface area in HTFT catalysts (Dry, 2004). Continuous disintegration of the catalyst due to chemical attrition would lead to a continuous increase in the surface area, but this is not observed. This indicates that the observed drop in surface area could be related to wax instead of an actual decrease in surface area with TOS. The pore volume measured for the Spent Cat-3 samples exhibits a maximum associated with the competing effects of an increase in porosity due to particle growth and eventual pore-blockage by wax that is not

efficiently removed at 440 °C. It has been shown from the particle size distributions (Section 5.2.4.1) that the level of disintegration is still at an early stage by the time the catalysts are removed from the reactor, even after 25 days on-stream. The initial increase in pore volume possibly has the same origin as the increase in surface area, namely the formation of the porous carbonaceous matrix. Evolution of this carbon to PAH sheets at 25 days on-stream possibly causes blockage of the porous structure. This would result in trapping the wax formed within the pores. It therefore becomes more difficult to remove the wax by thermal desorption.

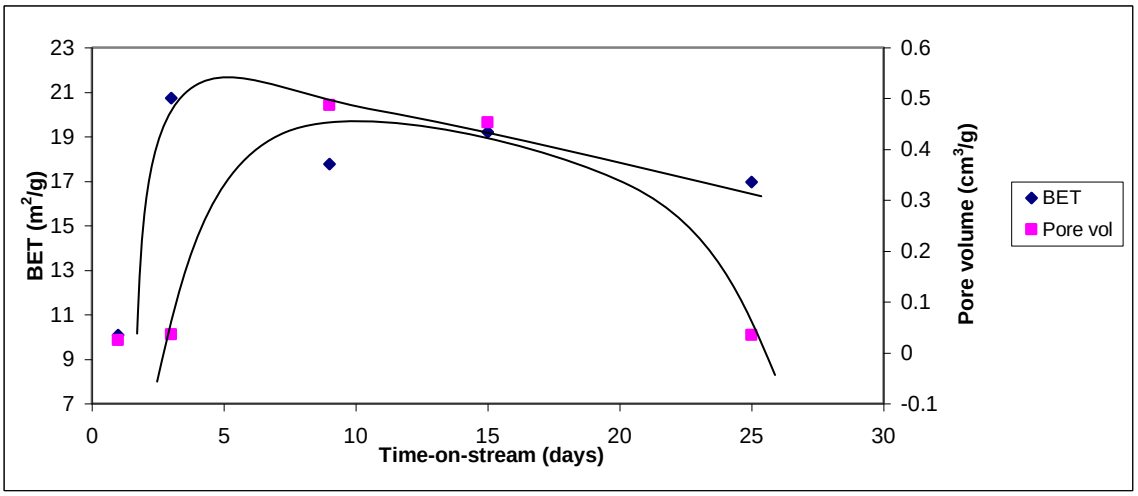

Figure 5-27: BET surface area and pore volume of spent iron Fischer-Tropsch catalysts recovered from the Berty reactor following wax removal by desorption at 440 °C as a function of time on-stream (TOS) under reaction conditions. Micromeritics Gemini VI

The particle density before thermal desorption at 440 °C decreases linearly as a function of TOS as illustrated in Figure 5.28. The error bars indicate a confidence interval of 95 %. It is also evident that the density decreases with an increase in the total carbon content on the catalyst. This is to be expected since the build-up of carbonaceous deposits is the main reason for the observed density decrease. Thermal desorption appears to decrease the bulk density of Spent Cat-3(1) and Spent Cat-3(3) particles, whereas the catalysts that experienced a longer time under FT conditions exhibit a slight increase in the measured bulk density upon this thermal treatment.

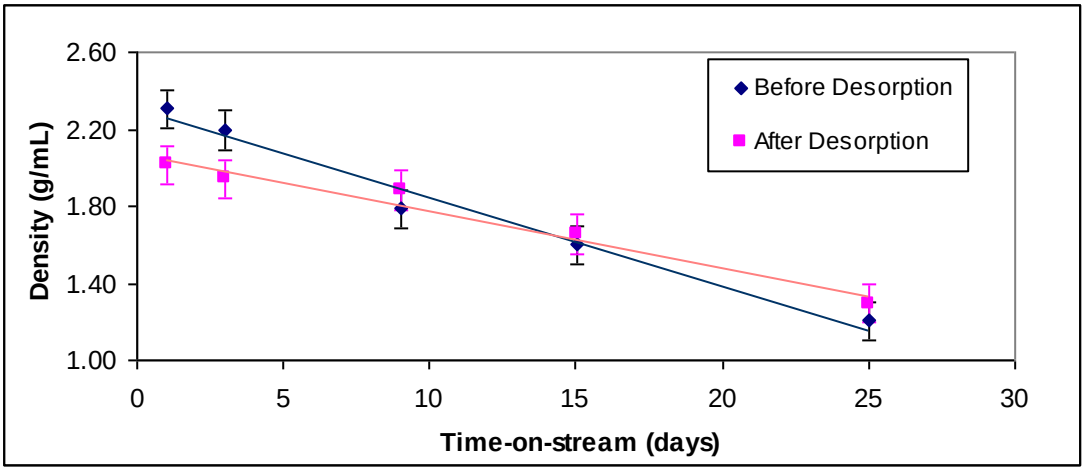

Figure 5-28: Bulk density of spent iron Fischer-Tropsch catalysts recovered from the Berty reactor before and after wax removal by thermal desorption at 440 °C, as a function of TOS under reaction conditions

Since it was shown that thermal desorption at 440 °C is too harsh for the catalysts, the measurements had to be repeated for the catalysts after desorption under reduced pressure at 350 °C. The BET and pore volume as a function of total carbon content of the Spent Cat-3 samples after vacuum desorption at 350 °C is given in Figure 5.29. The BET surface area presented follows a similar trend to that of the Spent Cat-3 samples after thermal desorption at 440 °C but is an order of magnitude smaller. Using too high a temperature for the thermal desorption introduces additional problems such as combustion/oxidation/thermal cracking of the hard carbon which probably accounts for this anomaly. On the other hand, a milder treatment could probably also be less effective at removing wax. The change in pore volume with TOS appears to follow a similar trend as the surface area. The exception is the Spent Cat-3(9) sample, where lower pore volume and surface area could be ascribed to the wax not being removed to the same extent as the other catalysts. This hypothesis is supported by CHN analysis, which indicates a smaller decrease in the carbon mass percentage for Spent Cat-3(9) (Table 5.4). Figure 5.29 indicates that the BET surface area and pore volume generally increase with an increase in carbon build-up.

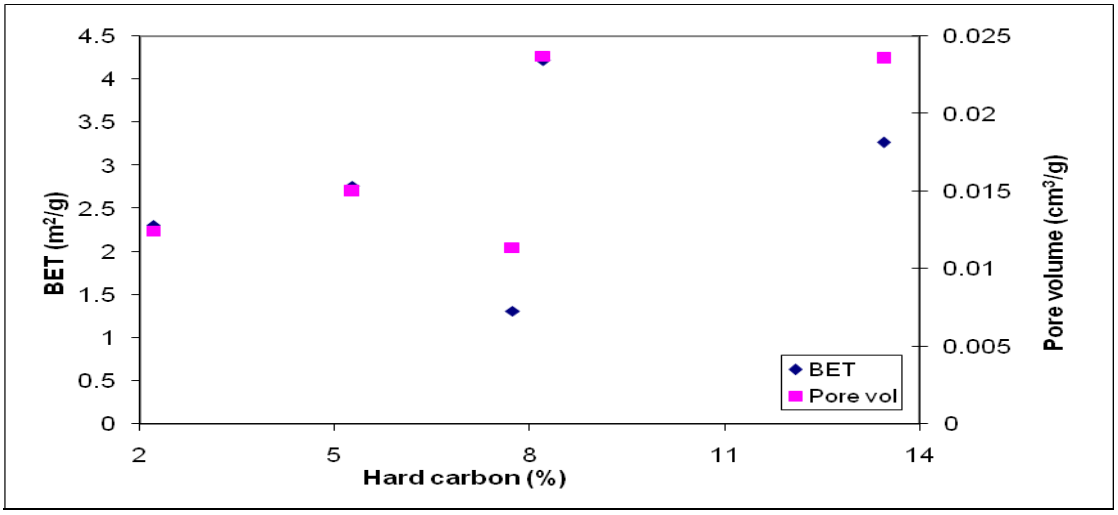

Figure 5-29: BET surface area and pore volume of spent iron Fischer-Tropsch catalysts recovered from the Berty reactor after wax removal by vacuum desorption at 350 °C, as a function of increasing hard carbon content. Micromeritics Gemini VI

Bulk density of the Spent Cat-3 samples before and after vacuum desorption at 350 °C is presented in Figure 5.30 and indicates an increase in the density with desorption. The change in density is similar for the different samples with the exception of Spent Cat-3(9), which shows a slightly larger increase in density after desorption. The mass of wax is shown to constitute at least 2 % of the catalyst (determined by TGA); this would lead to an incremental decrease (less than 0.05 g/ml) in density instead of the observed increase. It appears more likely that a change in density is more strongly correlated with a phase transformation of the bulk catalyst. Although there are complications from phase transformations during thermal treatment which might affect the density, Figure 5.30 clearly shows that there is a decrease in density with carbon build-up.

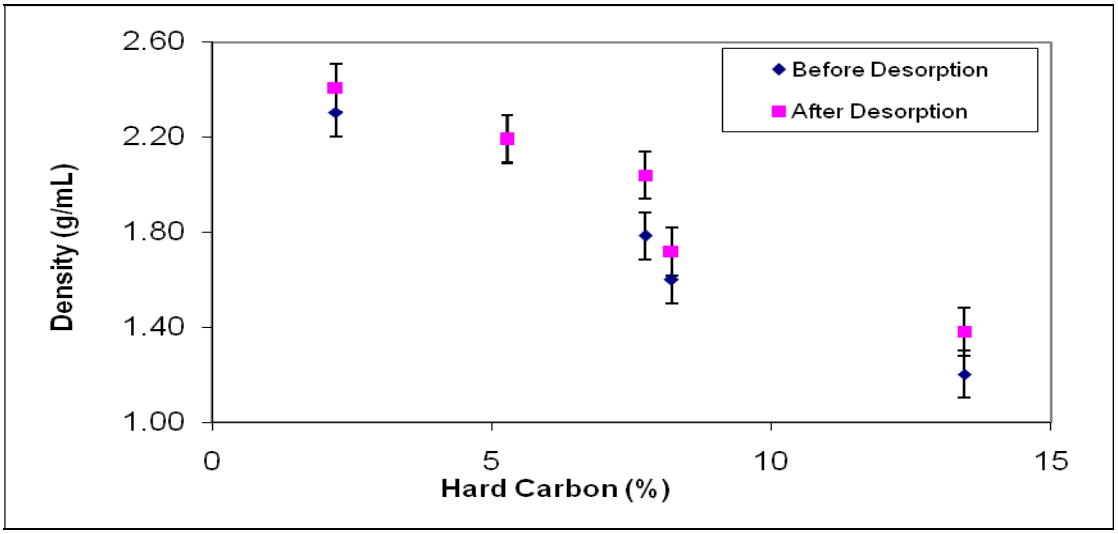

Figure 5-30: Bulk density of spent iron Fischer-Tropsch catalysts recovered from the Berty reactor before and after wax removal by vacuum desorption at 350 °C, shown as a function of increasing hard carbon content

5.3 Discussions

The main aim in this chapter was the quantification of carbon deposited on high temperature Fischer-Tropsch (HTFT) catalysts. This proved to be quite challenging and certain modifications had to be made to standard measurements in order to accurately determine the amount of carbon present. Subsequently, we attempted to draw correlations between the continuous build-up of carbon and the chemical and physical properties. The samples for this study were generated in a Berty micro-reactor.

The observed drop in synthesis gas conversion was shown to correspond to an increase in the amount of carbon present on the catalyst. The carbon gradually envelops the catalyst particles with time on-stream. This leads to growth of the particles and break-up. The mass distributions of the carbonaceous deposits increased in maximum molecular weight, but seem to remain polymeric and polycyclic aromatic hydrocarbonaceous in nature. Carbon filaments and sheets were observed on some of the samples. A linear decrease in density was also observed with carbon build-up.

The phase composition indicates (Section 5.2.3.1) that there is not a significant change in the relative abundance of iron carbide. Therefore the

increase in total carbon mainly represents the build-up of hard and soft carbon on the catalyst with TOS. It is known that carbon is steadily deposited after the initial formation of carbide phases on catalysts during HTFT synthesis (Dry, 2004). The difficulties associated with determination of the carbon and hydrogen content in the catalyst by CHN microanalysis have therefore been highlighted. The intrinsic nature of the spent catalyst complicates the analysis of these materials by standard instrumentation, but this can be overcome by using a horizontal furnace. The total amount of carbon was found to increase linearly with TOS. This carbon consists of iron carbides, waxes, polymeric carbon and polycyclic aromatic hydrocarbons. The presence of adsorbed wax complicates the quantification of hard carbon. The inability of Soxhlet extraction to remove soft hydrocarbons (wax) was discussed in Section 3.2.1.5. Removing soft carbon by vacuum desorption at a suitable temperature facilitated the determination of the rate of hard carbon formation over time. The rate of hard carbon deposition is determined to decrease with TOS.

Section 5.2.3.1 shows that the ($CO+CO_2$) conversion to FT products is fairly constant over the 25 day timescale, while ($CO+H_2$) conversion decreases. This suggests that the active sites for FT are blocked by hard carbon. Blocking of active sites would lead to less atomic carbon being available and the R_{CF} eventually levelling off, which is in fact observed. Performing more experiments to find the other factors that control R_{CF} would also facilitate proposing a rate equation. The benefit of such a relation is that the rate of carbon formation can be predicted in order to determine the lifetime of the catalyst and therefore the frequency at which catalysts should be replaced in continuous operation.

Throughout the chapter it can be seen that Spent Cat-3(15) behaves differently than expected. There is less hard carbon present on this catalyst than predicted by the trend observed with the other catalysts. The catalyst activity (Section 5.2.3.1) shows that more CO is converted to CO_2 *via* the water-gas shift (WGS) reaction, thereby reducing the amount of carbon that is

available for hydrogenation into FT products or deposition as hard carbon on the surface. Looking at the product slate, it is clear that there is a higher availability of hydrogen in this case. This is evident from higher methane selectivity, higher paraffin-to-olefin ratios and less oxygenates.

The progressive build-up of carbonaceous species on the catalyst surface was investigated using microscopy and Raman mapping, the results of which suggest the core-shell structure and the particles increasing in size when hard carbonaceous material is deposited over the crystalline facets of the catalyst. This growth of the particles caused by the build-up of carbonaceous species was also observed by PSD measurements.

Optical images of polished segments of Spent Cat-3 particles fixed in resin do not show reaction (and therefore carbon deposition) initiating at the surface of the particles. Reaction rather appears to initiate at occlusions and grain boundaries within the catalyst particle. This suggests that the promoter-rich regions located in the grain boundaries serve as preferred sites for FT synthesis, whereas on a particle in a fluidised-bed SAS reactor this occurs initially at the potassium-rich areas located on the surface and subsequently along these grain boundaries (see Section 3.2.3). It is known that potassium migrates to the surface during reaction (Riedel *et al.*, 2003, Prasad *et al.*, 2008; Bonzel & Krebs, 1981). It seems unlikely that the lack of fluidisation in the Berty reactor decreases the migration of potassium to the surface of the catalyst, especially considering that Riedel *et al*. performed their experiments in fixed bed systems. This migration improves the distribution of potassium on the catalyst surface. It has been shown that when finely ground potassium silicate is added separately to a fused catalyst its performance in the FT synthesis is similar to that of a catalyst prepared by the addition of the potassium promoter during the fusion of magnetite (Loggenberg *et al.*, 1990).

SEM images show breaking up of the particles with TOS. Since there is no fluidisation in the Berty reactors, this suggests chemical attrition (discussed in Section 3.2.3). Chemical attrition is known to produce carbide crystallites that

are present on the surface of larger magnetite particles (Zhao *et al.*, 2001) and is possibly one of the mechanisms by which the particles disintegrate during reaction. The presence of these small particles is also demonstrated by PSD studies (see Section 5.2.4.1) and become more numerous with an increase in TOS. This chemical attrition occurs even in the absence of fluidisation and appears to be inherent to iron-based catalysts. The deposition of carbonaceous species in the form of hard carbon seems to make the particles rougher on the edges as observed on the surface of the catalysts at 15 and 25 days on-stream. This is linked to the growth of amorphous carbon on the surface enveloping the catalyst, as seen from the Raman studies.

It is widely believed that the activity of a FT catalyst is dependent on the carbide content (Dictor & Bell, 1986; Rao *et al.*, 1994; Hayakawa *et al.*, 2006; Amelse *et al*., 1978; Raupp & Delgass, 1979a, b; Shroff *et al*., 1995; Jung & Thomson, 1992). The observed decrease in carbide phases determined by quantitative XRD correlates with the decrease in ($CO+H_2$) conversion with TOS in the Berty reactor. This decrease in the carbide content with TOS is often observed (Malan et al., 1961; Dry, 2004) and can be explained by re-oxidation of surface carbides. This can occur by the presence of CO_2 and product water during FTS, while it could also be associated with passivation and/or exposure to air. The implication of the direct correlation between the relative abundance of carbide phase and conversion is that the disperse iron carbide species is apparently directly responsible for FT activity. The effect of increased surface area associated with carbide formation probably also contributes to the apparent activity of iron carbides. This is in agreement with literature reports where the relative abundance of the iron carbide phase has been related to the activity of the FT catalyst. The drop in ($CO+H_2$) conversion indicates that the activity of the catalyst towards the WGS reaction is increased with TOS, which is in fact observed. The fact that carbon deposition occurs simultaneously to this phase transformation should be taken into account, since it could negate the correlation discussed above.

It was stated in Section 3.1 that in the SAS reactor, the need for catalyst replenishment results from changes in fluidisation dynamics due to carbon build-up. This leads to less catalyst in the optimal temperature zone and eventually a drop in productivity. The significance of observing a drop in activity in the Berty micro-reactors is that this deactivation (by a combination of phase transformation and blockage of active sites) is likely to also occur in the SAS and Pilot Plant reactors. The drop in productivity is probably far greater than the decrease in intrinsic FT activity in the large fluidising reactors, thereby overshadowing this deactivation. The benefit of studying activity in the absence of fluidisation is therefore demonstrated, and challenges the current beliefs within Sasol.

The evolution of the carbonaceous deposits was studied by MALDI-TOF MS and HRTEM, which indicated that the amount and molecular mass distributions of the deposits increased with TOS and furthermore changed from amorphous carbon to polycyclic aromatic hydrocarbons (PAHs) in the form of filamentous carbon and polycyclic aromatic sheets (graphene). The formation of carbon depositing in the form of filaments has been reported in the literature (Sommen *et al.*, 1985) and occurs in the presence of hydrogen (Nolan *et al.*, 1994). The observed change in the morphology of carbonaceous species possibly relates to the decrease in abundance of surface hydrogen at the FTS sites. This is probably due to the active sites being embedded in a carbonaceous matrix consisting of trapped wax, hard carbon and iron carbide crystallites.

We believe that a cause of deactivation is related to phase change as well as carbon formation. This catalyst exhibits a steady drop in activity in terms of ($CO+H_2$) conversion with TOS although the deposits grow to larger than 4000 Da. Growth of PAHs into large molecules seems to be a continuous process and does not seem to reach a critical mass, beyond which the activity dramatically stops. According to the classification of catalytic reactions into coke sensitive or insensitive (Menon, 1990), it is accepted that FTS is coke insensitive (Bartholomew, 2001). In coke-sensitive reactions, the deposition of

coke on active sites leads to a decrease in activity, while in coke-insensitive reactions coke precursors are readily hydrogenated. For instance, PAHs are not readily hydrogenated and are often considered to be responsible for deactivation. In this classification the location of the coke (in terms of blocking active sites), the nature, structure and morphology of these species is more important in affecting catalytic activity than the quantity or mass of coke. The deactivation rate depends strongly on the difference in the rates of formation and gasification of the coke precursors. By reason of the activity shown for the Berty experiments the active sites appear to be gradually blocked by the carbonaceous deposits.

On the mechanism of hard carbon formation, we do not believe that the observed PAHs are formed from the aromatic product of the HTFT reaction. Since the product selectivity does not change significantly with carbon build-up these aromatic species are not likely to be the precursors of coke. Furthermore, it is known that coke also forms in reactions where aromatic compounds are absent. In the Hydrogen Abstraction C_2H_2 Addition (HACA) mechanism, acetylene is believed to be the monomer for the growth of PAHs. While we are not proposing HACA as the growth mechanism, it is important to note that acetylene is not typically formed during FTS, although we cannot discount it forming as an intermediate. This suggests that additional carbon (polymeric carbon) that is deposited on the catalyst surface (after saturation of the metal lattice) possibly rearranges into these stable PAH sheets.

A three-step carbide cycle has been proposed as a mechanism for the formation of PAH structures (Dias & Assaf, 2004). The first step is the formation of a carbon monolayer followed by the formation of a graphitic carbon by polymerisation of the carbon atoms. The third step occurs as a result of a carbon concentration gradient between the top of the surface and the bottom of the metal or carbide particle. This leads to carbon diffusion across the crystal (corrosion or carbide decomposition) and eventually the growth of a PAH filament or sheet. This mechanism explains our observation of amorphous polymeric carbon and PAHs.

Attrition resistance is strongly related to the carbon that deposits continuously on the catalyst. The structural integrity was observed to become compromised after 10% total carbon was formed on the catalyst (Section 5.2.4.1). In the investigation by Kalakkad and co-workers (1995), it was reported that exposure to CO at high temperature leads to deposition of carbon with the associated swelling of the catalyst particles. This carbon apparently further enhances attrition due to an increased likelihood of collision between particles within the reactor. The morphology of the deposits has been shown to affect the structural integrity of a catalyst, as demonstrated in metal dusting experiments (Grabke *et al.*, 2001) where carbon filaments are known to lead to disintegration of the catalyst particle. The morphology of the carbonaceous species on the Spent Cat-3 samples has been discussed in Section 5.2.3.3. Generally, the amount and type of deposits formed depend strongly on the temperature (Dry, 1970b), CO/H_2 ratio in the feed (Grabke *et al.*, 2001) and the presence of sulphur (Kim *et al.*, 1993; Schneider *et al.*, 2000), while alloying with a second transition metal (e.g. chromium) also seems to affect the formation of carbonaceous species (Machocki, 1991; Park & Baker, 1999; Lohitharn *et al.*, 2008; Ott *et al.*, 1980; de la Peña O'Shea *et al.*, 2007). The rates of carbon deposition on smaller crystallites are also expected to be decreased, since deleterious carbon deposition is assumed to occur predominantly on large iron carbide particles (Jin & Datye, 2000; Shroff *et al*., 1995; Arakawa & Bell, 1983). Using this knowledge, minimising the loss in structural integrity of HTFT catalysts could be achieved simply by reducing the degree of carbon deposition. However, this is not so straightforward since a change in the operating conditions would also alter the catalyst activity, stability and product selectivity.

An alternative approach is to explore the addition of small amounts of sulphur to the feed stream or as a promoter on the catalyst. A great deal of work has been invested in this topic since sulphur is widely believed to act as a poison in FTS. A promising aspect of sulphur promotion was reported by Bromfield and Coville (1999), namely that the activity and olefin/paraffin selectivity was

increased at low loadings of sulphide ions on a precipitated iron-based catalyst. The authors report that the formation of iron carbide is enhanced at low sulphide loadings.

Fused catalysts are non-porous and consequently have virtually zero Brunauer-Emmett-Teller (BET) surface area. Reduction of these catalysts is therefore essential to create surface area required for reaction. The reduction step is normally performed in H_2 in the region of 350 to 450 °C, producing catalyst with a surface area of 5 – 15 m^2/g (Dry, 2004). In the presence of CO during HTFT, highly dispersed Hägg carbide crystallites are formed and this is normally accompanied by the deposition of carbon. This carbonaceous matrix forms the reactive surface area.

For the catalysts desorbed at 440 °C, the initial drop in density upon thermal desorption can be explained by the fact that the mass loss due to removal of the wax occurs and is not accompanied by a decrease in the particle volume. This is because the wax is predominantly located in the pores of the catalyst, as shown by BET studies. With an increase in TOS, the difference in density before and after desorption is smaller, but seems to increase as of 9 days on-stream. This could be ascribed to the wax still being trapped in the carbon matrix. This wax on the catalysts after 9, 15 and 25 days on-stream is not effectively removed by thermal desorption since the wax becomes more difficult to remove in the presence of the hard carbon matrix, as demonstrated by CHN analysis (Section 5.2.1). An alternative explanation is that the observed phase transformation associated with the thermal treatment demonstrated in Section 5.2.3.1 leads to a mass increase of the iron-based catalyst. However, it was shown that catalysts that have experienced longer times on-stream are shielded from phase transformation by the carbonaceous matrix (Section 5.2.1), thereby placing doubt on this rationalization. A more viable possibility is that thermal treatment during desorption leads to the collapse of the porous structure of the carbonaceous overlayer. This would result in a decrease in volume and thereby increase the measured bulk density. This is corroborated by results from attrition studies (Section 5.2.4.1),

where it was demonstrated that a critical carbon content exists beyond which structural integrity of the particle is compromised. This again relates to extensive chemical attrition for these catalysts.

5.4 Concluding remarks

The benefits of simplifying the problems encountered in characterising the catalyst recovered from the Sasol Advanced Synthol reactors are demonstrated in this chapter. A better understanding of the correlation between the amount of hard carbon and physical properties of high temperature Fischer-Tropsch (HTFT) catalysts has been obtained.

The evolution of the HTFT catalyst with time has been determined by studying catalysts from the Berty micro-reactor. A slight decrease in FTS activity of the catalyst as determined by synthesis gas conversions was demonstrated. Hard carbon formation is believed to affect the activity by blocking the active sites. It was also shown that the phase composition of the catalyst changes with time on-stream to become richer in magnetite. These findings suggest the carbide model of FTS, where the active species is a surface carbide crystallite. It is difficult to draw conclusions from the available data since the approach toward the study is not conducive to phase-activity relationships. Narrowing down the number of variables or *in situ/operando* experiments would facilitate this.

Carbon deposition was shown to have a direct correlation to the structural integrity of the catalyst particles by subjecting the materials to physical attrition *ex situ*. The volume frequency of fine particles was also found to be higher on the catalysts after longer durations under FT conditions due to chemical attrition during FTS. Chemical attrition refers to corrosion of the catalyst, which occurs by the formation of fine carbide-rich particles (which forms in the absence of physical attrition).

The BET surface area and pore volume increases initially with the deposition of carbonaceous species and subsequently seems to mirror the carbide and hard carbon build-up with TOS, suggesting that surface area is created by the formation of carbonaceous species. The bulk density of the catalysts was found to decrease linearly with increased exposure time to FT conditions and, more importantly, also with an increase in the amount of carbon.

It was demonstrated that coke or hard carbon is continuously formed on the catalysts. Fouling due to carbon can occur either chemically due to chemisorption and carbide formation, or physically due to blocking of active sites, encapsulation of the metal crystallites, plugging of pores and destruction of catalyst particles by carbonaceous matrix.

There is a recurring theme of the role that is played by hydrogen throughout this thesis. It is believed to enhance CO adsorption by the reduction of iron carbide to metallic iron, while it could also act as an electron donor enhancing the metal to carbon bond and weakening the carbon to oxygen bond on CO (Dry *et al*., 1970b). The competition model proposes that high availability of hydrogen enhances hydrocarbon synthesis via the Fischer-Tropsch reaction, while the incorporation of carbon into the bulk catalyst metal and carbon deposition will be reduced (Niemantsverdriet & van der Kraan, 1981). However, the presence of hydrogen was found to increase the amount of filamentous carbon versus graphene sheets formed (Ando & Kimura, 1989; Nolan *et al*., 1994). In fundamental studies it was similarly found that the presence of hydrogen inhibits the coupling of surface carbon atoms (Cao *et al*., 2008).

Hydrogen availability reflects on the typical Fischer-Tropsch product slate by an increased selectivity to lighter hydrocarbons such as methane, higher paraffin to olefin ratios and the production of fewer oxygenated products. This is unfavourable where petrol (gasoline) is the end product, and therefore a slightly lower hydrogen partial pressure should be maintained during synthesis. The advantage is that less catalyst break-up will occur, since

filamentous carbon formation should be diminished (Grabke *et al*., 2001). A possible disadvantage could be blocking of active FT sites by increased graphene-like carbon formation.

6.CONCLUSIONS AND OUTLOOK

6.1 Spent HTFT catalysts

This thesis deals with the investigation of carbonaceous deposits on spent high temperature Fischer-Tropsch (HTFT) catalysts. Carbon build-up on HTFT catalysts leads to a drop in productivity with time on-stream. This has been largely attributed to changes in fluidisation dynamics within the reactor but could also be related to a genuine loss in activity caused by blockage of active sites. Importantly, it is the build-up of hard carbon (coke) that is a major contributing factor to changes in particle size distribution and density, which affects fluidisation properties and is also often implicated as a cause of activity loss through fouling. Understanding the pathways to carbon formation and its effect on both chemical and physical properties is therefore key to the development of next generation catalysts that are more resistant to carbon build-up. Thus, the aim of the work described in this thesis was to develop a more detailed understanding of the mechanism of hard carbon formation and its influence on catalyst activity, selectivity, structural integrity, density, etc. Various catalyst samples were obtained from Sasol in order to study different aspects of a typical iron-based spent catalyst.

The research described in this thesis has provided invaluable insight into various aspects of HTFT synthesis from the evolution of the catalyst structure, nature of carbonaceous deposits, the quantification of total and hard carbon and its effect on physical and chemical behaviour of the catalyst with time on-stream. Chapter 3 describes the structure of a working HTFT catalyst and focuses on interpretation of Temperature Programmed Oxidation (TPO) data. The typical TPO profile reveals desorption of hydrocarbons, oxidative dehydrogenation processes, the combustion of hard carbon and iron carbide transformations and finally iron oxide phase transformations to hematite, listed in order of onset temperature. Hard carbon is a hydrogen-deficient species that is fairly resistant to oxidation, and is commonly referred to as coke in other studies. Simultaneous desorption, partial oxidation and oxidative hydrogenation has been shown to occur during TPO measurements and this

complicates quantitative interpretation of TPO data. The significance of the oxidative dehydrogenation peak is that it can be used to determine the hydrogen content of hard carbonaceous deposits, which can be extremely challenging particularly when hydrogen content is low. Phase transformations that occur during TPO were investigated by X-ray Diffraction (XRD) and Raman spectroscopy. Raman and energy-dispersive X-ray spectroscopy maps of the spent catalyst set in resin, together with Back-scattered Scanning Electron Microscopy, revealed a core-shell structure in which the core is comprised of magnetite and the shell is a hard carbonaceous matrix with embedded iron carbide crystallites and product wax. Similar structures have been proposed previously where the presence of an oxidic core was ascribed to re-oxidation of the catalyst by product water at a reaction boundary. From studies of catalysts that have experienced prolonged exposure to HTFT conditions, we believe that this oxidic core is actually a consequence of inefficient reduction during the catalyst activation step.

In Chapter 4 the nature of carbonaceous deposits formed on HTFT catalysts is described. Factors which determine the type of carbon that is formed include temperature (Dry, 1970b), hydrogen availability (Grabke *et al*., 2001) and the presence of sulphur (Kim *et al*., 1993; Schneider *et al*., 2000). Graphitic carbon has been proposed as a prominent form of coke, although most of the techniques used in these investigations are not specifically suited to distinguish between different carbon forms. Chapter 4 describes the use of X-ray Photoelectron Spectroscopy (XPS), High Resolution Transmission Electron Microscopy (HRTEM) and Raman Spectroscopy in the study of carbonaceous species (hard carbon) deposited on catalysts. The use of these techniques provided evidence for amorphous and a more crystalline (graphite-like) form of carbon, as well as some oxygenated species. We have developed the application of Matrix-Assisted Laser Desorption/Ionisation-Time of Flight Mass Spectrometry (MALDI-TOF MS) to the analysis of deposits on spent catalysts. Carbonaceous materials are difficult to analyse owing to their general insolubility and limited chemical functionality. It is for this reason that MALDI-TOF MS has proven to be such a powerful technique since it

overcomes the necessity for solubilisation and provides accurate mass data for ionisable components in the mixture. The coke deposits were found to consist of predominantly polycyclic aromatic hydrocarbons (PAHs), as evidenced by a molecular weight distribution in which major ion peaks are separated by 24 Da, with a molecular weight extending up to 5000 Da. Similar observations have been made in the analysis of flame-formed PAHs where an Hydrogen Abstraction C_2H_2 Addition (HACA) mechanism is a commonly accepted mechanism for PAH growth. We do not suggest that HACA is responsible for PAH growth during HTFT synthesis, but merely indicate that the growth of PAHs lead to 24 Da separations. C_2H_2 species are not observed during Fischer-Tropsch synthesis, but could exist as intermediates.

It is important to understand how the structure of the catalyst evolves and coke is deposited with time on-stream. Ideally, *in-situ* or more fundamental investigations of well-defined model systems would be used to study catalyst behaviour, and this is discussed further in Section 6.3. The core of Chapter 5 focussed on the quantification of hard carbon and its effect on the catalyst's physical and chemical properties. Quantification was achieved by a combination of CHN microanalysis, phase analysis (ideally through Mössbauer Absorption Spectroscopy) and elemental Fe analysis. A drop in the rates of both Fischer-Tropsch Synthesis (FTS) activity and carbon deposition was observed and, in the absence of fluidisation dynamics effects, this was ascribed to blockage of active sites. We propose that graphitic or laminar carbon forms would lead to blockage of sites. FTS activity is often related to the abundance of iron carbide phases in the catalyst. Relating the observed drop in FT activity to phase composition, where a general drop in the iron carbide content was observed, could not be done unambiguously because it is difficult to separate the effects of phase transformation and carbon deposition, which occur simultaneously. Furthermore, the catalyst composition measured *ex situ* is unlikely to represent the actual composition during active catalysis.

The molecular weight of carbonaceous material increases progressively as a function of time on-stream, but there is no critical point beyond which FT activity suddenly drops. Amorphous carbon, filaments and graphene-like sheets were observed on the catalyst. The gradual drop in structural integrity of the catalyst was investigated through sonication during Particle Size Analysis. Particle growth due to the deposition of carbon was observed, while the loss in mechanical strength of the particles is strongly linked to increasing carbon content. There is a distinct drop in the density of the catalyst particle with an increase in the hard carbon content. This corresponds to the original observations associated with the drop in productivity in the industrial reactor (Dry, 2004) and masks any true loss of activity.

The findings presented in Chapters 3, 4 and 5 provide a fundamental understanding of the structure and evolution of HTFT catalysts with time on-stream. This ultimately aids in obtaining insight into the mechanisms responsible for the inevitable losses in activity over time. The methodologies employed herein suggest that the HTFT activity decreases with an increase in deposited carbon. Activity is not affected by the nature or molecular weight of deposited carbon. We concede to the fact that the deleterious effects of carbon are also physical.

The stresses and strains typically present in the core-shell structure of a reacting particle are partly responsible for the observed attrition. The formation of iron carbides is inherently accompanied by corrosion, which results in the production of carbon-rich fines. These fines bring about differences in fluidisation dynamics within the reactor, which leads to a reduced mass of catalyst being present in the optimal temperature zone for FTS. The role of specifically hard carbon in this attrition has been determined. Identifying the exact composition of the spent catalysts also provides an idea of the properties and influence of each component in the FTS mechanism i.e. harmless or harmful for the HTFT process. This could facilitate feasibility studies into the regeneration of the catalysts which may perhaps be more cost effective than constantly replenishing the catalyst.

6.2 Method development

The most challenging aspect of this work was to develop methodologies to study spent catalysts. A relatively simple technique would typically need to be modified in order to be employed in this type of application. TPO was shown to only represent species that are actually oxidised in the experiment, omitting anything that undergoes desorption. In this way, we could not quantify the hard and soft carbon as well as the iron carbides present. This could possibly be overcome by the use of thermogravimetry (TGA/TPO) or first performing a desorption experiment.

The alternative method we used in carbon quantification was CHN microanalysis, and it was shown that the normal vertical furnace set-up could not accurately determine total carbon. Simple mortar and pestle grinding also improved the results obtained. Linked with this quantification method, determining the phase composition was shown to be inaccurately determined by XRD combined with Rietveld refinement. Mössbauer Spectroscopy was demonstrated to be a superior tool to determine the phase of metal-based spent catalysts.

The intricacy of Particle Size Analysis lies in the physical ability of the instrument used. The analyser needs to be capable of sufficiently high pump speeds in order to fluidise all the particles in the water medium. In addition, the carbon-rich fines that typically float on the surface need to be wetted using a Triton X-100 solution. Sample inhomogeneity may also complicate the analysis, but using a larger sample or repeat experiments can overcome this obstacle.

Although Raman Spectroscopy is one of the easier techniques to apply to the study of spent catalysts, the difficulty is that the information obtained is fairly limited due to a mixture of species present. The influence of the laser beam on the samples and the challenges when attempting to deconvolute the

spectra play a role in the decision to employ this technique to samples consisting of mixtures of species.

The signal of any given element obtained by Energy Dispersive X-ray Spectroscopy is influenced by the angle at which the X-ray beam impacts the surface. For this reason, powders are notorious for being difficult to study. Inhomogeneity further exacerbates the quality of measurements possible by this technique. Setting the powders in resin and polishing down to obtain a smooth surface is a useful way of addressing these issues. The problem with inhomogeneity is also manifested during HRTEM and SEM measurements, where only a small portion of the catalyst is typically imaged. This is unlikely to be representative of the entire sample.

Studying spent catalysts by traditional techniques such as Size Exclusion Chromatography or GC-MS techniques is limited by the insolubility of the samples. GC-MS would be useful if it were possible to volatilise the adsorbed species by some thermal technique (e.g. flash pyrolysis). The transformations brought on by these techniques could possibly introduce a further complication, but the benefits of knowing on a molecular level the nature of adsorbed species would be useful.

One of the major considerations in the characterisation of any aspect of spent catalysts is being able to compare the results to other studies. Building up an understanding of the behaviour of various catalysts and associated forms of coke deposits should simplify future investigations. In this way, comparisons between various fields may become a possibility.

6.3 Future work

The work presented here provides a platform for studying spent catalysts. Not only have we demonstrated the pitfalls of certain techniques and methodologies, but also paved the way to overcome them. This should enable

future researchers in this field to study spent catalysts in a way that will allow comparisons and a good understanding of various aspects of the problem.

Ideally, a move towards *in situ* or *in operando* studies would solve many problems associated with meta-stable species that only exist under reaction conditions. For instance, as alluded to previously, the catalyst composition determined *ex situ* may not represent the actual composition during active catalysis. It is therefore difficult to associate any observed change with catalytic behaviour. This problem could be overcome by studying changes in phase composition using *in situ* XRD, which has been demonstrated for the study of FT catalysts (Du Plessis, 2008) and carbide crystal structures could be measured in real time. *In situ* Raman measurements have been performed (Stair, 2002) and can provide information about the solid catalyst and molecular reagents in a single measurement. *In situ* XPS (Bluhm *et al*., 2007) could also be a promising technique for studying the evolution of surface species on HTFT catalysts in a synthesis gas environment. Developing a fundamental understanding of various systems could be addressed more simply by studying model systems, which can then be applied to industrial reaction conditions.

Studies of model systems would grant access to techniques such as X-ray Absorption Near Edge Structure (XANES) and Extended X-ray Absorption Fine Structure (EXAFS), which provide information about oxidation states and local atomic structure of crystalline or non-crystalline material in their natural state. This has been demonstrated for alkali promoted iron catalysts in a Fischer-Tropsch environment (Ribeiro *et al*., 2010). Elegant HRTEM measurements (Moodley, 2010) of a defined group of catalyst particles on a grid before and after certain treatments and reaction times would also become a possibility. These approaches would be ideal for the observation of carbonaceous deposition. However, such measurements would have to be performed in parallel to the generation of larger sample volumes required for measurements including attrition studies and so on. Regardless, the

advantages of *in situ* methods to study the changes in catalyst composition as a function of exposure to HTFT conditions are clear.

Considering the work presented in this thesis, it is possible to design new catalyst systems for HTFT. A feature of the current catalyst that needs to be addressed lies in the inhomogeneous distribution of promoter elements. This leads to the localised production of carbon-rich fines that create weakness in catalyst particle structure and are strongly linked to the drop in productivity. The main difficulties with changing the catalyst or conditions in order to minimise carbon deposition and therefore deactivation is that the activity and selectivity are often affected as well. Bearing this in mind, there are several possibilities that could be investigated. These include the addition of sulphur to the system or alloying the iron with a metal less prone to corrosion. The role of hydrogen on FTS activity and selectivity, as well as the type of carbon formed (graphitic versus filamentous) also needs to be better understood in order to find the ideal hydrogen partial pressures for HTFT. The success of new designs of catalyst systems hinges on the ability to stabilise iron carbides i.e. inhibition of corrosion. Improving the stability of iron-based catalyst employed in HTFT could have a tremendous impact on the economic viability of current HTFT operations.

7.REFERENCES

Alstrup, I. & Tavares, T. 1993, 'Kinetics of carbon formation from CH_4 + H_2 on silica-supported Nickel and Ni-Cu catalysts', *Journal of Catalysis*, vol. 139, pp. 513-524.

Amelse, J.A., Butt, J.B. & Schwartz, L.H. 1978, 'Carburization of supported iron synthesis catalysts', *Journal of Physical Chemistry*, vol. 82, pp. 558-563.

Anderson, R.B., Seligman, B., Shultz, J.F., Kelly, R. & Elliott, M.A. 1952, Fischer-Tropsch Synthesis. Some important variables of the synthesis on iron catalysts', *Engineering and Process Development*, vol. 44, pp. 391-397.

Ando, S. & Kimura, H. 1989, 'Effect of hydrogen on carbon deposition on iron in CO-H_2 mixtures', *Scripta Metallurgica*, vol. 23, pp. 1767-1772.

Apicella, B., Carpentieri, A., Alfè, M., Barbella, R., Tregrossi, A., Pucci, P. & Ciajolo, A. 2007, 'Mass spectrometric analysis of large PAH in a fuel-rich ethylene flame', *Proceedings of the Combustion Institute*, vol. 31, pp. 547-553.

Apicella, B., Ciajolo, A., Millan, M., Galmes, C., Herod, A.A. & Kandiyoti, R. 2004, 'Oligomeric carbon and siloxane series observed by matrix-assisted laser desorption/ionisation and laser desorption/ionisation mass spectrometry during the analysis of soot formed in fuel-rich flames', *Rapid Communications in Mass Spectrometry*, vol. 18, pp. 331-338.

Apicella, B., Millan, M., Herod, A.A., Carpentieri, A., Pucci, P. & Ciajolo, A. 2006, 'Separation and measurement of flame-formed high molecular weight polycyclic aromatic hydrocarbons by size-exclusion chromatography and laser desorption/ionization time-of-flight mass spectrometry', *Rapid Communications in Mass Spectrometry*, vol. 20, pp. 1104-1108.

Arakawa, H. & Bell, A.T. 1983, 'Effects of potassium promotion on the activity and selectivity of iron Fischer-Tropsch catalysts', *Industrial and Engineering Chemistry Process Design and Development*, vol. 22, pp. 97-103.

Axelsson, J., Hoberg, A.-M., Waterson, C., Myatt, P., Shield, G.L., Varney, J., Haddleton, D.M. & Derrick, P.J. 1997, 'Improved reproducibility and increased signal intensity in matrix assisted laser desorption/ionization as a result of electrospray sample preparation', *Rapid Communications in Mass Spectrometry*, vol. 11, pp. 209-213.

Bartholomew, C.H. 2001, 'Mechanisms of catalyst deactivation', *Applied Catalysis A: General*, vol. 212, pp. 17-60.

Bauer, F., Chen, W.H., Bilz, E., Freyer, A., Sauerland, V. & Liu, S.B. 2007, 'Surface modification of nano-sized HZSM-5 and HFER by pre-coking and silanization', *Journal of Catalysis*, vol. 251, pp. 258-270.

Bauschlicher, C.W., Ricca, A. & Rosi, M. 2002, 'Mechanisms for the growth of polycyclic aromatic hydrocarbon (PAH) cations', *Chemical Physics Letters*, vol. 355, pp. 159-163.

Belcher, R. 1976, 'The elements of organic analysis', *Proceedings of the Analytical Division of the Chemical Society*, Glasgow, 7 April 1976. Cambridge: RSC Publishing, pp. 153-164.

Beyssac, O., Goffé, B., Petitet, J.P., Froigneux, E., Moreau, M. & Rouzaud, J.N. 2003, 'On the characterization of disordered and heterogeneous carbonaceous materials by Raman spectroscopy', *Spectrochimica Acta Part A*, vol. 59, pp. 2267-2276.

Bi, X.X., Ganguly, B., Huffman, G.P., Huggins, F.E., Endo, M. & Ekland, P.C. 1993, 'Nanocrystalline α-Fe, Fe_3C and Fe_7C_3 produced by CO_2 laser pyrolysis', *Journal of Materials Research*, vol. 8, pp. 1666-1674.

Bian, G., Oonuki, A., Kobayashi, Y., Koizumi, N. & Yamada, M. 2001, 'Syngas adsorption on precipitated iron catalyst reduced by H_2, syngas or CO and on those used for high-pressure FT synthesis by in situ diffuse reflectance FTIR spectroscopy', *Applied Catalysis A: General*, vol. 219, pp. 13-24.

Bian, G., Oonuki, A., Koizumi, N., Nomoto, H. & Yamada, M. 2002, 'Studies with a precipitated iron Fischer-Tropsch catalyst reduced by H_2 or CO', *Journal of Molecular Catalysis A: Chemical*, vol. 186, pp. 203-213.

Bluhm, H., Havecker, M., Knop-Gericke, A., Kiskinova, M., Schlogl, R. & Salmeron, M. 2007, 'In situ X-ray photoelectron spectroscopy studies of gas-solid interfaces at near-ambient conditions', *Materials Research Society Bulletin*, vol. 32, pp. 1022-1030.

Bockhorn, H., Fetting, F. & Wenz, H.W. 1983, 'Investigation of the Formation of high molecular hydrocarbons and soot in premixed hydrocarbon-oxygen flames', *Berichte der Bunsen-Gesellschaft für Physikalische Chemie*, vol. 87, pp. 1067-1073.

Bonzel, H.P. & Krebs, H.J. 1980, 'On the chemical nature of the carbonaceous deposits on iron after CO hydrogenation', *Surface Science*, vol. 91, pp. 499-513.

Bonzel, H.P. & Krebs, H.J. 1981, 'Enhanced rate of carbon deposition during Fischer-Tropsch synthesis on K promoted Fe', *Surface Science Letters*, vol. 109, pp. L527-L531.

Bromfield, T.C. & Coville, N.J. 1999, 'The effect of sulphide ions on a precipitated iron Fischer-Tropsch catalyst', *Applied Catalysis A: General*, vol. 186, pp. 297-307.

Bukur, D.B., Mukesh, D. & Patel, S.A. 1990, 'Promoter effects on precipitated iron catalysts for Fischer-Tropsch synthesis', *Industrial & Engineering Chemistry Research*, vol. 29, pp. 194-204.

Bukur, D.B., Okabe, K., Rosynek, M.P., Li, C., Wang, D., Rao, K.R.P.M. & Huffman, G.P. 1995a, 'Activation studies with a precipitated iron catalyst for Fischer-Tropsch synthesis I. Characterization studies', *Journal of Catalysis*, vol. 155, pp. 3353-365.

Bukur, D.B., Nowicki, L., Manne, R.K. & Lang, X. 1995b, 'Actication studies with a precipitated catalyst for Fischer-Tropsch synthesis II. Reaction studies', *Journal of Catalysis*, vol. 155, pp. 366-275.

Bukur, D.B., Koranne, M., Lang, X., Rao, K.R.P.M. & Huffman, G.R. 1995c, 'Pretreatment effect studies with a precipitated iron Fischer-Tropsch catalyst', *Applied Catalysis A: General*, vol. 126, pp. 85-113.

Butt, J.B. 1990, 'Carbide phase on iron-based Fischer-Tropsch synthesis catalyst Part I: Characterization studies', *Catalysis Letters*, vol. 7, pp. 61-82.

Caceres, P.G. 2006, 'Low-temperature synthesis of nanostructures χ-Fe_5C_2 platelets in $CO+H_2$ atmospheres', *Materials Characterization*, vol. 56, pp. 26-31.

Campos, A., Lohitharn, N., Roy, A., Lotero, E., Goodwin, J.G. (JR) & Spivey, J.J. 2010, 'An activity and XANES study of Mn-promoted, Fe-based Fischer-Tropsch catalysts', *Applied Catalysis A: General*, vol. 375, pp. 12-16.

Cao, D.-B., Zhang, F.-Q., Li, Y.-W. & Jiao, H. 2004, 'Density functional theory study of CO adsorption on Fe_5C_2(001), -(100), and –(110) surfaces', *Journal of Physical Chemistry B*, vol. 108, pp. 9094-9104.

Cao, D.-B., Zhang, F.-Q., Li, Y.-W., Wang, J. & Jiao, H. 2005a, 'Density functional theory study of hydrogen adsorption on Fe_5C_2(001), Fe_5C_2(100), and Fe_5C_2(110)', *Journal of Physical Chemistry B*, vol. 109, pp. 833-844.

Cao, D.-B., Zhang, F.-Q., Li, Y.-W., Wang, J. & Jiao, H. 2005b, 'Structures and energies of coadsorbed CO and H_2 on Fe_5C_2(001), Fe_5C_2(100), and Fe_5C_2(110)', *Journal of Physical Chemistry B*, vol. 109, pp. 10922-10935.

Cao, D.-B., Wang, S.-G., Li, Y.-W., Wang, J. & Jiao, H. 2007, 'What is the product of ketene hydrogenation on Fe_5C_2(001): oxygenates or hydrocarbons', *Journal of Molecular Catalysis A: Chemical*, vol. 272, pp. 275-287.

Cao, D.-B., Li, Y.-W., Wang, J. & Jiao, H. 2008, 'Adsorption and reaction of surface carbon species on Fe_5C_2(001)', *Journal of Physical Chemistry C*, vol. 112, pp. 14883-14890.

Carré, V., Vernex-Loset, L., Krier, G., Manuelli, P. & Muller, J. 2004, 'Laser desorption/ionization mass spectrometry of diesel particulate matter with charge-transfer complexes', *Analytical Chemistry*, vol. 76, no. 14, pp. 3979-3987.

Casanova, R., Cabrera, A.L., Heinemann, H. & Somorjai, G.A. 1983, 'Calcium oxide and potassium hydroxide catalysed low temperature methane production from graphite and water', *Fuel*, vol. 62, pp. 1138-1144.

Cerqueira, H.S., Sievers, C., Joly, G., Magnoux, P. & Lercher, J.A. 2005, 'Mulitechnique characterization of coke produced during commercial resid FCC operation', *Industrial & Engineering Chemistry Research*, vol. 44, pp. 2069-2077.

Cervo, E.C. & Thies, M.C. 2007, 'Control of the molecular weight distribution of petroleum pitched via dense-gas extraction', *Chemical Engineering Technology*, vol. 30, pp. 742-748.

Cervo, E.C., Thies, M.C. & Fathollahi, B. 2008, 'Controlling the oligomeric composition of carbon-fiber precursors by dense-gas extraction', *Journal of the American Ceramic Society*, vol. 91, pp. 1416-1422.

Cheng, J., Hu, P., Ellis, P., French, S., Kelly, G. & Lok, C.M. 2010, 'Density functional theory study of iron and cobalt carbides for Fischer-Tropsch synthesis', *Journal of Physical Chemistry C*, vol. 114, pp. 1085-1093.

Ciobîcă, I.M., van Santen, R.A., van Berge, P.J. & van de Loosdrecht, J. 2008, 'Adsorbate induced reconstruction of cobalt surfaces', *Surface Science*, vol. 602, pp. 17-27.

Claeys, M. & van Steen, E. 2004, 'Basic studies'. In Steynberg, A., Dry, M., Eds. *Studies in Surface Science and Catalysis Vol. 152.* Elsevier: Amsterdam. Chapter 8.

Craxford, S.R. & Rideal, E. 1939, 'Die Fischer-Tropsch-Synthese von Kohlenwasserstoffen und einige verwante Reaktionen', *Brennstof Chemie*, vol. 20, pp. 263-270.

Cristadoro. A., Kulkarni, S.U., Burgess, W.A., Cervo, E.G., Räder, H.J., Müllen, K., Bruce, D.A. & Thies, M.C. 2009, 'Structural characterization of the oligomeric constituents of petroleum pitches', *Carbon*, vol. 47, pp. 2358-2370.

Dass, C. 2007. *Fundamentals of contemporary mass spectrometry*, New Jersey: John Wiley & Sons.

Davis, B.H. 2007, Fischer-Tropsch synthesis: Comparison of performances of iron and cobalt catalysts', *Industrial & Engineering Chemistry Research*, vol. 46, pp. 8938-8945.

Davis, B.H. 2009, 'Fischer-Tropsch synthesis: reaction mechanisms for iron catalysts', *Catalysis Today*, vol. 141, pp. 25-33.

De Faria, D.L.A., Silva, S.V. & de Oliveira, M.T. 1997, 'Raman microspectroscopy of some iron oxides and oxyhydroxides', *Journal of Raman Spectroscopy*, vol. 28, pp. 873-878.

De la Peña O'Shea, V.A., Homs, N., Fierro, J.L.G. & Ramírez de la Piscina, P. 2006, 'Structural changes and activation treatment in a Co/SiO_2 catalyst for Fischer-Tropsch synthesis', *Catalysis Today*, vol. 114, pp. 422-427.

De la Peña O'Shea, V.A., Álvarez-Galván, M.C., Campos-Martín, J.M. & Fierro, J.L.G. 2007, 'Fischer-Tropsch synthesis on mono- and bimetallic Co and Fe catalysts in fixed-bed and slurry reactors', *Applied Catalysis A: General*, vol. 326, pp. 65-73.

Dias, J.A.C. & Assaf, J.M. 2004, 'The advantages of air addition on the methane steam reforming over $Ni/\gamma\text{-}Al_2O_3$', *Journal of Power Sources*, vol. 137, pp. 264-268.

Dictor, R.A. & Bell, A.T. 1986, 'Fischer-Tropsch synthesis over reduced and unreduced iron oxide catalysts', *Journal of Catalysis*, vol. 97, pp. 121-136.

Dirand, M. & Afqir, L. 1983, 'Identification structurale precise des carbures precipites dans les aciers faiblement allies aux divers stades du revenue. Mecanismes de precipitation', *Acta Metallurgica*, vol. 31, pp. 1089-1107.

Dobbins, R.A., Fletcher, R.A., Benner, B.A. (JR) & Hoeft, S. 2006, 'Polycyclic aromatic hydrocarbons in flames, in diesel fuels, and in diesel emissions', *Combustion and Flame*, vol.144, pp. 773-781.

Dobbins, R.A., Fletcher, R.A. & Chang, H.-C. 1998, 'The evolution of soot precursor particles in a diffusion flame', *Combustion and Flame*, vol. 115, pp. 285-298.

Dobbins, R.A., Fletcher, R.A. & Lu, W. 1995, 'Laser microprobe analysis of soot precursor particles and carbonaceous soot', *Combustion and Flame*, vol. 100, pp. 301-309.

Domin, M., Moreea, R., Lazaro, M.-J., Herod, A.A. & Kandiyoti, R. 1997, 'Effect of polydispersity on the characterization of coal-derived liquids by matrix-assisted laser desorption/ionization time-of-flight mass spectrometry : Interferences from results for mixtures of polystyrene molecular mass standards', *Rapid Communications in Mass Spectrometry*, vol. 11, pp. 1845-1952.

Dry, M., 1981. The Fischer-Tropsch Synthesis. In J.R. Anderson, & M. Boudart, eds. *Catalysis: Science and Technology* Vol. 1, New York: Springer. pp 159-255.

Dry, M.E. 1990, 'Fischer-Tropsch synthesis over iron catalysts', *Catalysis Letters*, vol. 7, pp. 241-252.

Dry, M.E. 1996, 'Practical and theoretical aspects of the catalytic Fischer-Tropsch process', *Applied Catalysis A: General*, vol. 138, pp. 319-344.

Dry, M.E. 2002, 'The Fischer-Tropsch process: 1950-2000', *Catalysis Today*, vol. 71, pp. 227-241.

Dry, M.E. 2004, 'FT Catalysts'. In Steynberg, A., Dry, M., Eds. *Studies in Surface Science and Catalysis Vol. 152.* Elsevier: Amsterdam. Chapter 7.

Dry, M.E., Shingles, T. & van H. Botha, C.S. 1970a, 'Factors influencing the formation of carbon on iron Fischer-Tropsch catalysts I. The influence of promoters', *Journal of Catalysis*, vol. 17, pp. 341-346.

Dry, M.E., Shingles, T. & van H. Botha, C.S. 1970b, 'Factors influencing the formation of carbon on iron Fischer-Tropsch catalysts II. The effect of temperature and of gases and vapors present during Fischer-Tropsch synthesis', *Journal of Catalysis*, vol. 17, pp. 347-354.

Du Plessis, H.E. 2008, 'The crystal structures of the iron carbides', Ph. D. Thesis, University of Johannesburg.

Du Plessis, H.E., de Villiers, J.P.R. & Kruger, G.J. 2007, 'Re-determination of the crystal structure of χ-Fe_5C_2 Hägg carbide', *Zeitschrift für Kristallographie*, vol. 222, pp. 211-217.

Dutta, T.K. & Harayama, S. 2001, 'Time-of-flight mass spectrometric analysis of high-molecular-weight alkanes in crude oil by silver nitrate chemical ionization after laser desorption', *Analytical Chemistry*, vol. 73, pp. 864-869.

Dwyer, D.J. & Somorjai, G.A. 1978, 'Hydrogenation of CO and CO_2 over iron foils', *Journal of Catalysis*, vol. 52, pp. 291-301.

Dwyer, D.J. & Hardenbergh, J.H. 1984, 'The catalytic reduction of carbon monoxide over iron surfaces: a surface science investigation', *Journal of Catalysis*, vol. 87, pp. 66-76.

Edwards, W.F., Jin, L. & Thies, M.C. 2003, 'MALDI-TOF mass spectrometry: obtaining reliable mass spectra for insoluble carbonaceous pitches', *Carbon*, vol. 41, pp. 2761-2768.

Edwards, W.F. & Thies, M.C. 2005, 'Dense-gas fractionation and MALDI characterization of carbonaceous pitches', *Energy & Fuels*, vol. 19, pp. 984-991.

Edwards, W.F. & Thies, M.C. 2006, 'Fractionation of pitches by molecular weight using continuous and semibatch dense-gas extraction', *Carbon*, vol. 44, pp. 243-252.

Ehlers, A.W., de Koster, C.G., Meier, R.J. & Lammertsma, K. 2001, 'MALDI-TOF MS of saturated polyolefins by coordination of metal cations: a theoretical study', *Journal of Physical Chemistry A*, vol. 105, pp. 8691-8695.

Eliason, S.A. & Bartholomew, C.H. 1999, 'Reaction and deactivation kinetics for Fischer-Tropsch synthesis on unpromoted and potassium-promoted iron catalysts', *Applied Catalysis A: General*, vol. 186, pp. 229-243.

Etherington, K.J., Rodger, A. & Hemming, P. 2001, 'CHN microanalysis – a technique for the 21st century?', *LabPlus International*, vol. Feb/March, pp. 26-27.

Feller, A., Zuazo, I., Guzman, A., Barth, J.O. & Lercher, J.A. 2003a, 'Common mechanistic aspects of liquid and solid acid catalyzed alkylation of isobutene with n-butene', *Journal of Catalysis*, vol. 216, pp. 313-323.

Feller, A., Barth, J.O., Guzman, Zuazo, I. & Lercher, J.A. 2003b, 'Deactivation pathways in zeolite-catalyzed isobutene/butene alkylation', *Journal of Catalysis*, vol. 220, pp. 192-206.

Ferrari, A.C., Meyer, J.C., Scardaci, V., Casiraghi, C., Lazzeri, M., Mauri, F., Piscanec, S., Jiang, D., Novoselov, K.S., Roth, S. & Geim, A.K. 2006, 'Raman spectrum of graphene and graphene layers', *Physical Review Letters*, vol. 97, pp. 187401:1-4.

Ferrari, A.C. & Robertson, J. 2000, 'Interpretation of Raman spectra of disordered and amorphous carbon', *Physical Review B*, vol. 61, pp. 14095-14107.

Ferrari, A.C. & Robertson, J. 2001, 'Resonant Raman spectroscopy of disordered, amorphous, and diamondlike carbon', *Physical Review B*, vol. 64, pp. 075414: 1-13.

Fischer, F. & Tropsch, H. 1923, 'Über die Herstellung synthetischer Ölgemische (Synthol) durch Aufbau aus Kohlenoxyd und Wasserstoff', *Brennstof Chemie*, vol 4, pp. 276-285.

Fischer, F. & Tropsch, H. 1926, 'Die Erodölsynthese bei gewöhnlichem Druck aus den Vergangsprodukten der Kohlen', *Brennstof Chemie*, vol 7, pp. 97-104.

Fletcher, R.A., Dobbins, R.A. & Chang, H.-C. 1998, 'Mass spectrometry of particles formed in a deuterated ethene diffusion flame', *Analytical Chemistry*, vol. 70, pp. 2745-2749.

Forzatti, P. & Lietti, L. 1999, 'Catalyst deactivation', *Catalysis Today*, vol. 52, pp. 165-181.

Freeman, S.K. 1974. *Applications of Laser Raman Spectroscopy*. New York: Wiley & Sons.

Frenklach, M. 2002, 'Reaction mechanism of soot formation in flames', *Physical Chemistry Chemical Physics*, vol. 4, pp. 2028-2037.

Frenklach, M., Clary, D.W., Gardiner, W.C., Stein, S.E. 1984, 'Detailed kinetic modelling of soot formation in shock-tube pyrolysis of acetylene', *Twentieth Symposium (International) on Combustion/The Combustion Institute*, pp. 887-901.

Fung, S.C., Querini, C.A. 1992, 'A highly sensitive detection method for temperature programmed oxidation if coke deposits: Methanation of CO_2 in the presence of O_2', *Journal of Catalysis*, vol. 138, pp. 240-254.

Galuszka, J., Sano, T. & Sawicki, J.A. 1992, 'Study of carbonaceous deposits on Fischer-Tropsch oxide supported iron catalysts', *Journal of Catalysis*, vol. 136. pp. 96-109.

Gherghel, L., Kübel, C., Lieser, G., Räder, H. & Mullen, K. 2002, 'Pyrolysis in the mesophase: a chemist's approach toward preparing carbon nano- and microparticles', *Journal of American Chemical Society*, vol. 124, pp. 13130-13138.

Goldstein, G.I., Newbury, D.E., Echlin, P., Joy, D.C., Fiori, C., Lifshin, E. 1981, *Scanning electron microscopy and x-ray microanalysis*. New York: Plenum Press.

Gormley, R.J., Zarochak, M.F., Deffenbaugh, P.W. & Rao, K.R.P.M. 1997, 'Effect of initial wax medium on the Fischer-Tropsch slurry reaction', *Applied Catalysis A: General*, vol. 116, pp. 263-279.

Gould, B.D., Chen, X. & Schwank, J.W. 2008, '*n*-Dodecane reforming over nickel-based monolith catalysts: deactivation and carbon deposition', *Applied Catalysis A: General*, vol. 334, pp. 277-290.

Grabke, H.J., Müller-Lorenz, E.M. & Schneider, A. 2001, 'Carburization and metal dusting on iron', *ISIJ International*, vol. 41, pp. S1-S8.

Gruber, T., Waldeck-Zerda, T. & Gerspacher, M. 1994, 'Raman studies of heat-treated carbon blacks', *Carbon*, vol. 32, pp. 1377-1382.

Hanton, S.D. & Parees, D.M. 2005, 'Extending the solvent-free MALDI sample preparation method', *Journal of American Society for Mass Spectrometry*, vol. 16, pp. 90-93.

Hayakawa, H., Tanaka, H. & Fujimoto, K. 2006, 'Studies on precipitated iron catalysts for Fischer-Tropsch synthesis', *Applied Catalysis A: General*, vol. 310, pp. 24-30.

Helveg, S., López-Cartes, C., Sehested, J., Hansen, P.L., Clausen, B.S., Rostrup-Nielsen, J.R., Abild-Pedersen, F. & Nørskov, J.K. 2004, 'Atomic scale imaging of carbon nanofibre growth', *Nature*, vol. 427, pp. 426-428.

Herod, A.A., Lazaro, M.J., Domin, M., Islas, C.A. & Kandiyoti, R. 2000, 'Molecular mass distributions and structural characterisation of coal derived liquids', *Fuel*, vol. 79, pp. 323-337.

Herranz, T., Rojas, S., Pérez-Alonso, F., Ojeda, M., Terreros, P. & Fierro, J.L.G. 2006, 'Genesis of iron carbides and their role in the synthesis of hydrocarbons from synthesis gas', *Journal of Catalysis*, vol. 243, pp. 199-211.

Janbroers, S., Louwen, J.N., Zandbergen, H.W. & Kooyman, P.J. 2009, 'Insight into the nature of iron-based Fischer-Tropsch catalysts from quasi in situ TEM-EELS and XRD', *Journal of Catalysis*, vol. 268, pp. 235-242.

Jin, Y. & Datye, A.K. 1998a, 'Phase transformations in iron Fischer-Tropsch synthesis (FTS) catalysts', *Proceedings of the 14th International Congress on Electron Microscopy Volume II*, Cancun, 31 August – 4 September 1998. Bristol: Institute of Physics Publishing, pp. 379-380.

Jin, Y. & Datye, A.K. 1998b, 'Characterization of bubble column slurry phase iron Fischer-Tropsch catalysts', *Proceedings of the 5th Natural Gas Conversion Symposium*, Giardini Naxos, 20-25 September 1998. Amsterdam: Elsevier, pp. 209-214.

Jin, Y. & Datye, A.K. 2000, 'Phase transformations in iron Fischer-Tropsch catalysts during temperature programmed reduction', *Journal of Catalysis*, vol.196, pp. 8-17.

Jin, Y., Xu, H. & Datye, A.K. 2002, 'Electron energy-loss spectroscopy of carbonaceous layers in iron surfaces in Fischer-Tropsch catalysts', *Proceedings of the 15th International Congress in Electron Microscopy Volume 1*, Durban, 1-6 September 2002. Bloemfontein: Microscopy Society of Southern Africa, pp. 363-364.

Johnson, A.D., Daley, S.P., Utz, A.L. & Ceyer, S.T. 1992, 'The chemistry of bulk hydrogen: reaction of hydrogen embedded in nickel with adsorbed CH_3', *Science*, vol. 257, pp. 223-225.

Johnson, B.R., Bartle, K.D., Domin, M., Herod, A.A. & Kandiyoti, R. 1998, 'Absolute calibration of size exclusion chromatography for coal derivatives through MALDI MS', *Fuel*, vol. 77, no. 9/10, pp.933-945.

Jung, H-J., Vannice, M.A., Mulay, L.N., Stanfield, R.M. & Delgass, W.N. 1982a, 'The characterisation of carbon-supported iron catalysts: Chemisorption, magnetization, and Mössbauer spectroscopy', *Journal of Catalysis*, vol.76, pp. 208-224.

Jung, H.-J., Walker, P.L. & Vannice, M.A. 1982b, 'CO hydrogenation over well-dispersed carbon-supported iron catalysts', *Journal of Catalysis*, vol. 75, pp. 416-422.

Jung, H. & Thomson, W.J. 1992, 'Dynamic X-ray diffraction study of an unsupported iron catalyst in Fischer-Tropsch synthesis', *Journal of Catalysis*, vol. 134, pp. 654-667.

Kahr, M.S. & Wilkins, C.L. 1993, 'Silver nitrate chemical ionization for analysis of hydrocarbon polymers by laser desorption Fourier Transform mass spectrometry', *Journal of American Society for Mass Spectrometry*, vol. 4, pp. 453-460.

Kalakkad, D.S., Shroff, M.D., Köhler, S., Jackson, N. & Datye, A.K. 1995, 'Attrition of precipitated iron Fischer-Tropsch catalysts', *Applied Catalyst A: General*, vol. 133, pp. 335-350.

Kalibaeva, G., Vuilleumier, R., Meloni, S., Alavi, A., Ciccotti, G. & Rosei, R. 2006, 'Ab initio simulation of carbon clustering on an Ni(111) surface: a model of the poisoning of nickel-based catalysts', *Journal of Physical Chemistry B*, vol. 110, pp. 3638-3646.

Karas, M. & Hillenkamp, F. 1988, 'Laser desorption ionization of proteins with molecular masses exceeding 10 000 Daltons', *Analytical Chemistry*, vol. 60, pp. 2299-2301.

Keating, K. & Knight, R. 2007, 'A laboratory study to determine the effects of iron oxides on proton NMR measurements', *Geophysics*, vol. 72, pp. E27-E32.

Kim, M.S., Rodriguez, N.M. & Baker, R.T.K. 1993, 'The interplay between sulphur adsorption and carbon deposition on cobalt catalysts', *Journal of Catalysis*, vol. 143, pp. 449-463.

Kölbel, H., Ackermann, P., Ruschenburg, E., Langheim, R. & Engelhardt, F. 1951, 'Beitrag zur Fischer-Tropsch Synthese on Eisenkontakten', *Chemie-Ingenieur-Technik*, vol. 23, pp. 153-157.

Krebs, H.J., Bonzel, H.P. & Gafner, G. 1979, 'A model study of the hydrogenation of CO over polycrystalline iron', *Surface Science*, vol. 88, pp. 269-283.

Kuivila, C.S., Butt, J.B. & Stair, P.C. 1988, 'Characterisation of surface species on iron synthesis catalysts by x-ray photoelectron spectroscopy', *Applied Surface Science*, vol. 32, pp. 99-121.

Kuivila, C.S., Stair, P.C. & Butt, J.B. 1989, 'Compositional aspects of iron Fischer-Tropsch catalysts: An XPS/reaction study', *Journal of Catalysis*, vol. 118, pp. 299-311.

Kühn, G., Weidner, St., Just U. & Hohner, G. 1996, 'Characterization of technical waxes. Comparison of chromatography techniques and matrix assisted laser-desorption/ionization mass spectrometry', *Journal of Chromatography A*, vol. 732, pp. 111-117.

Kuzman, E., Nagy, S., Vertes, A. 2003, 'Critical review of analytical applications of Mössbauer spectroscopy illustrated by mineralogical and geological examples', *Pure and Applied Chemistry*, vol. 75, pp. 801-858.

Larson, A.C. & von Dreele, R.B. 1987, 'GSAS', *Los Alamos National Laboratory Report*. No. LA-UR-87-748.

Lázaro, M.J., Herod, A.A., Cocksedge, M., Domin, M. & Kandiyoti, R. 1997, 'Molecular mass determinations in coal-derived liquids by MALDI mass spectrometry and size-exclusion chromatography', *Fuel*, vol. 76, pp. 1225-1233.

Lazzeri, M., Piscanec, S., Mauri, F., Ferrari, A.C. & Robertson, J. 2006, 'Phonon linewidths and electron-phonon coupling in graphite and nanotubes', *Physical Review B*, vol. 73, pp. 115426:1-6.

Li, S., Ding, W., Meitzner, G.D. & Iglesia, E. 2002, 'Spectroscopic and transient kinetic studies of site requirements in iron-catalyzed Fischer-Tropsch synthesis', *Journal of Physical Chemistry B*, vol. 106, pp. 85-91.

Li, S., Meitzner, G.D. & Iglesia, E. 2001, 'Structure and site evolution of iron oxide catalyst precursors during the Fischer-Tropsch synthesis', *Journal of Physical Chemistry B*, vol. 105, pp. 5743-5750.

Liu, J. 2000, 'Contrast of highly dispersed metal nanoparticles in high-resolution secondary electron and backscattered electron images of supported metal catalysts', *Microscopy and Microanalysis*, vol. 6, pp. 388-399.

Loaiza-Gil, A., Fontal, B., Rueda, F., Mendialdua, J. & Casanova, R. 1999, 'On carbonaceous deposit formation in carbon monoxide hydrogenation on a natural iron catalyst', *Applied Catalysis A: General*, vol. 177, pp. 193-203.

Loggenberg, P.M., Dry, M.E. & Copperthwaite, R.G. 1990, 'A surface study of the CO hydrogenation reaction on fused iron catalysts', *Surface and Interface Analysis*, vol. 16, pp. 347-351.

Lohitharn, N., Goodwin, J.G. & Lotero, E. 2008, 'Fe-based Fischer-Tropsch synthesis catalysts containing carbide-forming transition-metal promoters', *Journal of Catalysis*, vol. 255, pp. 104-113.

Macha, S.F., McCarley, T.D. & Limbach, P.A. 1999, 'Influence of ionization energy on charge-transfer ionization iin matrix-assisted laser desorption/ionization mass spectrometry', *Analytica Chimica Acta*, vol. 397, pp. 235-245.

Machocki, A. 1991, 'Formation of carbonaceous deposit and its effect on carbon monoxide hydrogenation on iron-based catalysts', *Applied Catalysis*, vol. 70, pp. 237-252.

Maddock, A.G. 1997. *Mössbauer Spectroscopy: Principles and Applications*. Chichester: Horwood Publishing.

Mahajan, D., Gütlich, P., Ensling, J., Pandya, K., Stumm, U. & Vijayaraghavan, P. 2003, 'Evaluation of nano-sized iron in slurry-phase Fischer-Tropsch synthesis', *Energy & Fuels*, vol. 17, pp. 1210-1221.

Maitlis, P.M., Long, H.C., Quyoum, R., Turner, M.L. & Wang, Z.-Q. 1996, 'Heterogeneous catalysis of C-C bond formation: black art or organometallic science?', *Chemical Communications*, pp. 1.

Maitlis, P.M., Quyoum, R., Long, H.C. & Turner, M.L. 1999, 'Towards a chemical understanding of the Fischer-Tropsch reaction: alkene formation', *Applied Catalysis A: General*, vol. 186, pp. 363-374.

Malan, O., Louw, J. & Ferreira, L. 1961, 'Eisencarbidphasen in Benzin-Sinthese-Katalysatoren', *Brennstoff Chemie*, vol. 42, pp. 209-212.

Mansker, L.D., Jin, Y., Bukur, D.B. & Datye, A.K. 1999, 'Characterization of slurry phase iron catalysts for Fischer-Tropsch synthesis', *Applied Catalysis A: General*, vol. 186, pp. 277-296.

Mathieu, O., Frache, G., Djebaili-Chaumeix, N., Paillard, C.-E., Krier, G., Muller, J.-F., Douce, F. & Manuelli, P. 2007, 'Characterization of adsorbed species on soot formed behind reflected shock waves', *Proceedings of the Combustion Institute*, vol. 31, pp. 511-519.

Mathieu, O., Frache, G., Djebaili-Chaumeix, N., Paillard, C.-E., Krier, G., Muller, J.-F., Douce, F. & Manuelli, P. 2009, 'Laser desorption-ionization time-of-flight mass spectrometry for analysis of heavy hydrocarbons adsorbed on soot formed behind reflected shock waves', *Proceedings of the Combustion Institute*, vol. 32, pp. 971-978.

Matsumoto, H. & Bennett, C.O. 1978, 'The transient method applied to the methanation and Fischer-Tropsch reactions over a fused iron catalyst', *Journal of Catalysis*, vol. 53, pp. 331-344.

Meima, G.R., Knijff, L.M., van Dillen, A.J., Geus, J.W., Bongaerts, J.E., van Buren, F.R. & Delcour, K. 1987, 'The effect of sub-surface oxygen on the catalytic properties of silver catalysts', *Catalysis Today*, vol. 1, pp. 117-131.

Menon, P.G. 1990, 'Coke on catalysts – harmful, harmless, invisible and beneficial types', *Journal of Molecular Catalysis*, vol. 59, pp. 207-220.

Miller, J.T., Fisher, R.B., Thiyagarajan, P., Winans, R.E. & Hunt, J.E. 1998, 'Subfractionation and characterization of Mayan asphaltene', *Energy & Fuels*, vol. 12, pp. 1290-1298.

Moodley, D.J. 2008, 'On the deactivation of cobalt-based Fischer-Tropsch catalysts', Ph. D. Thesis, Technische Universiteit Eindhoven.

Moodley, P. 2010, 'Iron nanoparticulate planar model systems – synthesis and applications', Ph.D. Thesis, Technische Universiteit Eindhoven.

Moulijn, J.A., van Diepen, A.E. & Kapteijn, F. 2001, 'Catalyst deactivation: is it predictable? What to do?', *Applied Catalysis A: General*, vol. 212, pp. 3-16.

Murad, E. & Cashion, J. 2004. *Mössbauer spectroscopy of environmental materials and their industrial utilisation*. Boston: Kluwer Academic Press.

Nielen, M.W.F. 1999, 'MALDI time-of-flight mass spectrometry of synthetic polymers', *Mass Spectrometry Reviews*, vol. 18, pp. 309-344.

Niemantsverdriet, J.W. 1993. *Spectroscopy in Catalysis*. Weinheim: VCH.

Niemantsverdriet, J.W. & van der Kraan, A.M. 1981, 'On the time-dependent behaviour of iron catalysts in Fischer-Tropsch synthesis', *Journal of Catalysis*, vol. 72, pp. 385-388.

Niemantsverdriet, J.W., van der Kraan, A.M., van Dijk, W.L. & van der Baan, H.S. 1980, 'Behavior of metallic iron catalysts during Fischer-Tropsch synthesis studied with Mössbauer spectroscopy, x-ray diffraction, carbon content determination, and reaction kinetic measurements', *Journal of Physical Chemistry*, vol. 84, pp. 3363-3370.

Ning, W., Koizumi, N., Chang, H., Mochizuki, T., Itoh, T. & Yamada, M. 2006, 'Phase transformation of unpromoted and promoted Fe catalysts and the formation of carbonaceous compounds during Fischer-Tropsch synthesis reaction', *Applied Catalysis A: General*, vol. 312, pp. 35-44.

Ning, W., Koizumi, N. & Yamada, M. 2007, 'Improvement of promoters on the Fischer-Tropsch activity of mechanically mixed Fe catalysts', *Catalysis Communications*, vol. 8, pp. 275-278.

Nolan, P.E., Lynch, D.C. & Cutler, A.H. 1998, 'Carbon deposition and hydrocarbon formation on group VIII metal catalysts', *Journal of Physical Chemistry B*, vol. 102, pp. 4165-4175.

Ott, G.L., Fleisch, T. & Delgass, W.N. 1980, 'Carbon deposition and activity changes over FeRu alloys during Fischer-Tropsch synthesis', *Journal of Catalysis*, vol. 65, pp. 253-262.

Paál, Z., Wootsch, A., Schlögl, R. & Wild, U. 2005, 'Carbon accumulation, deactivation and reactivation of Pt catalysts upon exposure to hydrocarbons', *Applied Catalysis A: General*, vol. 282, pp. 135-145.

Panzner, G. & Diekmann, W. 1985, 'The bonding state of carbon segregated to α-iron surfaces and on iron carbide surfaces studied by electron spectroscopy', *Surface Science*, vol. 160, pp. 253-270.

Park, C. & Baker, R.T.K. 2000, 'Carbon deposition on iron-nickel during interaction with ethylene-carbon monoxide-hydrogen mixtures', *Journal of Catalysis*, vol. 190, pp. 104-117.

Park, E., Zhang, J., Thomson, S., Ostrovski, O. & Howe, R. 2001, 'Characterization of phases formed in the iron carbide process by x-ray diffraction, Mossbauer, x-ray photoelectron spectroscopy, and Raman spectroscopy', *Metallurgical and Materials Transactions B*, vol. 32B, pp. 839-845.

Park, H.J., Meyer, J., Roth, S. & Skákalova, V. 2010, 'Growth and properties of few-layer graphene prepared by chemical vapour deposition', *Carbon*, vol. 48, pp. 1088-1094.

Patzlaff, J., Liu, Y., Graffmann, C. & Gaube, J. 1999, 'Studies on product distributions of iron and cobalt catalyzed Fischer-Tropsch synthesis', *Applied Catalysis A: General*, vol. 186, pp. 109-119.

Pichler, H. & Schulz, H. 1970, 'Neuere Erkenntnisse auf dem Gebiet der Synthese von Kohlenwasserstoffen aus CO und H_2', *Chemie Ingenieur Technik*, vol. 42, pp. 1162-1174.

Pijolat, M., Perrichon, V. & Bussière, P. 1987, 'Study of the carburization of an iron catalyst during the Fischer-Tropsch synthesis: influence on its catalytic activity', *Journal of Catalysis*, vol. 107, pp. 82-91.

Pindoria, R.V., Megaritis, A., Chatzakis, I.N., Vasanthakumar, L.S., Zhang, S., Lazaro, M., Herod, A.A., Garcia, X.A., Gordon, A.L. & Kandiyoti, R. 1997, 'Structural characterization of tar from a coal gasification plant', *Fuel*, vol. 76, no. 2, pp. 101-113.

Piscanec, S., Lazzeri, M., Robertson, J., Ferrari, A.C. & Mauri, F. 2007, 'Optical phonons in carbon nanotubes: Kohn anomalies, Peierls distortions, and dynamic effects', *Physical Review B*, vol. 75, pp. 035427:1-22.

Podgurski, H.H., Kummer, J.T., De Witt, T.W. & Emmett, P.H. 1950, 'Preparation, stability and absorptive properties of the carbides of iron', *Journal of the American Chemical Society*, vol. 72, pp. 5382-5388.

Prasad, P.S.S., Bae, J.W., Jun, K.-W. & Lee, K.-W. 2008, 'Fischer-Tropsch synthesis by carbon dioxide hydrogenation on Fe-based catalysts', *Catalysis Surveys from Asia*, vol. 12, pp. 170-183.

Pruns, J.K., Vietzke, J.-P., Strassner, M., Rapp, C., Hintze, U. & König, W.A. 2002, 'Characterization of low molecular weight hydrocarbon oligomers by laser desorption/ionization time-of-flight mass spectrometry using a solvent-free sample preparation method', *Rapid Communications in Mass Spectrometry*, vol. 16, pp. 208-211.

Przybilla, L., Brand, J., Yoshimura, K., Räder, H.J. & Müllen, K. 2000, 'MALDI-TOF mass spectrometry of insoluble giant polycyclic aromatic hydrocarbons by a new method of sample preparation', *Analytical Chemistry*, vol. 72, pp. 4591-4597.

Räder, H.J., Spickermann, J., Kreyenschmidt, M. & Müllen, K. 1996, 'MALDI-TOF mass spectrometry in polymer analytics, molecular weight analysis of rigid-rod polymers', *Macromolecular Chemistry and Physics*, vol. 197, pp. 3285-3296.

Rao, K.R.P.M., Huggins, F.E., Mahajan, V., Huffman, G.P., Bukur, D.B. & Rao, V.U.S. 1994, 'Mössbauer study of CO-precipitated Fischer-Tropsch catalysts', *Hyperfine Interactions*, vol. 93, pp. 1751-1754.

Raupp, G.B. & Delgass, W.N. 1979a, 'Mössbauer investigation of supported Fe and FeNi catalysts I. Effect of pre-treatment on particle size', *Journal of Catalysis*, vol. 58, pp. 337-347.

Raupp, G.B. & Delgass, W.N. 1979b, 'Mössbauer investigation of supported Fe and FeNi catalysts II. Carbides formed by Fischer-Tropsch synthesis', *Journal of Catalysis*, vol. 58, pp. 348-360.

Raupp, G.B. & Delgass, W.N. 1979c, 'Mössbauer investigation of supported Fe and FeNi catalysts III. In situ kinetics and spectroscopy during Fischer-Tropsch synthesis', *Journal of Catalysis*, vol. 58, pp. 361-369.

Reymond, J.P., Mériaudeau, P. & Teichner, S.J. 1982, 'Changes in the surface structure and composition of an iron catalyst of reduced or unreduced Fe_2O_3 during the reaction of carbon monoxide and hydrogen', *Journal of Catalysis*, vol. 75, pp. 39-48.

Ribeiro, M.C., Jacobs, G., Davis, B.H., Cronauer, D.C., Kropf, A.J. & Marshall, C.L. 2010, 'Fischer-Tropsch synthesis: an in situ TPR-EXAFS/XANES investigation of the influence of Group I alkali promoters on the local atomic and electronic structure of carburized iron/silica catalysts', *Journal of Physical Chemistry C*, vol. 114, pp. 7895-7903.

Riedel, T., Schulz, H., Schaub, G., Jun, K.-W., Hwang, J.-S. & Lee, K.-W. 2003, 'Fischer-Tropsch on iron with H_2/CO and H_2/CO_2 as synthesis gases: the episodes of formation of the Fischer-Tropsch regime and construction of the catalyst', *Topics in Catalysis*, vol. 26, pp. 41-54.

Rietveld, H.M. 1969, 'A profile refinement method for nuclear and magnetic structures', *Journal of Applied Crystallography*, vol. 2, pp. 65-71.

Rodriguez, N.M., Anderson, P.E., Wootsch, A., Wild, U., Schlögl, R. & Paál, Z. 2001, 'XPS, EM, and catalytic studies of the accumulation of carbon on Pt black', *Journal of Catalysis*, vol. 197, pp. 365-377.

Sadezky, A., Muckenhuber, H., Grothe, H., Niessner, R. & Pöschl, U. 2005, 'Raman microspectroscopy of soot and related carbonaceous materials: spectral analysis and structural information', *Carbon*, vol. 1731-1742.

Saib, A.M., Moodley, D.J., Ciobîcă, I.M., Hauman, M.M., Sigwebela, B.H., Westrate, C.J., Niemantsverdriet, J.W. & van de Loosdrecht, J. 2010 'Fundamental understanding of deactivation and regeneration of cobalt Fischer-Tropsch synthesis catalysts', *Catalysis Today*, vol. 154, pp. 271-282.

Sarkar, A., Seth, D., Dozier, A.K., Neathery, J.K., Hamdeh, H.H. & Davis, B.H. 2007, 'Fischer-Tropsch synthesis: Morphology, phase transformation and particle size growth of nano-scale particles', *Catalysis Letters*, vol. 117, pp. 1-17.

Schneider, A., Inden, G., Grabke, H.J., Wei, Q., Pippel, E. & Woltersdorf, J. 2000, 'Effect of H_2S on formation and decomposition of Fe_3C and Fe_5C_2 under metal dusting conditions', *Steel Research*, vol. 71, pp. 179-184.

Schulz, H. & Claeys, M. 1999, 'Reactions of α-olefins of different chain length added during Fischer–Tropsch synthesis on a cobalt catalyst in a slurry reactor', *Applied Catalysis A: General*, vol. 186, pp. 71-90.

Schulz, H. Nie, Z. & Ousmanov, F. 2002, 'Construction of the Fischer–Tropsch regime with cobalt catalysts', *Catalysis Today*, vol. 71, pp. 351-360.

Schulz, H., Schaub, G., Claeys, M. & Riedel, T. 1999, 'Transient initial kinetic regimes of Fischer-Tropsch synthesis', *Applied Catalysis A: General*, vol. 186, pp. 215-227.

Šedo, O., Alberti, M., Janča, J. & Havel, J. 2006, 'Laser desorption-ionization time of flight mass spectrometry of various carbon materials', *Carbon*, vol. 44, pp. 840-847.

Shang, N.G., Papakonstantinou, P., McMullan, M., Chu, M., Stamboulis, A., Potenza, A., Dhesi, S.S. & Marchetto, H. 2008, 'Catalyst-free efficient growth, orientation and biosensing properties of multilayer graphene nanoflake films with sharp edge planes', *Advanced Functional Materials*, vol. 18, pp. 3506-3514.

Shroff, M.D. & Datye, A.K. 1996, 'The importance of passivation in the study of iron Fischer-Tropsch catalysts', *Catalysis Letters*, vol. 37, pp. 101-106.

Shroff M.D., Kalakkad, D.S., Coulter, K.E., Köhler, S.D., Harrington, M.S., Jackson, N.B., Sault, A.G. & Datye, A.K. 1995, 'Activation of precipitated iron Fischer-Tropsch synthesis catalysts', *Journal of Catalysis*, vol. 156, pp. 185-207.

Shukla, B., Susa, A., Miyoshi, A. & Koshi, M. 2007, 'In situ direct sampling mass spectrometric study on the formation of polycyclic aromatic hydrocarbons in toluene pyrolysis', *Journal of Physical Chemistry A*, vol 111, pp. 8308-8324.

Shukla, B., Susa, A., Miyoshi, A. & Koshi, M. 2008, 'Role of phenyl radicals in the growth of polycyclic aromatic hydrocarbons', *Journal of Physical Chemistry A*, vol. 112, pp. 2362-2369.

Simpson, C.D., Brand, J.D., Berresheim, A.J., Przybilla, L., Räder, H.J. & Müllen, K. 2002, 'Synthesis of a giant 222 carbon graphite sheet', *Chemistry – A European Journal*, vol. 8, no. 6, pp. 1424-1429.

Skelton, R., Dubois, F. & Zenobi, R. 2000, 'A MALDI sample preparation method suitable for insoluble polymers', *Analytical Chemistry*, vol. 72, pp. 1707-1710.

Skoog, D.A., Holler, F.J. & Nieman, T.A. 1998. *Principles of Instrumental Analysis*. 5th ed. Harcourt College: Brooks Cole.

Smith, E. & Dent, G. 2004. *Modern Raman Spectroscopy: a practical approach*. Chichester: John Wiley & Sons.

Sommen, A.P.B., Stoop, F. & van der Wiele, K. 1985, 'Synthesis gas conversion on carbon supported iron catalysts and the nature of deactivation', *Applied Catalysis*, vol. 14, pp. 277-288.

Spivey, J.J. & Roberts, G.W. eds. 2004. *Catalysis, Volume 17*. Cambridge: The Royal Society of Chemistry.

Stair, P.C. 2002, 'In situ Ultraviolet Raman Spectroscopy'. In Haw, J.F. Ed. *In-Situ Spectroscopy in Heterogeneous Catalysis*. Wiley-VCH: Weinheim. Chapter 5.

Steynberg, A.P. 2004, 'Introduction to Fischer-Tropsch Technology'. In Steynberg, A., Dry, M., Eds. *Studies in Surface Science and Catalysis Vol. 152.* Elsevier: Amsterdam, Chapter 1.

Steynberg, P.J., van den Berg, J.A. & Janse van Rensburg, W. 2008, 'Bulk and surface analysis of Hägg Fe carbide (Fe_5C_2): a density functional theory study', *Journal of Physics: Condensed Matter*, vol. 20, pp. 064238(1)-(11).

Storch, H.H., Golumbic, N. & Anderson, R.B. 1951. *The Fischer-Tropsch and Related Synthesis*. New York: John Wiley & Sons.

Swart, J.C.W., Ciobîcă, I.M., van Santen, R.A. & van Steen, E. 2008, 'Intermediates in the formation of graphitic carbon on a flat FCC-Co(111) surface', *Journal of Physical Chemistry C*, vol. 112, pp. 12899-12904.

Swart, J.C.W., van Steen, E., Ciobîcă, I.M. & van Santen, R.A. 2009, 'Interaction of graphene with FCC-Co(111)', *Physical Chemistry Chemical Physics*, vol. 11, pp. 803-807.

Tavares, M.T., Alstrup, I., Bernardo, C.A. & Rostrup-Nielsen, J.R. 1994, 'CO disproportionation in silica-supported nickel and nickel-copper catalysts', *Journal of Catalysis*, vol. 147, pp. 525-234.

Thomson, K., Ziskind, M., Mihesan, C., Therssen, E., Desgroux, P. & Focsa, C. 2007, 'Influence of the photoionization process on the fragmentation of laser desorbed polycyclic aromatic hydrocarbons', *Applied Surface Science*, vol. 253, pp. 6435-6441.

Trimm, D.L. 1999, 'Catalysis for the control of coking during steam reforming', *Catalysis Today*, vol. 49, pp. 3-10.

Trimpin, S., Rouhanipour, A., Az, R., Räder, H.J. & Müllen, K. 2001, 'New aspects in matrix-assisted laser desorption/ionization time-of-flight mass spectrometry: a universal solvent-free sample preparation', *Rapid Communications in Mass Spectrometry*, vol. 15, pp. 1364-1373.

Trinquier, G. & Hoffmann, R. 1984, 'Dinuclear reductive eliminations', *Organometallics*, vol. 3, pp. 370-380.

Unterreiner, B.V., Sierka, M. & Ahlrichs, R. 2004, 'Reaction pathways for growth of polycyclic aromatic hydrocarbons under combustion conditions, a DFT study', *Physical Chemistry Chemical Physics*, vol. 6, pp. 4377-4384.

van der Laan, G.P. & Beenackers, A.A.C.M 2000, 'Intrinsic kinetics of the gas-solid Fischer-Tropsch and water gas shift reactions over a precipitated iron catalyst', *Applied Catalysis A: General*, vol. 193, pp. 39-53.

Vannice, M.A. 1975, 'The catalytic synthesis of hydrocarbons from H_2/CO mixtures over the Group VIII metals I. The specific activities and product distributions of supported metals', *Journal of Catalysis*, vol. 37, pp. 449-461.

Violi, A. 2004, 'Modelling of soot particle inception in aromatic and aliphatic premixed flames', *Combustion and Flame*, vol. 139, pp. 279-287.

Vorm, O., Roepstorff, P. & Mann, M. 1994, 'Improved resolution and very high sensitivity in MALDI TOF of matrix surfaces made by fast evaporation', *Analytical Chemistry*, vol. 66, pp. 3281-3287.

Wang, S.-G., Liao, X.-Y., Cao, D.-B., Li, Y.-W., Wang, J. & Jiao, H. 2007, 'Formation of carbon species on Ni(111): structure and stability', *Journal of Physical Chemistry C*, vol. 111, pp. 10894-10903.

Wu, C.S. ed. 1995. *Size Exclusion Chromatography*. New York: Marcel Dekker.

Xu, J. & Bartholomew, C.H. 2005, 'Temperature-programmed hydrogenation (TPH) and in situ Mössbauer spectroscopy studies of carbonaceous species on silica-supported iron Fischer-Tropsch catalysts', *Journal of Physical Chemistry B*, vol. 109, pp. 2392-2403.

Xu, J., Bartholomew, C.H., Sudweeks, J. & Eggett, D.L. 2003, 'Design, synthesis, and catalytic properties of silica-supported, Pt-promoted iron Fischer-Tropsch catalysts', *Topics in Catalysis*, vol. 26, pp. 55-71.

Yang, X., Dou, X., Rouhanipour, A., Zhi, L., Räder, H.J. & Müllen, K. 2008, 'Two-dimensional graphene nanoribbons', *Journal of the American Chemical Society*, vol. 130, pp. 4216-4217.

Yang, Q.Y., Maynard, K.J., Johnson, A.D. & Ceyer, S.T. 1995, 'The structure and chemistry of CH_3 and CH radicals adsorbed on Ni(111)', *Journal of Chemical Physics*, vol. 102, pp. 7734-7749.

Young, R.A. 1995. *The Rietveld Method*. Oxford: Oxford University Press.

Zaera, F. 2003, 'Surface chemistry of hydrocarbon fragments on transition metals: towards understanding catalytic processes', *Catalysis Letters*, vol. 91, pp. 1-10.

Zhang, R., Bai, L., Yang, Y., Xiang, H., Li, Y. & Zhou, J. 2004, 'Phase change of precipitated iron catalyst during reaction process of Fischer-Tropsch synthesis', *Chinese Journal of Catalysis*, vol. 25, pp. 409-412.

Zhao, R., Goodwin, J.G. & Oukaci, R. 1999, 'Attrition assessment for slurry bubble column reactor catalysts', *Applied Catalysis A: General*, vol. 189, pp. 99-116.

Zhao, R., Goodwin, J.G., Jothimurugesan, K., Spivey, J.J. & Gangwal, S.K. 2000, 'Comparison of attrition test methods: ASTM standard fluidized bed vs. jet cup', *Industrial & Engineering Chemistry Research*, vol. 39, pp. 1155-1158.

Zhao, R., Goodwin, J.G., Jothimurugesan, K., Gangwal, S.K. & Spivey, J.J 2001, 'Spray-dried iron Fischer-Tropsch catalyst. 2. Effect of carburization on catalyst attrition resistance', *Industrial & Engineering Chemistry Research*, vol. 40, pp. 1320-1328.

Zheng, C., Apeloig, Y. & Hoffmann, R. 1988, 'Bonding and coupling of C_1 fragments on metal surfaces', *Journal of the American Chemical*